



**FEDERAL UNIVERSITY OF CEARÁ**  
**CENTER OF TECHNOLOGY**  
**DEPARTMENT OF CHEMICAL ENGINEERING**  
**GRADUATE PROGRAM IN CHEMICAL ENGINEERING**

**BRUNO RAMON BATISTA FERNANDES**

**IMPLICIT AND SEMI-IMPLICIT TECHNIQUES FOR THE COMPOSITIONAL  
PETROLEUM RESERVOIR SIMULATION BASED ON VOLUME BALANCE**

**FORTALEZA**

**2014**

**BRUNO RAMON BATISTA FERNANDES**

**IMPLICIT AND SEMI-IMPLICIT TECHNIQUES FOR THE COMPOSITIONAL  
RESERVOIR SIMULATION BASED ON VOLUME BALANCE**

Thesis presented to the Graduate Program in  
Chemical Engineering of Federal University of  
Ceará as a partial requirement for obtaining  
the Master's degree in Chemical Engineering.  
Concentration Area: Chemical Processes.

Supervisor: Prof. Dr. Francisco Marcondes.  
Co-Supervisor: Prof. Dr. Kamy Sepehrnoori.

**FORTALEZA**

**2014**

Dados Internacionais de Catalogação na Publicação  
Universidade Federal do Ceará  
Biblioteca de Pós-Graduação em Engenharia - BPGE

- 
- F398i      Fernandes, Bruno Ramon Batista.  
            Implicit and semi-implicit techniques for the compositional Petroleum reservoir simulation based on volume balance / Bruno Ramon Batista Fernandes. – 2014.  
            167 f. : il. color., enc. ; 30 cm.
- Dissertação (mestrado) – Universidade Federal do Ceará, Centro de Tecnologia, Departamento de Engenharia Química, Programa de Pós-Graduação em Engenharia Química, Fortaleza, 2014.  
            Área de Concentração: Processos Químicos.  
            Orientação: Prof. Dr. Francisco Marcondes.  
            Coorientação: Prof. Dr. Kamy Sepehrnoori.
1. Engenharia Química. 2. Simulação. 3. Volumes finitos. 4. Mecânica dos fluidos. 5. Escoamento em meios porosos. I. Título.

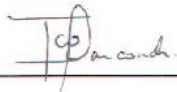
**BRUNO RAMON BATISTA FERNANDES**

**IMPLICIT AND SEMI-IMPLICIT TECHNIQUES FOR THE COMPOSITIONAL  
RESERVOIR SIMULATION BASED ON VOLUME BALANCE**

Thesis presented to the Graduate Program in  
Chemical Engineering of Federal University of  
Ceará as a partial requirement for obtaining  
the Master's degree in Chemical Engineering.  
Concentration Area: Chemical Processes.

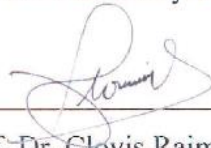
Approved in: 26/06/2014.

COMITEE MEMBERS



---

Prof. Dr. Francisco Marcondes (Supervisor)  
Federal Univeristy of Ceará (UFC)



---

Prof. Dr. Clovis Raimundo Maliska  
Federal Univeristy of Santa Catarina (UFSC)



---

Prof. Dr. Sebastião Mardônio Pereira de Lucena  
Federal University of Ceará (UFC)

To my father and mother.

## ACKNOWLEDGEMENTS

I would like to express my sincere gratitude to my supervisor, Professor Francisco Marcondes, for all his teaching, guidance, help and patience during these years, and for all the opportunities. I am really grateful for joining his research group. I would like to acknowledge my co-supervisor, Professor Kamy Sepehrnoori, for all his help and opportunities as well. I am grateful for all the helpful comments of Dr. Abdojalil Varavei.

I would like to thank my parents, especially my mother for entrusting her dream of studying for me. I would like to thank my brother for all his fellowship, and for always believing in me.

I would like to express my gratitude to my fiancée, Ana Beatriz Gentil, for all her support, affection, patience, for believing in my potential, and for always standing on my side, even in the bad times.

I thank my friends from the 3D Lab for all their help and fellowship, in special for Pedro Felipe and Victor Aias. I thank my friends, Leonardo Farias and Ítalo Waldimíro, for their fellowship. I would like to thank the friends of the LDFC, in special for Frank Webston for all his help when I joined the group. I acknowledge my friend Dr. Luiz Otávio Schmal dos Santos and his wife, Rubia, for all their help and care during my time at UT Austin, and also with all his important comments for the development of this work.

I would like to express my sincere gratitude to Professor Sebastião Mardônio Pereira de Lucena for all his help and attention towards our group. I also thank the other professors of the Chemical Engineering Department for their teaching, in special for Professor Samuel Jorge Marques Cartaxo.

I thank the members of the qualification and defense committees: Prof. Francisco Marcondes, Prof. Clovis Raimundo Maliska, Prof. Sebastião Mardônio Pereira de Lucena and Prof. Diana Cristina Silva de Azevedo.

I would like to acknowledge the Abu Dhabi National Oil Company, CAPES and PETROBRAS S/A, for the financial support for this research.

I would like to thank the Center for Petroleum and Geosystems Engineering at the University of Texas at Austin for allowing us to use the UTCOMP simulator for the development of this work. Also, I thank ESSS for allowing us to use their post-processor, Kraken<sup>®</sup>.

“Man would not have attained the possible unless time and again he had reached out for the impossible.”

-Max Weber

## ABSTRACT

In reservoir simulation, the compositional model is one of the most used models for enhanced oil recovery. However, the physical model involves a large number of equations with a very complex interplay between equations. The model is basically composed of balance equations and equilibrium constraints. The way these equations are solved, the degree of implicitness, the selection of the primary equations, primary and secondary variables have a great impact on the computation time. In order to verify these effects, this work proposes the implementation and comparison of some implicit and semi-implicit methods. The following formulations are tested: an IMPEC (implicit pressure, explicit composition), an IMPSAT (implicit pressure and saturations), and two fully implicit formulations, in which one these formulations is being proposed in this work. However, the literature reports some intrinsic inconsistencies of the IMPSAT formulation mentioned. In order to verify it, an iterative IMPSAT is implemented to check the quality of the IMPSAT method previously mentioned. The finite volume method is used to discretize the formulations using Cartesian grids and unstructured grids in conjunction with the EbFVM (Element based finite volume method) for 2D and 3D reservoirs. The implementations have been performed in the UTCOMP simulator from the University of Texas at Austin. The results of several case studies are compared in terms of volumetric oil and gas rates and the total CPU time. It was verified that the FI approaches increase their performance, when compared to the other approaches, as the grid is refined. A good performance was observed for the IMPSAT approach when compared to the IMPEC formulation. However, as more complex stencils are used, the IMPSAT performance reduces.

**Keywords:** Compositional Simulation, EbFVM, IMPEC, IMPSAT, Fully Implicit, Unstructured grids.



## RESUMO

Em simulação de reservatórios, o modelo composicional é um dos mais usados para a recuperação avançada de petróleo. Entretanto, o modelo físico envolve um grande número de equações com uma complexa interrelação entre elas. O modelo é basicamente composto por equações de balanço e restrições de equilíbrio. A forma como essas equações são resolvidas como, o grau de implicitude, a seleção das equações primárias, variáveis primárias e secundárias tem um grande impacto no tempo de computação. Com o intuito de verificar esse efeito, esse trabalho propõe a implementação e comparação de alguns métodos implícitos e semi-implícitos. As seguintes formulações são testadas: uma IMPEC (*implicit pressure, explicit composition*), uma IMPSAT (*implicit pressure and saturations*), e duas formulações totalmente implícitas, das quais uma destas está sendo proposta neste trabalho. Entretanto, a literatura relata algumas inconsistências intrínsecas da formulação IMPSAT mencionada. Para verificar isso, um IMPSAT iterativo foi implementado para verificar a qualidade nos resultados do método IMPSAT previamente mencionado. O método de volumes finitos é usado para discretizar as formulações usando malhas Cartesianas e não-estruturadas em conjunto com o EbFVM (*Element based finite volume method*) para reservatórios 2D e 3D. A implementação foi realizada no simulador UTCOMP da *Univeristy of Texas at Austin*. Os resultados de diversos casos de estudo são comparados em termos das vazões volumétricas de óleo e gás e do tempo total de CPU. Verificou-se que as abordagens totalmente implícitas melhoram sua performance, quando comparado com os demais métodos, a medida que a malha é refinada. Um bom desempenho foi observado para as formulações IMPSAT quando comparadas com a formulação IMPEC. Entretanto, com o uso de conexões mais complexas entre os blocos da malha, o desempenho da formulação IMPSAT reduziu.

**Palavras-chave:** Simulação Composicional, EbFVM, IMPEC, IMPSAT, Totalmente Implícito, Malhas não-estruturadas.

## LIST OF ILLUSTRATIONS

### CHAPTER 1

Figure 1.1 – Illustration of a typical oil and gas reservoir.....22

### CHAPTER 2

Figure 2.1 – Illustration of the REV .....38

### CHAPTER 3

Figure 3.1 – Cartesian control volume. a) three dimensional view; b) x-y plane view.....63

Figure 3.2 – Illustration of a dual mesh for the EbFVM approach ..... 66

Figure 3.3 – 2D elements in the physical and computational planes. a) Triangle element; b) quadrilateral element ..... 67

Figure 3.4 – 3D elements into the physical plane and computational local plane. a) Hexahedron element; b) tetrahedron element; c) prism element; d) pyramid element .....69

### CHAPTER 4

Figure 4.1 – Flowchart of the IMPEC formulation for a time-step.....76

Figure 4.2 – Flowchart of the IMPSAT-0 formulation for a time-step .....78

Figure 4.3 – Flowchart of the IMPSAT-1 formulation for a time-step .....79

Figure 4.4 – Flowchart of the IMPSAT-2 formulation for a time-step .....81

Figure 4.5 – Flowchart for performing one time-step FI-0 formulation .....87

Figure 4.6 – Flowchart for performing one time-step for the FI-1 formulation.....88

### CHAPTER 5

Figure 5.1 – Five-spot layout (quarter of five-spot filled).....90

Figure 5.2 – 2D Cartesian grids - Case 1. Injectors in blue and producers in red. ....92

Figure 5.3 – Production rates comparison between IMPEC and IMPSAT-0 – Case 1. a) oil; and b) gas.....94

Figure 5.4 – Production rates comparison between IMPEC and IMPSAT-1 – Case 1. a) oil; and b) gas.....94

Figure 5.5 – Production rates comparison between IMPEC and IMPSAT-2 – Case 1. a) oil; and b) gas.....95

Figure 5.6 – Production rates comparison between IMPEC and FI-0* – Case 1. a) oil; and b) gas. ....	95
Figure 5.7 – Production rates comparison between IMPEC and FI-1* – Case 1. a) oil; and b) gas. ....	96
Figure 5.8 – Production rates comparison between IMPEC and FI-0 – Case 1. a) oil; and b) gas. ....	96
Figure 5.9 – Production rates comparison between IMPEC and FI-1 Case 1. a) oil; and b) gas. ....	97
Figure 5.10 – Time-stepping profiles for all formulations – Case 1. a) 20x20; b) 40x40; and c) 80x80. ....	98
Figure 5.11 – Gas saturation fields at 500 days for all formulations - Case 1 using a 20x20 Cartesian grid. a) IMPEC; b) IMPSAT-0; c) IMPSAT-1; d) IMPSAT-2; e) FI-0; and f) FI-1. ....	99
Figure 5.12 – Gas saturation fields at 500 days for all formulations - Case 1 using a 40x40 Cartesian grid. a) IMPEC; b) IMPSAT-0; c) IMPSAT-1; d) IMPSAT-2; e) FI-0; and f) FI-1. ....	100
Figure 5.13 – Gas saturation fields at 500 days for all formulations - Case 1 using a 80x80 Cartesian grid. a) IMPEC; b) IMPSAT-0; c) IMPSAT-1; d) IMPSAT-2; e) FI-0; and f) FI-1. ....	101
Figure 5.14 – 3D Cartesian grids - Case 1. a) 20x20x5; b) 40x40x10; and c) 60x60x15. ....	103
Figure 5.15 – Production rates comparison for 3D Cartesian 60x60x15 between IMPEC and IMPSAT-0 - Case 1. a) oil; and b) gas. ....	104
Figure 5.16 – Production rates comparison for 3D Cartesian 60x60x15 between IMPEC and FI-0 for Case 1. a) oil; and b) gas. ....	104
Figure 5.17 – Time-stepping profiles for all formulations – Case 1 using 3D Cartesian grids. ....	105
Figure 5.18 – Gas saturation fields at 700 days for all formulations - Case 1 using a 60x60x15 Cartesian grid. a) IMPEC; b) IMPSAT-0; c) IMPSAT-1; d) IMPSAT-2; e) FI-0; and f) FI-1. ....	106
Figure 5.19 – 2D regular quadrilateral element grids - Case 1. a) 20x20; b) 40x40; and c) 60x60. ....	107
Figure 5.20 – 2D unstructured quadrilateral grids - Case 1. a) 1199 vertices (1134 elements); b) 2661 vertices (2568 elements); and c) 3387 vertices (3282 elements). ....	108

Figure 5.21 – 2D unstructured triangular grids - Case 1. a) 1220 vertices (2310 elements); b) 2330 vertices (4482 elements); and c) 3329 vertices (6444 elements).....	108
Figure 5.22 – Production rates comparison between IMPEC and IMPSAT-0 - Case 1, using 2D regular quadrilateral grids. a) oil; and b) gas. ....	109
Figure 5.23 – Production rates comparison between IMPEC and FI-0 - Case 1, using 2D regular quadrilateral grids. a) oil; and b) gas. ....	109
Figure 5.24 – Production rates comparison between IMPEC and IMPSAT-0 - Case 1 for 2D unstructured quadrilateral grid. a) oil; and b) gas. ....	110
Figure 5.25 – Production rates comparison between IMPEC and FI-0 - Case 1 for 2D unstructured quadrilateral grid. a) oil; and b) gas. ....	110
Figure 5.26 – Production rates comparison between IMPEC and IMPSAT-0 - Case 1 for 2D unstructured triangular grid. a) oil; and b) gas. ....	111
Figure 5.27 – Production rates comparison between IMPEC and FI-0 - Case 1 for 2D unstructured triangular grid. a) oil; and b) gas. ....	111
Figure 5.28 – Gas saturation field at 500 days for 2D EbFVM - Case 1. a) quadrilateral 60x60 IMPEC; b) quadrilateral 60x60 IMPSAT-0; c) quadrilateral 60x60 FI-0; d) quadrilateral 3387 vertices IMPEC; e) quadrilateral 3387 vertices IMPSAT-0; f) quadrilateral 3387 vertices FI-0; g) triangle 3329 vertices IMPEC; h) triangle 3329 vertices IMPSAT-0; and i) triangle 3329 vertices FI-0. ....	112
Figure 5.29 – 3D hexahedron element grids - Case 1. a) 1024 vertices; b) 6480 vertices; and c) 11767 vertices. ....	114
Figure 5.30 – 3D tetrahedron element grids - Case 1. a) 1024 vertices; b) 4056 vertices; and c) 16810 vertices. ....	115
Figure 5.31 – 3D prism element grids - Case 1. a) 1024 vertices; b) 4056 vertices; and c) 13448 vertices. ....	115
Figure 5.32 – 3D pyramid element grids - Case 1. a) 1699 vertices; b) 7181 vertices; and c) 24648 vertices. ....	116
Figure 5.33 – Production rates comparison between IMPEC and IMPSAT-0 - Case 1 for 3D unstructured hexahedron grid. a) oil; and b) gas. ....	117
Figure 5.34 – Production rates comparison between IMPEC and FI-0 - Case 1 for 3D unstructured hexahedron grid. a) oil; and b) gas. ....	117
Figure 5.35 – Production rates comparison between IMPEC and IMPSAT-0 - Case 1 for 3D unstructured tetrahedron grid. a) oil; and b) gas. ....	118

Figure 5.36 – Production rates comparison between IMPEC and FI-0 - Case 1 for 3D unstructured tetrahedron grid. a) oil; and b) gas.....	118
Figure 5.37 – Production rates comparison between IMPEC and IMPSAT-0 - Case 1 for 3D unstructured prism grid. a) oil; and b) gas.....	119
Figure 5.38 – Production rates comparison between IMPEC and FI-0 - Case 1 for 3D unstructured prism grid. a) oil; and b) gas.....	119
Figure 5.39 – Production rates comparison between IMPEC and IMPSAT-0 - Case 1 for 3D unstructured pyramid grid. a) oil; and b) gas.....	120
Figure 5.40 – Production rates comparison between IMPEC and FI-0 - Case 1 for 3D unstructured pyramid grid. a) oil; and b) gas.....	120
Figure 5.41 – Gas saturation field at 700 days for 3D hexahedron EbFVM with 11767 vertices - Case 1. a) IMPEC; b) IMPSAT-0; and c) FI-0. ....	121
Figure 5.42 – Gas saturation field at 700 days for 3D tetrahedron EbFVM with 16810 vertices - Case 1. a) IMPEC; b) IMPSAT-0; and c) FI-0. ....	121
Figure 5.43 – Gas saturation field at 700 days for 3D prism EbFVM with 13448 vertices - Case 1. a) IMPEC; b) IMPSAT-0; and c) FI-0.....	121
Figure 5.44 – Gas saturation field at 700 days for 3D pyramid EbFVM with 24648 vertices - Case 1. a) IMPEC; b) IMPSAT-0; and c) FI-0.....	122
Figure 5.45 – Hybrid grid: 20298 vertices; 3254 triangle elements and 18195 quadrilateral elements - Case 2. ....	126
Figure 5.46 – Production rates comparison between IMPEC and IMPSAT-0 - Case 2. a) oil; and b) gas.....	126
Figure 5.47 – Production rates comparison between IMPEC and FI-0 - Case 2. a) oil; and b) gas. ....	127
Figure 5.48 – Gas saturation fields at 6000 days of simulation - Case 2. a) IMPEC; b) IMPSAT-0; and c) FI-0. ....	127
Figure 5.49 – 2D 40x80 Cartesian grid - Case 3. ....	131
Figure 5.50 – Heterogeneous absolute permeability in X and Y directions field - Case 3. ....	131
Figure 5.51 – Production rates comparison between IMPEC and IMPSAT-0 - Case 3 for the Cartesian grid. a) oil; and b) gas.....	132
Figure 5.52 – Production rates comparison between IMPEC and FI-0 - Case 3 for the Cartesian grid. a) oil; and b) gas.....	132
Figure 5.53 – Gas saturation field at 3000 days for 2D Cartesian grid - Case 3. a) IMPEC; b) IMPSAT-0; and c) FI-0. ....	133

Figure 5.54 – Second hydrocarbon liquid saturation field at 3000 days for 2D Cartesian grid - Case 3. a) IMPEC; b) IMPSAT-0; and c) FI-0.....	133
Figure 5.55 – Time-stepping profiles for the IMPEC, IMPSAT-0 and FI-0 formulations – Case 3 using Cartesian grid. ....	134
Figure 5.56 – 2D 3016 vertices grid with 818 triangular and 2490 quadrilateral elements - Case 3. ....	136
Figure 5.57 – Heterogeneous absolute permeability in X and Y directions field for the element grid - Case 3.....	136
Figure 5.58 – Production rates comparison between IMPSAT-0 and FI-0 - Case 3 for the EbFVM. a) oil; and b) gas. ....	137
Figure 5.59 – Gas saturation field at 3500 days for 2D element grid - Case 3. a) IMPSAT-0; and b) FI-0. ....	138
Figure 5.60 – Second liquid hydrocarbon phase saturation field at 3500 days for 2D element grid - Case 3. a) IMPSAT-0; and b) FI-0. ....	138
Figure 5.61 – Time-stepping profiles for the IMPSAT-0 and FI-0 formulations – Case 3 using the element grid. ....	139
Figure 5.62 – 40x40x5 Cartesian grid - Case 4. ....	142
Figure 5.63 – Heterogeneous absolute permeability in X and Y directions field - Case 4. ...	142
Figure 5.64 – Production rates comparison between IMPEC and IMPSAT-0 - Case 4. a) oil; and b) gas.....	143
Figure 5.65 – Production rates comparison between IMPEC and IMPSAT-1 - Case 4. a) oil; and b) gas.....	143
Figure 5.66 – Production rates comparison between IMPEC and IMPSAT-2 - Case 4. a) oil; and b) gas.....	144
Figure 5.67 – Production rates comparison between IMPEC and FI-0 - Case 4. a) oil; and b) gas. ....	144
Figure 5.68 – Production rates comparison between IMPEC and FI-1 - Case 4. a) oil; and b) gas. ....	145
Figure 5.69 – Gas saturation field at 250 days - Case 4. a) IMPEC; b) IMPSAT-0; c) IMPSAT-1; d) IMPSAT-2; e) FI-0; and f) FI-1. ....	145
Figure 5.70 – Time-stepping profiles – Case 4. a) IMPEC and IMPSAT formulations; and b) IMPEC and FI formulations. ....	146

## LIST OF TABLES

### CHAPTER 1

Table 1.1 – Variables in compositional reservoir simulation.....	26
Table 1.2 – General concepts of the formulations for compositional reservoir simulation. ....	32

### CHAPTER 5

Table 5.1 – Reservoir data for Case 1. ....	90
Table 5.2 – Fluid composition data for Case 1.....	90
Table 5.3 – Component data for Case 1. ....	91
Table 5.4 – Binary interaction coefficients for Case 1.....	91
Table 5.5 – Relative permeability data for Case 1. ....	91
Table 5.6 – CPU time (s) for all simulations - Case 1 using 2D Cartesian grids. ....	102
Table 5.7 – CPU time (s) of all simulations - Case 1 using 3D Cartesian grids. ....	105
Table 5.8 – CPU time (s) of all simulations - Case 1 using 2D regular quadrilateral grids. ..	113
Table 5.9 – CPU time (s) of all simulations - Case 1 using 2D unstructured quadrilateral grids. .....	113
Table 5.10 – CPU time (s) of all simulations - Case 1 using 2D unstructured triangular grids. .....	113
Table 5.11 – CPU time (s) of all simulations - Case 1 using 3D hexahedron grids.....	122
Table 5.12 – CPU time (s) of all simulations - Case 1 using 3D tetrahedron grids. ....	122
Table 5.13 – CPU time (s) of all simulations - Case 1 using 3D prism grids. ....	123
Table 5.14 – CPU time (s) of all simulations – Case 1 using 3D pyramid grids.....	123
Table 5.15 – Reservoir data for Case 2. ....	124
Table 5.16 – Fluid composition data for Case 2.....	124
Table 5.17 – Component data for Case 2. ....	125
Table 5.18 – Binary interaction coefficients for Case 2.....	125
Table 5.19 – Relative permeability data for Case 2. ....	125
Table 5.20 – CPU time (s) of all simulations – Case 2. ....	128
Table 5.21 – Reservoir data for Case 3. ....	129
Table 5.22 – Fluid composition data for Case 3.....	129
Table 5.23 – Component data for Case 3. ....	130
Table 5.24 – Binary interaction coefficients for Case 3.....	130
Table 5.25 – Relative permeability data for Case 3. ....	130

Table 5.26 – CPU time (s) for all simulations - Case 3 using a 40x80 2D Cartesian grid.....	135
Table 5.27 – CPU time (s) for all simulations - Case 3 using a hybrid grid with 3016 vertices. .....	139
Table 5.28 – Reservoir data for Case 4. ....	140
Table 5.29 – Fluid composition data for Case 4.....	140
Table 5.30 – Component data for Case 4. ....	141
Table 5.31 – Binary interaction coefficients for Case 4.....	141
Table 5.32 – Relative permeability data for Case 4. ....	141
Table 5.33 – CPU time (s) of all simulations – Case 4. ....	146

## APPENDIX A

Table A.1. Time-stepping control parameters for Case 1 using 2D Cartesian grids.....	157
Table A.2. Time-stepping control parameters for Case 1 using 3D Cartesian grids.....	158
Table A.3. Time-step control parameters - Case 1 using 2D uniform quadrilateral grids. ....	159
Table A.4. Time-step control parameters for Case 1 using 2D unstructured quadrilateral grids. .....	160
Table A.5. Time-step control parameters for Case 1 using 2D unstructured triangular grids. .....	161
Table A.6. Time-step control parameters for Case 1 using 3D unstructured hexahedron grids. .....	162
Table A.7. Time-step control parameters for Case 1 using 3D unstructured tetrahedron grids. .....	163
Table A.8. Time-step control parameters for Case 1 using 3D unstructured prism grids. ....	164
Table A.9. Time-step control parameters for Case 1 using 3D unstructured pyramid grids..	165
Table A.10. Time-step control parameters for Case 2.....	165
Table A.11. Time-step control parameters for Case 3 using Cartesian grid. ....	166
Table A.12. Time-step control parameters for Case 3 using the element grid.....	166
Table A.13. Time-step control parameters for Case 4.....	167



## LIST OF ABBREVIATIONS AND ACRONYMS

BF	Boundary Fitted
CP	Corner Point
CV	Control-Volume
CVFEM	Control Volume Finite Element Method
EbFVM	Element based Finite Volume Method
EOR	Enhanced Oil Recovery
EOS	Equation of State
FEM	Finite Element Method
FI	Fully Implicit
FVM	Finite Volume Method
IFT	Interfacial Tension
IMPEC	Implicit Pressure, Explicit Compositions
IMPEM	Implicit Pressure, Explicit Overall Mass/Moles
IMPES	Implicit Pressure, Explicit Saturations
IMPSAT	Implicit Pressure and Saturations
IP	Integration Point
MAW	Mass Weighted Upwind
MCM	Multiple Contacts Miscibility
MVNR	Minimum Variable Newton-Raphson
NOBF	Non-Orthogonal Boundary Fitted
PEBI	Perpendicular Bisector
PREOS	Peng-Robinson Equation of State
REV	Representative Elementary Volume
SCV	Subcontrol-Volume
SUCV	Streamline Upwind Control-Volume
TVD	Total Variation Diminishing
UTCOMP	University of Texas Compositional Simulator

## LIST OF SYMBOLS

$a$	Equation of state parameter.
$A$	Equation of state parameter or area ( $\text{m}^2$ ).
$b$	Equation of state parameter or back interface.
$B$	Equation of state parameter or back control-volume.
$C_f$	Formation compressibility ( $\text{MPa}^{-1}$ ).
$C_w$	Water compressibility ( $\text{MPa}^{-1}$ ).
$D$	Depth (m).
$e$	East interface.
$E$	East control-volume.
$f$	Fractionary flow (dimensionless) or fugacity (MPa).
$F$	Volumetric flow rate ( $\text{m}^3/\text{d}$ ).
$g$	Gravity acceleration ( $\text{m}/\text{d}^2$ ).
$G$	Gibbs free energy ( $J$ ).
$j$	Mole flux transported by dispersion ( $\text{kmol}/\text{m}^2\text{d}$ ).
$L$	Phase mole fraction (dimensionless).
$k_r$	Relative permeability (dimensionless).
$\bar{\bar{K}}$	Absolute permeability tensor ( $\text{m}^2$ ).
$n_c$	Number of components.
$n_p$	Number of phases.
$n_j$	Number of moles of phase $j$ (kmol).
$n_{ij}$	Number of moles of component $i$ in phase $j$ (kmol).
$n_f$	Number of control volume interfaces.
$n_v$	Number of element vertices.
$N$	Total number of moles (kmol) or shape function.
$\tilde{N}$	Total number of moles per pore volume ( $\text{kmon}/\text{m}^3$ ).
$P$	Pressure (MPa).
$P_c$	Capillary pressure (MPa).
$\dot{q}$	Mole rate being injected or produced ( $\text{kmol}/\text{d}$ ).
$\dot{Q}$	Volumetric flow rate injected or produced ( $\text{m}^3/\text{d}$ ).
$R$	Gases universal constant ( $\text{MPa m}^3 \text{ kmol}^{-1} \text{ K}^{-1}$ ).

$S$	Saturation (dimensionless).
$t$	Time (days).
$T$	Temperature (K) or transmissibility ( $\text{m}^3$ ).
$\vec{U}$	Velocity vector (m/d).
$V$	Volume ( $\text{m}^3$ ).
$\bar{V}$	Partial molar volume ( $\text{m}^3/\text{kmol}$ ).
$w$	West interface.
$W$	West control-volume.
$WI$	Well index ( $\text{m}^3$ ).
$x$	Cartesian coordinate in X direction (m).
$x_{ij}$	Mole fraction of component $i$ in phase $j$ (dimensionless).
$y$	Cartesian coordinate in Y direction (m).
$z$	Cartesian coordinate in Z direction (m).
$z_i$	Overall mole fraction of component $i$ (dimensionless).
$Z$	Compressibility factor (dimensionless).

### **Greek letters**

$\zeta$	Mole density ( $\text{kmol}/\text{m}^3$ ) or coordinate in the computational plane.
$\lambda$	Mobility ( $\text{MPa}^{-1} \text{d}^{-1}$ ).
$\mu$	Viscosity ( $\text{MPa d}$ ).
$\rho$	Mass density ( $\text{kg}/\text{m}^3$ ).
$\eta$	Coordinate in the computational plane.
$\gamma$	Coordinate in the computational plane.
$\phi$	Porosity (dimensionless).
$\kappa$	Binary interaction coefficient (dimensionless).
$\omega$	Acentric factor (dimensionless).
$\Phi$	Hydraulic potential (MPa).

### **Subscripts**

$b$	Bulk.
$g$	Gas phase.
$l$	Second liquid phase.

$o$	Oil phase.
$p$	Pore or control-volume P.
$T$	Total.
$w$	Water phase or component.

### **Superscripts**

$n$	Previous time-step.
$n+1$	Current time-step.
$m$	Implicit level to be defined.
$0$	Reference condition.

## SUMMARY

1	INTRODUCTION.....	21
1.1	<i>Literature review</i> .....	24
1.1.1	<i>Numerical formulations</i> .....	24
1.1.2	<i>Gridding techniques</i> .....	33
1.2	<i>Layout of this work</i> .....	35
2	MATHEMATICAL MODEL .....	37
2.1	<i>Transport equations</i> .....	37
2.2	<i>Phase behavior</i> .....	44
2.3	<i>Physical properties</i> .....	47
3	APPROXIMATE EQUATIONS .....	60
3.1	<i>Spatial discretization</i> .....	60
3.1.1	<i>Cartesian grid discretization</i> .....	63
3.1.2	<i>EbFVM grid discretization</i> .....	66
3.2	<i>Time-step size selection</i> .....	73
4	FORMULATIONS .....	75
4.1	<i>Ács et al. (IMPEC)</i> .....	75
4.2	<i>Watts (IMPSAT-0)</i> .....	76
4.3	<i>Modified Watts (IMPSAT-1)</i> .....	78
4.4	<i>Iterative IMPSAT (IMPSAT-2)</i> .....	80
4.5	<i>Collins et al. (FI-0)</i> .....	82
4.6	<i>New FI approach (FI-1)</i> .....	87
5	RESULTS AND DISCUSSION .....	89
5.1	<i>Case study 1</i> .....	89
5.1.1	<i>Case study 1: 2D Cartesian grid</i> .....	92
5.1.2	<i>Case study 1: 3D Cartesian grid</i> .....	103
5.1.3	<i>Case study 1: 2D EbFVM</i> .....	107
5.1.4	<i>Case study 1: 3D EbFVM</i> .....	114
5.2	<i>Case study 2: 2D EbFVM</i> .....	124
5.3	<i>Case study 3</i> .....	129
5.3.1	<i>Case study 3: 2D Cartesian grid</i> .....	131
5.3.2	<i>Case study 3: 2D EbFVM</i> .....	136

5.4	<i>Case study 4: 3D Cartesian</i> .....	140
6	CONCLUSIONS AND FUTURE WORK .....	147
6.1	<i>Future work</i> .....	148
7	REFERENCES.....	149

**APPENDICES**

APPENDIX A	TIME-STEPPING CONTROL PARAMETERS.....	157
------------	---------------------------------------	-----

## 1 INTRODUCTION

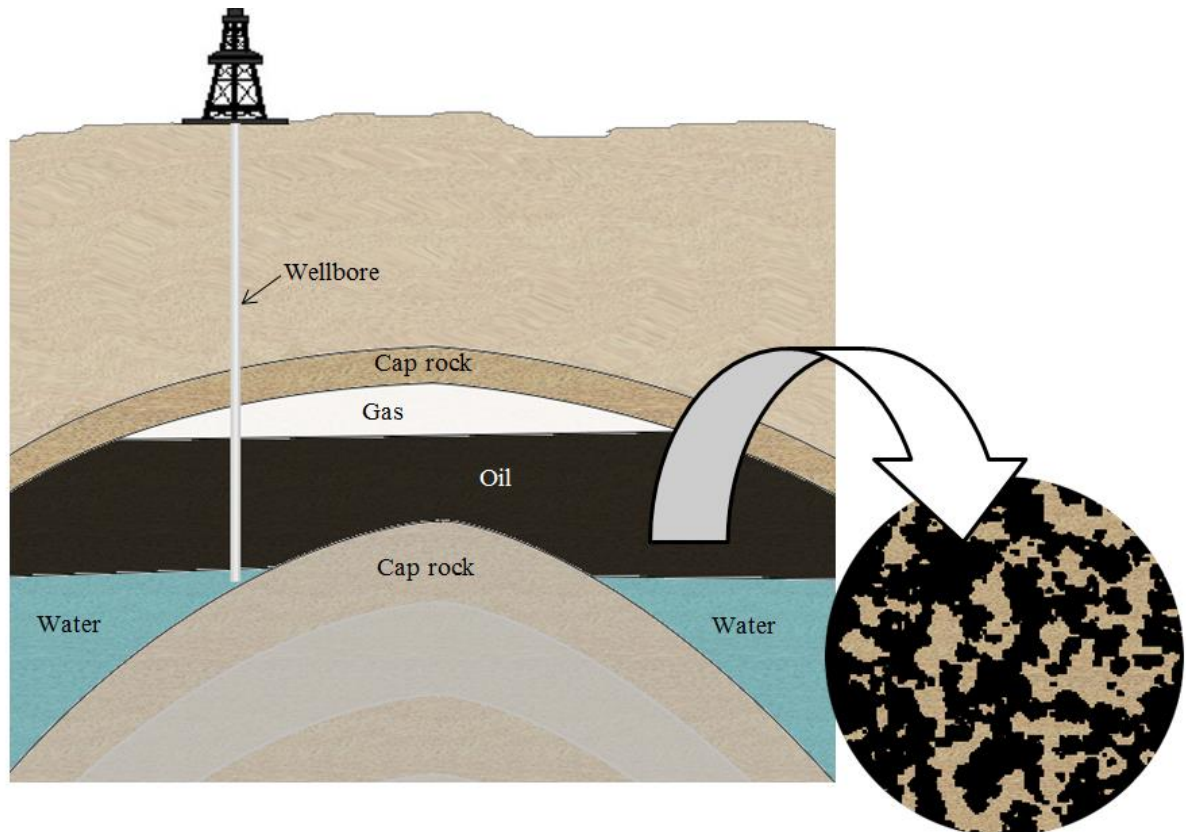
Petroleum is one of the most important items in the modern society. Not only petroleum is the main energy source in the world, but it is also used as a raw material in countless consumer goods and has numerous applications in industrial processes. The importance of the oil impacts all areas of the society including politics, environment, science, and technology.

Petroleum is a non-renewable mixture of hydrocarbons found naturally in rock formations in the subsurface. Two theories try to explain the origin of these mixtures: the biogenic and abiogenic theories. The biogenic theory, the most accepted one, claims that the hydrocarbon mixtures are formed through the deposition of dead organic matter under lakes and seas through millions of years. During this period, these remains are continuously covered by layers of sediments which become later sedimentary rocks. The heat and pressure under these layers generates innumerable complex chemical reactions converting the organic remains in oil and gas in a very slow process. On the other hand, the abiogenic theory claims that petroleum was formed without the need of biological remains. One of the abiogenic hypothesis, proposed that the petroleum comes from deep carbon deposits as old as the Earth formation. The hydrocarbons then migrate upward reaching the reservoir rocks. Since the biogenic theory has been more successful in the discovery of oil and gas fields, it is much more popular and supported than the abiogenic theory, as concluded by Glasby (2006).

The oil rock formations are permeable porous media called reservoirs. These reservoirs are usually surrounded by impermeable rocks called trap, seal, or cap rocks. The hydrocarbons present in the rock pores at reservoir conditions can have complex phase behavior and can form phases such as oil, gas, another liquid or solid (such as asphaltene). Water is always present in oil reservoirs, thus an aqueous phase is always present. To produce the oil from the fields it is necessary to drill wells to connect the reservoir with the surface. Figure 1.1 illustrates a well drilled through the formation. If the pressure difference between the reservoir and the surface is enough to produce a fluid flow from the reservoir to the producing wells, this recovery process is called primary recovery, and it consists of the simplest recovery mechanism. After the initial depletion, the reservoir pressure decreases and also the production rates. In order to continue the production, it is possible to inject water or recycled gas into the reservoir to increase the reservoir pressure; this mechanism is called secondary recovery. Any oil recovery technique that is not classified as primary or secondary recovery is called tertiary recovery or enhanced oil recovery (EOR). The EOR can be

summarized as thermal recovery, gas flooding, chemical injection, among others. The EOR techniques can recover up to 60% (U.S. Department of Energy, 2011) of the original oil in place, while the primary recovery goes up to 20%, and the secondary recovery up to 40% (EPRI, 1999). It is important to mention that these recovered amounts depend on the oil type and reservoir depth.

Figure 1.1 – Illustration of a typical oil and gas reservoir.



The modelling and simulation of oil and gas recovery processes allows engineers to have a good idea of the oil and gas production rates, which aids the formulation of economic analysis and in the selection of the recovery strategies. Modelling oil recovery processes consists of mass, volume, and energy balances that can reproduce the fluid dynamics inside the reservoir with the desirable degree of realism and accuracy. These balances form a set of nonlinear differential equations that cannot be solved without the use of numerical approaches unless several simplifications are made. These models have been used in reservoir simulations since the 1930's (Coats, 1982a; Coats, 1982b). According to Coats (1982a; 1982b), the early simulations consisted of analytical solutions, zero-dimensional material balances and one dimensional Buckley-Leverett (Buckley and Leverett, 1942) calculations. The use of computers to solve these models started at the beginning of the 1960's and became a great advance in petroleum reservoir area, extending the solution of



monophasic one-dimension flow to two and three dimensions, with multiphase flow in transient regime and heterogeneous media (Coats, 1982a; Coats, 1982b). Before the 70's, the computational models were mainly based on Black-Oil models. The Black-Oil model assumes that three pseudo-components exist inside the reservoir: oil, gas and water. In general, the gas component can exist in the oil and gas phase, but the oil and water components cannot be transferred to the other phases. Although the Black-Oil model is simple and has a low computational cost, it lacks realism and it is suitable only for heavy oils. The increase in oil prices led to the development of many EOR techniques. These processes could not be modelled with the Black-Oil model unless large errors in the predictions with this model were acceptable. Several models emerged to treat each EOR processes. However these models were soon replaced by multipurpose models that could handle several processes. According to Ács et al. (1985), two reasons led to this: first, the expenses involved in training, development and maintenance of these multiple models; and second, the search for a model which could have a common basis to help surveys and comparisons for the understanding of different oil recovery mechanisms.

The reservoir simulation had a great evolution since its beginning, not only in the physical modelling equations used but also in many other features such as: numerical formulations, gridding, flux approximation schemes, phase behavior calculations, geomechanics models, fractures and fault models and linear solvers.

Solving the equations involved is still a difficult task, consuming even days of computation even with the most modern computers to provide a single result. In order to provide feasible computation times, many algorithms were proposed for all types of models, from black-oil to thermal compositional models, differing in complexity, robustness and consistency. These algorithms are called numerical formulations. Although the development of compositional simulators is underway for more than three decades, this is still a challenging task, given the large number of partial differential equations to be solved and the large number of variables that must be determined. The main goal of this work is to investigate several numerical formulations using Cartesian and unstructured grids, with the goal of evaluating the performance of each formulation in terms of accuracy and overall computational cost for processes like miscible and immiscible gas flooding and CO<sub>2</sub> injection for isothermal compositional reservoir simulation.

The numerical formulations of reservoir models can be classified as IMPES (Implicit Pressure, Explicit Saturations), IMPSAT (Implicit Pressure and Saturations), AIM (Adaptive Implicit Method), and FI (Fully Implicit). The IMPES formulations are also called

by IMPEM (Implicit Pressure, Explicit Overall Mass/Moles) (Wong and Aziz, 1989) and IMPEC (Implicit Pressure, Explicit Compositions). The IMPES, IMPEM and IMPEC formulations share the same basis of evaluating in which only pressure is evaluated implicitly and the use of each one of these nomenclatures are used according to the variables that are computed explicitly through the other material balance equations. Since saturation is not a common term in chemical engineering field, it is important to mention that it refers to the volumetric fraction of each phase that resides into the pore volume.

## ***1.1 Literature review***

A literature review is presented in this section. First, a review of the numerical formulations for isothermal compositional simulation, then a review of the gridding techniques used in reservoir simulation is presented.

### *1.1.1 Numerical formulations*

The physical models used in petroleum reservoir simulation evolved in realism and robustness through time, but they also increased their complexity as a consequence. One of the first models used was the Buckley-Leverett model (1942). This model describes an incompressible/immiscible multiphase flow. Buckley and Leverett (1942) also presented the analytical solution for the two-phase flow of oil and water using this model. Muskat (1949) developed the three-phase Black-Oil model which was improved and modified for several applications in the oil industry being used up to date. The compositional models are relatively more recent. The development of compositional reservoir models was supported by the development of accurate Equations of State (EOS) for the phase behavior of oil and gas calculations. Although the use of EOS increased the computational cost of the models, the use of these models was encouraged by the evolution in the computers' processing power.

The early compositional models neither used fugacity nor EOS. Physical properties were evaluated through correlations. These simulators presented several convergence problems. Fussel and Fussel (1979) were the first to use an EOS to evaluate properties and phase behavior and have overcome the convergence problems of the previous simulators. Thele (1984) presents a review of the compositional models that did not use EOS.

Some of the most important methods developed are presented next. The differences between the formulations are the choices and nature of the balance equations, the

coupling with the phase equilibrium equations, and the choice of the variables to be solved with the balance equations.

Before looking at the compositional formulations it is necessary to define the concept of primary and secondary variables. The hypothesis of local equilibrium is usually accepted in the field of reservoir engineering and considers that each point of the reservoir is in a thermodynamic equilibrium related to the conditions and overall compositions at that point. This assumption makes valid the Gibbs' phase rule:

$$F_{thermo} = N + 2 - N_P, \quad (1.1)$$

where  $F_{thermo}$  is the degree of freedom,  $N_P$  is the number of phases in equilibrium, and  $N$  is the number of components present in the phases in equilibrium. The degrees of freedom are the number of independent intensive parameters that determine the all other intensive variables of the system. Water component is not usually included into flash calculations; therefore there is no mass transfer between the water phase and the other hydrocarbon phases. With these assumptions, the value of  $N$  becomes  $n_c$  and the value of  $N_P$  becomes  $n_p - 1$ , where  $n_c$  is the number of components excluding water and  $n_p$  is the number of phases existing inside the reservoir. If the model is to be considered isothermal, then one of the independent intensive parameters is fixed and one parameter less needs to be determined. Additionally, in multiphase flow in porous media, it is necessary to determine the phase saturations in order to compute the phase flow; this will include  $n_p$  more independent variables to be determined. However, one saturation can be eliminated with the saturation constraint, which is given by

$$\sum_{j=1}^{n_p} S_j = 1. \quad (1.2)$$

Applying the above assumptions, eliminating one parameter with Eq. (1.2), and substituting it in Eq. (1.1), the number of independent variables reduces to

$$F_{thermo} = n_c + 1. \quad (1.3)$$

The  $n_c + 1$  intensive parameters that must be determined are called *primary variables*, and are usually determined through the flow equations. If the extensive state of the system is desired, then another degree of freedom is included and we have to solve the system for  $n_c + 2$  primary variables. The primary variables determine all other variables in the system. The main variables used in compositional reservoir simulation are presented in Table 1.1.

Table 1.1 – Variables in compositional reservoir simulation.

Variable	Definition	Total quantity	Number eliminated	Final quantity
$P_j$	Phase pressures.	$n_p$	$n_p-1$	1
$S_j$	Phase saturations.	$n_p$	1	$n_p-1$
$x_{ij}$	Phase compositions.	$n_c(n_p-1)$	$n_p-1$	$(n_c-1)(n_p-1)$
Total:		$n_p(n_c+2)-n_c$	$2n_p-1$	$n_c(n_p-1)+1$

As shown in Table 1.1, the total number of variables to be determined are  $n_p(n_c+2)-n_c$ . All other properties and parameters involved in a isothermal reservoir simulation considering local equilibrium can be obtained using these variables. Note that quantities in Table 1.1 are taken assuming that water is present only in water phase and the water component cannot be found in any of the hydrocarbon phases. The phase pressures are related to each other through the capillary pressure relations. The capillary pressure relations allow selecting just one phase pressure as a reference and then computing the others from this reference. This eliminates  $n_p-1$  variables. One of the saturations is also dependent from the others through the saturation constraint and eliminates one more variable, as it was shown previously. Also, the phase compositions of each phase must sum up to one. It adds one more equation to determine the composition for each hydrocarbon phases, therefore  $n_p-1$  variables can be eliminated. Finally, after the elimination of all depending variables,  $n_c(n_p-1)+1$  variable still remain, as shown in Table 1.1. If the most typical situation in a reservoir is assumed, namely a three phase system (water, oil and gas), then the number of variables becomes  $2n_c+1$ . Since the  $n_c+1$  primary variables are usually determined from the flow equations, it will be necessary to compute  $n_c(n_p-2)$  more variables. These variables are called the *secondary variables*, and most models use the equilibrium relations to determine them. The equilibrium relations are the isofugacity equations. The equilibrium relations will be discussed later in chapter 2.

Most of the numerical formulations use the concepts of primary and secondary variables. The literature review of the numerical formulations will be now addressed.

Fussel and Fussel (1979) were the first ones to develop a simulator using EOS for both phase equilibrium and density calculations. This approach solved the convergence problems faced by the previous compositional approaches. The model proposed by Fussel and Fussel (1979) were tridimensional, three-phase and used the modified Redlich-Kwong EOS (Zudkevitch and Joffe, 1970). The authors did not consider the effects of physical dispersion

and capillary pressure. Additionally, the mass transfer between the hydrocarbon and the water phase was not considered. This formulation differs from all other isothermal compositional formulations since it is the only formulation that uses constraint equations (equilibrium equations and volume constraint) to solve  $n_c+1$  primary variables. This formulation is an IMPES-type and uses a Minimum Variable Newton-Raphson (MVNR) method to reduce the number of equations and variables by a Gauss elimination procedure. The primary variables are not fixed and are selected according to the predominance of oil or gas in a given grid block. The phase predominance is determined by verifying which phase has the greater number of moles per pore volume. If liquid phase prevails in a grid block, then the primary variables will be the pressure, the number of moles per pore volume of gas phase and  $n_c-1$  compositions of the gas phase  $\{P, \tilde{N}_g, x_{2g}, \dots, x_{n_{cg}}\}$ . On the other hand, if the gas phase prevails, then the set of variables will be the pressure, the number of moles per pore volume of oil phase and  $n_c-1$  compositions of the oil phase  $\{P, \tilde{N}_o, x_{2o}, \dots, x_{n_{co}}\}$ . The authors called the MVRN using the first set of variables by V-Y-P iteration and the MVRN using the second set by L-X-P iteration. All the flow equations of this formulation are based on mole balance equations.

Coats (1980) presented the first FI formulation for the isothermal compositional model. The model considered three dimensions and three phases, and the gravity and capillary pressure effects were taken into account. Furthermore, the capillary pressure and relative permeabilities are considered as functions of saturations and also of the interfacial tensions (IFT). The modified Redlich-Kwong EOS (Zudkevitch and Joffe, 1970) was used by the author for the density and phase equilibrium calculations. This model also does not consider mass transfer between the water phase and the hydrocarbon phases. The primary equations are the  $n_c$  hydrocarbon material balance equations and the water balance equation. A Newton-Raphson method is used to solve the discretized set of equations, generating a block Jacobian matrix in which each entry has  $(2n_c+1) (2n_c+1)$  size for the two hydrocarbon phases presented into the system. It is worthwhile to mention that primary and secondary variables are coupled into the Jacobian matrix. In order to decouple them, a Gauss elimination approach is used reducing each block of the Jacobian matrix to a  $(n_c+1) (n_c+1)$ . The secondary variables are then computed after solving the primary variables. The primary variables for a grid block with both oil and gas phases are the gas phase pressure, oil and gas saturations, and  $n_c-2$  compositions of the gas phase  $\{P_g, S_o, S_g, x_{3g}, \dots, x_{n_{cg}}\}$ . If the grid block has only gas

phase, the primary variables are:  $\{P_g, S_g, x_{2g}, \dots, x_{n_g}\}$ . If the grid block has only oil phase, the primary variables will be:  $\{P_o, S_o, x_{2o}, \dots, x_{n_o}\}$ . The author also mentions that for grid blocks with immobile water, the water saturation is kept constant and one more saturation is eliminated. Coats (1980) treated the phase disappearance verifying the saturation value at the end of a Newton iteration; if a saturation is less than zero, the saturation of the grid-block is set to zero for the next Newton iteration. The phase appearance was treated by calculating a saturation pressure. If the saturation pressure is less than the grid block pressure, then the grid-block is single hydrocarbon phase, otherwise the grid block is considered to have two hydrocarbon phase and the value of the saturation of the absent phase is set to 0.001. The great advantage of the Coats formulation is that most terms of the Jacobian matrix are directly calculated, since most of the primary variables are explicitly in the mole balance equations. Due to this feature, this set of primary variables is normally called the natural variables. On the other hand, the flash procedure is treated in a special way, making impossible to use general flash algorithms. In his paper, the author used the formulation to solve problems of multicontact-miscibility (MCM) problems. According to Coats (1980) these simulations are characterized by a great amount of numerical dispersion.

Nghiem et al. (1981) developed an IMPES-type formulation that differs from the previous ones by solving pressure and compositions separately. Nghiem et al. (1981) considered a three dimensional model with three phase flow. The Peng-Robinson (1976) EOS was used and the effects the IFT were included into the relative permeabilities and capillary pressures. The physical dispersion was not considered. The Nghiem et al. (1981) formulation is a modification of the Kazemi et al. (1978). Basically, the authors have modified the weighting factors of the pressure equation proposed by Kazemi et al. (1978). Wong and Aziz (1989) emphasized that this modification has the great advantage of making the Jacobian matrix strictly diagonal dominant and symmetric. A Newton-Raphson method was used to linearize this equation in terms of pressure. Observing that the pressure sometimes oscillates, Mansoori (1982) suggested the use of numerical approximation for the jacobian, what would require an extra flash calculation per iteration. Nghiem (1982) suggested the use of a damping function to avoid the oscillations.

Young and Stephenson (1983) developed a new approach based on the formulation proposed by Fussel and Fussel (1979). As in the original formulation, it is also an IMPES-type formulation. The major difference between the Fussel and Fussel (1979) and the Young and Stephenson (1983) formulations were in the selection of the primary variables and

in the ordering of the equations. In this formulation, the ordering and variables are the same whether oil or gas prevails. For single phase grid blocks, the residues of the equilibrium constraints are set to zero and only diagonal terms corresponding to these equations are equal to one. The primary variables chosen are:  $\{P, \tilde{N}_g, x_{2g}, \dots, x_{n_{cg}}\}$ . The authors used the Redlich-Kwong (1949) EOS, and the capillary pressure and gravity were not considered.

Another FI model was proposed by Chien et al. (1985). In this model the primary equations are obtained from the material balance equations for each component. The authors proposed a set of primary variables similar to that one proposed by Coats (1980), except that gas mole fractions were replaced by the equilibrium ratios (*K-values*). The authors used this formulation to solve multiple contacts miscibility problems for one, two and three dimensions.

Ács et al. (1985) proposed a new IMPES formulation that shares the primary variables of Kazemi et al. (1978) and Nghiem et al. (1981). Although the pressure equation is based on a volume balance as in the other two works, this equation is obtained in a special way. Ács et al. (1985) used a Taylor series truncated in the first order terms to expand the porous volume and the total fluid volume at the new time-step level. Then, they equate these two expansions in order to obtain an equation fully decoupled from the flash calculation. Additionally, the discretized form of this equation is already linear and thus, no Newton's iterations are required. Also, the expansion of the volumes naturally gives rise to a term called volume discrepancy. This volume discrepancy is the error between the porous volume computed through the conservation equation and the fluid volume computed after the flash calculation. This discrepancy is used to control the volume error that can arise and then allow the use of a flash calculation per time-step. The authors suggest two possible set of primary variables:  $n_c+1$  for the intensive state or  $n_c+2$  for the extensive state. The set for intensive variables are the oil pressure, the water number of moles per pore volume, and  $n_c-1$  overall compositions:  $\{P_o, \tilde{N}_w, z_1, \dots, z_{n_c-1}\}$ ; the set for the extensive state is the oil pressure and the total number of moles per pore volume of all components including water:  $\{P_o, \tilde{N}_w, \tilde{N}_1, \dots, \tilde{N}_{n_c}\}$ . It is important to mention that at least one extensive parameter is necessary to be included in the extensive parameter set. The solution of the equations is performed in a sequential way. First, the pressure is computed implicitly from the total volume balance. Then, the overall mole fractions or the total moles for each component are evaluated. If the total moles are solved, then the overall compositions are calculated with them. Finally, an

isothermal flash calculation is performed using the pressure and overall compositions to determine the compositions and amounts of each phase. The saturations are computed using the densities and the phase mole fractions. The drawback of this formulation is the total fluid derivatives needed in the pressure equation. The evaluation of these derivatives is not an easy task and were described analytically only after the development of this formulation in two different ways by Subramanian et al. (1987) and by Wong et al. (1987).

Watts (1986) combined the method of Ács et al. (1985) with the method of Spillette et al. (1973). The author combined the idea of a one iteration per time-step of Ács et al. (1985) with the sequential IMPSAT of Spillette et al. (1973), generating a new IMPSAT formulation. Watts (1986) mentions that inaccuracies can be obtained due to an inconsistency that is intrinsic of the formulation. However, he do not address this inconsistency. The Watts formulation uses the same pressure equation as does the Ács et al. formulation, but  $n_p-1$  new equations are included to solve the saturations. The saturation equations are volume balance equations obtained using the same idea as that done for pressure. It is obviously that one of these equations is not solved because one of the saturations is always set as a dependent variable through the volume constraint. As the pressure is solved using transmissibilities completely explicit, the saturations then use a special form of velocity in order to obtain the same mass transferred after the calculation of the new saturations. This semi-implicit velocity is used to evaluate the total moles of the  $n_c+1$  components and water. Thus, a total of  $n_c+n_p+1$  is solved as primary variables. After this process the flash is performed and all other variables at the new time-step level are calculated. Watts (1986) considered only the advective terms into his formulation and has shown the model for both compositional and black-oil models. Although the author do not present any result he mention that this formulation was implemented and tested in the simulator presented by Kendall et al. (1983).

Quandalle and Savary (1989) worked in the formulation proposed by Watts (1986) with the goal of identifying and solving the inconsistency issue of it. The authors pointed out the first inconsistency as the own semi-implicit nature of the solution. This inconsistency is the use of explicit transmissibilities for evaluating the pressure and then changing these transmissibilities during the calculation of the saturations. However, this inconsistency is not the critical one. The second inconsistency is mentioned by the authors to be the  $n_c+2$  using only  $n_c+1$  flow equations (material balance). The authors also mention that the problem for this is that the PVT packages usually considers the saturations of the hydrocarbon phases as secondary variables resulting from the phase equilibrium calculation, while they are very important in the implicit treatment to compute the relative permeability



and capillary pressure. To overcome this limitation, the authors included the solution of  $n_c-2$  new variables into the material balance equations. The new variables can be compositions of the oil or gas phase and are related to the relative quantity of each phase.

Collins et al. (1992) presented an adaptive implicit approach (AIM) for isothermal compositional formulation. The equations of this formulation are the  $n_c+1$  material balances and the volume constraint. The primary variables are the total number of moles per bulk volume of the  $n_c$  components and water.

Branco and Rodriguez (1996) proposed a new IMPSAT formulation based on the formulation of Coats (1980). The authors neglect some terms of the coupled Jacobian matrix and freeze the compositions for each iteration, solving each iteration only for pressure and saturations. After solving the pressure and saturations the compositions of the phases are updated and a new iteration is performed until convergence is achieved. The primary variables are the same of the Coats (1980) formulation. The authors validate their model with the steady-state solution provided by Chopra and Carter (1986) that considers that in some point of the reservoir the oil-gas mobility ratio is equal to the oil-gas mole ratio of the original fluid in place at the pressure and temperature of that point.

Wang et al. (1997) proposed a new FI formulation. In this formulation the flow equations and the equilibrium constraints are all assembled into the Jacobian matrix; the size of each entry of the Jacobian matrix is equal to  $(n_c(n_p-1)+1)(n_c(n_p-1)+1)$ . The variables solved in this formulation are:  $\{P, \tilde{N}_w, \tilde{N}_1, \dots, \tilde{N}_{n_c}, \ln(K_1), \dots, \ln(K_{n_c})\}$ .

Haukas et al. (2004) improved the approach of Quandalle and Savary (1990) by changing the primary variables. In Haukas et al. (2005) a better interpretation of these parameters is given. The authors called the new parameters by isochoric parameters. A stability criterion it was also given in Haukas et al. (2005).

Santos (2013) implemented and compared several formulations. It includes the FI and IMPSAT formulations of Coats (1980), Collins et al. (1990), Branco and Rodriguez (1996), and Wang et al. (1997) formulations and a new IMPES formulation. He pointed out that for cases investigated the Coats formulation was generally better in performance than the other formulations. The new IMPES formulation was based on the ideas of Branco and Rodriguez to reduce the equations to an equation for pressure only.

As suggested by Cao (2002), most of the formulations presented were classified according to the nature of the pressure equation into two categories: material balance and

volume balance formulations. Table 1.2 summarizes the primary variables and some concepts of the formulations presented here.

Table 1.2 – General concepts of the formulations for compositional reservoir simulation.

<b>Formulation</b>	<b>Implicitness degree</b>	<b>Classification</b>	<b>Primary variables</b>
Fussel and Fussel (1979)	IMPES	None	$\{P, \tilde{N}_g, x_{2g}, \dots, x_{n_{cg}}\}$ or $\{P, \tilde{N}_o, x_{2o}, \dots, x_{n_{co}}\}$
Coats (1980)	FI	Material balance	$\{P_g, S_o, S_g, x_{3g}, \dots, x_{n_{cg}}\}$
Nghiem et al. (1981)	IMPES	Volume balance	$\{P, \tilde{N}_w, \tilde{F}_T, z_1, \dots, z_{n_c}\}$ or $\{P, S_w, \tilde{F}_T, z_1, \dots, z_{n_c}\}$
Young and Stephenson (1983)	IMPES	None	$\{P, \tilde{N}_g, x_{2g}, \dots, x_{n_{cg}}\}$
Chien et al. (1985)	FI	None	$\{P, \tilde{N}_w, z_1, \dots, z_{n_c-1}\}$ or $\{P, \tilde{F}_T, z_1, \dots, z_{n_c-1}\}$
Ács et al. (1985)	IMPEC	Volume balance	$\{P_o, \tilde{N}_w, z_1, \dots, z_{n_c-1}\}$ or $\{P_o, \tilde{N}_w, \tilde{N}_1, \dots, \tilde{N}_{n_c}\}$
Watts (1986)	IMPSAT	Volume balance	$\{P_o, S_w, S_g, N_w, N_1, \dots, N_{n_c}\}$
Quandalle and Savary (1989)	IMPSAT	Volume balance	$\{P, S_w, S_g, x_{2o}, \dots, x_{n_c-1o}\}$ or $\{P, S_w, S_g, x_{2g}, \dots, x_{n_c-1g}\}$
Collins et al. (1992)	AIM (FI and/or IMPEC)	Volume balance	$\{P_o, N_w, N_1, \dots, N_{n_c}\}$
Branco and Rodriguez (1996)	IMPSAT	Material balance	$\{P_o, S_w, S_g, x_{1o}, \dots, x_{n_c-2o}\}$
Wang et al. (1997)	FI	Material balance	$\{P, \tilde{N}_w, \tilde{N}_1, \dots, \tilde{N}_{n_c}, \ln(K_1), \dots, \ln(K_{n_c})\}$
Haukas et al. (2004)	IMPSAT	Volume balance	$\{P, S_w, S_g, \kappa_1, \dots, \kappa_{n_c-n_p}\}$

Wong and Aziz (1989) present a detailed review of most of the formulations addressed in this text.

The next subsection will provide a literature survey of another important topic in reservoir simulation: the gridding techniques. This is an important topic for this work because the formulations will be tested here for Cartesian and Unstructured grids.

### *1.1.2 Gridding techniques*

The gridding techniques are the methods of spatial discretization and mapping. This subsection intends to show the development of these methods in compositional reservoir simulation focusing on the use of unstructured grids.

Most of the formulations presented previously were based on Cartesian grids in conjunction with the Finite Volume Method (FVM). However, all the formulations can be implemented for any spatial discretization since their derivations are relatively independent of the grid. However, as Cartesian grid is the simplest way to discretize the domain, the complexity of the implementation of a given formulation for other type of grid will increase sharply.

One of the most famous discretization used in reservoir simulation is the boundary fitted (BF) grids, commonly called corner point (CP) grids in the reservoir literature. Although the BF grids have the capability of computing the non-orthogonal portion of the flux, most simulators neglect it for the sake of computational cost. The use of BF grids is really old in reservoir simulation (Sheldon and Dougherty, 1961; Hirasaki and O'Dell, 1970; Wadsley, 1980). However the concept of non-orthogonal BF (NOBF) grids was presented by Chu (1971), but became famous only after Thompson et al. (1974). The great advantage of the NOBF is the possibility of distorting the grid without great losses in the physical quality of the results. Leventhal et al. (1985) chose grids with grid lines tangent to the streamlines of a single flow solution, what makes the mixed derivatives negligible. Cunha et al. (1994) solved the two-phase flow (water and oil) problem using NOBF for 2D reservoirs; they verified a great reduction in the grid orientation effects. Maliska et al. (1994) presented an extension of the work of Cunha et al. (1994) for three dimensions. Later, Maliska et al. (1997) presented their three dimensional NOBF for the three-phase flow in conjunction with the black-oil model using mass fractions and pressure as independent variables. Edwards (1998) used the two dimensional NOBF grid in conjunction with a two-phase flow and IMPES approach with a full permeability tensor and a high order scheme. Edwards (1998) also compared the results

of 9 point stencil (NOBF) with 5 point stencil (Cartesian grid); from this comparison, it was possible to see that the NOBF is able to reduce the grid orientation effect and increase the numerical accuracy. Coutinho (2002) implemented a NOBF using 2D grids for a fully implicit two-phase black-oil model using a mass fraction formulation that was later extended by Araújo (2005) for 3D reservoirs. Sarmiento (2009) continued the work of Araújo by extending the model for three-phase flow. Marcondes et al. (2005) implemented the NOBF method in a FI, isothermal, compositional reservoir simulator called GPAS (General Purpose Adaptive Simulator) from the University of Texas at Austin. Marcondes et al. (2008) compared the effect of the cross derivatives; they figured out that the neglect of these terms have a great impact in compositional reservoir simulation since a portion of the flux is not being considered.

The unstructured grids are more general in terms of modelling important features of the reservoirs. The unstructured grids are usually related to the concept of elements. However, during many years this concept was used only by the Finite Element Method (FEM) until the work of Baliga and Patankar (1980); they combined the conservative approach of the FVM with the idea of elements and shape functions of the FEM creating a new method that they named Control Volume Finite Element Method (CVFEM). Later, Maliska (2004) suggested that the CVFEM denomination is unsuitable, since the CVFEM gives a wrong idea that we have a finite element approach that is based on material balance. Maliska (2004) suggested calling this approach as Element based Finite-Volume Method (EbFVM). We strongly feel that such denomination is much more adequate, since the approach presented by Baliga and Patankar (1980) borrows from finite element only the idea of elements and shape functions, but still performs a material balance in order to obtain the approximate equations. For this reason, in the rest of this text, we will always refer to this approach as EbFVM.

The first use of unstructured grids in reservoir simulation was done by Heinemann and Brand (1988) and Heinemann et al. (1991) with the use of PEBI grids (Perpendicular Bisector). These grids are also called Voronoi grids. Although the PEBI grids are cell-vertex as the EbFVM method, the nature of the discretization is different. PEBI grids are tessellated in a way that the control volume interfaces are always perpendicular to the line joining the two control volumes centers. By doing this the fluxes can be approximated using just two points. The first use of EbFVM in reservoir simulation was performed by Rozon (1989) that used it to solve a single-phase flow using quadrilateral elements. Rozon (1989) also presented a comparison of the truncation errors between the EbFVM and the Cartesian grids, showing

that for regular grids composed of quadrilateral elements the EbFVM method is more accurate. Fung et al. (1992) used PEBI grids based on triangular element in a thermal general purpose simulator. Cordazzo (2006) solved the two-phase flow (water and oil) in conjunction with the EbFVM using triangular and quadrilateral elements. Nogueira (2011) implemented the EbFVM for 2D reservoirs using a black-oil model based on the mass fractions formulation in conjunction with a fully implicit approach. Marcondes and Sepehrnoori (2010) used the EbFVM for the solution of an isothermal composition formulation using a FI approach in conjunction with triangular and quadrilateral elements. Recently, Marcondes et al. (2013) implemented the EbFVM for 3D reservoirs, and isothermal compositional simulation using four element types: hexahedron, tetrahedron, pyramid, and prism.

Also, using the EbFVM approach, Fernandes et al. (2013) has investigated the use of several interpolation functions in conjunction with compositional reservoir simulation. They adapted the Darwish and Moukaled (2003) approach, for evaluating the successive slope ratio for using in TVD (Total Variation Diminishing), originally proposed for cell-centered, for the EbFVM approach. In addition to TVD scheme, they also investigated the original Mass Weighted Upwind scheme (MAW) (Masson et al., 1994; Saabas and Baliga, 1994a; Saabas and Baliga, 1994b) and modified version of MAW (Hurtado et al., 2007), a stream-Line based Upwind scheme (SUCV) (Swaminathan and Voller, 1992a; Swaminathan and Voller, 1992b), and the TVD scheme using two flux limiters: MINMOD (Roe, 1986) and Koren (Koren, 1993).

## ***1.2 Layout of this work***

In this study, five new formulations were implemented into the UTCOMP simulator for both Cartesian and unstructured grids in conjunction with the EbFVM. The following formulations were implemented: three IMPSAT and two FI formulations. The three IMPSAT formulations are all based on the Watts (1986) formulation where one of them is the original Watts' formulation and the other two formulations are suggested in this work. We implemented the FI formulation of Collins et al (1992) and extended the original IMPEC formulation of Ács et al. (1985) in a FI framework. To the best of our knowledge, this is the first time that the Ács et al. (1985) formulation has been implemented in a FI framework. We also like to stress that this is the first time that these IMPSAT formulations and the Ács et al. (1985) formulation in a FI framework have been implemented in conjunction with the EbFVM.

In chapter 2 we will present the mathematical model for the isothermal compositional approach, as well as the physical properties such as models used for compute viscosity and relative permeability used in this study, and the phase behavior calculation.

Chapter 3 will present the approximate equations for both Cartesian and EbFVM.

Chapter 4 will show the algorithm and implicitness level of all formulations implemented and tested in this study.

In chapter 5, all results will be shown and discussed.

Finally, chapter 6 comes up with the main conclusions and final remarks of this work, as well as the possible future study.

## 2 MATHEMATICAL MODEL

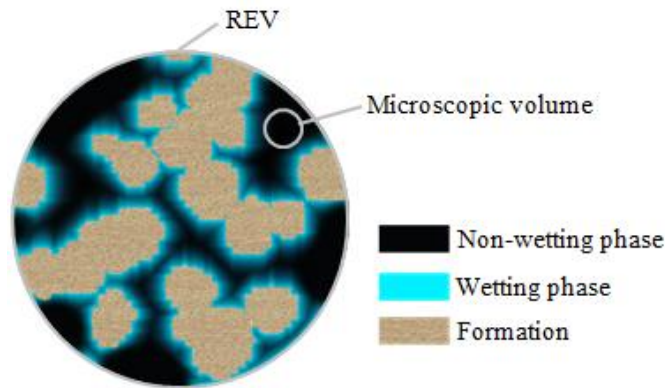
The mathematical model used in reservoir simulation involves transport equations to describe the fluid flow, correlations to describe fluid properties, and thermodynamic equations to describe equilibrium relations. All the implementations of this thesis will be performed into UTCOMP simulator, as mentioned in the introduction. The UTCOMP simulator is an isothermal EOS based compositional reservoir simulator. In this work, the models will consider up to four phases that can be classified as water, oil, gas and a second liquid hydrocarbon phase which, in general, is basically composed of CO<sub>2</sub>. The mass transfer between the water phase and the hydrocarbon phases is not considered. All the implementations will be performed considering both two and three dimensions with the gravity and capillary pressure terms, but the physical dispersion is not taken into account. Additionally, the local equilibrium between hydrocarbon phases is considered.

This section will be divided into three subsections: transport equations, thermodynamic relations, and fluid properties.

### *2.1 Transport equations*

The petroleum reservoirs are complex pore media with a multicomponent/multiphase system. In a microscopic point of view, each phase is separated by an interface. The properties of a given phase are only continuous until the interface, where a great discontinuity between physical properties arises. It is worthwhile to mention that the phase interfaces are also very complex and hard to predict. The properties discontinuity, the complexity of the pore media and interfaces, and the very small pore size scale would make the simulation of this problem almost impossible. In order to avoid such difficulties, a continuum model is used. The continuum model is employed in order to reduce the properties discontinuity and simplify such issues as the complexity of the pore media and the phase interfaces. In order to obtain the continuum model equations, the microscopic equations and properties are averaged into a Representative Elementary Volume (REV). The REV is chosen such that a bit of each phase is presented in it. Figure 2.1 illustrates the REV. The development of the continuum model from the microscopic equations is really complex and will not be treated here. A brief review about this topic is presented by Wong and Aziz (1988).

Figure 2.1 – Illustration of the REV.



As in compositional reservoir simulation several pseudo-components describe the fluid, some amount of each component will compose each phase. The mole balance equation for the  $k$ -th component is given as

$$\frac{1}{V_b} \frac{\partial N_k}{\partial t} = - \sum_{j=1}^{n_p} \bar{\nabla} \cdot (x_{kj} \xi_j \bar{U}_j) - \sum_{j=1}^{n_p} \bar{\nabla} \cdot (\phi S_j \bar{J}_{kj}) - \dot{q}_k, \quad k = 1, \dots, n_c, n_c + 1, \quad (2.1)$$

where  $N_k$  is the total moles of component  $k$ ,  $V_b$  is the bulk volume,  $x_{kj}$  is the molar fraction of component  $k$  in phase  $j$ ,  $\xi_j$  is the mole density of phase  $j$ ,  $\bar{U}_j$  is the velocity vector of phase  $j$ ,  $\phi$  is the porosity,  $S_j$  is the saturation of phase  $j$ ,  $\bar{J}_{kj}$  is the dispersion mole flux of component  $k$  in phase  $j$ , and  $\dot{q}_k$  is the source/sink term of component  $k$ .

Due to the complexity of the implementations in this work, the physical dispersion will not be considered here. The velocity vector in Eq. (2.1) is approximated through the modification of Darcy's law for multiphase flow. According to Wong and Aziz (1988), the Darcy's flux is the result of the averaging of the advective terms into a REV. The velocity is then written as

$$\bar{U}_j = - \frac{1}{\mu_j} \bar{\bar{K}}_j \cdot \bar{\nabla} \Phi_j \quad j = 1, \dots, n_p, \quad (2.2)$$

where  $\bar{\bar{K}}_j$  is the effective permeability tensor of phase  $j$ ,  $\mu_j$  is the viscosity of phase  $j$ , and  $\Phi_j$  is the hydraulic potential of phase  $j$  defined as

$$\Phi_j = P_j - \rho_j g D \quad j = 1, \dots, n_p, \quad (2.3)$$

where  $P_j$  is the pressure of phase  $j$ ,  $g$  is the gravity acceleration,  $D$  is the depth which is positive in the downward direction, and  $\rho_j$  is the mass density of phase  $j$ .



The effective permeability tensor shown in Eq. (2.2) is usually written in terms of the absolute rock permeability as

$$\bar{\bar{K}}_j = k_{rj} \bar{\bar{K}} \quad j = 1, \dots, n_p, \quad (2.4)$$

where  $\bar{\bar{K}}$  is the rock absolute permeability tensor and  $k_{rj}$  is the relative permeability of phase  $j$ .

The phase pressures used in Eq. (2.3) are related to a reference phase through the capillary pressure relations. In this work, the oil phase is the reference phase; the pressure for the other phases are evaluated through the capillary pressure relations by

$$P_j = P_r + P_{cjr} \quad j = 1, \dots, n_p, \quad (2.5)$$

where  $P_r$  is the reference pressure, that will be referred from now on just by  $P$ , and  $P_{cjr}$  is the capillary pressure of the phase  $j$  related to the reference phase, which is zero when  $j$  is equal to  $r$ . It is worth to mention, that in this text, the phase subscripts  $l$  or  $w$  will refer to water phase, 2 or  $o$  will refer to oil phase, 3 or  $g$  will refer to gas phase, and 4 or  $l$  will refer to a second liquid hydrocarbon phase.

In this work, the water is not included into any phase equilibrium calculation, and therefore no mass transfer is considered between the water and the hydrocarbon phases. As a result, the mole balance equations (Eq. 2.1) can be written for any hydrocarbon components as

$$\frac{1}{V_b} \frac{\partial N_k}{\partial t} = \sum_{j=2}^{n_p} \bar{\nabla} \cdot \left( x_{kj} \xi_j \frac{k_{rj}}{\mu_j} \bar{\bar{K}} \cdot \bar{\nabla} \Phi_j \right) - \frac{\dot{q}_k}{V_b}, \quad k = 1, \dots, n_c, \quad (2.6)$$

and for water

$$\frac{1}{V_b} \frac{\partial N_w}{\partial t} = \bar{\nabla} \cdot \left( \xi_w \frac{k_{rw}}{\mu_w} \bar{\bar{K}} \cdot \bar{\nabla} \Phi_w \right) - \frac{\dot{q}_w}{V_b}, \quad (2.7)$$

where the subscript  $w$  denotes the water component or phase.

The molar phase compositions of each hydrocarbon phase must sum up to one which is given by,

$$\sum_{k=1}^{n_c} x_{kj} = 1, \quad j = 1, \dots, n_p. \quad (2.8)$$

The same goes for the overall compositions,

$$\sum_{k=1}^{n_c} z_k = 1. \quad (2.9)$$

A saturation constraint is also considered as given by Eq. (1.2). Equation (1.2) is rewritten bellow as:

$$\sum_{j=1}^{n_p} S_j = 1. \quad (2.10)$$

The saturation constraint can be interpreted as one way to express the volume constraint. The volume constraint in porous media means that the amount of fluid ( $V_T$ ) must occupy the pore volume ( $V_p$ ), which is expressed by

$$dV_p = dV_T. \quad (2.11)$$

As the total fluid volume for an isothermal system is function only of pressure and of the total number of moles of each component, the total volume derivative gives

$$dV_T = \left( \frac{\partial V_T}{\partial P} \right)_N dP + \sum_{k=1}^{n_c+1} \left( \frac{\partial V_T}{\partial N_k} \right)_{P, N_i(i \neq k)} dN_k. \quad (2.12)$$

The first derivative in Eq. (2.12) is the total fluid's compressibility and the second derivative the total fluid's partial molar volume and will be written here as

$$\left( \frac{\partial V_T}{\partial N_k} \right)_{P, N_i(i \neq k)} = \bar{V}_{Tk}, \quad (2.13)$$

for simplicity. The subscript into the total fluid compressibility will also be omitted here for simplicity.

On the other hand, the pore volume is considered to be function of only pressure. Therefore, the total derivative of pore volume can be written as

$$dV_p = \frac{\partial V_p}{\partial P} dP, \quad (2.14)$$

where the pore volume is defined as

$$V_p = \phi V_b, \quad (2.15)$$

where  $V_b$  is the bulk volume and the porosity ( $\phi$ ) is computed as

$$\phi = \phi^0 \left[ 1 + C_f (P - P_f) \right], \quad (2.16)$$

where  $\phi^0$  is the rock porosity evaluated at a reference pressure  $P_f$ , and  $C_f$  is the rock compressibility. After substituting Eq. (2.15) into Eq. (2.14) and deriving Eq. (2.16) respect to pressure, we obtain:

$$dV_p = V_b \phi^0 C_f dP. \quad (2.17)$$

Substituting Eqs. (2.12) and (2.17) into Eq. (2.11) and deriving with respect to time, dividing by the bulk volume and manipulating yields

$$\left( \phi^0 C_f - \frac{1}{V_b} \frac{\partial V_T}{\partial P} \right) \frac{\partial P}{\partial t} = \frac{1}{V_b} \sum_{k=1}^{n_c+1} \bar{V}_{Tk} \frac{\partial N_k}{\partial t}. \quad (2.18)$$

Substituting the molar rates from Eq. (2.6) into Eq. (2.18), the final form of the pressure equation is obtained.

$$\begin{aligned} \left( \phi^0 C_f - \frac{1}{V_b} \frac{\partial V_T}{\partial P} \right) \frac{\partial P}{\partial t} = & \bar{V}_{Tw} \bar{\nabla} \cdot \left( \xi_w \frac{k_{rw}}{\mu_w} \bar{\bar{K}} \cdot \bar{\nabla} \Phi_w \right) \\ & + \sum_{k=1}^{n_c} \bar{V}_{Tk} \sum_{j=2}^{n_p} \bar{\nabla} \cdot \left( x_{kj} \xi_j \frac{k_{rj}}{\mu_j} \bar{\bar{K}} \cdot \bar{\nabla} \Phi_j \right) - \sum_{k=1}^{n_c+1} \bar{V}_{Tk} \frac{\dot{q}_k}{V_b}. \end{aligned} \quad (2.19)$$

The saturation equation used by the Watts formulation is obtained using a similar procedure. The simple volume balance of a phase  $\ell$  is given as

$$d(S_\ell V_p) = dV_\ell. \quad (2.20)$$

Deriving Eq. (2.20) with respect to time, we obtain

$$V_p \frac{\partial S_\ell}{\partial t} + S_\ell \frac{\partial V_p}{\partial t} = \frac{\partial V_\ell}{\partial t}. \quad (2.21)$$

Applying Eq. (2.15) into Eq. (2.21)

$$\phi V_b \frac{\partial S_\ell}{\partial t} + S_\ell V_b \frac{\partial \phi}{\partial t} = \frac{\partial V_\ell}{\partial t}. \quad (2.22)$$

The total derivative of the phase volume can be written as

$$dV_\ell = \left( \frac{\partial V_\ell}{\partial P} \right)_N dP + \sum_{k=1}^{n_c+1} \left( \frac{\partial V_\ell}{\partial N_k} \right)_{P, N_i (i \neq k)} dN_k. \quad (2.23)$$

Deriving Eq. (2.23) with respect to time and substituting the result into Eq. (2.22), using a definition similar to that of Eq. (2.13) for the partial molar volume of phase  $\ell$ , omitting the subscript of the phase volume compressibility yields

$$\phi V_b \frac{\partial S_\ell}{\partial t} + S_\ell V_b \frac{\partial \phi}{\partial t} = \frac{\partial V_\ell}{\partial P} \frac{\partial P}{\partial t} + \sum_{k=1}^{n_c+1} \bar{V}_{\ell k} \frac{\partial N_k}{\partial t}. \quad (2.24)$$

Applying the chain rule for the porosity derivative and substituting Eq. (2.16) results in

$$\phi V_b \frac{\partial S_\ell}{\partial t} + \left[ S_\ell V_b \phi^0 C_f - \frac{\partial V_\ell}{\partial P} \right] \frac{\partial P}{\partial t} = \sum_{k=1}^{n_c+1} \bar{V}_{\ell k} \frac{\partial N_k}{\partial t}. \quad (2.25)$$

The Watts (1986) formulation uses a special treatment for the saturation equations. Therefore, we will develop the saturation equation in a way this treatment become clear. For this procedure, the molar rates used must have the phase velocities visible. Therefore, the molar rates in Eq. (2.25) are substituted using Eq. (2.1), neglecting the physical dispersion terms, and dividing the resulting equation by the bulk volume yields:

$$\phi \frac{\partial S_\ell}{\partial t} + \left[ S_\ell \phi^0 C_f - \frac{1}{V_b} \frac{\partial V_\ell}{\partial P} \right] \frac{\partial P}{\partial t} = -\bar{V}_{\ell w} \bar{\nabla} \cdot (\xi_w \vec{U}_w) - \sum_{k=1}^{n_c} \bar{V}_{\ell k} \sum_{j=2}^{n_p} \bar{\nabla} \cdot (x_{kj} \xi_j \vec{U}_j) - \sum_{k=1}^{n_c+1} \bar{V}_{\ell k} \frac{\dot{q}_k}{V_b}. \quad (2.26)$$

The phase velocities can be expressed in terms of the total fluid velocity. The total fluid velocity is given by

$$\vec{U}_T = \sum_{m=1}^{n_p} \vec{U}_m. \quad (2.27)$$

The velocity of phase  $j$  can be rewritten using the concept of phase mobility (relative permeability divided by viscosity) as

$$\vec{U}_j = -\lambda_j \bar{\bar{K}} \cdot (\bar{\nabla} P + \bar{\nabla} P_{cjr} - \rho_j g \bar{\nabla} D) \quad j = 1, \dots, n_p. \quad (2.28)$$

Applying Eq. (2.28) into Eq. (2.27) gives

$$\vec{U}_T = -\bar{\bar{K}} \cdot \bar{\nabla} P \sum_{m=1}^{n_p} \lambda_m - \sum_{m=1}^{n_p} \lambda_m \bar{\bar{K}} \cdot \bar{\nabla} P_{cmr} + \sum_{m=1}^{n_p} \lambda_m \bar{\bar{K}} \cdot (\rho_m g \bar{\nabla} D), \quad (2.29)$$

where the first term in the right-hand side of Eq. (2.29) can be obtained from Eq. (2.28) as

$$\bar{\bar{K}} \cdot \bar{\nabla} P = -\frac{\vec{U}_j}{\lambda_j} - \bar{\bar{K}} \cdot (\bar{\nabla} P_{cjr} - \rho_j g \bar{\nabla} D) \quad j = 1, \dots, n_p. \quad (2.30)$$

Performing some algebraic manipulations in Eq. (2.29), we obtain the first term of Eq. (2.30) in terms of total velocity as

$$\bar{\mathbf{K}} \cdot \bar{\nabla} P = - \frac{1}{\sum_{m=1}^{n_p} \lambda_m} \left[ \bar{\mathbf{U}}_T + \sum_{m=1}^{n_p} \lambda_m \bar{\mathbf{K}} \cdot \bar{\nabla} P_{cmr} - \sum_{m=1}^{n_p} \lambda_m \bar{\mathbf{K}} \cdot (\rho_m \mathbf{g} \bar{\nabla} D) \right]. \quad (2.31)$$

Equating (2.30) and (2.31), we obtain the following equation to phase velocity in terms of total velocity as

$$\bar{\mathbf{U}}_j = f_{rj} \left[ \bar{\mathbf{U}}_T + \sum_{m=1}^{n_p} \lambda_m \bar{\mathbf{K}} \cdot (\bar{\nabla} P_{cmr} - \bar{\nabla} P_{cjr}) - \sum_{m=1}^{n_p} \lambda_m (\rho_m - \rho_j) \mathbf{g} \bar{\mathbf{K}} \cdot \bar{\nabla} D \right], \quad (2.32)$$

where  $f_{rj}$  is the fractionary flow of the  $j$ -th phase which is defined as

$$f_{rj} = \frac{\lambda_j}{\sum_{m=1}^{n_p} \lambda_m}. \quad (2.33)$$

Finally, the reservoir simulator usually considers thermodynamic equilibrium between the hydrocarbon phases. At the equilibrium condition the Gibbs free energy is minimum. The Gibbs free energy for a multiphase system is written as

$$G^T = \sum_{j=2}^{n_p} \sum_{i=1}^{n_c} n_{ij} \bar{\mu}_{ij}, \quad (2.34)$$

where  $n_{ij}$  is the moles of component  $i$  in phase  $j$  and  $\bar{\mu}_{ij}$  is the chemical potential of component  $i$  in phase  $j$  defined as

$$\bar{\mu}_{ij} = \bar{\mu}_{ij}^0 + RT \ln \frac{f_{ij}}{f_{ij}^0}, \quad i = 1, \dots, n_c, \quad j = 2, \dots, n_p, \quad (2.35)$$

where  $\bar{\mu}_{ij}^0$  and  $f_{ij}^0$  are the chemical potential and fugacity at a reference state, respectively.

Considering that the reference state is such that the chemical potential is zero when the fugacity is the unity, the chemical potential expression is simplified to

$$\bar{\mu}_{ij} = RT \ln f_{ij}, \quad i = 1, \dots, n_c, \quad j = 2, \dots, n_p, \quad (2.36)$$

where  $f_{ij}$  is the fugacity of component  $i$  in phase  $j$ .

Thus the minimization of the Gibbs free energy is obtained when

$$\frac{\partial}{\partial n_{ij}} \left( \frac{G^T}{RT} \right) = \ln f_{ij} - \ln f_{ir} = 0, \quad i = 1, \dots, n_c, \quad j = 2, \dots, n_p (j \neq r), \quad (2.37)$$

where  $r$  is a reference phase, defined in UTCOMP as the oil phase. Notice that choosing any phase as dependent will yield the same result.

Since the transport equations are determined, it is important to present the phase behavior procedures used into UTCOMP simulator, since these will determine the number of phases and the equilibrium phase compositions needed for the transport equations.

## 2.2 Phase behavior

The UTCOMP simulator has three EOS implemented. However, all the case studies in this work will be tested considering only the Peng and Robinson (1976) EOS (PREOS) which was originally implemented in the UTCOMP by Perschke (1988):

$$P = \frac{RT}{v-b} - \frac{a}{v(v+b)+b(v-b)}, \quad (2.38)$$

where  $a$  and  $b$  are the PREOS parameters defined for a pure substance as

$$a = \Omega_a \frac{\alpha (RT_c)^2}{P_c}, \quad (2.39)$$

and

$$b = \Omega_b \frac{RT_c}{P_c}, \quad (2.40)$$

where

$$\Omega_a = 0.45724, \quad (2.41)$$

$$\Omega_b = 0.0778, \quad (2.42)$$

and

$$\alpha = \left[ 1 + m \left( 1 - \left( \frac{T}{T_c} \right)^{0.5} \right) \right]^2, \quad (2.43)$$

with the parameter  $m$  is evaluated as suggested by Peng and Robinson (1978):

$$m = \begin{cases} 0.37464 + 1.54226\omega - 0.26992\omega^2 & \text{if } \omega \leq 0.49 \\ 0.379642 + 1.48503\omega - 0.164423\omega^2 + 0.016666\omega^3 & \text{if } \omega > 0.49 \end{cases}, \quad (2.44)$$

The PREOS is written in function of the compressibility factor  $Z$  as

$$Z^3 - (1 - B)Z^2 + (A - 3B^2 - 2B)Z - (AB - B^2 - B^3) = 0, \quad (2.45)$$

where

$$A = \frac{aP}{(RT)^2}, \quad (2.46)$$

and

$$B = \frac{bP}{RT}. \quad (2.47)$$

For a multiphase, multicomponent system, Eqs. (2.38) and (2.45) become

$$P = \frac{RT}{v_j - b_j} - \frac{a_j}{v_j(v_j + b_j) + b_j(v_j - b_j)}, \quad j = 2, \dots, n_p, \quad (2.48)$$

and

$$Z_j^3 - (1 - B_j)Z_j^2 + (A_j - 3B_j^2 - 2B_j)Z_j - (A_j B_j - B_j^2 - B_j^3) = 0, \quad j = 2, \dots, n_p, \quad (2.49)$$

where  $a_j$  and  $b_j$  are the PREOS parameters for a phase  $j$  and are obtained using the mixing rules as follows

$$a_j = \sum_{i=1}^{n_c} \sum_{k=1}^{n_c} x_{ij} x_{kj} a_{ik}, \quad j = 2, \dots, n_p, \quad (2.50)$$

where

$$a_{ik} = (1 - \kappa_{ik})(a_i a_k)^{0.5}, \quad j = 2, \dots, n_p, \quad (2.51)$$

and

$$b_j = \sum_{i=1}^{n_c} x_{ij} b_i, \quad j = 2, \dots, n_p, \quad (2.52)$$

where  $a_i$  and  $b_i$  are the PREOS parameters for a component  $i$  obtained from Eqs. (2.39) and (2.40), respectively; and  $\kappa_{ik}$  is the binary interaction coefficient. The parameters  $A_j$  and  $B_j$  are computed following Eqs. (2.46) and (2.47), but considering the PREOS parameters defined as in Eqs. (2.50) and (2.52), respectively.

Obviously, the solution of Eq. (2.49) can provide up to three real roots. If more than one real root is obtained, the real root that provides the lower Gibbs free energy is chosen for that phase, as mentioned by Perchke (1988). Additionally, the pressure considered in all the above calculations is the oil pressure.

The fugacity coefficient for the PREOS is computed as

$$\ln \phi_{ij} = \frac{b_i}{b_j} (Z_j - 1) - \ln (Z_j - B_j) - \frac{A_j}{2\sqrt{2}B_j} \left( 2 \sum_{k=1}^{n_c} \frac{x_{kj} a_{ik}}{a_j} - \frac{b_i}{b_j} \right) \ln \left( \frac{Z_j + (1 + \sqrt{2})B_j}{Z_j + (1 - \sqrt{2})B_j} \right), \quad i = 1, \dots, n_c, \quad j = 2, \dots, n_p. \quad (2.53)$$

The phase mole densities are computed as follows:

$$\xi_j = \frac{P}{Z_j RT}, \quad j = 2, \dots, n_p. \quad (2.54)$$

A volume-shift approach based on the work of Jhaveri and Youngren (1988) is also available for liquid density correction.

The phase appearance and disappearance is treated using stability test calculations. Another way to treat the phase disappearance is considered when using the Watts (1986) formulation, but this approach will be discussed only in the next chapter. Two phase stability test algorithms are implemented in UTCOMP simulator: the stationary point location method (Michelsen, 1982) and the Gibbs free energy minimization algorithm that is similar to the Trangenstein (1987) method and was modified by Perschke (1988) to deal with the equilibrium of three hydrocarbon phases. In general, as commented by Perschke (1988) the stationary method is faster than Gibbs free energy minimization method.

After the phase stability, a procedure to solve the mole fractions and amount of each hydrocarbon phase using the fugacity constraint equations is performed. This calculation is usually named flash calculation. The flash calculation used in UTCOMP is a combination of the Accelerated Successive Substitution (ACSS) method (Mehra et al., 1983) with the modified version of the Gibbs free energy minimization method (Perschke, 1988). At the beginning of the flash procedure, we use the ACSS method in order to provide a reasonable initial estimation, and then we switch to the Gibbs free energy minimization method in order to accelerate the convergence. The switching criteria to change from one method to another is given by Chang (1990) as

$$\max |\ln f_{ij} - \ln f_{ir}| \leq \varepsilon_{swi}, \quad i = 1, \dots, n_c, \quad j = 2, \dots, n_p (j \neq r) \quad (2.55)$$

where  $r$  is a reference phase, generally assumed as oil. The switching criteria ( $\varepsilon_{swi}$ ) suggested by Chang (1990) is equal to 0.01.



### 2.3 Physical properties

After the flash calculation, it is possible to evaluate the physical properties. Some properties depend on the EOS and others depend on correlations. We now describe the equations used to compute the densities, saturations, relative permeabilities, capillary pressures, viscosities and the volume derivatives.

The hydrocarbon mole densities are evaluated by Eq. (2.54), while the water mole density is assumed to be slightly compressible and given by

$$\xi_w = \xi_w^0 [1 + C_w (P - P_w)], \quad (2.56)$$

where  $\xi_1^0$  is a reference molar density evaluated at a  $P_w$  pressure and  $C_w$  is the water compressibility. The mass density of water is evaluated as

$$\rho_w = MW_w \xi_w, \quad (2.57)$$

where  $MW_w$  is the molar mass of water. The mass density of the hydrocarbon phases are evaluated in a similar way.

$$\rho_j = \xi_j \sum_{i=1}^{n_c} x_{ij} MW_i, \quad j = 2, \dots, n_p. \quad (2.58)$$

The water saturation is computed as the volume of water over the porous volume

$$S_w = \frac{N_w v_w}{V_p}, \quad (2.59)$$

where  $v_w$  is molar volume of the water phase.

The saturation of the hydrocarbon phases are evaluated as

$$S_j = (1 - S_w) \frac{L_j / \xi_j}{\sum_{m=2}^{n_p} L_m / \xi_m}, \quad j = 2, \dots, n_p - 1, \quad (2.60)$$

where the last saturation is always computed through the saturation constraint, Eq. (2.10).

The relative permeabilities are considered to be function of saturations only and the effect of hysteresis is not considered. Although several models are implemented in UTCOMP simulator, only two of them will be used in this work: the modified Stone II model (Stone, 1973), and the Corey model (Corey, 1986).

For a two-phase system, e.g. water and oil, the relative permeabilities are written as

$$k_{rw} = k_{rw}^0 \left( \frac{S_w - S_{wr}}{1 - S_{wr} - S_{or}} \right)^{e_w}, \quad (2.61)$$

and

$$k_{ro} = k_{ro}^0 \left( \frac{S_o - S_{or}}{1 - S_{wr} - S_{or}} \right)^{e_o}, \quad (2.62)$$

where  $k_r^0$  refers to the end-point permeability,  $e$  is an exponent, and  $S_{wr}$  and  $S_{or}$  are the residual saturations of water and oil, respectively.

For a three-phase system (water, oil and gas), the Stone II model is written as

$$k_{rw} = k_{rw}^0 \left( \frac{S_w - S_{wr}}{1 - S_{wr} - S_{orw}} \right)^{e_w}, \quad (2.63)$$

$$k_{rg} = k_{rg}^0 \left( \frac{S_g - S_{gr}}{1 - S_{gr} - S_{wr} - S_{org}} \right)^{e_g}, \quad (2.64)$$

and

$$k_{ro} = k_{row}^0 \left[ \left( \frac{k_{row}}{k_{row}^0} + k_{rw} \right) \left( \frac{k_{rog}}{k_{row}^0} + k_{rg} \right) - (k_{rw} + k_{rg}) \right], \quad (2.65)$$

where  $S_{orw}$  is the residual saturation of oil in water,  $S_{org}$  is the residual saturation of oil in gas,  $k_{row}^0$  is the end-point relative permeability of oil in water, and  $k_{row}$  and  $k_{rog}$  are the relative permeabilities of oil in water and oil in gas, respectively; and are given as

$$k_{row} = k_{row}^0 \left( \frac{1 - S_w - S_{orw}}{1 - S_{wr} - S_{orw}} \right)^{e_{ow}}, \quad (2.66)$$

and

$$k_{rog} = k_{rog}^0 \left( \frac{1 - S_g - S_{wr} - S_{org}}{1 - S_{wr} - S_{gr} - S_{org}} \right)^{e_{og}}, \quad (2.67)$$

where  $k_{rog}^0$  is the end-point relative permeability of oil in gas,  $e_{ow}$  is the exponent of oil in water, and  $e_{og}$  is the exponent of oil in gas.

Finally, the Stone II model, for the four-phase system, computes the relative permeabilities of water and gas in the same way as shown for the three-phase system and the relative permeabilities of oil, and the second liquid hydrocarbon phase is given by

$$k_{ro} = k_{row}^0 \frac{S_o}{S_o + S_l} \left[ \left( \frac{k_{row}}{k_{row}^0} + k_{rw} \right) \left( \frac{k_{rog}}{k_{row}^0} + k_{rg} \right) - (k_{rw} + k_{rg}) \right], \quad (2.68)$$

and

$$k_{rl} = k_{row}^0 \frac{S_l}{S_o + S_l} \left[ \left( \frac{k_{row}}{k_{row}^0} + k_{rw} \right) \left( \frac{k_{rog}}{k_{row}^0} + k_{rg} \right) - (k_{rw} + k_{rg}) \right]. \quad (2.69)$$

The Corey model for a three-system is written as

$$k_{rw} = k_{rw}^0 \left( \frac{S_w - S_{wr}}{1 - S_{wr} - S_{orw} - S_{gr}} \right)^{e_w}, \quad (2.70)$$

$$k_{ro} = k_{ro}^0 \left( \frac{S_o - S_{or}}{1 - S_{wr} - S_{orw} - S_{gr}} \right)^{e_o}, \quad (2.71)$$

and

$$k_{rg} = k_{rg}^0 \left( \frac{S_g - S_{gr}}{1 - S_{wr} - S_{orw} - S_{gr}} \right)^{e_g}, \quad (2.72)$$

where

$$S_{or} = S_{orw} \left( 1 - \frac{S_g}{1 - S_{wr} - S_{org}} \right) + S_{org} \left( \frac{S_g}{1 - S_{wr} - S_{org}} \right). \quad (2.73)$$

The Corey model for a four-phase system is given by the following equations:

$$k_{rw} = k_{rw}^0 \left( \frac{S_w - S_{wr}}{1 - S_{wr} - S_{orw} - S_{gr} - S_{lr}} \right)^{e_w}, \quad (2.74)$$

$$k_{ro} = k_{ro}^0 \left( \frac{S_o - S_{or}}{1 - S_{wr} - S_{orw} - S_{gr} - S_{lr}} \right)^{e_o}, \quad (2.75)$$

$$k_{rg} = k_{rg}^0 \left( \frac{S_g - S_{gr}}{1 - S_{wr} - S_{orw} - S_{gr} - S_{lr}} \right)^{e_g}, \quad (2.76)$$

and

$$k_{rl} = k_{rl}^0 \left( \frac{S_l - S_{lr}}{1 - S_{wr} - S_{orw} - S_{gr} - S_{lr}} \right)^{e_l}, \quad (2.77)$$

where  $k_{rl}^0$ ,  $S_{lr}$  and  $e_l$  are the end-point relative permeability, residual saturation, and exponent of the second liquid hydrocarbon phase.

The capillary pressure is considered function of the saturations and IFT (interfacial tension). For a three-phase system (water, oil and gas), the capillary pressures are

$$P_{cwo} = -C_{pc} \sigma_{wo} \sqrt{\frac{\phi}{k_y}} (1 - \bar{S}_w)^{E_{pc}}, \quad (2.78)$$

and

$$P_{cog} = -C_{pc} \sigma_{og} \sqrt{\frac{\phi}{k_y}} \left( \frac{\bar{S}_w}{\bar{S}_o + \bar{S}_g} \right)^{E_{pc}}, \quad (2.79)$$

where  $C_{pc}$  and  $E_{pc}$  are parameters adjusted experimentally,  $\sigma_{wo}$  is the IFT for water-oil,  $\sigma_{og}$  is the IFT for oil-gas, and  $\bar{S}$  denotes the normalized saturation defined for the Corey model as

$$\bar{S}_w = \frac{S_w - S_{wr}}{1 - S_{wr} - S_{orw} - S_{gr}}, \quad (2.80)$$

$$\bar{S}_o = \frac{S_o - S_{or}}{1 - S_{wr} - S_{orw} - S_{gr}}, \quad (2.81)$$

and

$$\bar{S}_g = \frac{S_g - S_{gr}}{1 - S_{wr} - S_{orw} - S_{gr}}. \quad (2.82)$$

The Macleod-Sugden (Macleod, 1923; Sugden, 1924) correlation, as presented by Polling et al. (2001), is used to compute the IFT for each pair of phase as

$$\sigma_{ij}^{0.25} = 0.016018 \sum_{k=1}^{n_c} \psi_k (\xi_i x_{ki} - \xi_j x_{kj}), \quad i = 1, \dots, n_p, \quad j = 1, \dots, n_p, \quad (2.83)$$

where  $\psi$  is the parachor parameter.

The UTCOMP simulator has implemented four viscosity models. Only the Lohrenz et al. (1964) model will be used in this work. As the water viscosity is considered constant, this model is used only for the hydrocarbon phases. The first step in computing the viscosities is evaluating the pure-component viscosities at low pressure using the Stiel and Thodos (1961) correlation.

$$\tilde{\mu}_i = \begin{cases} \frac{3.4 \times 10^{-4} T_{ri}^{0.94}}{\zeta_i} & \text{if } T_{ri} \leq 0.15 \\ \frac{1.776 \times 10^{-4} (4.58 T_{ri} - 1.67)^{5/8}}{\zeta_i} & \text{if } T_{ri} > 0.15 \end{cases}, \quad i = 1, \dots, n_c, \quad (2.84)$$

where

$$\zeta_i = \frac{5.44T_{ci}^{1/6}}{MW_i^{1/2}P_c^{2/3}}, \quad i = 1, \dots, n_c. \quad (2.85)$$

The viscosity of the mixture at low pressure is found for each phase using the equation given by Hering and Zipperer (1936).

$$\mu_j^* = \frac{\sum_{i=1}^{n_c} x_{ij} \tilde{\mu}_i \sqrt{MW_i}}{\sum_{i=1}^{n_c} x_{ij} \sqrt{MW_i}}, \quad j = 1, \dots, n_p. \quad (2.86)$$

Finally, the viscosity of each phase at the pressure  $P$  is computed through the correlation of Jossi et al (1962).

$$\mu_j = \begin{cases} \mu_j^* + 2.05 \times 10^{-4} \frac{\xi_{jr}}{\eta_j} & \text{if } \xi_{jr} \leq 0.18 \\ \frac{\mu_j^* + (\chi_j^4 - 1)}{10^4 \eta_j} & \text{if } \xi_{jr} > 0.18 \end{cases}, \quad j = 1, \dots, n_p, \quad (2.87)$$

where the phase reduced density ( $\xi_{jr}$ ) is computed as

$$\xi_{jr} = \xi_j \sum_{i=1}^{n_c} x_{ij} v_{ci}, \quad j = 1, \dots, n_p, \quad (2.88)$$

where  $v_{ci}$  is the critical molar volume of each component. The parameters  $\eta_j$  and  $\chi_j$  are given by

$$\eta_j = \frac{5.44 \left( \sum_{i=1}^{n_c} x_{ij} T_{ci} \right)^{1/6}}{\left( \sum_{i=1}^{n_c} x_{ij} W_i \right)^{1/2} \left( \sum_{i=1}^{n_c} x_{ij} P_{ci} \right)^{2/3}}, \quad j = 1, \dots, n_p, \quad (2.89)$$

$$\chi_j = 1.023 + 0.23364 \xi_{jr} + 0.58533 \xi_{jr}^2 - 0.40758 \xi_{jr}^3 + 0.093324 \xi_{jr}^4, \quad j = 1, \dots, n_p. \quad (2.90)$$

Finally, we need to compute the volume derivatives which are necessary for the Ács et al. (1985), the Watts (1986) and the new FI formulations. In UTCOMP, these derivatives were originally computed analytically only for the total fluid volume as suggested by Chang (1990). However, for the Watts formulation it is also necessary to evaluate the

derivatives of each phase volume. Therefore we will show the equations for each phase, and then sum them up to evaluate the derivative of total fluid volume. The analytical procedure for developing these derivatives were originally proposed by Subramanian et al. (1987) and by Wong et al. (1987) as previously mentioned.

The derivative with relation to the number of moles of water is given by

$$\bar{V}_{ww} = \frac{\partial}{\partial N_w} \left( \frac{N_w}{\xi_w} \right) = \frac{1}{\xi_w}. \quad (2.91)$$

The procedure to evaluate the derivatives with relation to the hydrocarbon phases is much more complicated. The derivation starts from

$$\bar{V}_{jk} = \frac{\partial (n_j v_j)}{\partial N_k}, \quad k = 1, \dots, n_c, \quad j = 2, \dots, n_p, \quad (2.92)$$

where  $n_j$  is the number of moles of phase  $j$  and is given by

$$n_j = \sum_{i=1}^{n_c} n_{ij}, \quad k = 1, \dots, n_c, \quad j = 2, \dots, n_p. \quad (2.93)$$

Evaluating the derivatives of Eq. (2.92), we obtain

$$\bar{V}_{jk} = v_j \sum_{i=1}^{n_c} \frac{\partial n_{ij}}{\partial N_k} + n_j \frac{\partial v_j}{\partial N_k}, \quad k = 1, \dots, n_c, \quad j = 2, \dots, n_p, \quad (2.94)$$

where the second derivative can be evaluated through the chain rule as

$$\frac{\partial v_j}{\partial N_k} = \frac{\partial v_j}{\partial P} \frac{\partial P}{\partial N_k} + \sum_{i=1}^{n_c} \frac{\partial v_j}{\partial n_{ij}} \frac{\partial n_{ij}}{\partial N_k}, \quad k = 1, \dots, n_c, \quad j = 2, \dots, n_p. \quad (2.95)$$

The first term on the right hand-side of Eq. (2.95) is eliminated since the derivative is taken at constant pressure (see Eq. (2.13)), thus the derivative of  $P$  with respect to  $N_k$  will be zero. Substituting Eq. (2.103) into Eq. (2.102) yields

$$\bar{V}_{jk} = \sum_{i=1}^{n_c} \frac{\partial n_{ij}}{\partial N_k} \left( v_j + n_j \frac{\partial v_j}{\partial n_{ij}} \right), \quad k = 1, \dots, n_c, \quad j = 2, \dots, n_p, \quad (2.96)$$

where

$$\frac{\partial v_j}{\partial n_{ij}} = \frac{\partial}{\partial n_{ij}} \left( \frac{Z_j RT}{P} \right) = \frac{RT}{P} \frac{\partial Z_j}{\partial n_{ij}}, \quad k = 1, \dots, n_c, \quad j = 2, \dots, n_p, \quad (2.97)$$

where the derivative of the compressibility factor can be obtained from the PREOS.

Therefore, the only unknown to obtain the volume derivatives are  $\frac{\partial n_{ij}}{\partial N_k}$ . To obtain

these derivatives, we consider the fugacity constraints (Eq. 2.37):

$$\ln f_{ij} = \ln f_{ir}. \quad (2.98)$$

We first show the process for the two-phase equilibrium system. In this case, the subscripts  $j$  and  $r$  in Eq. (2.98) can assume the  $o$  and  $g$  for the oil-gas system;  $o$  and  $l$  for the oil-second liquid system; or  $g$  and  $l$  for the gas-second liquid system.

Deriving Eq. (2.98) with respect to  $N_k$  yields

$$\frac{\partial \ln f_{ij}}{\partial N_k} = \frac{\partial \ln f_{ir}}{\partial N_k}, \quad i = 1, \dots, n_c; \quad k = 1, \dots, n_c, \quad (2.99)$$

where, through the chain rule,

$$\frac{\partial \ln f_{ir}}{\partial N_k} = \sum_{s=1}^{n_c} \frac{\partial \ln f_{ir}}{\partial n_{sr}} \frac{\partial n_{sr}}{\partial N_k} + \frac{\partial \ln f_{ir}}{\partial P} \frac{\partial P}{\partial N_k}, \quad i = 1, \dots, n_c; \quad k = 1, \dots, n_c, \quad (2.100)$$

and

$$\frac{\partial \ln f_{ij}}{\partial N_k} = \sum_{s=1}^{n_c} \frac{\partial \ln f_{ij}}{\partial n_{sr}} \frac{\partial n_{sr}}{\partial N_k} + \frac{\partial \ln f_{ij}}{\partial P} \frac{\partial P}{\partial N_k}, \quad i = 1, \dots, n_c; \quad k = 1, \dots, n_c, \quad (2.101)$$

where once again the derivative of pressure with respect to  $N_k$  will be zero. For this reason,

$$\sum_{s=1}^{n_c} \frac{\partial \ln f_{ij}}{\partial n_{sj}} \frac{\partial n_{sj}}{\partial N_k} = \sum_{s=1}^{n_c} \frac{\partial \ln f_{ir}}{\partial n_{sr}} \frac{\partial n_{sr}}{\partial N_k}, \quad i = 1, \dots, n_c; \quad k = 1, \dots, n_c, \quad (2.102)$$

where

$$N_s = n_{sr} + n_{sj}, \quad s = 1, \dots, n_c, \quad (2.103)$$

and

$$\frac{\partial N_s}{\partial N_k} = \delta_{sk} = \frac{\partial n_{sr}}{\partial N_k} + \frac{\partial n_{sj}}{\partial N_k}, \quad s = 1, \dots, n_c; \quad k = 1, \dots, n_c, \quad (2.104)$$

and

$$\frac{\partial n_{sj}}{\partial N_k} = \delta_{sk} - \frac{\partial n_{sr}}{\partial N_k}, \quad s = 1, \dots, n_c; \quad k = 1, \dots, n_c, \quad (2.105)$$

where  $\delta_{sk}$  is 1 for  $s=k$  and 0 for  $s \neq k$ .

Substituting Eq. (2.105) into Eq. (2.102) and making some algebraic manipulation yields

$$\sum_{s=1}^{n_c} \left( \frac{\partial \ln f_{ir}}{\partial n_{sr}} + \frac{\partial \ln f_{ij}}{\partial n_{sj}} \right) \frac{\partial n_{sr}}{\partial N_k} = \frac{\partial \ln f_{ij}}{\partial n_{kj}}, \quad i = 1, \dots, n_c; \quad k = 1, \dots, n_c. \quad (2.106)$$

Observe that Eq. (2.106) contains  $n_c$  derivatives of moles of phase  $r$  with respect to the total number of moles of component  $k$  ( $N_k$ ) and is obtained using only the fugacity of the  $i$ -th component. For determining these derivatives, the expressions for the remaining fugacities are written such that the following linear system is assembled:

$$\begin{bmatrix} \frac{\partial \ln f_{1r}}{\partial n_{1r}} + \frac{\partial \ln f_{1j}}{\partial n_{1j}} & \dots & \frac{\partial \ln f_{1r}}{\partial n_{n_cr}} + \frac{\partial \ln f_{1j}}{\partial n_{n_cj}} \\ \vdots & \ddots & \vdots \\ \frac{\partial \ln f_{n_cr}}{\partial n_{1r}} + \frac{\partial \ln f_{n_cj}}{\partial n_{1j}} & \dots & \frac{\partial \ln f_{n_cr}}{\partial n_{n_cr}} + \frac{\partial \ln f_{n_cj}}{\partial n_{n_cj}} \end{bmatrix} \begin{bmatrix} \frac{\partial n_{1r}}{\partial N_k} \\ \vdots \\ \frac{\partial n_{n_cr}}{\partial N_k} \end{bmatrix} = \begin{bmatrix} \frac{\partial \ln f_{1j}}{\partial n_{kj}} \\ \vdots \\ \frac{\partial \ln f_{n_cj}}{\partial n_{kj}} \end{bmatrix}, \quad k = 1, \dots, n_c. \quad (2.107)$$

Notice that Eq. (2.107) must be solved  $n_c$  times for each component. Additionally, the coefficients matrix is independent of the  $N_k$  for which we are solving. Therefore, the same coefficients matrix is shared for all  $n_c$  systems of equations. Once the derivatives for phase  $r$  are computed, the derivatives for phase  $j$  can be obtained from Eq. (2.105).

For the three-phase system (oil-gas-second liquid), we have

$$\frac{\partial \ln f_{io}}{\partial N_k} = \frac{\partial \ln f_{ig}}{\partial N_k}, \quad i = 1, \dots, n_c; \quad k = 1, \dots, n_c, \quad (2.108)$$

and

$$\frac{\partial \ln f_{ig}}{\partial N_k} = \frac{\partial \ln f_{il}}{\partial N_k}, \quad i = 1, \dots, n_c; \quad k = 1, \dots, n_c, \quad (2.109)$$

Applying the chain rule to the above equations, we obtain

$$\sum_{s=1}^{n_c} \frac{\partial \ln f_{io}}{\partial n_{so}} \frac{\partial n_{so}}{\partial N_k} = \sum_{s=1}^{n_c} \frac{\partial \ln f_{ig}}{\partial n_{sg}} \frac{\partial n_{sg}}{\partial N_k}, \quad i = 1, \dots, n_c; \quad k = 1, \dots, n_c, \quad (2.110)$$

and

$$\sum_{s=1}^{n_c} \frac{\partial \ln f_{ig}}{\partial n_{sg}} \frac{\partial n_{sg}}{\partial N_k} = \sum_{s=1}^{n_c} \frac{\partial \ln f_{il}}{\partial n_{sl}} \frac{\partial n_{sl}}{\partial N_k}, \quad i = 1, \dots, n_c; \quad k = 1, \dots, n_c. \quad (2.111)$$

where

$$N_s = n_{so} + n_{sg} + n_{sl}, \quad s = 1, \dots, n_c, \quad (2.112)$$

and



$$\frac{\partial N_s}{\partial N_k} = \delta_{sk} = \frac{\partial n_{so}}{\partial N_k} + \frac{\partial n_{sg}}{\partial N_k} + \frac{\partial n_{sl}}{\partial N_k}, \quad s = 1, \dots, n_c; \quad k = 1, \dots, n_c, \quad (2.113)$$

Choosing the gas phase as dependent, one obtains

$$\frac{\partial n_{sg}}{\partial N_k} = \delta_{sk} - \frac{\partial n_{so}}{\partial N_k} - \frac{\partial n_{sl}}{\partial N_k}, \quad s = 1, \dots, n_c; \quad k = 1, \dots, n_c. \quad (2.114)$$

Substituting Eq. (2.114) into Eq. (2.110) and Eq. (2.114) into Eq. (2.111), and performing the algebraic manipulating, we obtain

$$\sum_{s=1}^{n_c} \left( \frac{\partial \ln f_{io}}{\partial n_{so}} + \frac{\partial \ln f_{ig}}{\partial n_{sg}} \right) \frac{\partial n_{so}}{\partial N_k} + \sum_{s=1}^{n_c} \frac{\partial \ln f_{ig}}{\partial n_{sg}} \frac{\partial n_{sl}}{\partial N_k} = \frac{\partial \ln f_{ig}}{\partial n_{kg}}, \quad i = 1, \dots, n_c; \quad k = 1, \dots, n_c. \quad (2.115)$$

$$\sum_{s=1}^{n_c} \frac{\partial \ln f_{ig}}{\partial n_{sg}} \frac{\partial n_{so}}{\partial N_k} + \sum_{s=1}^{n_c} \left( \frac{\partial \ln f_{ig}}{\partial n_{sg}} + \frac{\partial \ln f_{il}}{\partial n_{sl}} \right) \frac{\partial n_{sl}}{\partial N_k} = \frac{\partial \ln f_{ig}}{\partial n_{kg}}, \quad i = 1, \dots, n_c; \quad k = 1, \dots, n_c. \quad (2.116)$$

From Eqs. (2.115) through and (2.116) we can see that now  $n_c$  systems of equations with  $2n_c$  unknowns will be solved. These equations can be restated in matrix form as

$$A_{is} = \begin{bmatrix} \frac{\partial \ln f_{io}}{\partial n_{so}} + \frac{\partial \ln f_{ig}}{\partial n_{sg}} & \frac{\partial \ln f_{ig}}{\partial n_{sg}} \\ \frac{\partial \ln f_{ig}}{\partial n_{sg}} & \frac{\partial \ln f_{ig}}{\partial n_{sg}} + \frac{\partial \ln f_{il}}{\partial n_{sl}} \end{bmatrix}; \quad B_{ik} = \begin{bmatrix} \frac{\partial \ln f_{ig}}{\partial n_{kg}} \\ \frac{\partial \ln f_{ig}}{\partial n_{kg}} \end{bmatrix}; \quad (2.117)$$

$$X_{sk} = \begin{bmatrix} \frac{\partial n_{so}}{\partial N_k} \\ \frac{\partial n_{sl}}{\partial N_k} \end{bmatrix}, \quad i = 1, \dots, n_c; \quad k = 1, \dots, n_c,$$

or

$$\begin{bmatrix} A_{11} & \cdots & A_{1n_c} \\ \vdots & \ddots & \vdots \\ A_{n_c 1} & \cdots & A_{n_c n_c} \end{bmatrix} \begin{bmatrix} X_{1k} \\ \vdots \\ X_{n_c k} \end{bmatrix} = \begin{bmatrix} B_{1k} \\ \vdots \\ B_{n_c k} \end{bmatrix}, \quad k = 1, \dots, n_c. \quad (2.118)$$

Once again the coefficients matrix is the same for all  $n_c$  linear systems.

Solving these derivatives, the Eq. (2.96) can be solved. The total volume derivative will be evaluated as

$$\bar{V}_{Tk} = \sum_{j=1}^{n_p} \bar{V}_{jk}, \quad k = 1, \dots, n_c. \quad (2.119)$$

The derivatives of the volume with the respect to pressure are the only variables left now. The derivative of the water volume with respect to pressure is given by

$$\frac{\partial V_w}{\partial P} = -\frac{N_w \xi_w^0 C_w}{\xi_w^2}. \quad (2.120)$$

Once again, the derivatives of the hydrocarbon phase volumes will be much more complex than for water. For a phase  $j$  this derivative is given by

$$\frac{\partial V_j}{\partial P} = \frac{\partial(n_j v_j)}{\partial P} = n_j \frac{\partial v_j}{\partial P} + v_j \frac{\partial n_j}{\partial P}, \quad j = 2, \dots, n_p. \quad (2.121)$$

Applying the chain rule to the mole volume derivative we obtain

$$\frac{\partial v_j}{\partial P} = \frac{\partial v_j}{\partial P} \frac{\partial P}{\partial P} + \sum_{i=1}^{n_c} \frac{\partial v_j}{\partial n_{ij}} \frac{\partial n_{ij}}{\partial P}, \quad j = 2, \dots, n_p. \quad (2.122)$$

Substituting result into Eq. (2.121), yields

$$\frac{\partial V_j}{\partial P} = n_j \frac{\partial v_j}{\partial P} + \sum_{i=1}^{n_c} \frac{\partial n_{ij}}{\partial P} \left( v_j + n_j \frac{\partial v_j}{\partial n_{ij}} \right), \quad j = 2, \dots, n_p, \quad (2.123)$$

where

$$\frac{\partial v_j}{\partial P} = \frac{\partial}{\partial P} \left( \frac{Z_j RT}{P} \right) = \frac{RT}{P} \left( \frac{\partial Z_j}{\partial P} - \frac{Z_j}{P} \right), \quad j = 2, \dots, n_p. \quad (2.124)$$

From Eq. (2.123), we can infer that is necessary to compute the derivatives of the number of moles with respect to pressure. In order to compute it, we use a similar approach to that shown for the derivatives with respect to the total number of moles of each component. We show the procedure for a two-phase system first. Deriving Eq. (2.98) with respect to pressure and applying the chain rule, yields

$$\sum_{s=1}^{n_c} \frac{\partial \ln f_{ir}}{\partial n_{sr}} \frac{\partial n_{sr}}{\partial P} + \frac{\partial \ln f_{ir}}{\partial P} = \sum_{s=1}^{n_c} \frac{\partial \ln f_{ij}}{\partial n_{sj}} \frac{\partial n_{sj}}{\partial P} + \frac{\partial \ln f_{ij}}{\partial P}, \quad i = 1, \dots, n_c, \quad (2.125)$$

where

$$N_s = n_{sr} + n_{sj}, \quad s = 1, \dots, n_c, \quad (2.126)$$

and

$$\frac{\partial N_s}{\partial P} = 0 = \frac{\partial n_{sr}}{\partial P} + \frac{\partial n_{sj}}{\partial P}, \quad s = 1, \dots, n_c, \quad (2.127)$$

thus

$$\frac{\partial n_{sj}}{\partial P} = -\frac{\partial n_{sr}}{\partial P}, \quad s = 1, \dots, n_c. \quad (2.128)$$

Substituting Eq. (2.128) into Eq. (2.125) and doing some algebraic manipulation yields

$$\sum_{s=1}^{n_c} \left( \frac{\partial \ln f_{ir}}{\partial n_{sr}} + \frac{\partial \ln f_{ij}}{\partial n_{sj}} \right) \frac{\partial n_{sr}}{\partial P} = \frac{\partial \ln f_{ij}}{\partial P} - \frac{\partial \ln f_{ir}}{\partial P}, \quad i = 1, \dots, n_c \quad (2.129)$$

The  $n_c$  Eqs. (2.129) results in a linear system with the same coefficient matrix as shown in Eq. (2.107), which it is presented below.

$$\begin{bmatrix} \frac{\partial \ln f_{1r}}{\partial n_{1r}} + \frac{\partial \ln f_{1j}}{\partial n_{1j}} & \dots & \frac{\partial \ln f_{1r}}{\partial n_{n_c r}} + \frac{\partial \ln f_{1j}}{\partial n_{n_c j}} \\ \vdots & \ddots & \vdots \\ \frac{\partial \ln f_{n_c r}}{\partial n_{1r}} + \frac{\partial \ln f_{n_c j}}{\partial n_{1j}} & \dots & \frac{\partial \ln f_{n_c r}}{\partial n_{n_c r}} + \frac{\partial \ln f_{n_c j}}{\partial n_{n_c j}} \end{bmatrix} \begin{bmatrix} \frac{\partial n_{1r}}{\partial P} \\ \vdots \\ \frac{\partial n_{n_c r}}{\partial P} \end{bmatrix} = \begin{bmatrix} \frac{\partial \ln f_{1j}}{\partial P} - \frac{\partial \ln f_{1r}}{\partial P} \\ \vdots \\ \frac{\partial \ln f_{n_c j}}{\partial P} - \frac{\partial \ln f_{n_c r}}{\partial P} \end{bmatrix}. \quad (2.130)$$

For the three-phase system, we can derive the fugacity constraints with respect to pressure, to obtain

$$\frac{\partial \ln f_{io}}{\partial P} = \frac{\partial \ln f_{ig}}{\partial P}, \quad i = 1, \dots, n_c, \quad (2.131)$$

and

$$\frac{\partial \ln f_{ig}}{\partial P} = \frac{\partial \ln f_{il}}{\partial P}, \quad i = 1, \dots, n_c. \quad (2.132)$$

Applying the chain rule to the above the equations, we obtain

$$\sum_{s=1}^{n_c} \frac{\partial \ln f_{io}}{\partial n_{so}} \frac{\partial n_{so}}{\partial P} + \frac{\partial \ln f_{io}}{\partial P} = \sum_{s=1}^{n_c} \frac{\partial \ln f_{ig}}{\partial n_{sg}} \frac{\partial n_{sg}}{\partial P} + \frac{\partial \ln f_{ig}}{\partial P}, \quad i = 1, \dots, n_c, \quad (2.133)$$

and

$$\sum_{s=1}^{n_c} \frac{\partial \ln f_{ig}}{\partial n_{sg}} \frac{\partial n_{sg}}{\partial P} + \frac{\partial \ln f_{ig}}{\partial P} = \sum_{s=1}^{n_c} \frac{\partial \ln f_{il}}{\partial n_{sl}} \frac{\partial n_{sl}}{\partial P} + \frac{\partial \ln f_{il}}{\partial P}, \quad i = 1, \dots, n_c, \quad (2.134)$$

where

$$N_s = n_{so} + n_{sg} + n_{sl}, \quad s = 1, \dots, n_c, \quad (2.135)$$

and

$$\frac{\partial N_s}{\partial P} = 0 = \frac{\partial n_{so}}{\partial P} + \frac{\partial n_{sg}}{\partial P} + \frac{\partial n_{sl}}{\partial P}, \quad s = 1, \dots, n_c, \quad (2.136)$$

Once again, setting the gas as a dependent phase, we obtain

$$\frac{\partial n_{sg}}{\partial P} = -\frac{\partial n_{so}}{\partial P} - \frac{\partial n_{sl}}{\partial P}, \quad s = 1, \dots, n_c. \quad (2.137)$$

Substituting Eq. (2.137) into Eq. (2.133), and Eq. (2.137) into Eq. (2.134), and doing some algebraic manipulation, we obtain

$$\sum_{s=1}^{n_c} \left( \frac{\partial \ln f_{io}}{\partial n_{so}} + \frac{\partial \ln f_{ig}}{\partial n_{sg}} \right) \frac{\partial n_{so}}{\partial P} + \sum_{s=1}^{n_c} \frac{\partial \ln f_{ig}}{\partial n_{sg}} \frac{\partial n_{sl}}{\partial P} = \frac{\partial \ln f_{ig}}{\partial P} - \frac{\partial \ln f_{io}}{\partial P}, \quad i = 1, \dots, n_c. \quad (2.138)$$

$$\sum_{s=1}^{n_c} \frac{\partial \ln f_{ig}}{\partial n_{sg}} \frac{\partial n_{so}}{\partial P} + \sum_{s=1}^{n_c} \left( \frac{\partial \ln f_{ig}}{\partial n_{sg}} + \frac{\partial \ln f_{il}}{\partial n_{sl}} \right) \frac{\partial n_{sl}}{\partial P} = \frac{\partial \ln f_{ig}}{\partial P} - \frac{\partial \ln f_{il}}{\partial P}, \quad i = 1, \dots, n_c, \quad (2.139)$$

The  $n_c$  Eqs. (2.138) and (2.139) forms a linear set of equations with  $2n_c$  unknowns. Once again, the coefficients matrix is the same as that obtained for the moles derivatives, given by Eqs. (2.117) and (2.118). The linear system can be written as

$$A_{is} = \begin{bmatrix} \frac{\partial \ln f_{io}}{\partial n_{so}} + \frac{\partial \ln f_{ig}}{\partial n_{sg}} & \frac{\partial \ln f_{ig}}{\partial n_{sg}} \\ \frac{\partial \ln f_{ig}}{\partial n_{sg}} & \frac{\partial \ln f_{ig}}{\partial n_{sg}} + \frac{\partial \ln f_{il}}{\partial n_{sl}} \end{bmatrix}; B_i = \begin{bmatrix} \frac{\partial \ln f_{ig}}{\partial P} - \frac{\partial \ln f_{io}}{\partial P} \\ \frac{\partial \ln f_{ig}}{\partial P} - \frac{\partial \ln f_{il}}{\partial P} \end{bmatrix}; \quad (2.140)$$

$$X_s = \begin{bmatrix} \frac{\partial n_{so}}{\partial P} \\ \frac{\partial n_{sl}}{\partial P} \end{bmatrix}, i = 1, \dots, n_c,$$

or in a form

$$\begin{bmatrix} A_{11} & \cdots & A_{1n_c} \\ \vdots & \ddots & \vdots \\ A_{n_c 1} & \cdots & A_{n_c n_c} \end{bmatrix} \begin{bmatrix} X_1 \\ \vdots \\ X_{n_c} \end{bmatrix} = \begin{bmatrix} B_1 \\ \vdots \\ B_{n_c} \end{bmatrix}. \quad (2.141)$$

Finally, the total volume derivative with respect to pressure will be given as

$$\frac{\partial V_T}{\partial P} = \sum_{j=1}^{n_p} \frac{\partial V_j}{\partial P}. \quad (2.142)$$

Finally, we present the treatment of the wells included in the mole balance equations. Three operational conditions are treated in this work: constant surface volumetric

rate injection, constant bottom hole pressure (BHP) for injection and producer wells. If the first option is considered, then the molar rate of each component is computed at surface conditions, which must be the same that will be included directly into the mole balance equations. If multiple layers are considered, then this rate must be distributed through each segment as follows:

$$\dot{q}_{k,s} = \frac{WI_s \sum_{j=1}^{n_p} \lambda_{j,s}}{\sum_{l=1}^{n_L} WI_l \sum_{j=1}^{n_p} \lambda_{j,l}} \dot{q}_{k,T}, \quad s = 1, \dots, n_s, \quad k = 1, \dots, n_c \quad (2.143)$$

where  $n_s$  is the number of segments of the well and  $WI_s$  is the Well Index (WI) of each segment  $s$  of the well. The WI is computed through the Peaceman model (Peaceman, 1978; Peaceman, 1983) for Cartesian grids and through the Fung et al. (1992) model for unstructured grids. The volumetric rate of each segment of the well can be computed as

$$\dot{Q}_{j,s} = \lambda_{j,s} WI_s (P_s + P_{cjr,s} - P_{wf,s}), \quad s = 1, \dots, n_s, \quad j = 1, \dots, n_p \quad (2.144)$$

where  $P$  is the block pressure that has a well and  $P_{wf,s}$  is the wellbore pressure at segment  $s$ .

For producer wells operating at constant BHP, the mole rate of a given hydrocarbon component and water are respectively, computed as

$$\dot{q}_{k,s} = \sum_{j=2}^{n_p} x_{kj,s} \xi_{j,s} \dot{Q}_{j,s}, \quad s = 1, \dots, n_s, \quad k = 1, \dots, n_c \quad (2.145)$$

$$\dot{q}_{w,s} = \xi_{w,s} \dot{Q}_{w,s}, \quad s = 1, \dots, n_s \quad (2.146)$$

For injector wells operating at constant BHP, the mole rate of the hydrocarbon components and water are respectively given as

$$\dot{q}_{k,s} = z_{k,inj} \frac{(1 - W_F)}{v_{T,inj}} \sum_{j=1}^{n_p} \dot{Q}_{j,s}, \quad s = 1, \dots, n_s, \quad k = 1, \dots, n_c \quad (2.147)$$

$$\dot{q}_{w,s} = z_{w,inj} \frac{W_F}{v_{T,inj}} \sum_{j=1}^{n_p} \dot{Q}_{j,s}, \quad s = 1, \dots, n_s, \quad (2.148)$$

where  $W_F$  is the fraction of water being injected,  $z_{k,inj}$  is the mole fraction of component  $k$  into the injection fluid and  $v_{T,inj}$  is the total molar volume of fluid injected.

### 3 APPROXIMATE EQUATIONS

In this chapter, we present the discretization of the mathematical model. First, the spatial discretization of the equations is presented. Second, the upwind scheme used in this work is presented. Finally, we present the criteria for the selection of the time-steps.

#### 3.1 Spatial discretization

The discretization of the flow equations shown in chapter 2 will be presented. The Finite Volume Method (FVM) will be considered in this work. First, we show the discretization of the pressure equation used for all formulations, except for the Collins et al. (1992) formulation, and the saturation equations for the IMPSAT formulations along with the mole balance equations for an arbitrary control volume. Then, the mole and the volume balances are discretized for the Cartesian grids. Finally, the same process is performed for the EbFVM approach for 2D and 3D reservoirs.

Integrating Eq. (2.18) in time and for an arbitrary volume  $P$ , we obtain

$$\left[ V_{b,P} \phi_P^0 C_f - \frac{\partial V_{T,P}^n}{\partial P} \right] (P_P^{n+1} - P_P^n) = (V_{T,P}^n - V_{p,P}^n) + \sum_{k=1}^{n_c+1} \bar{V}_{Tk,P}^n \int_{V,t} \frac{1}{V_b} \frac{\partial N_k}{\partial t} dV dt, \quad (3.1)$$

where the first term in parenthesis on the right-hand side is the volume discrepancy term. This term comes from a special time discretization suggested by Ács et al. (1985). The volume discrepancy acts as an error control parameter that allows the formulation to perform only one flash calculation per time-step. In order to not making the derivation of the approximate equations confusing, we do not show this treatment. The reader may follow the procedure presented by Ács et al. (1985) and Watts (1986) in order to see how this term arises. The integration of the molar rate after applying the Green-Gauss theorem for the hydrocarbon components and water are respectively, given by

$$\int_{V,t} \frac{1}{V_b} \frac{\partial N_k}{\partial t} dV dt =$$

$$(N_{k,P}^{n+1} - N_{k,P}^n) = \Delta t \sum_{j=2}^{n_p} \int_A \left( x_{kj}^m \xi_j^m \frac{k_{rj}^m}{\mu_j^m} \bar{K} \cdot \vec{\nabla} (P^{n+1} + P_{cjr}^m - \rho_j^m gD) \right) \cdot d\vec{A} \quad (3.2)$$

$$- \Delta t \dot{q}_{k,P}^m, \quad k = 1, \dots, n_c,$$

$$\int_{V,t} \frac{1}{V_b} \frac{\partial N_w}{\partial t} dVdt =$$

$$\left( N_{w,P}^{n+1} - N_{w,P}^n \right) = \Delta t \int_A \left( \xi_w^m \frac{k_{rw}^m}{\mu_w^m} \bar{K} \cdot \bar{\nabla} (P^{n+1} + P_{cwr}^m - \rho_w^m gD) \right) \cdot d\bar{A} \quad , \quad (3.3)$$

$$- \Delta t \dot{q}_{w,P}^m$$

In Eqs. (3.1), (3.2) and (3.3) the superscript  $n$  and  $n+1$  denote properties evaluated at the previous and current time-step, respectively; and  $m$  is equal to  $n$  when the physical properties are evaluated at the previous time-step or equal to  $n+1$  when the physical properties are evaluated at the current time-step. The selection of the implicitness degree will be discussed later.

The integration of Eq. (3.1) for either Cartesian or unstructured grids will provide the final form of the pressure equation.

The same approach can be performed for the saturation equation (Eq. 2.25):

$$V_{b,P} S_\ell^{n+1} \phi^{n+1} = V_{\ell,P}^n + \frac{\partial V_{\ell,P}^n}{\partial P} (P_P^{n+1} - P_P^n) + \sum_{k=1}^{n_c+1} \bar{V}_{\ell k,P}^n \int_{V,t} \frac{1}{V_b} \frac{\partial N_k}{\partial t} dVdt, \quad \ell = 1, \dots, n_p. \quad (3.4)$$

The mole rate in Eq. (3.4) is treated in a special way when using the Watts formulation, which is presented bellow for the hydrocarbon components and water, respectively as

$$\int_{V,t} \frac{1}{V_b} \frac{\partial N_k}{\partial t} dVdt = -\Delta t \sum_{j=2}^{n_p} \int_A (x_{kj}^n \xi_j^n \bar{U}_j^{n+1}) \cdot d\bar{A} - \Delta t \dot{q}_{k,P}^n, \quad k = 1, \dots, n_c, \quad (3.5)$$

$$\int_{V,t} \frac{1}{V_b} \frac{\partial N_w}{\partial t} dVdt = -\Delta t \int_A (\xi_w^n \bar{U}_w^{n+1}) \cdot d\bar{A} - \Delta t \dot{q}_{w,P}^n, \quad (3.6)$$

The velocities, in Eqs. (3.5) and (3.6), are computed using Eq. (2.32), which are show bellow.

$$\bar{U}_j^{n+1} = f_{rj}^{n+1} \bar{U}_T^{n+1}$$

$$+ f_{rj}^{n+1} \left[ \sum_{s=1}^{n_p} \lambda_s^{n+1} \bar{K} \cdot (\bar{\nabla} P_{csr}^{n+1} - \bar{\nabla} P_{cjr}^{n+1}) - \sum_{s=1}^{n_p} \lambda_s^{n+1} (\rho_s^n - \rho_j^n) g \bar{K} \cdot \bar{\nabla} D \right], \quad (3.7)$$

where the expressions for total velocity, fractional flow, and phase mobility are respectively, given by

$$\bar{U}_T^{n+1} = - \sum_{s=1}^{n_p} \lambda_s^n \bar{K} \cdot \bar{\nabla} (P^{n+1} + P_{csr}^n - \rho_s^n g \bar{\nabla} D), \quad (3.8)$$

$$f_{rj}^{n+1} = \frac{\lambda_j^{n+1}}{\sum_{s=1}^{n_p} \lambda_s^{n+1}}, \quad (3.9)$$

$$\lambda_j^{n+1} = \frac{k_{rj}^{n+1}}{\mu_j^n}. \quad (3.10)$$

Notice that as the viscosity is not function of the saturation, it is always treated explicitly for the IMPSAT formulations.

The well terms treatment are not explained by Watts (1986) neither by authors that tried to extend his work (Quandalle and Savary, 1989; Haukas et al., 2004; Haukas, 2005). We know from experience (Fernandes et al.; 2014a), that the well treatment is a key parameter for the Watts formulation and therefore for all IMPSAT formulations that will be presented here. The wells rates need to be evaluated in a way that the total volumetric rates are conserved. The procedure shown here will be important for wells operating under prescribed BHP, since for wells operating under constant volumetric rates no additional procedure is required to conserve the volumetric rates. By summing up the volumetric rates for all phases (Eq. 2.144) and manipulating them in a similar way as it was performed for velocity, we obtain that the volumetric rate of a given phase can be written as

$$\dot{Q}_j^{n+1} = f_{rj}^{n+1} \left[ \dot{Q}_T^{n+1} + WI \sum_{s=1}^{n_p} \lambda_s^{n+1} (P_{cjr}^{n+1} - P_{csr}^{n+1}) \right], \quad (3.11)$$

where

$$\dot{Q}_T^{n+1} = \sum_{j=1}^{n_p} \lambda_j^n WI (P^{n+1} + P_{cjr}^n - P_w^n). \quad (3.12)$$

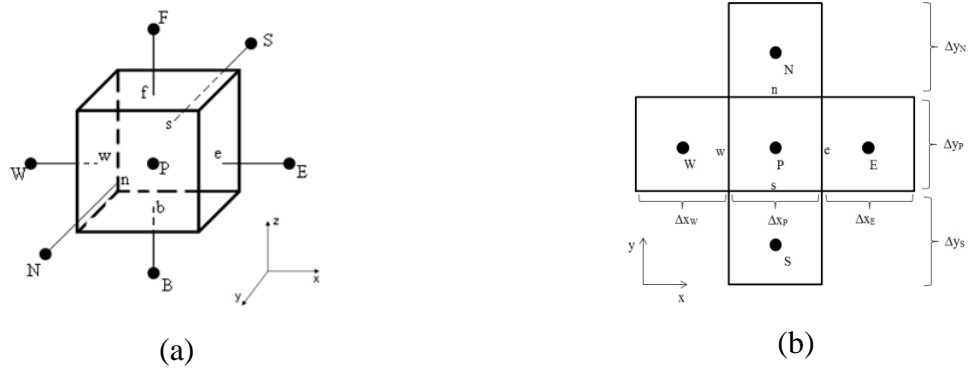
The degree of implicitness of each of these equations will be specified in the next chapter, where the flowchart of each formulation will be presented.



### 3.1.1 Cartesian grid discretization

For the Cartesian grids, the equations are integrated into a Cartesian volume as shown in Figure 3.1.

Figure 3.1 – Cartesian control volume. a) three dimensional view; b) x-y plane view.



The properties are considered uniform in each control surface, and therefore Eq.

(3.2) can be written as

$$\begin{aligned} (N_{k,P}^{n+1} - N_{k,P}^n) = \Delta t \sum_{j=2}^{n_p} \sum_{l=1}^{n_f} \left( x_{kj}^m \xi_j^m \frac{k_{rj}^m}{\mu_j^m} \bar{\bar{K}} \cdot \vec{\nabla} (P^{n+1} + P_{cjr}^m - \rho_j^m gD) \right)_l \cdot \vec{A}_l \\ - \Delta t \dot{q}_{k,P}^m, \quad k = 1, \dots, n_c, \end{aligned} \quad (3.13)$$

where  $n_f$  is the number of faces of the control volume P (six for the 3D control volume shown in Fig. 3.1),  $\vec{A}_l$  is the normal area of face  $l$  which is always oriented outward of the control-volume faces. These faces are shown in Figure 3.1 as  $w, e, s, n, b, f$ .

The inner products of the permeability tensor, potential gradient, and area of Eq. (3.13) is given by

$$\begin{aligned} \left[ \bar{\bar{K}} \cdot \vec{\nabla} \Phi_j^m \cdot \vec{A} \right]_l = \left( K_{xx} \frac{\partial \Phi_j^m}{\partial x} + K_{xy} \frac{\partial \Phi_j^m}{\partial y} + K_{xz} \frac{\partial \Phi_j^m}{\partial z} \right)_l A_{x,l} \\ + \left( K_{yx} \frac{\partial \Phi_j^m}{\partial x} + K_{yy} \frac{\partial \Phi_j^m}{\partial y} + K_{yz} \frac{\partial \Phi_j^m}{\partial z} \right)_l A_{y,l} \\ + \left( K_{zx} \frac{\partial \Phi_j^m}{\partial x} + K_{zy} \frac{\partial \Phi_j^m}{\partial y} + K_{zz} \frac{\partial \Phi_j^m}{\partial z} \right)_l A_{z,l}, \end{aligned} \quad (3.14)$$

If  $l$  is equal to  $e$ , for instance, we can evaluate the gradient at this interface, as

$$\left( \frac{\partial \Phi_j^m}{\partial x} \right)_{l=e} = \frac{2}{\Delta x_E + \Delta x_P} \left[ (P_{j,E}^{n+1} - P_{j,P}^{n+1}) + (P_{cjr,E}^m - P_{cjr,P}^m) - \rho_{j,e}^m g (D_E - D_P) \right], \quad (3.15)$$

where

$$\rho_{j,e}^{n+1,n} = \frac{V_{p,P}^m}{V_{p,P}^m + V_{p,E}^m} \rho_{j,P}^m + \frac{V_{p,E}^m}{V_{p,P}^m + V_{p,E}^m} \rho_{j,E}^m. \quad (3.16)$$

For Cartesian grids, the normal vectors to the faces are always aligned to one of the Cartesian coordinates. Therefore, for the faces  $e$  and  $w$ , which are aligned to the  $x$  direction, the normal vector hasn't any component in  $y$  and  $z$  directions. Additionally, the cross derivatives, such as a derivative of the potential with respect to  $y$  in a face  $e$  or  $w$  is neglected, because in general a diagonal tensor is used for Cartesian grids. Therefore, for the face  $e$ , Eq. (3.14) is simplified to

$$\left[ \bar{\bar{K}} \cdot \vec{\nabla} \Phi_j^m \cdot \vec{A} \right]_e = \left( K_{xx} \frac{\partial \Phi_j^m}{\partial x} \right)_e A_{x,e}, \quad (3.17)$$

where

$$A_{x,e} = \Delta y_p \Delta z_p. \quad (3.18)$$

In computational fluid dynamics is common to define transmissibilities which takes into account geometrical and conductivity parameters. For the face  $e$ , the transmissibility is given as

$$T_e = K_{xx,e} \frac{2A_{x,e}}{\Delta x_E + \Delta x_P}. \quad (3.19)$$

The transmissibilities are convenient since it accounts only for the geometrical and the permeability terms, which will be constant for the whole simulation and will simplify the writing of the equations. The transmissibilities for the other faces are obtained in a similar way of Eq. (3.19).

With all these assumptions, Eq. (3.13) becomes

$$\begin{aligned} (N_{k,P}^{n+1} - N_{k,P}^n) = \Delta t \sum_{j=2}^{n_p} \sum_{l=1}^{n_f} \left\{ (x_{kj}^m \xi_j^m \lambda_j^m)_l T_l \left[ \Delta P_l^{n+1} + \Delta P_{cjr,l}^m - \rho_{j,l}^m g \Delta D_l \right] \right\} \\ - \Delta t \dot{q}_{k,P}^m, \quad k = 1, \dots, n_c, \end{aligned} \quad (3.20)$$

where the operator  $\Delta$  is defined for a face  $l$  such that

$$\Delta P_l = P_L - P_P, \quad (3.21)$$

and the subscript  $L$  refers to the neighborhood control volume that shares the face  $l$  with the control volume  $P$ .

For the Cartesian mesh, all physical properties are evaluated at the center of each control volume. However, as we can see in Eq. (3.20) it is necessary to extrapolate physical properties like molar density, mole fraction, relative permeability, and viscosity from the center of the control volume to the control volume interfaces. For all approaches investigated in this work, we use the upwind scheme for both Cartesian and EbFVM. The upwind scheme considering the mobility, for instance, at the east interface of control volume  $P$  shown in Figure 3.1, is computed as

$$\lambda_j^m \Big|_e = \begin{cases} \lambda_{j,P}^m & \text{if } F_j^m \Big|_e \leq 0 \\ \lambda_{j,E}^m & \text{if } F_j^m \Big|_e > 0 \end{cases}. \quad (3.22)$$

A similar approach is performed for the EbFVM that will be shown later in this chapter.

The pressure equation is finally written for Cartesian grids as

$$\left[ V_{b,P} \phi_P^0 C_f - \frac{\partial V_{T,P}^n}{\partial P} \right] (P_P^{n+1} - P_P^n) = (V_{T,P}^n - V_{p,P}^n) + \sum_{k=1}^{n_c+1} \bar{V}_{Tk,P}^n (N_{k,P}^{n+1} - N_{k,P}^n). \quad (3.23)$$

The same process can be performed for the saturation equation, Eq. (3.5). However, the expression for the mole rate will be computed in a different way. This expression is obtained from Eq. (3.5) for the control volume  $P$  shown in Figure 3.1 as

$$(N_{k,P}^{n+1} - N_{k,P}^n) = -\Delta t \sum_{j=2}^{n_p} \sum_{l=1}^{n_f} \vec{\nabla} \cdot (x_{kj}^n \xi_j^n \vec{U}_j^{n+1} \cdot \vec{A})_l - \Delta t \dot{q}_{k,P}^n, \quad k = 1, \dots, n_c, \quad (3.24)$$

or

$$(N_{k,P}^{n+1} - N_{k,P}^n) = -\Delta t \sum_{j=2}^{n_p} \sum_{l=1}^{n_f} \vec{\nabla} \cdot (x_{kj}^n \xi_j^n F_j^{n+1})_l - \Delta t \dot{q}_{k,P}^n, \quad k = 1, \dots, n_c, \quad (3.25)$$

where

$$F_{j,l}^{n+1} = f_{rj,l}^{n+1} F_{T,l}^{n+1} - f_{rj,l}^{n+1} \left[ \sum_{s=1}^{n_p} \lambda_{s,l}^{n+1} T_l (\Delta P_{csr,l}^{n+1} - \Delta P_{cjr,l}^{n+1}) + \sum_{s=1}^{n_p} \lambda_{s,l}^{n+1} (\rho_{s,l}^n - \rho_{j,l}^n) g T_l \Delta D_l \right], \quad (3.26)$$

and

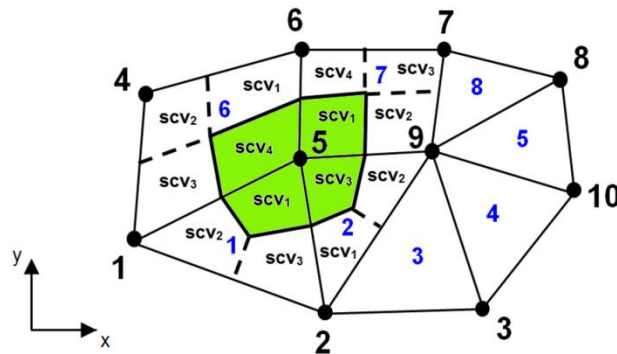
$$F_{T,i}^{n+1} = \vec{U}_{T,i}^{n+1} \cdot \vec{A}_i. \quad (3.27)$$

A similar procedure is performed to obtain the net molar flow of water.

### 3.1.2 EbFVM grid discretization

In the EbFVM approach, the domain is discretized by elements, and each element is divided into sub-elements according to the number of vertices. Next, the conservative equations are integrated for each one of these sub-elements. These sub-elements are called sub-control volumes (SCV). After the conservative equations are integrated to each one of these sub-control volumes, we assemble the control volume (CV) equations by obtaining the contributions of all sub-control volumes that shares the same vertex of the grid. This feature is called dual mesh and gives rise to a cell-vertex approach. The great advantage of this approach is that all calculations are based on the elements of the grid. An illustration of the dual mesh is shown in Figure 3.2. As presented in Figure 3.2, the blue labels represent the elements and the black labels represent the control volumes. The control volume associated with vertex 5 of the grid shown in Fig. 3.2 is given by green area.

Figure 3.2 – Illustration of a dual mesh for the EbFVM approach.



Shape functions are used to interpolate any property inside an element, including the gradient. Figure 3.3 shows the triangle and quadrilateral elements in the physical and computational planes that are used for 2D calculations. All the integrations are performed at the computational planes. In this way, the calculations are identically, no matter an element can be distorted in the physical plane. The shape functions are written, for an arbitrary property (including physical coordinates)  $\phi$  inside an element, so that

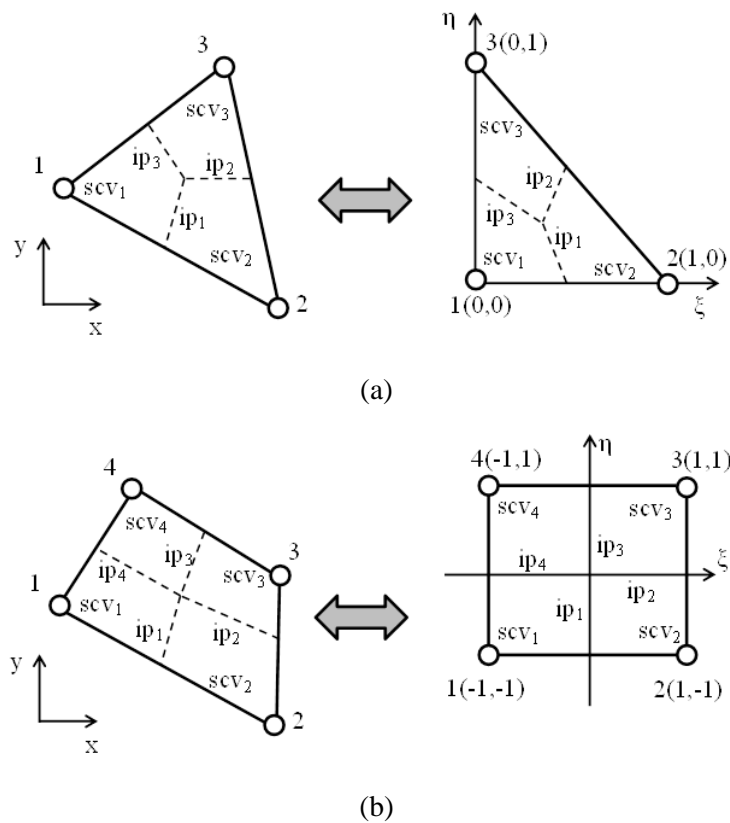
$$\phi(\xi, \eta, \gamma) = \sum_{i=1}^{n_v} N_i(\xi, \eta, \gamma) \Phi_i, \quad (3.28)$$

where  $\Phi$  is the value of the property evaluated at the nodes,  $\xi$ ,  $\eta$  and  $\gamma$  are the local plane coordinates, and  $N$  is the shape function. For 2D elements, triangles and quadrilaterals, the shape functions are respectively, given by

$$N_1(\xi, \eta) = 1 - \xi - \eta; \quad N_2(\xi, \eta) = \xi; \quad N_3(\xi, \eta) = \eta, \quad (3.29)$$

$$\begin{aligned} N_1(\xi, \eta) &= \frac{1}{4}(1 - \xi)(1 - \eta); & N_2(\xi, \eta) &= \frac{1}{4}(1 + \xi)(1 - \eta); \\ N_3(\xi, \eta) &= \frac{1}{4}(1 + \xi)(1 + \eta); & N_4(\xi, \eta) &= \frac{1}{4}(1 - \xi)(1 + \eta). \end{aligned} \quad (3.30)$$

Figure 3.3 – 2D elements in the physical and computational planes. a) Triangle element; b) quadrilateral element.



For 3D discretization four types of elements (Fig. 3.4) can be used: hexahedron, tetrahedron, prism, and pyramid. In general, prism and pyramid are considered transition elements because they allow the use of mixed grids combining in the same grid hexahedron and tetrahedron elements. Since prism and pyramid match the triangular areas of tetrahedron and quadrangular areas of the hexahedron these elements are used between hexahedron and tetrahedron elements. Once hexahedron has more vertices, it should be used in most parts of the reservoir. However, the tetrahedron is more indicated to perform local grid refinement,

specially around wells, fractures, and discrete fractures. The shape functions for the hexahedron, tetrahedron, prism, and pyramid elements are respectively, given by

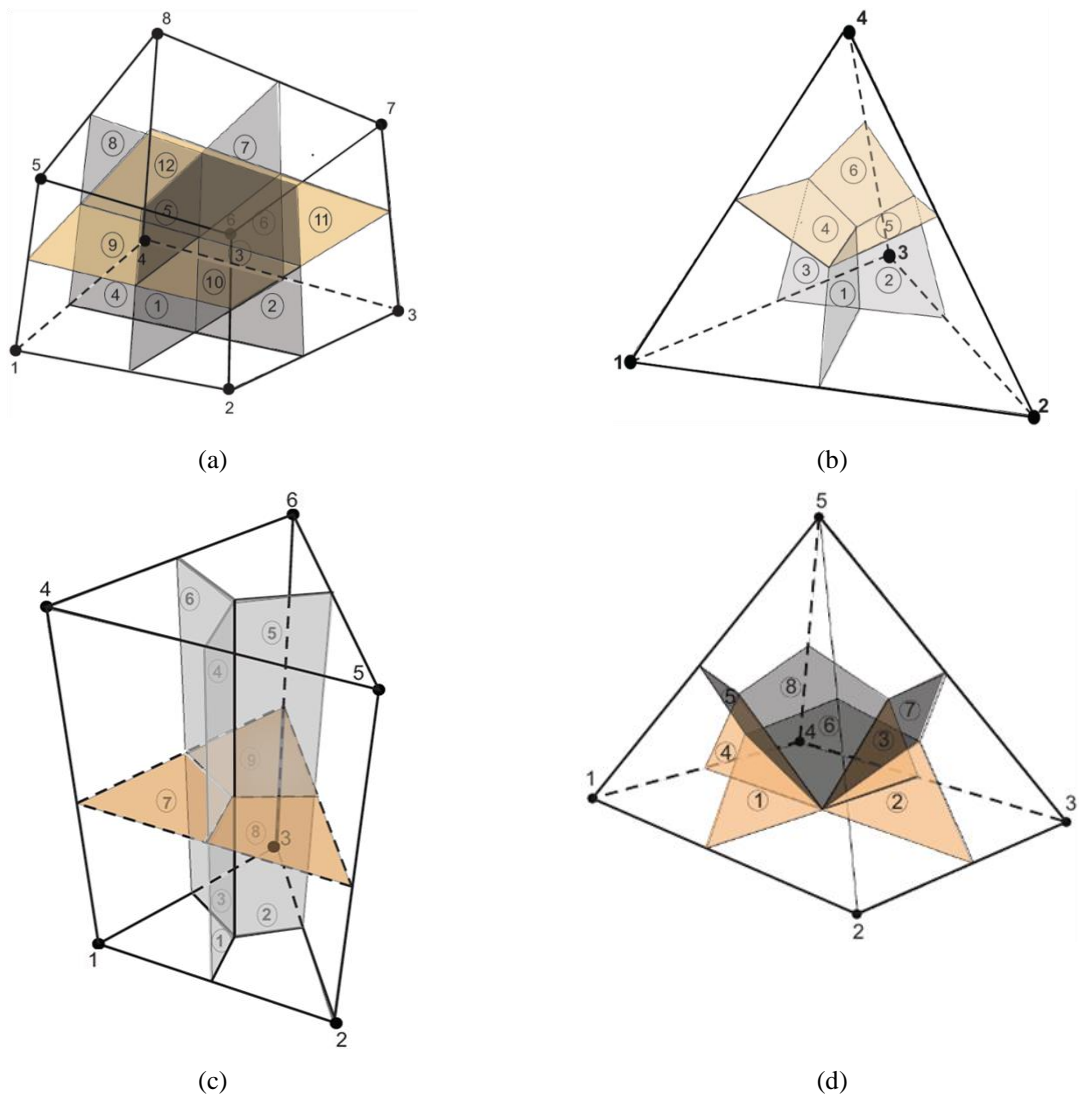
$$\begin{aligned}
 N_1(\xi, \eta, \gamma) &= \frac{1}{8}(1+\xi)(1-\eta)(1+\gamma); & N_2(\xi, \eta, \gamma) &= \frac{1}{8}(1+\xi)(1-\eta)(1-\gamma); \\
 N_3(\xi, \eta, \gamma) &= \frac{1}{8}(1-\xi)(1-\eta)(1-\gamma); & N_4(\xi, \eta, \gamma) &= \frac{1}{8}(1-\xi)(1-\eta)(1+\gamma); \\
 N_5(\xi, \eta, \gamma) &= \frac{1}{8}(1+\xi)(1+\eta)(1+\gamma); & N_6(\xi, \eta, \gamma) &= \frac{1}{8}(1+\xi)(1+\eta)(1-\gamma); \\
 N_7(\xi, \eta, \gamma) &= \frac{1}{8}(1-\xi)(1+\eta)(1-\gamma); & N_8(\xi, \eta, \gamma) &= \frac{1}{8}(1-\xi)(1+\eta)(1+\gamma),
 \end{aligned} \tag{3.31}$$

$$N_1(\xi, \eta, \gamma) = 1 - \xi - \eta - \gamma; \quad N_2(\xi, \eta, \gamma) = \xi; \quad N_3(\xi, \eta, \gamma) = \eta; \quad N_4(\xi, \eta, \gamma) = \gamma, \tag{3.32}$$

$$\begin{aligned}
 N_1(\xi, \eta, \gamma) &= (1 - \xi - \eta)(1 - \gamma); & N_2(\xi, \eta, \gamma) &= \xi(1 - \gamma); \\
 N_3(\xi, \eta, \gamma) &= \eta(1 - \gamma); & N_4(\xi, \eta, \gamma) &= \gamma(1 - \xi - \eta); \\
 N_5(\xi, \eta, \gamma) &= \xi\gamma; & N_6(\xi, \eta, \gamma) &= \eta\gamma,
 \end{aligned} \tag{3.33}$$

$$\begin{aligned}
 N_1(\xi, \eta, \gamma) &= \frac{1}{4} \left[ (1 - \xi)(1 - \eta) - \gamma + \frac{\xi\eta\gamma}{1 - \gamma} \right]; \\
 N_2(\xi, \eta, \gamma) &= \frac{1}{4} \left[ (1 + \xi)(1 - \eta) - \gamma - \frac{\xi\eta\gamma}{1 - \gamma} \right]; \\
 N_3(\xi, \eta, \gamma) &= \frac{1}{4} \left[ (1 + \xi)(1 + \eta) - \gamma - \frac{\xi\eta\gamma}{1 - \gamma} \right]; \\
 N_4(\xi, \eta, \gamma) &= \frac{1}{4} \left[ (1 - \xi)(1 + \eta) - \gamma - \frac{\xi\eta\gamma}{1 - \gamma} \right]; \\
 N_5(\xi, \eta, \gamma) &= \gamma,
 \end{aligned} \tag{3.34}$$

Figure 3.4 – 3D elements into the physical plane and computational local plane. a) Hexahedron element; b) tetrahedron element; c) prism element; d) pyramid element.



The gradient inside any element are evaluated using the shape functions as

$$\frac{\partial \phi}{\partial x} = \sum_{i=1}^{n_v} \frac{\partial N_i}{\partial x} \Phi_i; \quad \frac{\partial \phi}{\partial y} = \sum_{i=1}^{n_v} \frac{\partial N_i}{\partial y} \Phi_i; \quad \frac{\partial \phi}{\partial z} = \sum_{i=1}^{n_v} \frac{\partial N_i}{\partial z} \Phi_i. \quad (3.35)$$

The derivatives of the shape functions with respect to x, y and z are obtained for 3D elements as

$$\begin{aligned} \frac{\partial N_i}{\partial x} &= \frac{1}{\det(J_i)} \left[ \left( \frac{\partial y}{\partial \eta} \frac{\partial z}{\partial \gamma} - \frac{\partial y}{\partial \gamma} \frac{\partial z}{\partial \eta} \right) \frac{\partial N_i}{\partial \xi} - \left( \frac{\partial y}{\partial \xi} \frac{\partial z}{\partial \gamma} - \frac{\partial y}{\partial \gamma} \frac{\partial z}{\partial \xi} \right) \frac{\partial N_i}{\partial \eta} + \left( \frac{\partial y}{\partial \xi} \frac{\partial z}{\partial \eta} - \frac{\partial y}{\partial \eta} \frac{\partial z}{\partial \xi} \right) \frac{\partial N_i}{\partial \gamma} \right]; \\ \frac{\partial N_i}{\partial y} &= \frac{1}{\det(J_i)} \left[ \left( \frac{\partial x}{\partial \eta} \frac{\partial z}{\partial \gamma} - \frac{\partial x}{\partial \gamma} \frac{\partial z}{\partial \eta} \right) \frac{\partial N_i}{\partial \xi} + \left( \frac{\partial x}{\partial \xi} \frac{\partial z}{\partial \gamma} - \frac{\partial x}{\partial \gamma} \frac{\partial z}{\partial \xi} \right) \frac{\partial N_i}{\partial \eta} - \left( \frac{\partial x}{\partial \xi} \frac{\partial z}{\partial \eta} - \frac{\partial x}{\partial \eta} \frac{\partial z}{\partial \xi} \right) \frac{\partial N_i}{\partial \gamma} \right]; \\ \frac{\partial N_i}{\partial z} &= \frac{1}{\det(J_i)} \left[ \left( \frac{\partial x}{\partial \eta} \frac{\partial y}{\partial \gamma} - \frac{\partial x}{\partial \gamma} \frac{\partial y}{\partial \eta} \right) \frac{\partial N_i}{\partial \xi} - \left( \frac{\partial x}{\partial \xi} \frac{\partial y}{\partial \gamma} - \frac{\partial x}{\partial \gamma} \frac{\partial y}{\partial \xi} \right) \frac{\partial N_i}{\partial \eta} + \left( \frac{\partial x}{\partial \xi} \frac{\partial y}{\partial \eta} - \frac{\partial x}{\partial \eta} \frac{\partial y}{\partial \xi} \right) \frac{\partial N_i}{\partial \gamma} \right], \end{aligned} \quad (3.36)$$

where

$$\det(J_t) = \frac{\partial x}{\partial \xi} \left( \frac{\partial y}{\partial \eta} \frac{\partial z}{\partial \gamma} - \frac{\partial y}{\partial \gamma} \frac{\partial z}{\partial \eta} \right) - \frac{\partial x}{\partial \eta} \left( \frac{\partial y}{\partial \xi} \frac{\partial z}{\partial \gamma} - \frac{\partial y}{\partial \gamma} \frac{\partial z}{\partial \xi} \right) + \frac{\partial x}{\partial \gamma} \left( \frac{\partial y}{\partial \xi} \frac{\partial z}{\partial \eta} - \frac{\partial y}{\partial \eta} \frac{\partial z}{\partial \xi} \right). \quad (3.37)$$

For 2D elements a similar expression is obtained:

$$\frac{\partial N_i}{\partial x} = \frac{1}{\det(J_t)} \left( \frac{\partial y}{\partial \eta} \frac{\partial N_i}{\partial \xi} - \frac{\partial y}{\partial \xi} \frac{\partial N_i}{\partial \eta} \right); \quad \frac{\partial N_i}{\partial y} = \frac{1}{\det(J_t)} \left( \frac{\partial x}{\partial \xi} \frac{\partial N_i}{\partial \eta} - \frac{\partial x}{\partial \eta} \frac{\partial N_i}{\partial \xi} \right), \quad (3.38)$$

where

$$\det(J_t) = \left( \frac{\partial x}{\partial \xi} \frac{\partial y}{\partial \eta} - \frac{\partial x}{\partial \eta} \frac{\partial y}{\partial \xi} \right). \quad (3.39)$$

The interfaces for 3D elements are computed as

$$d\vec{A} = \left( \frac{\partial y}{\partial m} \frac{\partial z}{\partial n} - \frac{\partial y}{\partial n} \frac{\partial z}{\partial m} \right) dmdn\hat{i} - \left( \frac{\partial x}{\partial n} \frac{\partial z}{\partial m} - \frac{\partial x}{\partial m} \frac{\partial z}{\partial n} \right) dmdn\hat{j} + \left( \frac{\partial x}{\partial m} \frac{\partial y}{\partial n} - \frac{\partial x}{\partial n} \frac{\partial y}{\partial m} \right) dmdn\hat{k}, \quad (3.40)$$

where  $m$  and  $n$  are any of the coordinates  $\xi$ ,  $\eta$  or  $\gamma$ . For 2D elements, the area of each interface, reading a counterclockwise, is given by

$$d\vec{A} = h(dy\hat{i} - dx\hat{j}), \quad (3.41)$$

where  $h$  is the thickness of the reservoir. Further details of the above expressions can be found in (Maliska, 2004; Marcondes and Sepehrnoori, 2010).

For the EbFVM approach, the integral of each term for a control volume can be performed for each SCV. Therefore, the calculations are performed in each SCV and then summed up in order to obtain the closure of the balance equations for each CV. These calculations are computed in an element level. For the mole balance equations, for instance, the integration in space and time, for the sub-control volumes of each element of the grid, can be written as

$$A_{cc_i}^{N_k} - F_{adv_i}^{N_k} - S_i^{N_k} = 0, \quad k = 1, \dots, n_c + 1; \quad i = 1, \dots, n_v, \quad (3.42)$$

where  $n_v$  is the number of vertices of the element;  $A_{cc_k,i}$  denotes the accumulation term of component  $k$  into SCV  $i$ ;  $F_{adv_k,i}$  denotes the advective net flux of component  $k$  across the SCV  $i$  faces; and  $S_{k,i}$  denotes the source/sink (wells) term of component  $k$  into SCV  $i$ . These terms for the hydrocarbon components and water are given bellow, where  $n_c+1$  denotes the water component.



$$A_{cc_i}^{Nk} = \left( \frac{N_{k,i}^{n+1} - N_{k,i}^n}{V_{b,i}} \right) V_{scv_i}, \quad k = 1, \dots, n_c + 1; \quad i = 1, \dots, n_v, \quad (3.43)$$

$$F_{adv_i}^{Nk} = \Delta t \sum_{j=2}^{n_p} \int_{A_i} \left( x_{kj}^m \xi_j^m \frac{k_{rj}^m}{\mu_j^m} \bar{\bar{K}} \cdot \bar{\nabla} (P^{n+1} + P_{cjr}^m - \rho_j^m gD) \right) \cdot d\bar{A}_i, \quad k = 1, \dots, n_c; \quad i = 1, \dots, n_v, \quad (3.44)$$

$$F_{cc_i}^{N_{n_c+1}} = \Delta t \int_{A_i} \left( \xi_w^m \frac{k_{rw}^m}{\mu_w^m} \bar{\bar{K}} \cdot \bar{\nabla} (P^{n+1} + P_{cwr}^m - \rho_w^m gD) \right) \cdot d\bar{A}_i, \quad i = 1, \dots, n_v, \quad (3.45)$$

and

$$S_i^{Nk} = -\Delta t \frac{V_{SCV_i}}{V_{b,i}} \dot{q}_{k,i}, \quad k = 1, \dots, n_c + 1; \quad i = 1, \dots, n_v, \quad (3.46)$$

where  $V_{SCV_i}$  is the volume of SCV  $i$ .

The integration of the advective terms (Eq. (3.43) and (3.44)) can be approximated by the summation over the SCV faces, which are usually named integration points (IP). For Eq. (3.43), it can be written as

$$F_{adv_i}^{Nk} = \Delta t \sum_{j=2}^{n_p} \sum_{l=1}^{n_{ip}} \left[ \left( x_{kj}^m \xi_j^m \frac{k_{rj}^m}{\mu_j^m} \bar{\bar{K}} \cdot \bar{\nabla} (P^{n+1} + P_{cjr}^m - \rho_j^m gD) \right) \cdot d\bar{A}_l \right], \quad (3.47)$$

$$k = 1, \dots, n_c; \quad i = 1, \dots, n_v,$$

where  $n_{ip}$  is the number of integration points of SCV  $i$ . For 2D elements (triangles and quadrilaterals), the number of integration points is always two. For 3D elements, the number of integration points of a given SCV is usually three, except for the sub-control volume associated with the apex of the pyramid, which has four integration points, please see Fig. 3.4d.

Approximating the gradients in Eq. (3.47) with the expressions of Eq. (3.35) yields

$$F_{adv_i}^{Nk} = \Delta t \sum_{j=2}^{n_p} \sum_{l=1}^{n_{ip}} \left[ \left( x_{kj}^m \xi_j^m \frac{k_{rj}^m}{\mu_j^m} \bar{\bar{K}} \cdot \sum_{h=1}^{n_v} \bar{\nabla} N_h (P_h^m + P_{cjr,h}^m - \rho_{j,elem}^m gD_h) \right) \cdot d\bar{A}_l \right], \quad (3.48)$$

$$k = 1, \dots, n_c; \quad i = 1, \dots, n_v,$$

where  $N$  in Eq. (3.48) stands for the shape function at integration point  $l$  and  $elem$  denotes the element where the calculations are performed. The mass density of the element that is necessary to compute the gravity term is evaluated as the volumetric mean of the densities of

all vertices of the element. Only nodes where the phase exists are considered into this calculation. This calculation option was selected after testing several approaches.

Although, the transmissibility concept is valid when the flux is evaluated using only two vertices, it is possible to define a pseudo-transmissibility for the EbFVM as

$$T_{ihl} = \bar{\bar{K}}_l \cdot \bar{\nabla} N_{h,l} \cdot d\bar{A}_l, \quad (3.49)$$

where  $T_{ihl}$  is the transmissibility of integration point  $l$  related to SCV  $i$  which is multiplied by the property of vertex  $h$ . Therefore, Eq. (3.48) is written as

$$F_{adv_i}^{N_k} = \Delta t \sum_{j=2}^{n_p} \sum_{l=1}^{n_{ip}} \left[ \left( x_{kj}^m \xi_j^m \frac{k_{rj}^m}{\mu_j^m} \sum_{h=1}^{n_v} T_{ihl} (P_h^m + P_{cjr,h}^m - \rho_{j,elem}^m g D_h) \right) \right]_l, \quad (3.50)$$

$$k = 1, \dots, n_c; \quad i = 1, \dots, n_v.$$

For the pressure equation (Eq. (3.1)), the accumulation, advection, and well terms are respectively, written as

$$A_{cc_i}^P = \left[ V_{scv_i} \phi_{elem}^0 C_f - \frac{V_{scv_i}}{V_{b,i}} \frac{\partial V_{T,i}^n}{\partial P} \right] (P_i^{n+1} - P_i^n) - \frac{V_{scv_i}}{V_{b,i}} (V_{T,i}^n - V_{p,i}^n), \quad i = 1, \dots, n_v, \quad (3.51)$$

$$F_{adv_i}^P = \Delta t \bar{V}_{Tw,i}^n \sum_{l=1}^{n_{ip}} \left[ \left( \xi_w^m \frac{k_{rw}^m}{\mu_w^m} \sum_{h=1}^{n_v} T_{ihl} (P_h^m + P_{cwr,h}^m - \rho_{w,elem}^m g D_h) \right) \right]_l \\ + \Delta t \sum_{k=1}^{n_c} \bar{V}_{Tk,i}^n \sum_{j=2}^{n_p} \sum_{l=1}^{n_{ip}} \left[ \left( x_{kj}^m \xi_j^m \frac{k_{rj}^m}{\mu_j^m} \sum_{h=1}^{n_v} T_{ihl} (P_h^m + P_{cjr,h}^m - \rho_{j,elem}^m g D_h) \right) \right]_l, \quad (3.52)$$

$$i = 1, \dots, n_v,$$

$$S_i^P = \Delta t \sum_{k=1}^{n_c+1} \bar{V}_{Tk,i}^n \frac{V_{SCV_i}}{V_{b,i}} \dot{q}_{k,i}^m, \quad i = 1, \dots, n_v. \quad (3.53)$$

Performing a similar process, we obtain the saturation equation as

$$A_{cc_i}^S = V_{scv_i} \phi_{elem}^{n+1} S_{\ell,i}^{n+1} + \frac{V_{scv_i}}{V_{b,i}} \frac{\partial V_{T,i}^n}{\partial P} (P_i^{n+1} - P_i^n) - \frac{V_{scv_i}}{V_{b,i}} V_{\ell,i}^n, \quad i = 1, \dots, n_v, \quad (3.54)$$

$$F_{adv_i}^S = \Delta t \bar{V}_{\ell w,i}^n \sum_{l=1}^{n_{ip}} \left[ \left( \xi_w^n F_{w,i}^{n+1} \right) \right]_l + \Delta t \sum_{k=1}^{n_c} \bar{V}_{\ell k,i}^n \sum_{j=2}^{n_p} \sum_{l=1}^{n_{ip}} \left[ \left( x_{kj}^n \xi_j^n F_{j,i}^{n+1} \right) \right]_l, \quad (3.55)$$

$$i = 1, \dots, n_v,$$

$$S_i^S = \Delta t \sum_{k=1}^{n_c+1} \bar{V}_{\ell k,i}^n \frac{V_{SCV_i}}{V_{b,i}} \dot{q}_{k,i}^n, \quad i = 1, \dots, n_v; \quad (3.56)$$

where

$$F_{j,il}^{n+1} = f_{rj,l}^{n+1} F_{T,il}^{n+1} - f_{rj,l}^{n+1} \left[ \sum_{s=1}^{n_p} \lambda_s^{n+1} \sum_{v=1}^{n_v} T_{ivl} (P_{csr,v}^{n+1} - P_{cjr,v}^{n+1}) + \sum_{s=1}^{n_p} \lambda_s^{n+1} (\rho_{s,elem}^n - \rho_{j,elem}^n) g \sum_{v=1}^{n_v} T_{ivl} D_v \right]_l. \quad (3.57)$$

### 3.2 Time-step size selection

In UTCOMP, four time-step selection criterion are available. These criteria are used to control the increasing or decreasing of the time-step during the simulation. The four criteria are pressure variation, saturations variation, total mole variation and total volume error. Each of these criteria are given as

$$\Delta t_p = \Delta t^n \frac{\Delta P_{lim}}{|\Delta P|_{max}}, \quad (3.58)$$

$$\Delta t_s = \Delta t^n \frac{\Delta S_{lim}}{|\Delta S|_{max}}, \quad (3.59)$$

$$\Delta t_n = \Delta t^n \frac{\Delta N_{lim}}{|\Delta N|_{max}}, \quad (3.60)$$

and

$$\Delta t_v = \Delta t^n \frac{\Delta V_{lim}}{|\Delta V|_{max}}, \quad (3.61)$$

where

$$|\Delta P|_{max} = \max(|\Delta P|_i), \quad i = 1, \dots, n_b, \quad (3.62)$$

$$|\Delta S|_{max} = \max(|\Delta S|_{ij}), \quad i = 1, \dots, n_b, \quad j = 1, \dots, n_p, \quad (3.63)$$

$$|\Delta N|_{max} = \max(|\Delta N|_{ik}), \quad i = 1, \dots, n_b, \quad k = 1, \dots, n_c + 1, \quad (3.64)$$

and

$$|\Delta V|_{\max} = \max(|\Delta V|_i), \quad i = 1, \dots, n_b, \quad (3.65)$$

and the variation for each grid-block is computed as

$$|\Delta P|_i = \frac{|P_i^{n+1} - P_i^n|}{P_i^{n+1}}, \quad i = 1, \dots, n_b, \quad (3.66)$$

$$|\Delta S|_{ij} = |S_{j,i}^{n+1} - S_{j,i}^n|, \quad i = 1, \dots, n_b, \quad j = 1, \dots, n_p, \quad (3.67)$$

$$|\Delta N|_{ik} = \frac{|N_{k,i}^{n+1} - N_{k,i}^n|}{N_{k,i}^{n+1}}, \quad i = 1, \dots, n_b, \quad k = 1, \dots, n_c + 1, \quad (3.68)$$

and

$$|\Delta V|_i = \frac{|V_{T,i}^{n+1} - V_{p,i}^{n+1}|}{V_{p,i}^{n+1}}, \quad i = 1, \dots, n_b. \quad (3.69)$$

Finally, the new time-step size is computed as

$$\Delta t^{n+1} = \min(\Delta t_p, \Delta t_s, \Delta t_n, \Delta t_v). \quad (3.70)$$

The parameters  $\Delta P_{lim}$ ,  $\Delta S_{lim}$ ,  $\Delta N_{lim}$ , and  $\Delta V_{lim}$  are adjusted empirically to obtain the best stable time-step sizes for each simulation.

## 4 FORMULATIONS

This chapter will present the algorithms for each formulation implemented in this work. Six formulations will be presented here. The first one presented is the original IMPEC formulation of Ács et al. (1985) originally implemented in the UTCOMP simulator for Cartesian grids by Chang (1990) and later extended for 2D EbFVM by Fernandes (2011) and Fernandes et al. (2012); and for 3D EbFVM by Araújo et al. (2013). The other formulations were implemented as a contribution of this work for Cartesian and unstructured grids in conjunction with the EbFVM.

### 4.1 Ács et al. (IMPEC)

The flow equations needed by the Ács et al. (1985) formulation are the pressure equation and the  $n_c+1$  mole balance equations. This is an IMPEC formulation, hence only pressure is computed implicitly by setting all  $m$  parameters to  $n$ . The degree of implicitness of each equation can be clearly seen bellow. Notice that only time integration was performed for the equations of pressure, total number of moles of each hydrocarbon component, and number of moles of water that are respectively shown below:

$$\left[ \phi^0 C_f - \frac{1}{V_b} \frac{\partial V_T^n}{\partial P} \right] (P^{n+1} - P^n) = \frac{(V_T^n - V_p^n)}{V_b} + \Delta t \sum_{k=1}^{n_c} \bar{V}_{Tk}^n \left\{ \sum_{j=2}^{n_p} \bar{\nabla} \cdot \left( x_{kj}^n \xi_j^n \frac{k_{rj}^n}{\mu_j^n} \bar{K} \cdot \bar{\nabla} (P^{n+1} + P_{cjr}^n - \rho_j^n gD) \right) - \frac{\dot{q}_k^n}{V_b} \right\}, \quad (4.1)$$

$$+ \Delta t \bar{V}_{Tw}^n \left\{ \bar{\nabla} \cdot \left( \xi_w^n \frac{k_{rw}^n}{\mu_w^n} \bar{K} \cdot \bar{\nabla} (P^{n+1} + P_{cwr}^n - \rho_w^n gD) \right) - \frac{\dot{q}_w^n}{V_b} \right\}$$

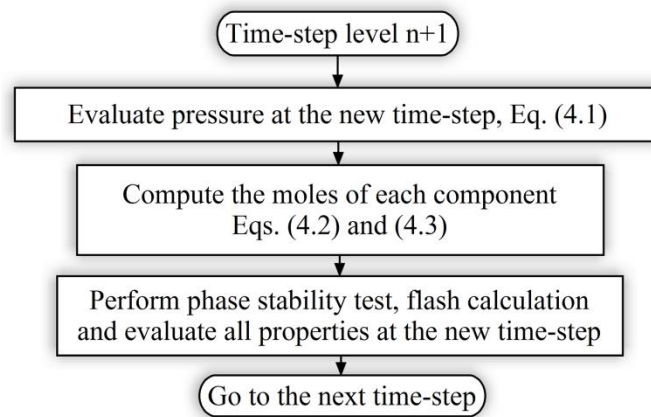
$$\frac{N_k^{n+1} - N_k^n}{V_b} = \Delta t \left\{ \sum_{j=2}^{n_p} \bar{\nabla} \cdot \left( x_{kj}^n \xi_j^n \frac{k_{rj}^n}{\mu_j^n} \bar{K} \cdot \bar{\nabla} (P^{n+1} + P_{cjr}^n - \rho_j^n gD) \right) - \frac{\dot{q}_k^n}{V_b} \right\} \quad k = 1, \dots, n_c, \quad (4.2)$$

$$\frac{N_w^{n+1} - N_w^n}{V_b} = \Delta t \left\{ \bar{\nabla} \cdot \left( \xi_w^n \frac{k_{rw}^n}{\mu_w^n} \bar{K} \cdot \bar{\nabla} (P^{n+1} + P_{cwr}^n - \rho_w^n gD) \right) - \frac{\dot{q}_w^n}{V_b} \right\}. \quad (4.3)$$

This formulation uses a discretized form of Eq. (4.1) to solve pressure, and then uses this new pressure to compute the moles of each component at the new time-step level through integrated forms of Eqs. (4.2) and (4.3). As the integration process was already explained, it will no longer be discussed here. Equation (4.1) will generate a linear set of equations. We use the PETSC package's solver (Balay et al., 1997; Balay et al., 2013; Balay et al., 2014) for solving the linear systems arising from all formulations and discretization presented in this work.

The flowchart of the IMPEC formulation is presented in Figure 4.1.

Figure 4.1 – Flowchart of the IMPEC formulation for a time-step.



Notice that in this formulation, the saturations at the new time-step level are computed only after the flash calculation through Eqs. (2.59) and (2.60). This formulation will be called in this work by just IMPEC.

#### 4.2 Watts (*IMPSAT-0*)

In this formulation, the pressure is solved in the same way as the Ács et al. (1985) formulation, (Eq. 4.1). Therefore, pressure is solved considering explicit relative permeabilities and capillary pressures. Since these properties are function of the saturation, they may drastically change when a new saturation is computed, which would provide a different volumetric flux from that used to solve pressure. To avoid it, a semi-implicit total velocity (or flux) is used to write the saturation equation. The saturation equation written in terms of the total velocity is given by

$$\begin{aligned}
S_\ell^{n+1} \phi^{n+1} &= \frac{V_\ell^n}{V_b} + \frac{1}{V_b} \frac{\partial V_\ell^n}{\partial P} (P^{n+1} - P^n) - \Delta t \sum_{k=1}^{n_c} \bar{V}_{\ell k}^n \left\{ \sum_{j=2}^{n_p} \bar{\nabla} \cdot (x_{kj}^n \xi_j^n \bar{U}_j^{n+1}) + \frac{\dot{q}_k^{n+1}}{V_b} \right\} \\
-\Delta t \bar{V}_{\ell w}^n &\left\{ \bar{\nabla} \cdot (\xi_w^n \bar{U}_w^{n+1}) + \frac{\dot{q}_w^{n+1}}{V_b} \right\}, \quad \ell = 1, \dots, n_p
\end{aligned} \tag{4.5}$$

Where the phase velocity, phase mobility and total velocity are respectively, given by

$$\begin{aligned}
\bar{U}_j^{n+1} &= f_{rj}^{n+1} \bar{U}_T^{n+1} \\
&+ f_{rj}^{n+1} \left[ \sum_{m=1}^{n_p} \lambda_m^{n+1} \bar{K} \cdot (\bar{\nabla} P_{cmr}^{n+1} - \bar{\nabla} P_{cjr}^{n+1}) - \sum_{m=1}^{n_p} \lambda_m^{n+1} (\rho_m^n - \rho_j^n) g \bar{K} \cdot \bar{\nabla} D \right],
\end{aligned} \tag{4.6}$$

$$\lambda_j^{n+1} = \frac{k_{rj}^{n+1}}{\mu_j^n}, \tag{4.7}$$

$$\bar{U}_T^{n+1} = - \sum_{m=1}^{n_p} \lambda_m^n \bar{K} \cdot \bar{\nabla} (P^{n+1} + P_{cmr}^n - \rho_m^n g \bar{\nabla} D), \tag{4.8}$$

and

$$\lambda_j^n = \frac{k_{rj}^n}{\mu_j^n}, \tag{4.9}$$

Equations (4.5) through (4.9) are solved together using the Newton-Raphson method.

The total number of moles at the new time-step level is then solved by using the same velocities that were used for the saturations:

$$\frac{N_k^{n+1} - N_k^n}{V_b} = -\Delta t \left\{ \sum_{j=2}^{n_p} \bar{\nabla} \cdot (x_{kj}^n \xi_j^n \bar{U}_j^{n+1}) + \frac{\dot{q}_k^{n+1}}{V_b} \right\}, \quad k = 1, \dots, n_c. \tag{4.10}$$

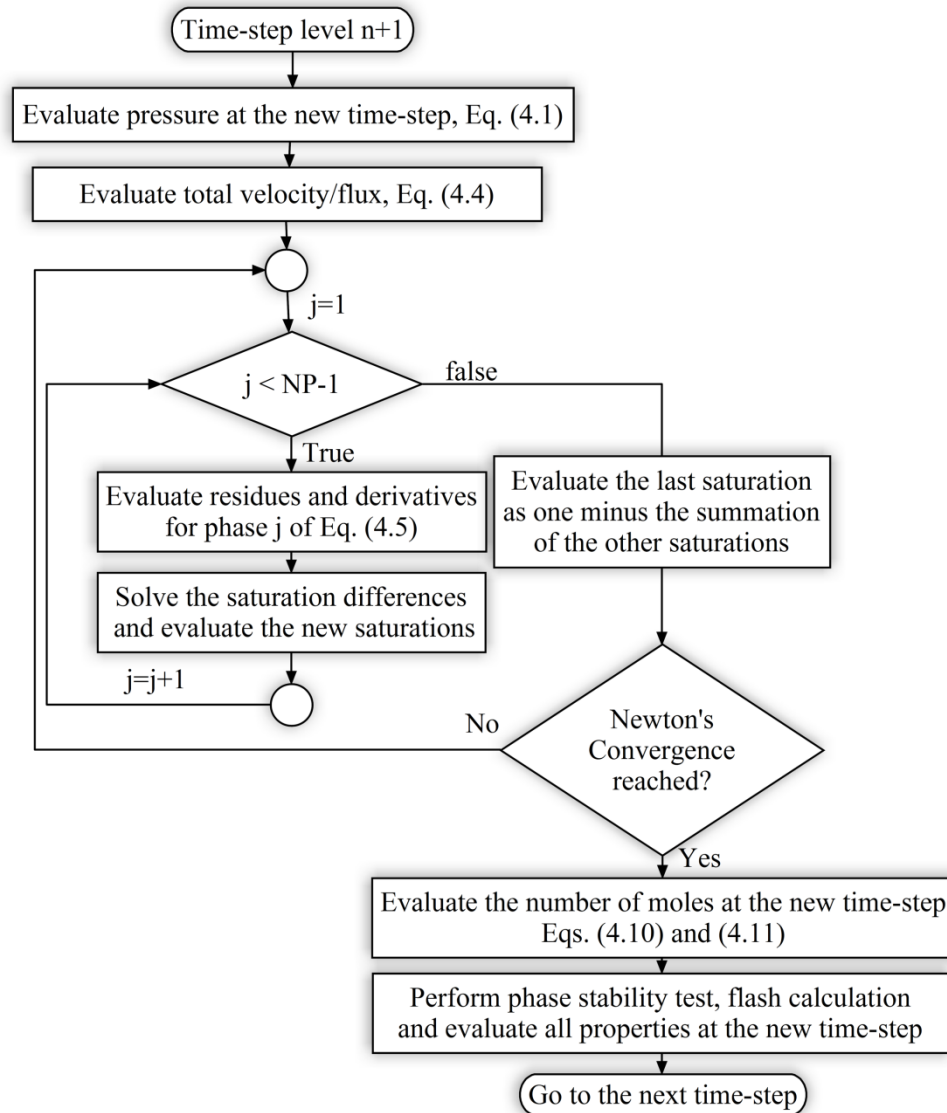
and

$$\frac{N_w^{n+1} - N_w^n}{V_b} = -\Delta t \left\{ \bar{\nabla} \cdot (\xi_w^n \bar{U}_w^{n+1}) + \frac{\dot{q}_w^{n+1}}{V_b} \right\}. \tag{4.11}$$

After obtaining the number of moles, the flash calculation is performed, but this time the saturations are not recalculated.

Figure 4.2 shows the flowchart of this formulation; we will name IMPSAT-0.

Figure 4.2 – Flowchart of the IMPSAT-0 formulation for a time-step.



### 4.3 Modified Watts (IMPSAT-1)

The IMPSAT-0 formulation has presented some inaccuracies for some cases as gas and water-alternating-gas (WAG) injection. Another form of this formulation was proposed and tested and the inaccuracies were greatly reduced. We suggested using the Buckley-Leverett velocity form only for the solution of the saturation equations. In this way, the mole balance equations are solved in the traditional form for the hydrocarbon components and water. These equations are shown below:



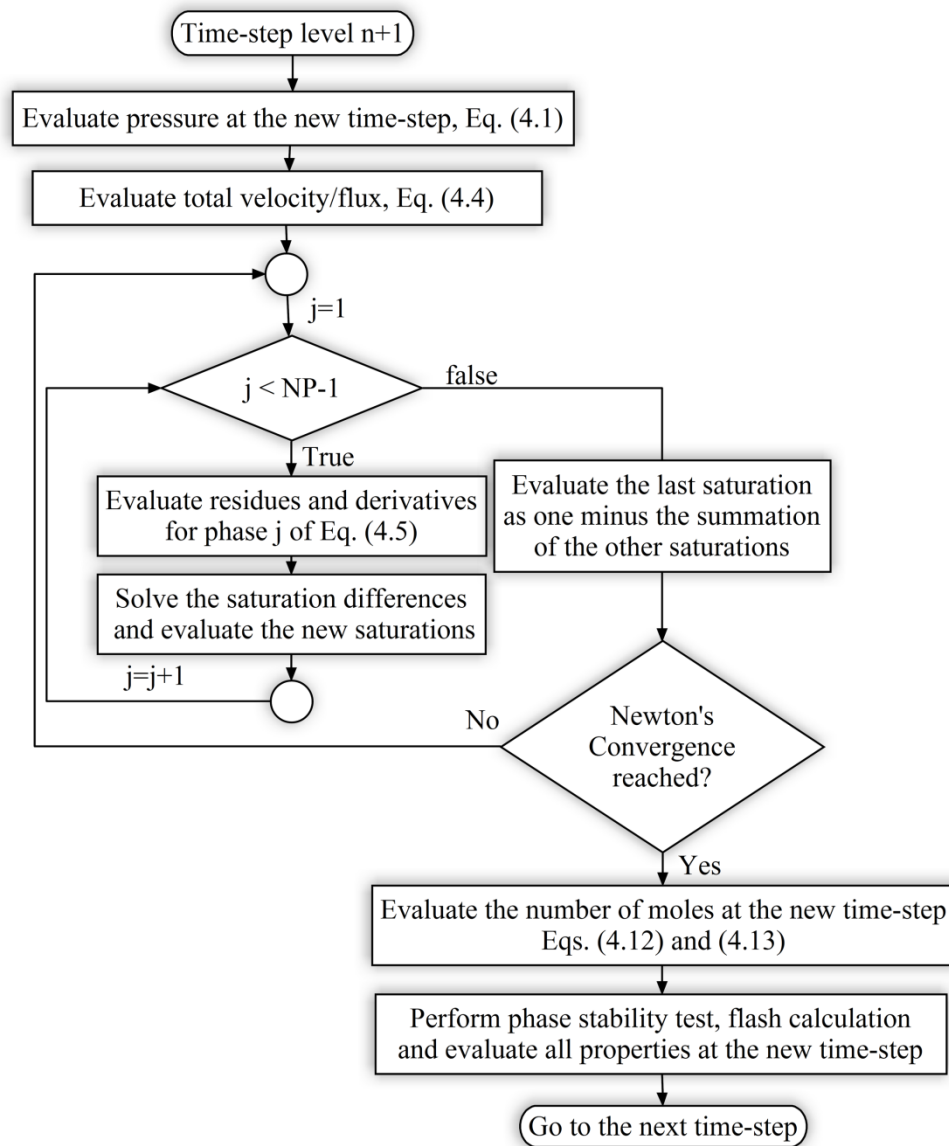
$$\frac{N_k^{n+1} - N_k^n}{V_b} = \Delta t \left\{ \sum_{j=2}^{n_p} \vec{\nabla} \cdot \left( x_{kj}^n \xi_j^n \frac{k_{rj}^{n+1}}{\mu_j^n} \bar{K} \cdot \vec{\nabla} (P^{n+1} + P_{cjr}^{n+1} - \rho_j^n gD) \right) - \frac{\dot{q}_k^n}{V_b} \right\} \quad k = 1, \dots, n_c, \quad (4.12)$$

and

$$\frac{N_w^{n+1} - N_w^n}{V_b} = \Delta t \left\{ \vec{\nabla} \cdot \left( \xi_w^n \frac{k_{rw}^{n+1}}{\mu_w^n} \bar{K} \cdot \vec{\nabla} (P^{n+1} + P_{cwr}^{n+1} - \rho_w^n gD) \right) - \frac{\dot{q}_w^n}{V_b} \right\}. \quad (4.13)$$

The algorithm is very similar to one presented in Figure 4.2 and it is shown in Figure 4.3.

Figure 4.3 – Flowchart of the IMPSAT-1 formulation for a time-step.



This formulation will be referred to as IMPSAT-1.

#### 4.4 Iterative IMPSAT (IMPSAT-2)

To avoid the problem of computing pressure, saturations and moles using different mole fluxes, we have implemented an iterative IMPSAT approach. After each calculation of the saturations, the pressure is recomputed using the correct relative permeabilities and capillary pressure. The new semi-implicit total velocity is then updated with pressure, relative permeabilities and capillary pressure and the saturations are recalculated. This procedure is done until convergence of pressure and saturations is reached. The result of this approach is that the pressure and saturations are solved using the same mole fluxes. Therefore, no inconsistency in this aspect is observed. The pressure equation is given by

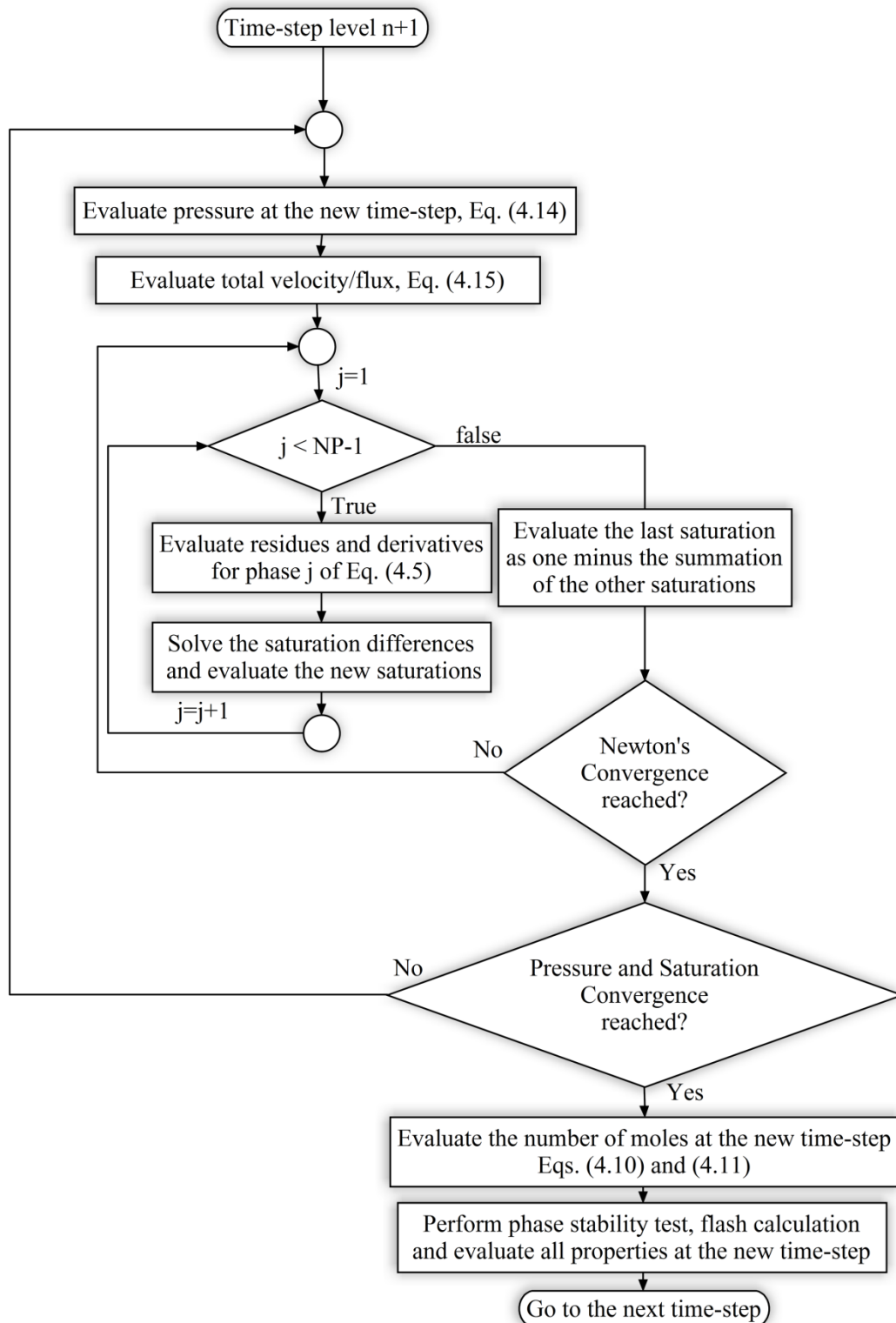
$$\begin{aligned}
 & \left[ \phi^0 C_f - \frac{1}{V_b} \frac{\partial V_T^n}{\partial P} \right] (P^{n+1} - P^n) = \frac{(V_T^n - V_p^n)}{V_b} \\
 & + \Delta t \sum_{k=1}^{n_c} \bar{V}_{Tk}^n \left\{ \sum_{j=2}^{n_p} \bar{\nabla} \cdot \left( x_{kj}^n \xi_j^n \frac{k_{rj}^{n+1}}{\mu_j^n} \bar{\bar{K}} \cdot \bar{\nabla} (P^{n+1} + P_{cjr}^{n+1} - \rho_j^n g D) \right) - \frac{\dot{q}_k^n}{V_b} \right\}, \\
 & + \Delta t \bar{V}_{Tw}^n \left\{ \bar{\nabla} \cdot \left( \xi_w^n \frac{k_{rw}^{n+1}}{\mu_w^n} \bar{\bar{K}} \cdot \bar{\nabla} (P^{n+1} + P_{cwr}^{n+1} - \rho_w^n g D) \right) - \frac{\dot{q}_w^n}{V_b} \right\}
 \end{aligned} \tag{4.14}$$

and

$$\bar{U}_T^{n+1,n} = - \sum_{m=1}^{n_p} \lambda_m^{n+1} \bar{\bar{K}} \cdot \bar{\nabla} (P^{n+1} + P_{cmr}^{n+1} - \rho_m^n g \bar{\nabla} D), \tag{4.15}$$

The algorithm of this approach is shown in Figure 4.4.

Figure 4.4 – Flowchart of the IMPSAT-2 formulation for a time-step.



This formulation will be referred to as IMPSAT-2.

#### 4.5 Collins et al. (FI-0)

One of FI considered in this work is one proposed by Collins et al. (1992). In this formulation, the number of moles of each component are computed using the same model as that of the previous formulations. However, the pressure equation is obtained by just equating the pore volume and the total fluid volume of a given grid-block at the new time-step level. All variables  $m$  are treated implicitly at  $(n+1)$  time level, then a non-linear set of equations is formed. To solve this non-linear system of equations, we write these equations in the residual form for pressure, number of moles of hydrocarbon components, respectively as

$$R_p = V_p^{n+1} - \sum_{j=1}^{n_p} \frac{n_j^{n+1}}{\xi_j^{n+1}}, \quad (4.16)$$

$$\frac{R_{N_k}}{V_b} = \frac{N_k^{n+1} - N_k^n}{V_b} - \Delta t \left\{ \sum_{j=2}^{n_p} \bar{\nabla} \cdot \left( x_{kj}^{n+1} \xi_j^{n+1} \frac{k_{rj}^{n+1}}{\mu_j^{n+1}} \bar{\bar{K}} \cdot \bar{\nabla} (P^{n+1} + P_{cjr}^{n+1} - \rho_j^{n+1} gD) \right) - \frac{\dot{q}_k^{n+1}}{V_b} \right\} \quad k = 1, \dots, n_c, \quad (4.17)$$

$$\frac{R_{N_w}}{V_b} = \frac{N_w^{n+1} - N_w^n}{V_b} - \Delta t \left\{ \bar{\nabla} \cdot \left( \xi_w^{n+1} \frac{k_{rw}^{n+1}}{\mu_w^{n+1}} \bar{\bar{K}} \cdot \bar{\nabla} (P^{n+1} + P_{cwr}^{n+1} - \rho_w^{n+1} gD) \right) - \frac{\dot{q}_w^{n+1}}{V_b} \right\}. \quad (4.18)$$

Each residue equation must be zero when the solution is reached. For solving Eqs. (4.14) to (4.16), the Newton-Raphson method is used so the following set of equations must be solved per Newton's iteration.

$$\begin{bmatrix} \bar{J}_{11} & \cdots & \bar{J}_{1n_b} \\ \vdots & \ddots & \vdots \\ \bar{J}_{n_b 1} & \cdots & \bar{J}_{n_b n_b} \end{bmatrix} \begin{bmatrix} \bar{X}_1 \\ \vdots \\ \bar{X}_{n_b} \end{bmatrix} = \begin{bmatrix} \bar{B}_1 \\ \vdots \\ \bar{B}_{n_b} \end{bmatrix}, \quad (4.19)$$

where  $n_b$  is the number of grid-blocks of the grid, and

$$\bar{J}_{ij} = \begin{bmatrix} \frac{\partial RP_i}{\partial P_j} & \frac{\partial RP_i}{\partial N_{1j}} & \dots & \frac{\partial RP_i}{\partial N_{n_c j}} & \frac{\partial RP_i}{\partial N_{w_j}} \\ \frac{\partial RN_{1i}}{\partial P_j} & \frac{\partial RN_{1i}}{\partial N_{1j}} & \dots & \frac{\partial RN_{1i}}{\partial N_{n_c j}} & \frac{\partial RN_{1i}}{\partial N_{w_j}} \\ \vdots & \vdots & \ddots & \vdots & \vdots \\ \frac{\partial RN_{n_c i}}{\partial P_j} & \frac{\partial RN_{n_c i}}{\partial N_{1j}} & \dots & \frac{\partial RN_{n_c i}}{\partial N_{n_c j}} & \frac{\partial RN_{n_c i}}{\partial N_{w_j}} \\ \frac{\partial RN_{w_i}}{\partial P_j} & \frac{\partial RN_{w_i}}{\partial N_{1j}} & \dots & \frac{\partial RN_{w_i}}{\partial N_{n_c j}} & \frac{\partial RN_{w_i}}{\partial N_{w_j}} \end{bmatrix}, \quad (4.20)$$

$$\bar{X}_i = \begin{bmatrix} \delta P_i \\ \delta N_{1i} \\ \vdots \\ \delta N_{n_c i} \\ \delta N_{w_i} \end{bmatrix}, \quad (4.21)$$

and

$$\bar{B}_i = \begin{bmatrix} -RP_i \\ -RN_{1i} \\ \vdots \\ -RN_{n_c i} \\ -RN_{w_i} \end{bmatrix}. \quad (4.22)$$

In order to obtain the derivatives of the residual equations is necessary to evaluate the derivative of each secondary variables with respect to the primary variables. These derivatives are given bellow as

$$\frac{\partial x_{kj}}{\partial N_i} = \frac{1}{n_j} \left( \frac{\partial n_{kj}}{\partial N_i} - x_{kj} \frac{\partial n_j}{\partial N_i} \right), \quad i = 1, \dots, n_c, \quad j = 2, \dots, n_p, \quad k = 1, \dots, n_c, \quad (4.23)$$

$$\frac{\partial \xi_j}{\partial N_i} = -\frac{1}{v_j^2} \sum_{k=1}^{n_c} \frac{\partial v_j}{\partial n_{kj}} \frac{\partial n_{kj}}{\partial N_i}, \quad i = 1, \dots, n_c, \quad j = 2, \dots, n_p, \quad (4.24)$$

$$\frac{\partial \xi_w}{\partial N_w} = 0, \quad (4.25)$$

$$\frac{\partial \mu_j}{\partial N_i} = \sum_{k=1}^{n_c} \frac{\partial n_{kj}}{\partial N_i} \frac{\partial \mu_j}{\partial n_{kj}}, \quad i = 1, \dots, n_c, \quad j = 2, \dots, n_p, \quad (4.26)$$

$$\frac{\partial \rho_j}{\partial N_i} = \frac{\partial \xi_j}{\partial N_i} \sum_{k=1}^{n_c} x_{kj} W_k + \xi_j \sum_{k=1}^{n_c} W_k \frac{\partial x_{kj}}{\partial N_i}, \quad i = 1, \dots, n_c, \quad j = 2, \dots, n_p, \quad (4.27)$$

$$\frac{\partial \rho_w}{\partial N_w} = 0, \quad (4.28)$$

$$\frac{\partial k_{ij}}{\partial N_i} = \sum_{k=1}^{n_p-1} \frac{\partial S_k}{\partial N_i} \frac{\partial k_{ij}}{\partial S_k}, \quad i = 1, \dots, n_c + 1, \quad j = 1, \dots, n_p, \quad (4.29)$$

$$\frac{\partial S_j}{\partial N_i} = (1 - S_w) \left\{ \frac{\left[ \frac{L_j}{\xi_j} \right] \sum_{k=2}^{n_p} \frac{L_j}{\xi_j} - \left[ \sum_{k=2}^{n_p} \frac{L_k}{\xi_k} \right] \frac{L_j}{\xi_j}}{\left( \sum_{k=2}^{n_p} \frac{L_j}{\xi_j} \right)^2} \right\}, \quad i = 1, \dots, n_c, \quad j = 2, \dots, n_p, \quad (4.30)$$

$$\frac{\partial S_w}{\partial N_w} = \frac{1}{V_p^2 \xi_w^2} \left[ V_p \xi_w - n_w V_p \frac{\partial \xi_w}{\partial N_w} \right], \quad (4.31)$$

$$\frac{\partial}{\partial N_i} \left( \frac{L_j}{\xi_j} \right) = \frac{1}{\xi_j} \left( \frac{\partial L_j}{\partial N_i} - \frac{L_j}{\xi_j} \frac{\partial \xi_j}{\partial N_i} \right), \quad i = 1, \dots, n_c, \quad j = 2, \dots, n_p, \quad (4.32)$$

$$\frac{\partial L_j}{\partial N_i} = \left( \sum_{k=2}^{n_p} n_k \right)^{-1} \left( \frac{\partial n_j}{\partial N_i} - L_j \frac{\partial}{\partial N_i} \left( \sum_{k=2}^{n_p} n_k \right) \right), \quad i = 1, \dots, n_c, \quad j = 2, \dots, n_p, \quad (4.33)$$

$$\frac{\partial P_{cjr}}{\partial N_i} = \sum_{k=1}^{n_p-1} \frac{\partial S_k}{\partial N_i} \frac{\partial P_{cjr}}{\partial S_k}, \quad i = 1, \dots, n_c + 1, \quad j = 1, \dots, n_p, \quad (4.34)$$

$$\frac{\partial x_{kj}}{\partial P} = \frac{1}{n_j} \left( \frac{\partial n_{kj}}{\partial P} - x_{kj} \frac{\partial n_j}{\partial P} \right), \quad j = 2, \dots, n_p, \quad k = 1, \dots, n_c, \quad (4.35)$$

$$\frac{\partial \xi_j}{\partial P} = -\frac{RT}{v_j^2 P} \left( \sum_{i=1}^{n_c} \left( \frac{\partial Z_j}{\partial n_{kj}} \right) \frac{\partial n_{ij}}{\partial P} + \frac{1}{P} \left[ P \frac{\partial Z_j}{\partial P} - Z_j \right] \right), \quad j = 2, \dots, n_p, \quad (4.36)$$

$$\frac{\partial \xi_w}{\partial P} = C_w \xi_w^0, \quad (4.37)$$

$$\frac{\partial \mu_j}{\partial P} = \sum_{k=1}^{n_c} \frac{\partial n_{kj}}{\partial P} \frac{\partial \mu_j}{\partial n_{kj}} + \left( \frac{\partial \mu_j}{\partial P} \right)_{n_{kj}}, \quad j = 2, \dots, n_p \quad (4.38)$$

$$\frac{\partial \rho_j}{\partial P} = \frac{\partial \xi_j}{\partial P} \sum_{k=1}^{n_c} x_{kj} W_k + \xi_j \sum_{k=1}^{n_c} W_k \frac{\partial x_{kj}}{\partial P}, \quad j = 2, \dots, n_p, \quad (4.39)$$

$$\frac{\partial \rho_w}{\partial P} = W_w \frac{\partial \xi_j}{\partial P}, \quad (4.40)$$

$$\frac{\partial k_{rj}}{\partial P} = \sum_{k=1}^{n_p-1} \frac{\partial S_k}{\partial P} \frac{\partial k_{rj}}{\partial S_k}, \quad j = 1, \dots, n_p, \quad (4.41)$$

$$\frac{\partial S_j}{\partial P} = (1 - S_w) \left\{ \frac{\left[ \frac{L_j}{\xi_j} \right] \sum_{k=2}^{n_p} \frac{L_j}{\xi_j} - \left[ \sum_{k=2}^{n_p} \frac{L_k}{\xi_k} \right] \frac{L_j}{\xi_j}}{\left( \sum_{k=2}^{n_p} \frac{L_j}{\xi_j} \right)^2} \right\} - \frac{\frac{L_j}{\xi_j}}{\sum_{k=2}^{n_p} \frac{L_k}{\xi_k}} \frac{\partial S_w}{\partial P}, \quad j = 2, \dots, n_p, \quad (4.42)$$

$$\frac{\partial S_w}{\partial P} = -\frac{1}{V_p^2 \xi_w^2} \left[ n_w V_p \frac{\partial \xi_w}{\partial P} + n_w \xi_w V_b \phi^0 C_f \right], \quad (4.43)$$

$$\frac{\partial}{\partial P} \left( \frac{L_j}{\xi_j} \right) = \frac{1}{\xi_j} \left( \frac{\partial L_j}{\partial P} - \frac{L_j}{\xi_j} \frac{\partial \xi_j}{\partial P} \right), \quad i = 1, \dots, n_c, \quad j = 2, \dots, n_p, \quad (4.44)$$

$$\frac{\partial L_j}{\partial P} = \left( \sum_{k=2}^{n_p} n_k \right)^{-1} \left( \frac{\partial n_j}{\partial P} - L_j \frac{\partial}{\partial P} \left( \sum_{k=2}^{n_p} n_k \right) \right), \quad j = 2, \dots, n_p, \quad (4.45)$$

and

$$\frac{\partial P_{cjr}}{\partial P} = \sum_{k=1}^{n_p-1} \frac{\partial S_k}{\partial P} \frac{\partial P_{cjr}}{\partial S_k}, \quad j = 1, \dots, n_p. \quad (4.46)$$

Some of the derivatives of the above expressions were already shown in Chapter 2 and the others are evaluated through the EOS.

The derivatives of relative permeability and capillary pressure with respect to saturations are computed numerically as

$$\frac{\partial k_{rj}}{\partial S_k} = \frac{k_{rj}(\dots, S_{j-1}, S_j + \Delta S_j, S_{j+1}, \dots) - k_{rj}(\dots, S_{j-1}, S_j, S_{j+1}, \dots)}{\Delta S_j}, \quad (4.47)$$

$$j = 1, \dots, n_p, \quad k = 1, \dots, n_p - 1,$$

and

$$\frac{\partial P_{cjr}}{\partial S_k} = \frac{P_{cjr}(\dots, S_{j-1}, S_j + \Delta S_j, S_{j+1}, \dots) - P_{cjr}(\dots, S_{j-1}, S_j, S_{j+1}, \dots)}{\Delta S_j}, \quad (4.48)$$

$$j = 1, \dots, n_p, \quad k = 1, \dots, n_p - 1.$$

The viscosity derivatives with respect to its phase moles of each component and pressure is obtained numerically as well,

$$\frac{\partial \mu_j}{\partial n_{kj}} = \frac{\mu_j(\dots, n_{k-1j}, n_{kj} + \Delta n_{kj}, n_{k+1j}, \dots, P) - \mu_j(\dots, n_{k-1j}, n_{kj}, n_{k+1j}, \dots, P)}{\Delta n_{kj}}, \quad (4.49)$$

$$j = 2, \dots, n_p, \quad k = 1, \dots, n_c,$$

and

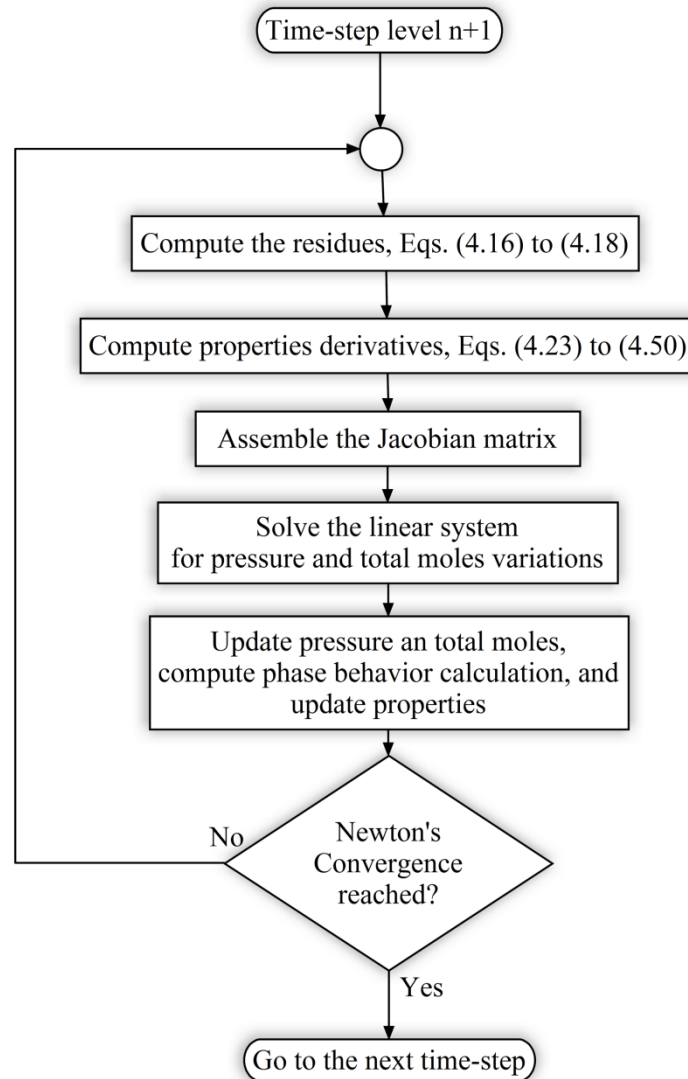
$$\left( \frac{\partial \mu_j}{\partial P} \right)_{n_{kj}} = \frac{\mu_j(\dots, n_{k-1j}, n_{kj}, n_{k+1j}, \dots, P + \Delta P) - \mu_j(\dots, n_{k-1j}, n_{kj}, n_{k+1j}, \dots, P)}{\Delta P}, \quad j = 2, \dots, n_p. \quad (4.50)$$

For all derivatives that are evaluated numerically we use the following variation for pressure and saturations:  $10^{-3}P$  and  $10^{-5}S$ .

Figure 4.5 presents the flowchart for a time-step calculation of the Collins et al. (1992) formulation; we will this approach FI-0 formulation.



Figure 4.5 – Flowchart for performing one time-step FI-0 formulation.



#### 4.6 New FI approach (FI-1)

The original approach of UTCOMP is the Ács et al. (1985) formulation. In order to preserve the nature of this formulation in the UTCOMP simulator, but using large time-steps we are proposing the use of the Ács et al. (1985) formulation in a fully implicit framework. We like to stress the main difference of this formulation and the Collins et al. (1992) formulation. In the pressure equation of the Collins et al. (1992) formulation the only terms that show up at the Jacobian matrix are in the diagonal block. On the other hand, in the pressure equation used in the current approach, non-zero derivatives will result for the diagonal and off-diagonal terms of each control volume. Therefore, we expect that that this

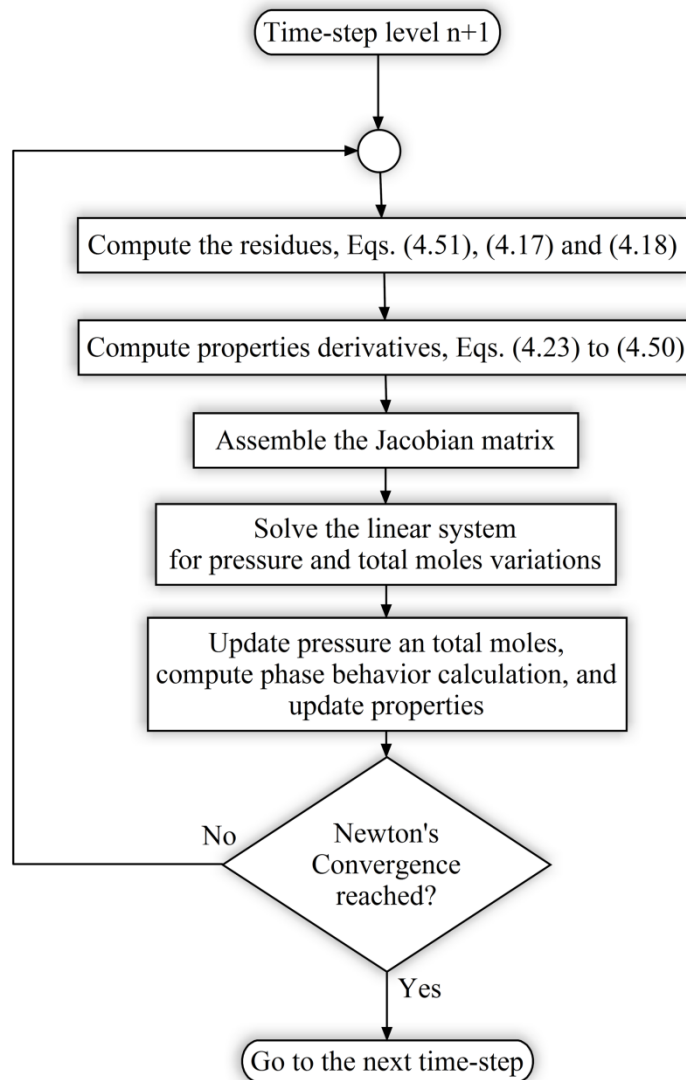
feature will have a large impact on the computational time. We name this approach FI-1 formulation. The new pressure equation is written as

$$R_p = \left[ \phi^0 C_f - \frac{1}{V_b} \frac{\partial V_T^n}{\partial P} \right] (P^{n+1} - P^n) - \frac{(V_T^n - V_p^n)}{V_b} - \Delta t \sum_{k=1}^{n_c} \bar{V}_{Tk}^n \left\{ \sum_{j=2}^{n_p} \bar{\nabla} \cdot \left( x_{kj}^{n+1} \xi_j^{n+1} \frac{k_{rj}^{n+1}}{\mu_j^{n+1}} \bar{\bar{K}} \cdot \bar{\nabla} (P^{n+1} + P_{cjr}^{n+1} - \rho_j^{n+1} gD) \right) - \frac{\dot{q}_k^{n+1}}{V_b} \right\}, \quad (4.51)$$

$$- \Delta t \bar{V}_{Tw}^n \left\{ \bar{\nabla} \cdot \left( \xi_w^{n+1} \frac{k_{rw}^{n+1}}{\mu_w^{n+1}} \bar{\bar{K}} \cdot \bar{\nabla} (P^{n+1} + P_{cwr}^{n+1} - \rho_w^{n+1} gD) \right) - \frac{\dot{q}_w^{n+1}}{V_b} \right\}$$

We use the same mole balance equations of the FI-0 formulation: Eqs. (4.17) and (4.18). Figure 4.6 presents the flowchart of this approach.

Figure 4.6 – Flowchart for performing one time-step for the FI-1 formulation.



## 5 RESULTS AND DISCUSSION

In this chapter, four case studies for testing and verification of all the formulations implemented in this work in conjunction with Cartesian and unstructured grids are presented. The results will be compared in terms of oil and gas production rates; time-stepping profiles; phase saturations and/or CO<sub>2</sub> overall composition fields; and overall CPU time. We validate all the new formulations with the original IMPEC formulation of UTCOMP, since it was severely tested and compared with several commercial simulators (Li, 2012). The field profiles are visualized using the ESSS Kraken<sup>®</sup> post-processor. The unstructured grids are generated using the ANSYS ICEM<sup>®</sup> and an in-house grid generator.

The following four case studies are used: a three component, three-phase CO<sub>2</sub> flooding; a six components, three-phase gas flooding; and two different seven components, four-phase CO<sub>2</sub> flooding cases.

All results for the IMPEC and IMPSAT approaches presented here were obtained for the maximum allowable time-step control parameters, that is, parameters that provide solutions without spurious oscillations.

### 5.1 Case study 1

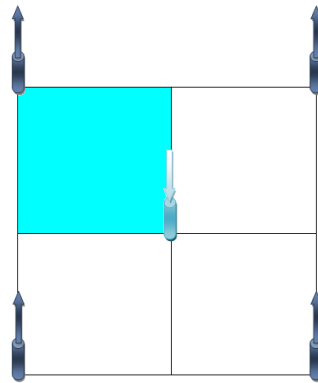
Case study 1 consists of a heavy oil characterized by three components: CO<sub>2</sub>, C<sub>1</sub> and nC<sub>16</sub>. The reservoir initially contains only water and oil phases. A fluid rich in CO<sub>2</sub> is injected which originates a new phase into reservoir. The reservoir investigated here is a quarter-of-five-spot configuration. Only immobile water exists in the reservoir during the whole simulation. Table 5.1 presents the reservoir data for this case.

Table 5.1 – Reservoir data for Case 1.

Property	Value
Length, width, and thickness	243.83 m, 243.83 m, and 60.96 m
Porosity	0.30
Initial Water Saturation	0.25
Initial Pressure	20.65 MPa
Permeability in x, y, and z directions	$1.97 \times 10^{-13} \text{ m}^2$ , $1.97 \times 10^{-13} \text{ m}^2$ , and $1.97 \times 10^{-14} \text{ m}^2$
Formation Temperature	299.82 K
Gas Injection Rate	$5.66 \times 10^5 \text{ m}^3/\text{d}$
Producer's Bottom Hole Pressure	20.65 MPa

The five-spot configuration is a common production layout used in petroleum engineering, which is basically constituted of 5 wells: one injector and four producer wells. Figure 5.1 shows the layout of this configuration. Due to symmetry just one quarter of this configuration is, in general, investigated.

Figure 5.1 – Five-spot layout (quarter of five-spot filled).



The original in place composition and the injected fluid composition for this case is shown in Table 5.2.

Table 5.2 – Fluid composition data for Case 1.

Component	Initial Reservoir Composition	Injection Fluid Composition
CO <sub>2</sub>	0.0100	0.9500
C <sub>1</sub>	0.1900	0.0500
nC <sub>16</sub>	0.8000	-

The components properties are displayed in Table 5.3.

Table 5.3 – Component data for Case 1.

Component	$P_c$ (MPa)	$T_c$ (K)	$v_c$ (m <sup>3</sup> /kmol)	$MW$ (kg/kmol)	<i>Acentric</i> <i>Factor</i> ( $\omega$ )
CO <sub>2</sub>	7.39	304.21	$9.40 \times 10^{-2}$	44.01	0.225
C <sub>1</sub>	4.60	190.60	$9.99 \times 10^{-2}$	16.04	0.022
nC <sub>16</sub>	1.74	734.68	$8.17 \times 10^{-1}$	222.00	0.684

The binary interaction coefficients and the relative permeabilities parameters are given in Tables 5.4 and 5.5, respectively.

Table 5.4 – Binary interaction coefficients for Case 1.

Component	CO <sub>2</sub>	C <sub>1</sub>	nC <sub>16</sub>
CO <sub>2</sub>	-	0.12	0.12
C <sub>1</sub>	0.12	-	-
nC <sub>16</sub>	0.12	-	-

Table 5.5 – Relative permeability data for Case 1.

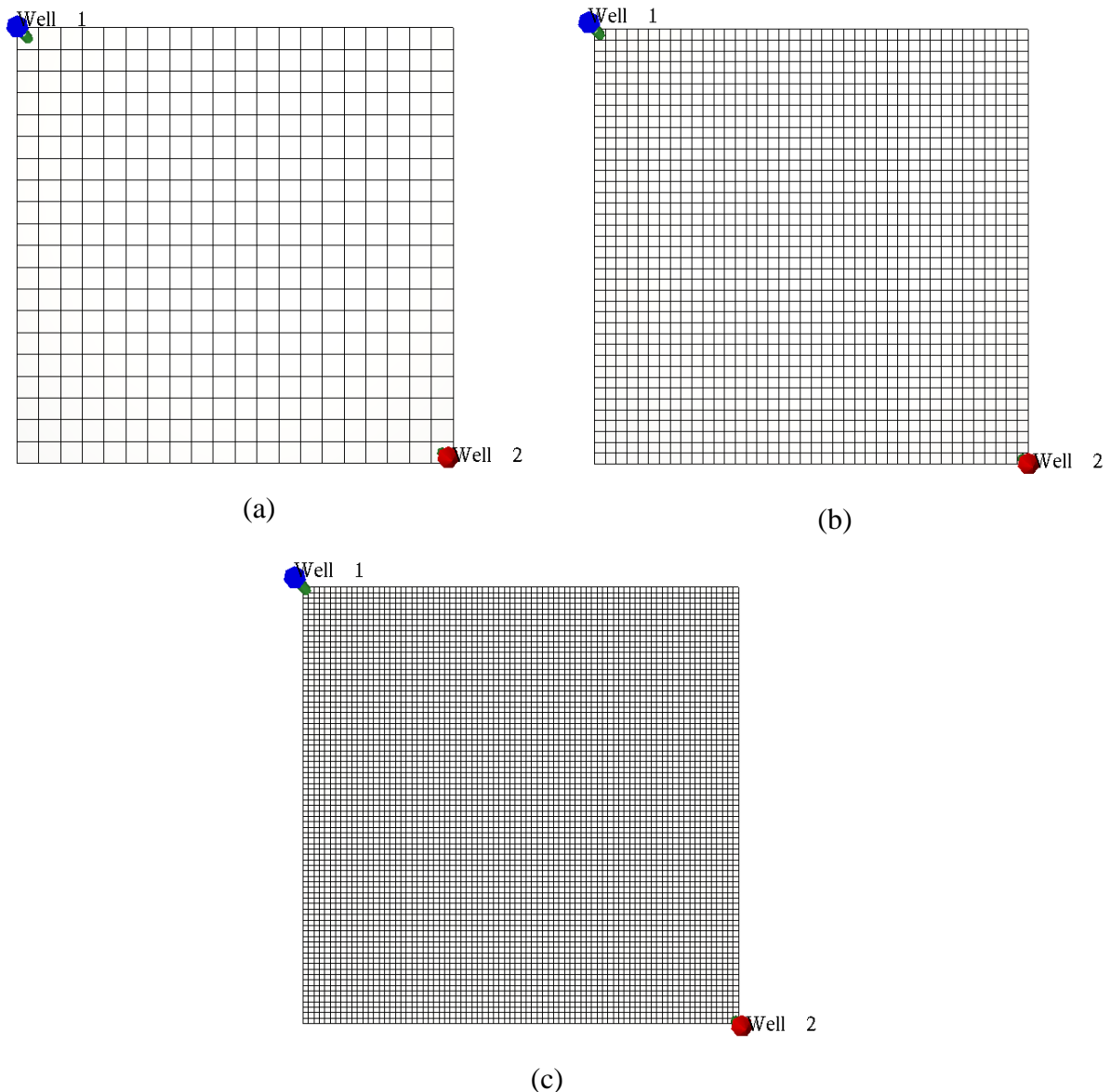
Parameter	Value
Model	Modified Stone II
End point relative permeabilities ( $k_{rw}^0$ , $k_{row}^0$ , $k_{rog}^0$ and $k_{rg}^0$ )	1.00, 1.00, 1.00 and 1.00
Residual saturations ( $S_{wr}$ , $S_{orw}$ , $S_{org}$ and $S_{gr}$ )	0.25, $10^{-6}$ , $10^{-6}$ and 0
Exponents ( $e_w$ , $e_{ow}$ , $e_{og}$ and $e_g$ )	1.00, 1.00, 1.00 and 1.00

Two and three dimensional reservoirs in conjunction with Cartesian and unstructured grids will be considered for this case study.

### 5.1.1 Case study 1: 2D Cartesian grid

Three grid refinements are used for this test: 20x20, 40x40 and 80x80. The purpose of using three different grids is to verify the performance of each formulation with the increase in the number of grid points. The grids are presented in Figure 5.2. For all reservoirs investigated, the blue arrows denote the injector wells, while the red arrows denote the producer wells.

Figure 5.2 – 2D Cartesian grids - Case 1. Injectors in blue and producers in red.



The time-step control parameters for the IMPEC and IMPSAT formulations are chosen in such way that no spurious oscillations are produced. The instability of the IMPEC and IMPSAT approaches can be noted as oscillations in the production curves. We want to avoid these oscillations by controlling the time-step as presented in chapter 3. Although the FI

approaches do not present this drawback, the use of large time-steps can lead to loss of numerical accuracy. Therefore, a time refinement needs to be performed in order to ensure that a time independent solution is obtained. For this study, the production rates using large time-steps for the FI approaches are denoted by (\*). The time-step control parameters for all cases presented in this chapter can be found in Appendix A.

Comparisons of the oil and gas production rates with the IMPEC formulation are presented in Figures 5.3 through 5.5 for the IMPSAT-0, IMPSAT-1, and IMPSAT-2 formulations. From these figures, one can observe a good agreement between the production curves for each grid. Figures 5.6 and 5.7 compare the production rates of the FI-0 and FI-1 using large time-steps (\*) with the IMPEC, respectively. From these figures, one can observe that the FI solutions are completely different from the IMPEC solution obtained for each mesh. In order to see if this difference is caused by the loss of accuracy due to using large time-steps, a time refinement will be performed for the FI approaches. The largest time-step, for each mesh, for the FI approaches is the one that provides the same production curves as the IMPEC. The curves obtained with this process are shown in Figures 5.8 and 5.9 for the FI-0 and FI-1 formulations, respectively. Now, we can observe a good agreement between the IMPEC and FI solutions for both approaches. From now on, all the results that will be presented for the FI approaches will be the ones that considered a time-step refinement.

As in this study we are interested only in the performance of the formulations, we do not carried out any grid refinement study. Results of grid refinement study using the UTCOMP simulator can be found in Fernandes et al. (2013) and Fernandes et al. (2014b).

The time-step profiles used by all grids and formulations are shown in Fig. 5.10. From this figure, it is possible to verify that FI approaches can handle large time-steps than the other approaches.

The gas saturation field at 500 days for all formulations are presented in Figures 5.11, 5.12, and 5.13 for the 20x20, 40x40, and 80x80 grids, respectively. From these figures, it is possible to see that the solutions are in very good agreement with the IMPEC formulation.

Figure 5.3 – Production rates comparison between IMPEC and IMPSAT-0 – Case 1. a) oil; and b) gas.

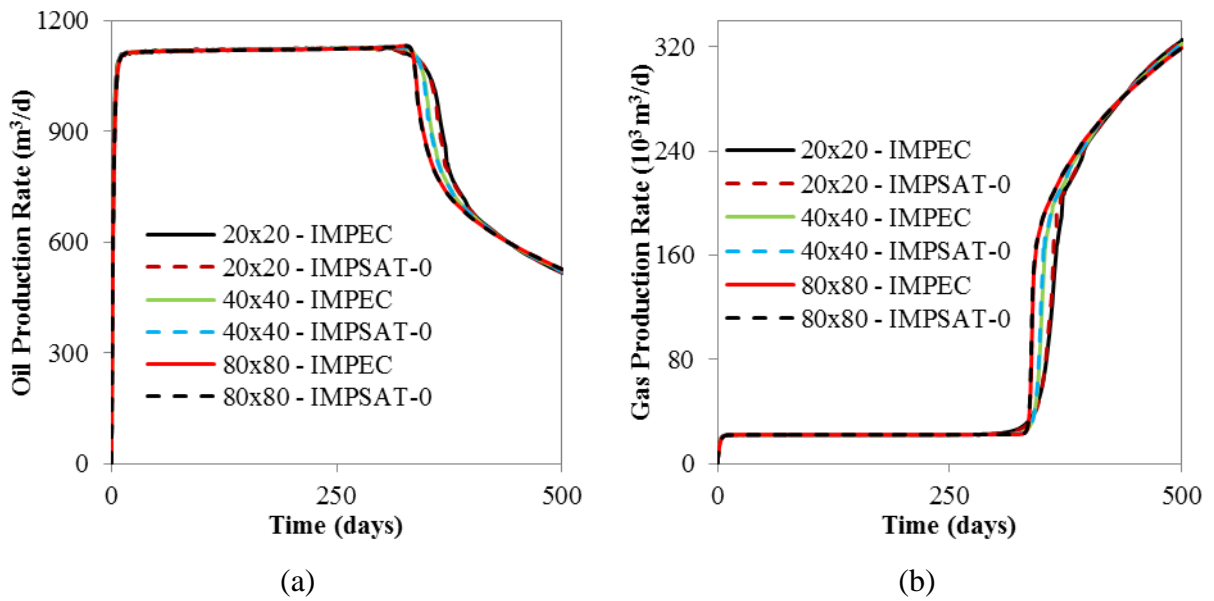


Figure 5.4 – Production rates comparison between IMPEC and IMPSAT-1 – Case 1. a) oil; and b) gas.

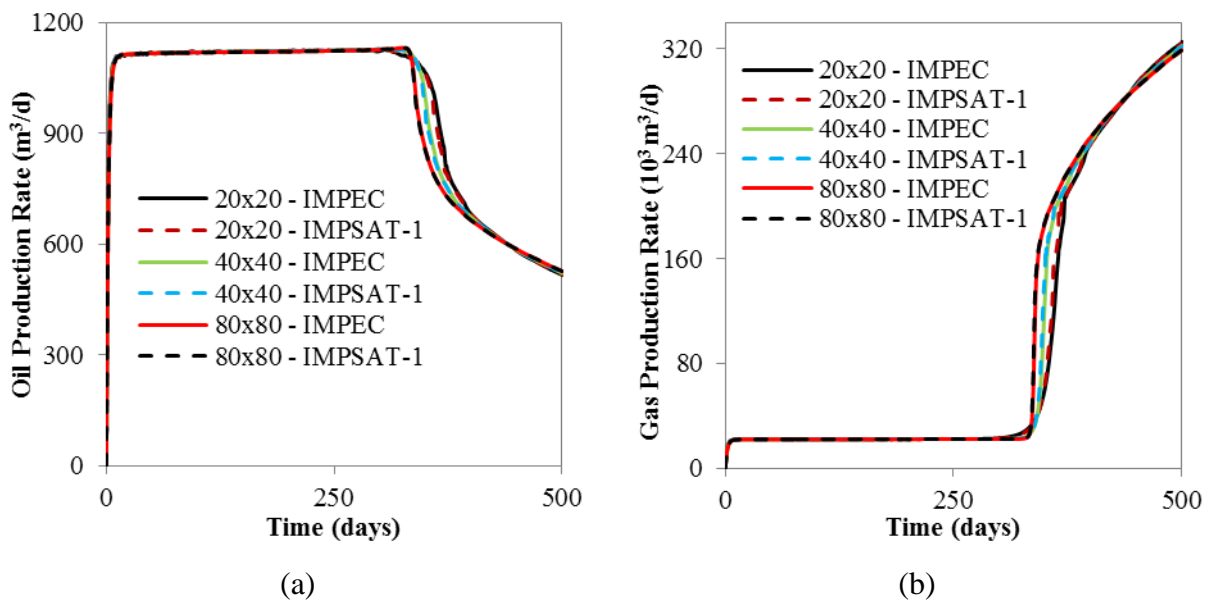




Figure 5.5 – Production rates comparison between IMPEC and IMPSAT-2 – Case 1. a) oil; and b) gas.

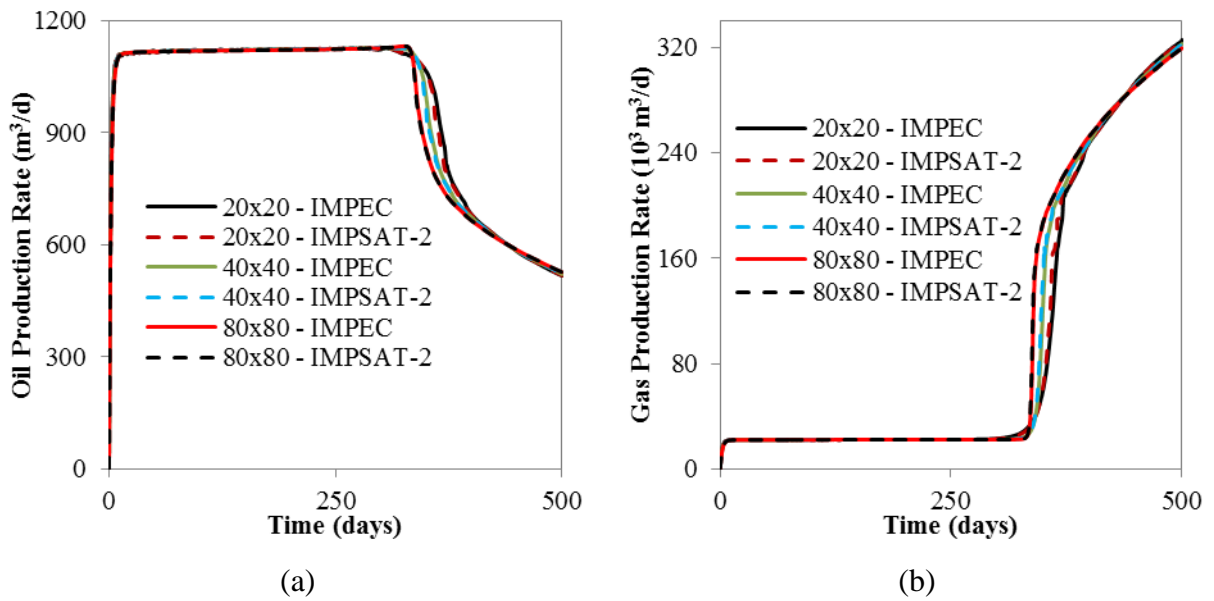


Figure 5.6 – Production rates comparison between IMPEC and FI-0\* – Case 1. a) oil; and b) gas.

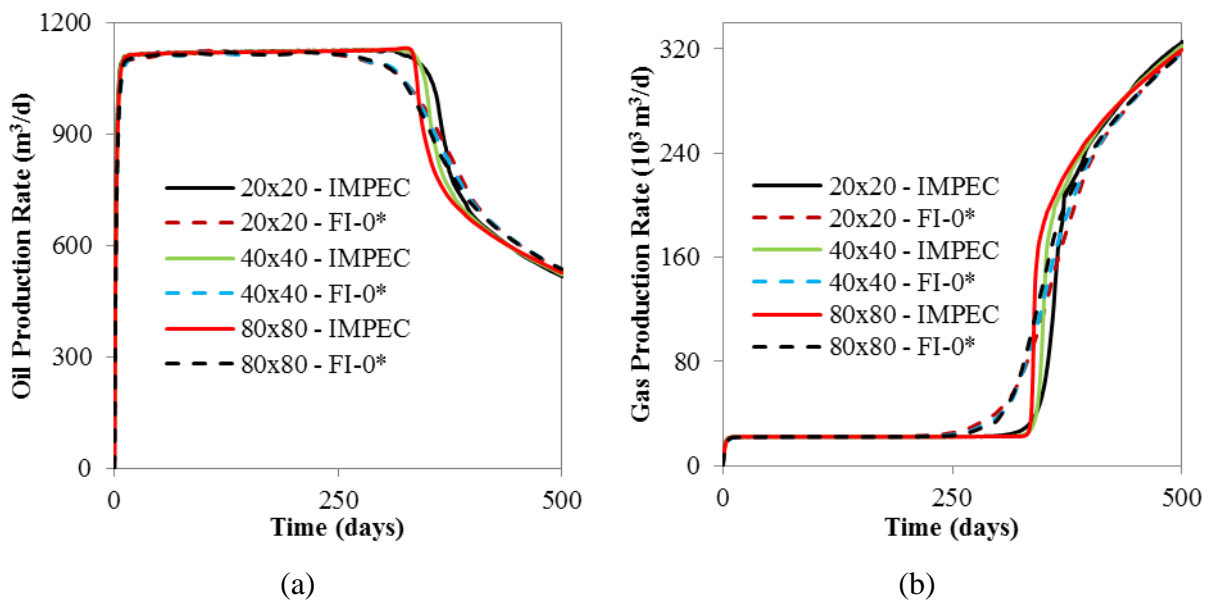


Figure 5.7 – Production rates comparison between IMPEC and FI-1\* – Case 1. a) oil; and b) gas.

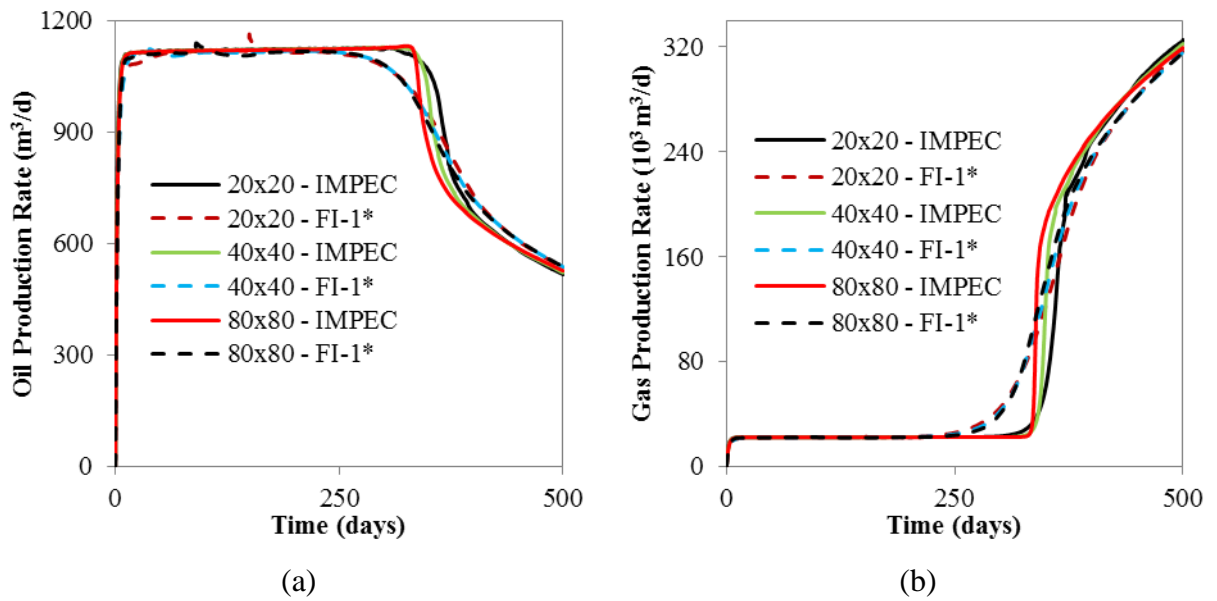


Figure 5.8 – Production rates comparison between IMPEC and FI-0 – Case 1. a) oil; and b) gas.

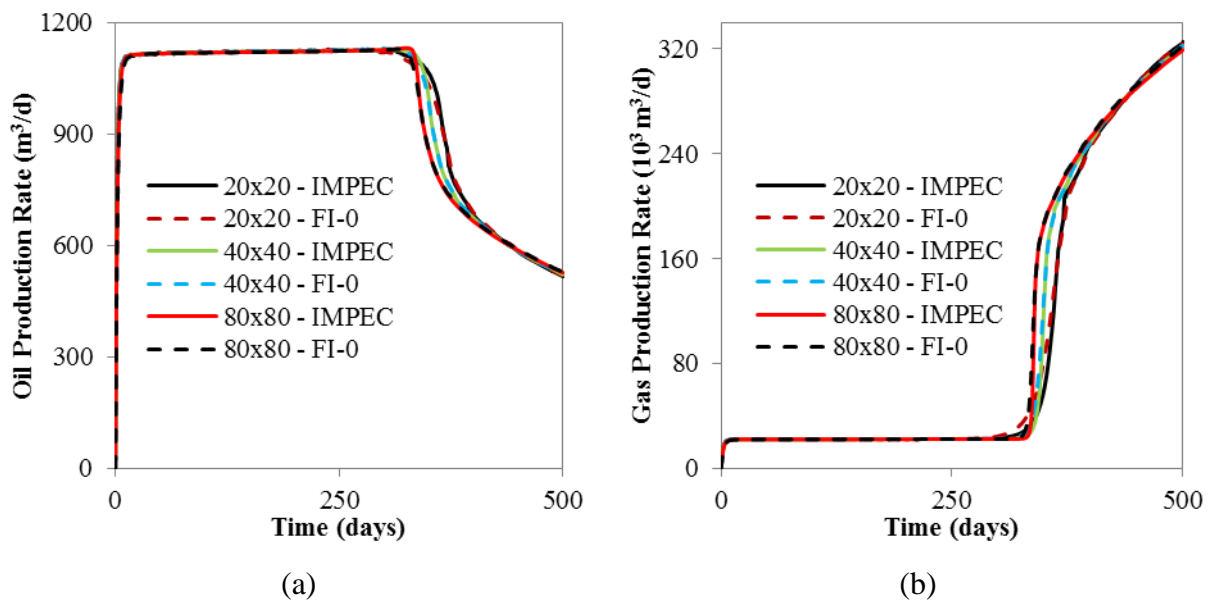
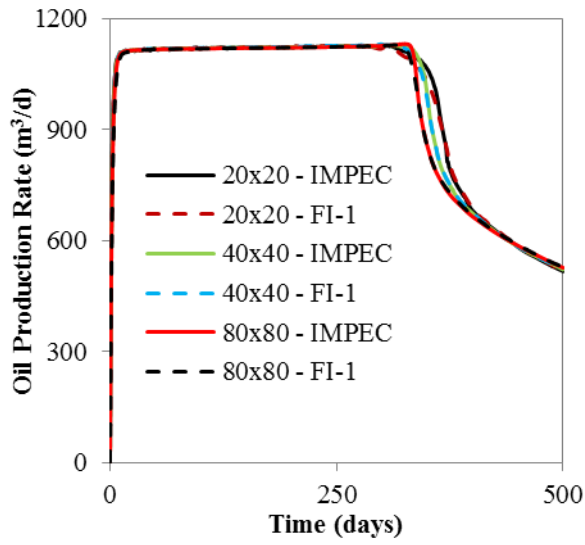
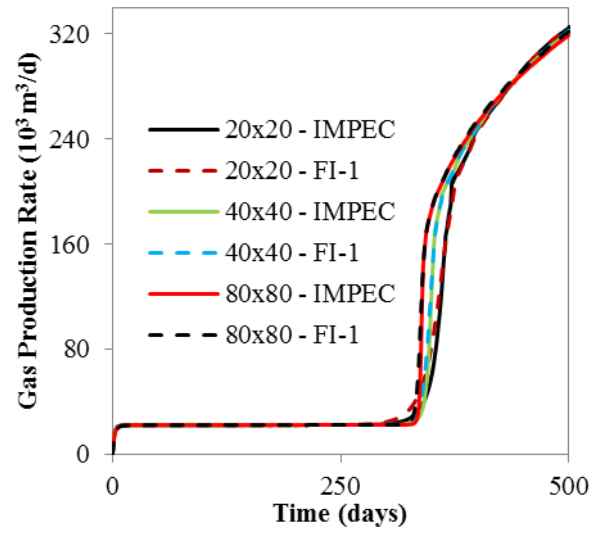


Figure 5.9 – Production rates comparison between IMPEC and FI-1 Case 1. a) oil; and b) gas.



(a)



(b)

Figure 5.10 – Time-stepping profiles for all formulations – Case 1. a) 20x20; b) 40x40; and c) 80x80.

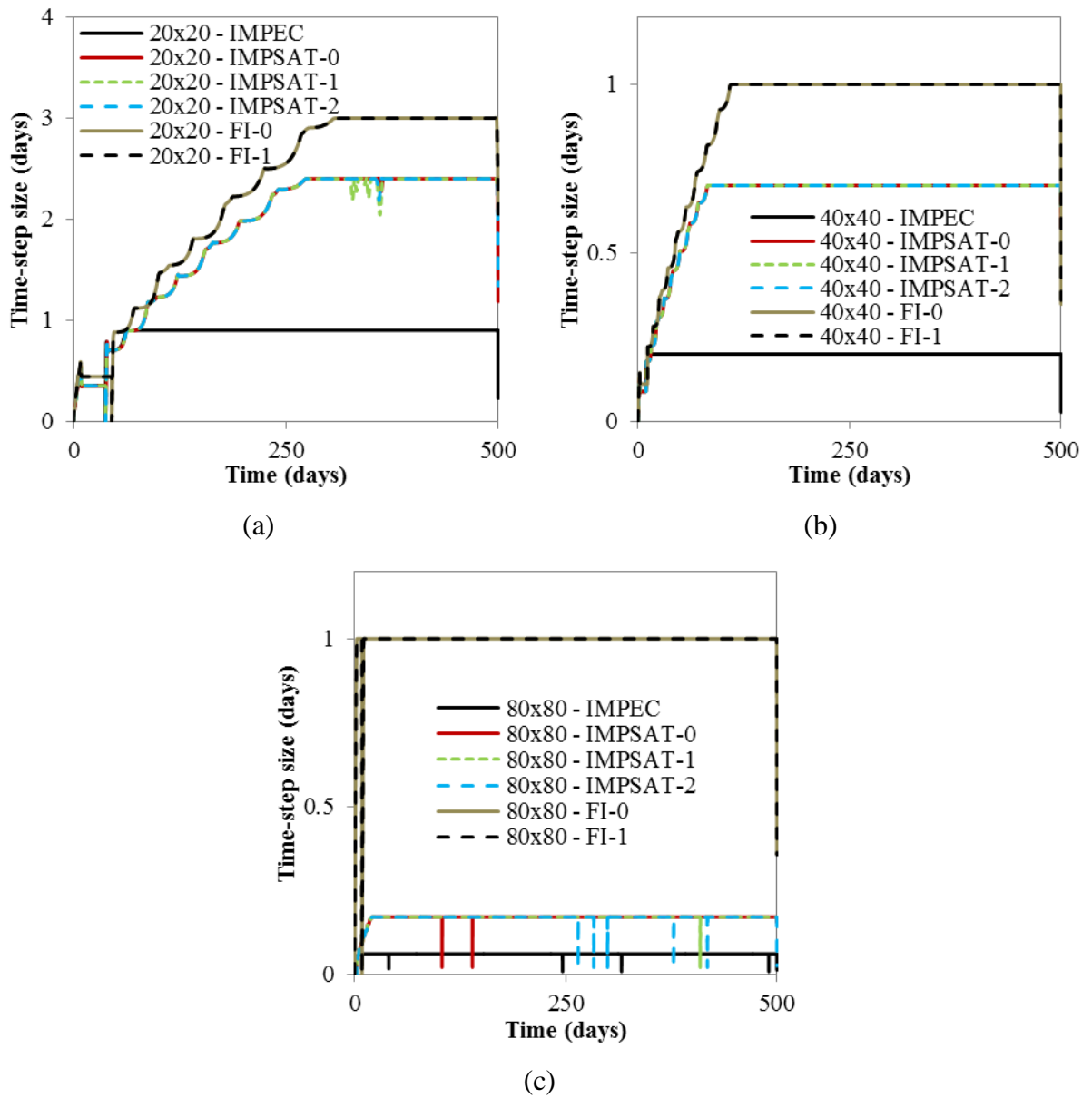


Figure 5.11 – Gas saturation fields at 500 days for all formulations - Case 1 using a 20x20 Cartesian grid. a) IMPEC; b) IMPSAT-0; c) IMPSAT-1; d) IMPSAT-2; e) FI-0; and f) FI-1

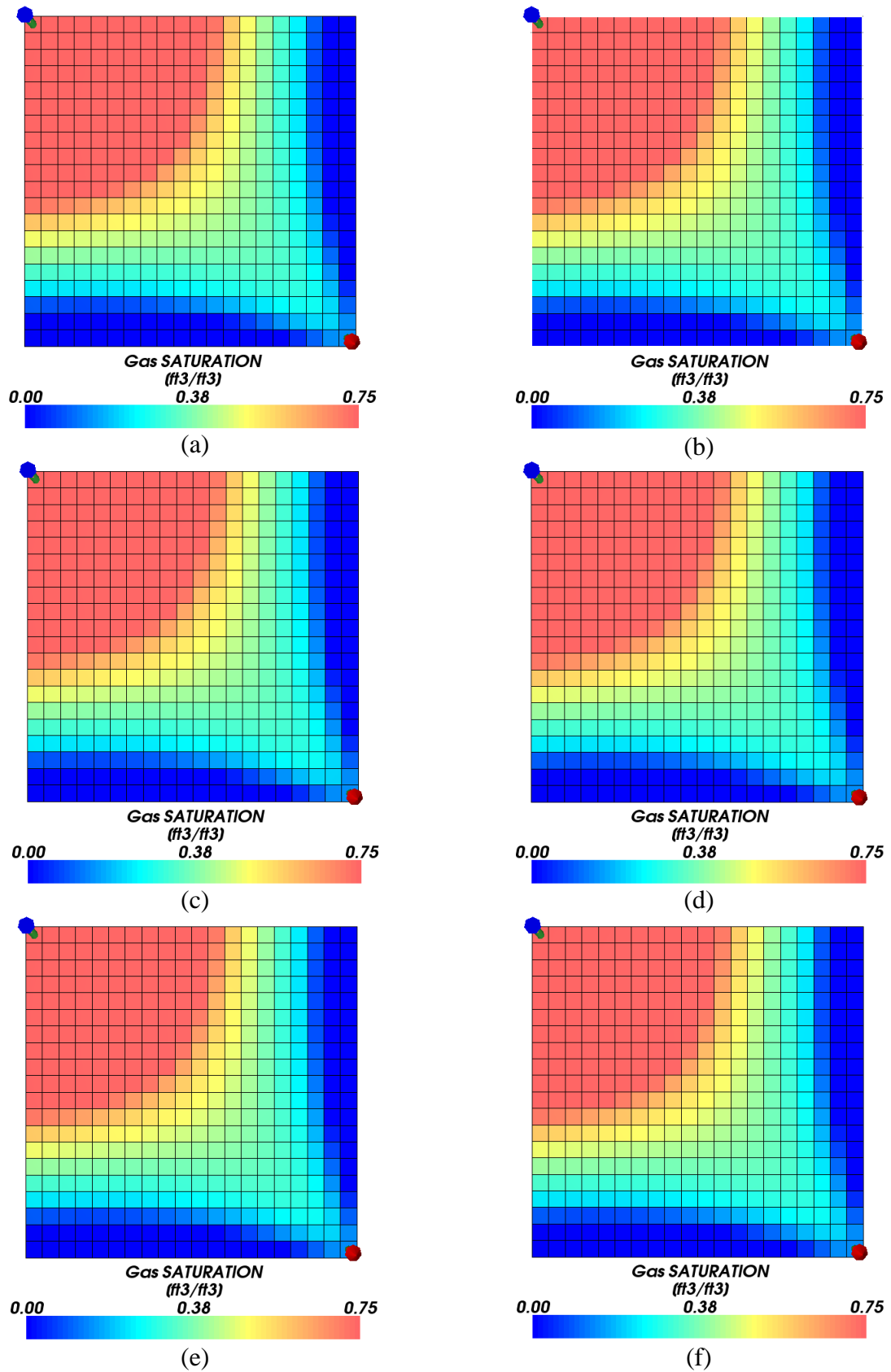


Figure 5.12 – Gas saturation fields at 500 days for all formulations - Case 1 using a 40x40 Cartesian grid. a) IMPEC; b) IMPSAT-0; c) IMPSAT-1; d) IMPSAT-2; e) FI-0; and f) FI-1

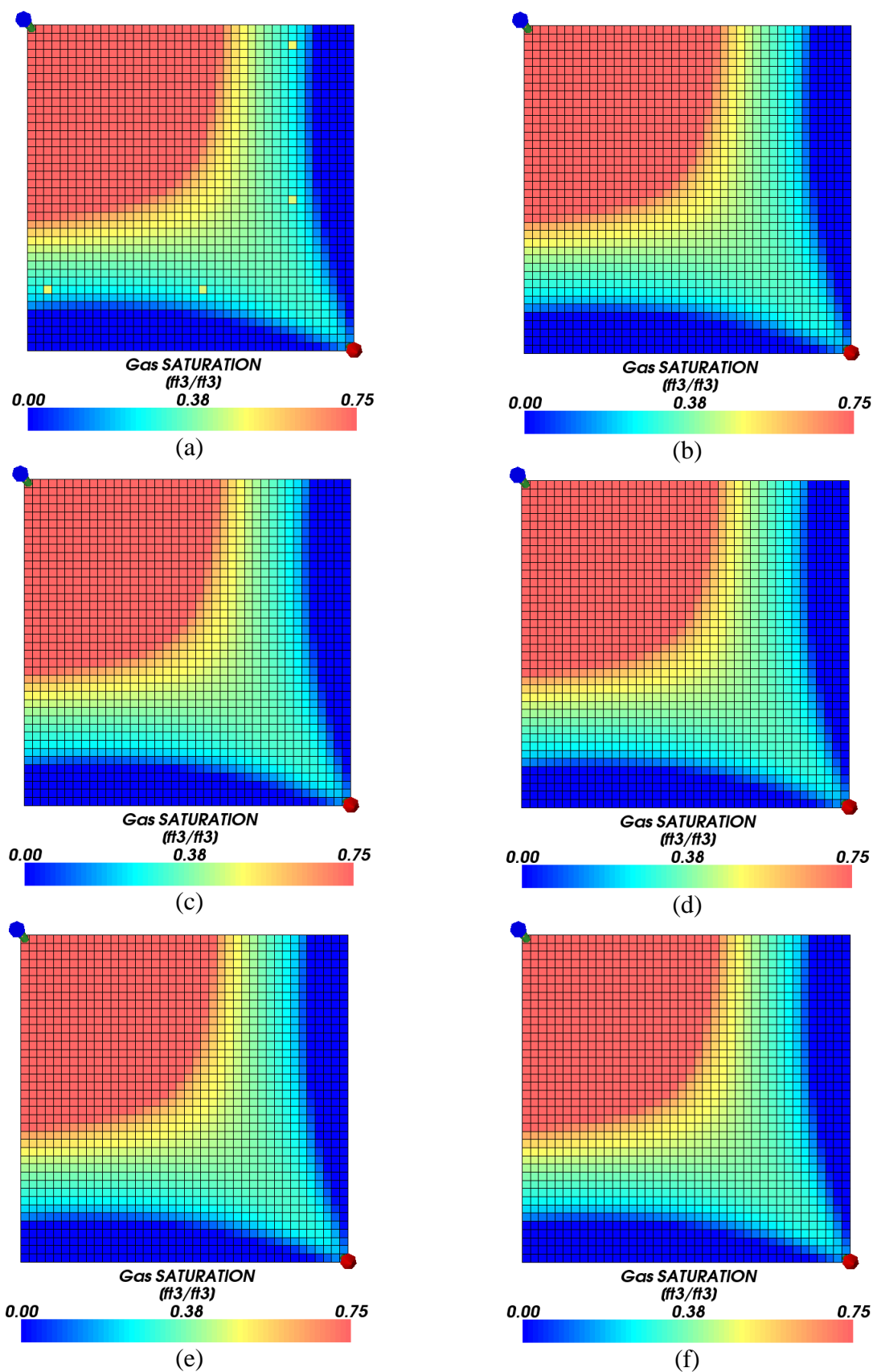
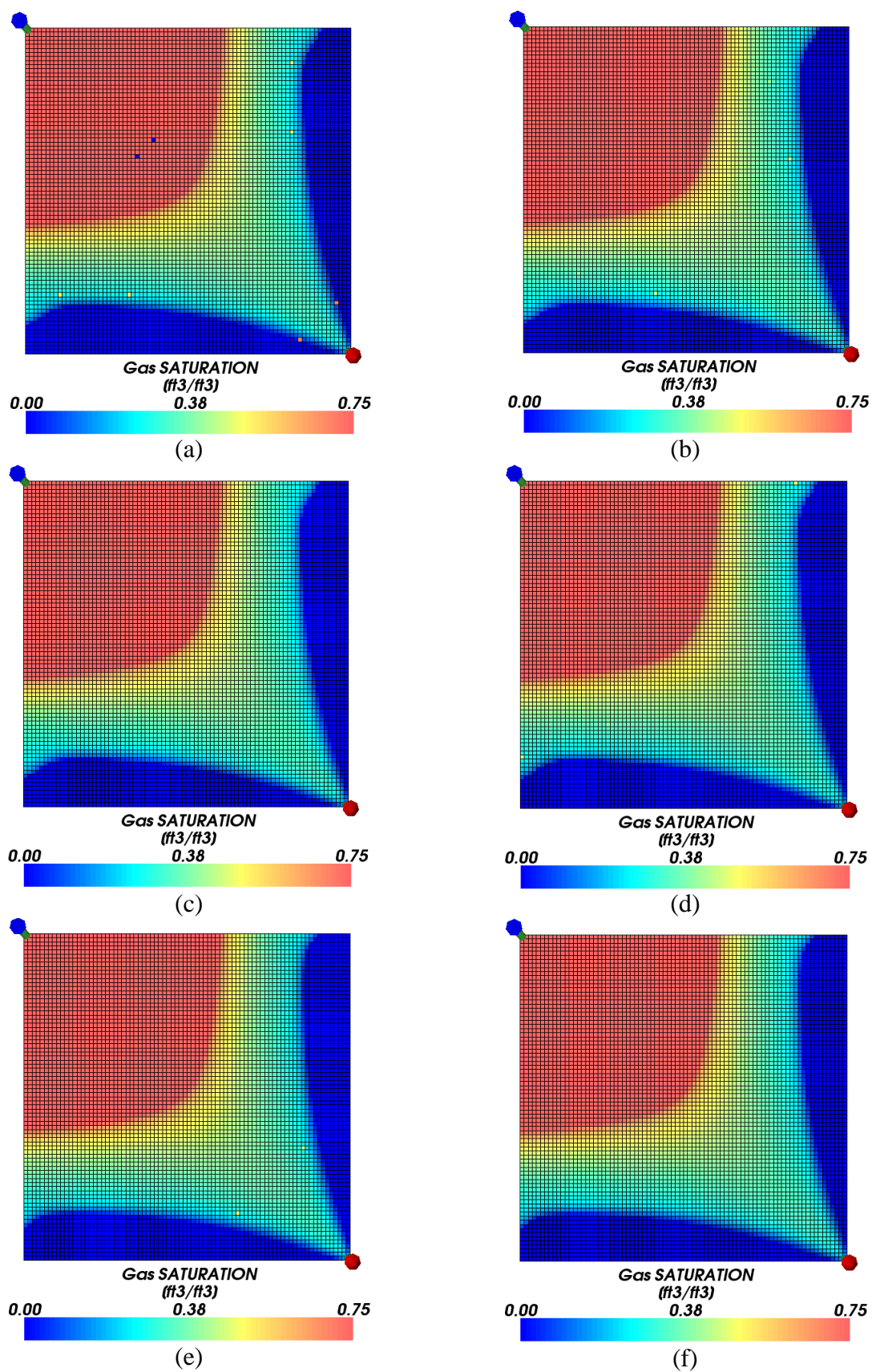


Figure 5.13 – Gas saturation fields at 500 days for all formulations - Case 1 using a 80x80 Cartesian grid. a) IMPEC; b) IMPSAT-0; c) IMPSAT-1; d) IMPSAT-2; e) FI-0; and f) FI-1



The CPU time for each of the formulations and grids is presented in Table 5.6. As it can be observed, the IMPEC formulation is one of the faster formulations for the coarser grid (20x20). However, when the grid is refined, the performance of the IMPEC and IMPSAT-2 formulations reduces and the other formulations increase. For the finest grid, the FI approaches performance sharply increase. This happens because as the other formulations decrease their time-step sizes due to numerical stability, while the FI approaches can use the maximum time.

Table 5.6 – CPU time (s) for all simulations - Case 1 using 2D Cartesian grids.

<b>Formulation</b>	<b>20x20</b>	<b>40x40</b>	<b>80x80</b>
IMPEC	3.96	67.98	1030.19
IMPSAT-0	3.76	38.11	630.84
IMPSAT-1	3.73	38.18	638.84
IMPSAT-2	4.94	40.56	953.99
FI-0	7.91	72.16	415.87
FI-1	7.86	69.70	408.59

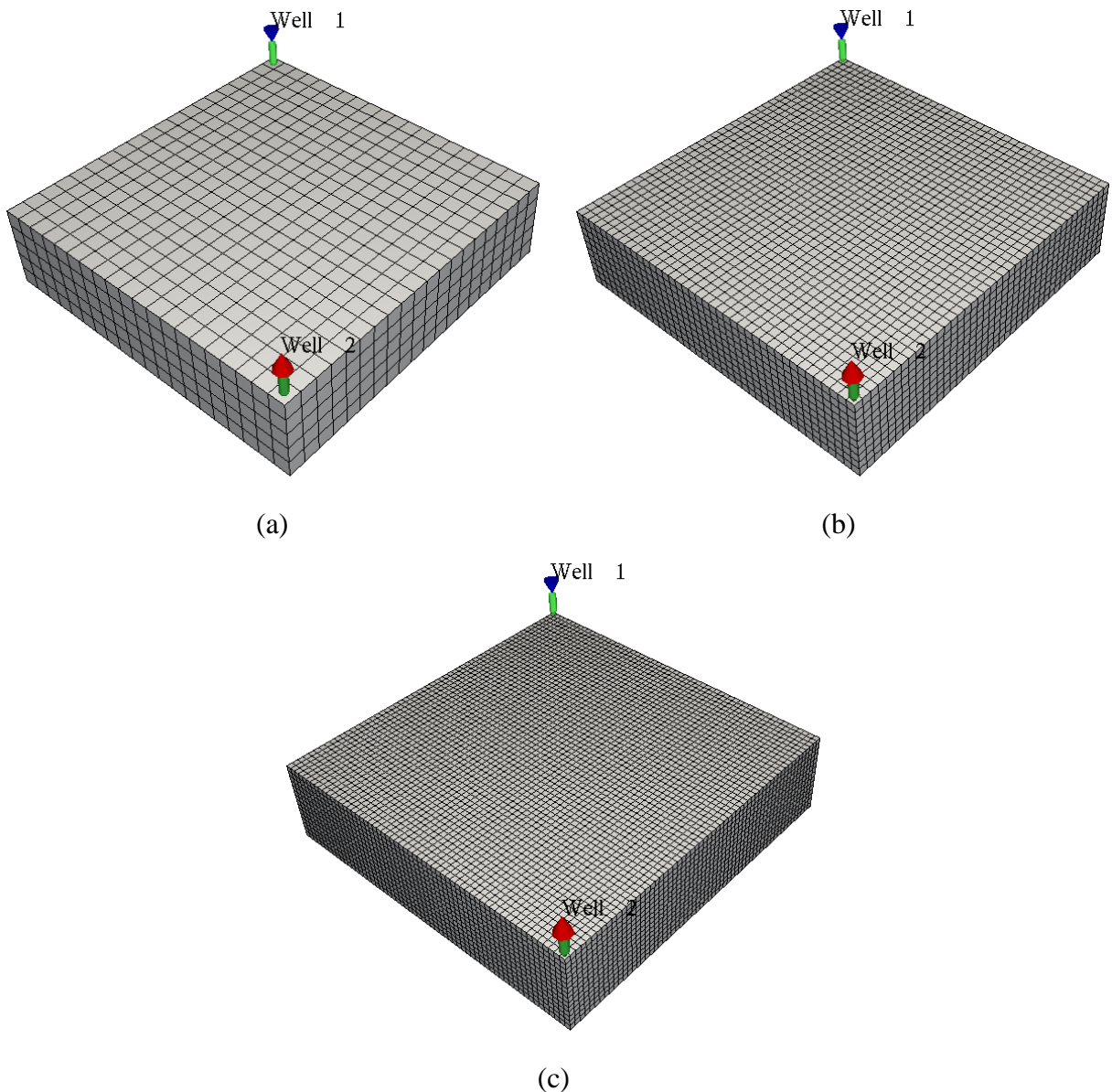


### 5.1.2 Case study 1: 3D Cartesian grid

In order to see the effect of variation in z direction, we run the 2D problem stated in section 5.1.1 as a 3D problem.

For the 3D Cartesian analysis of Case 1 we consider three grids: 20x20x5, 40x40x10, and 80x80x15. The grids are shown in Figure 5.14. The time-step control parameters are presented in Appendix A.

Figure 5.14 – 3D Cartesian grids - Case 1. a) 20x20x5; b) 40x40x10; and c) 60x60x15.



As the solutions for the IMPSAT formulations are very similar for this case, we present only the results for the IMPSAT-0, considering the finest grid. For the same reason we present only the results for the FI-0. The oil and gas rates are presented in Figure 5.15 and 5.16. From these figures, it is possible to see that all the formulations are in good agreement.

Figure 5.15 – Production rates comparison for 3D Cartesian 60x60x15 between IMPEC and IMPSAT-0 - Case 1. a) oil; and b) gas.

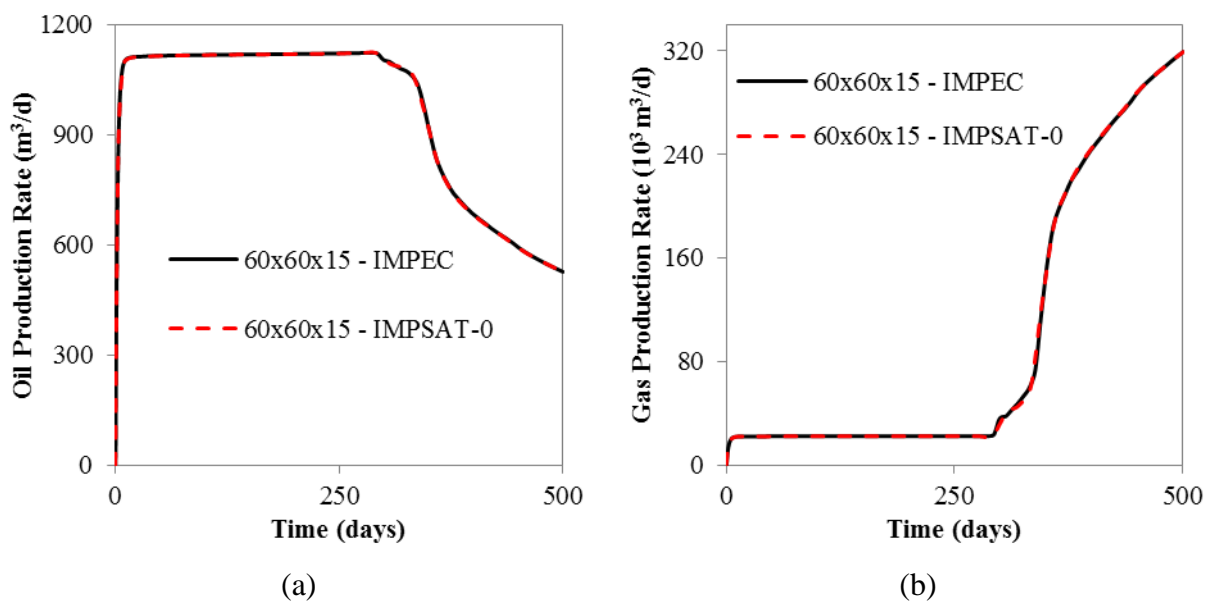
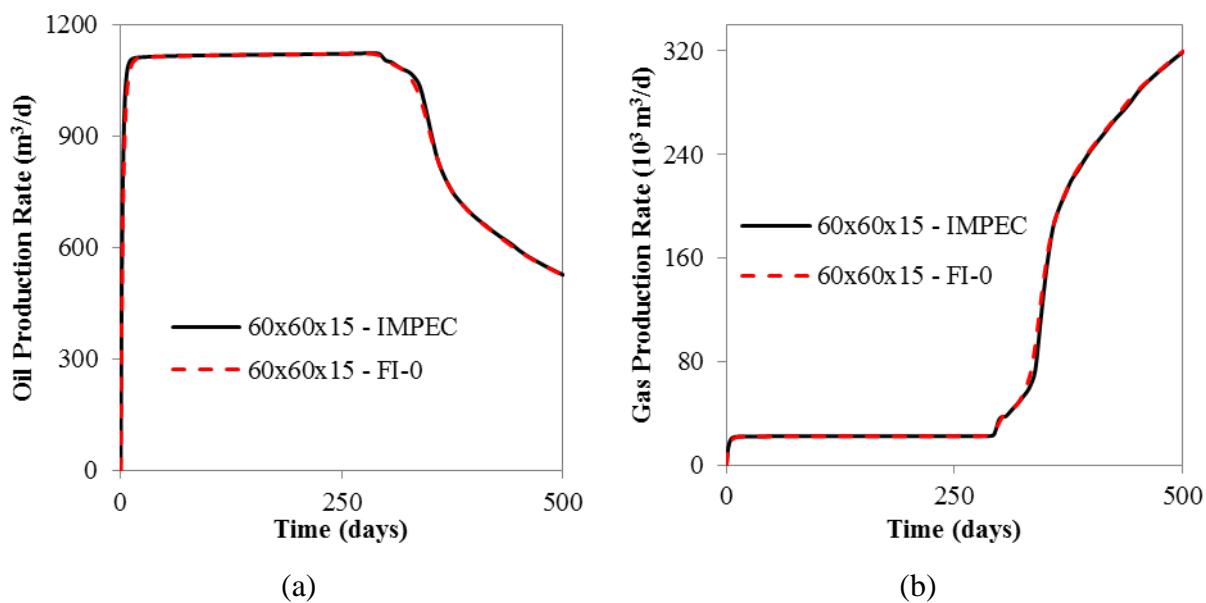


Figure 5.16 – Production rates comparison for 3D Cartesian 60x60x15 between IMPEC and FI-0 for Case 1. a) oil; and b) gas.



The time-step profiles for the 60x60x15 grid are presented in Figure 5.17. From this figure, it is possible to see that the IMPEC reached the lowest values of time-step size. Also, the maximum time-step for the FI approaches are about 20 times larger than the ones used by the IMPSAT approaches.

Figure 5.17 – Time-stepping profiles for all formulations – Case 1 using 3D Cartesian grids.

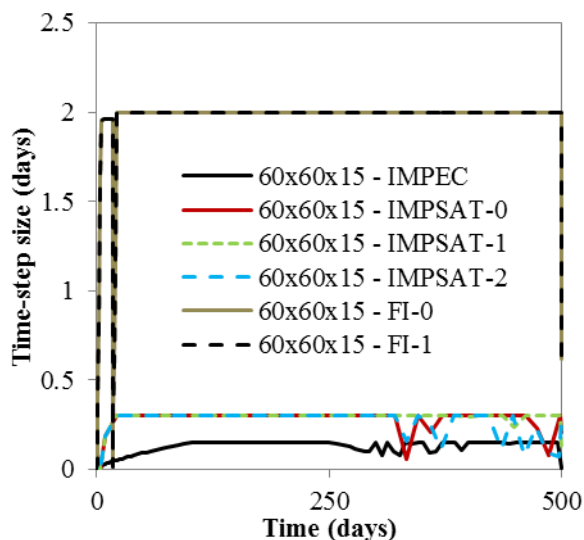


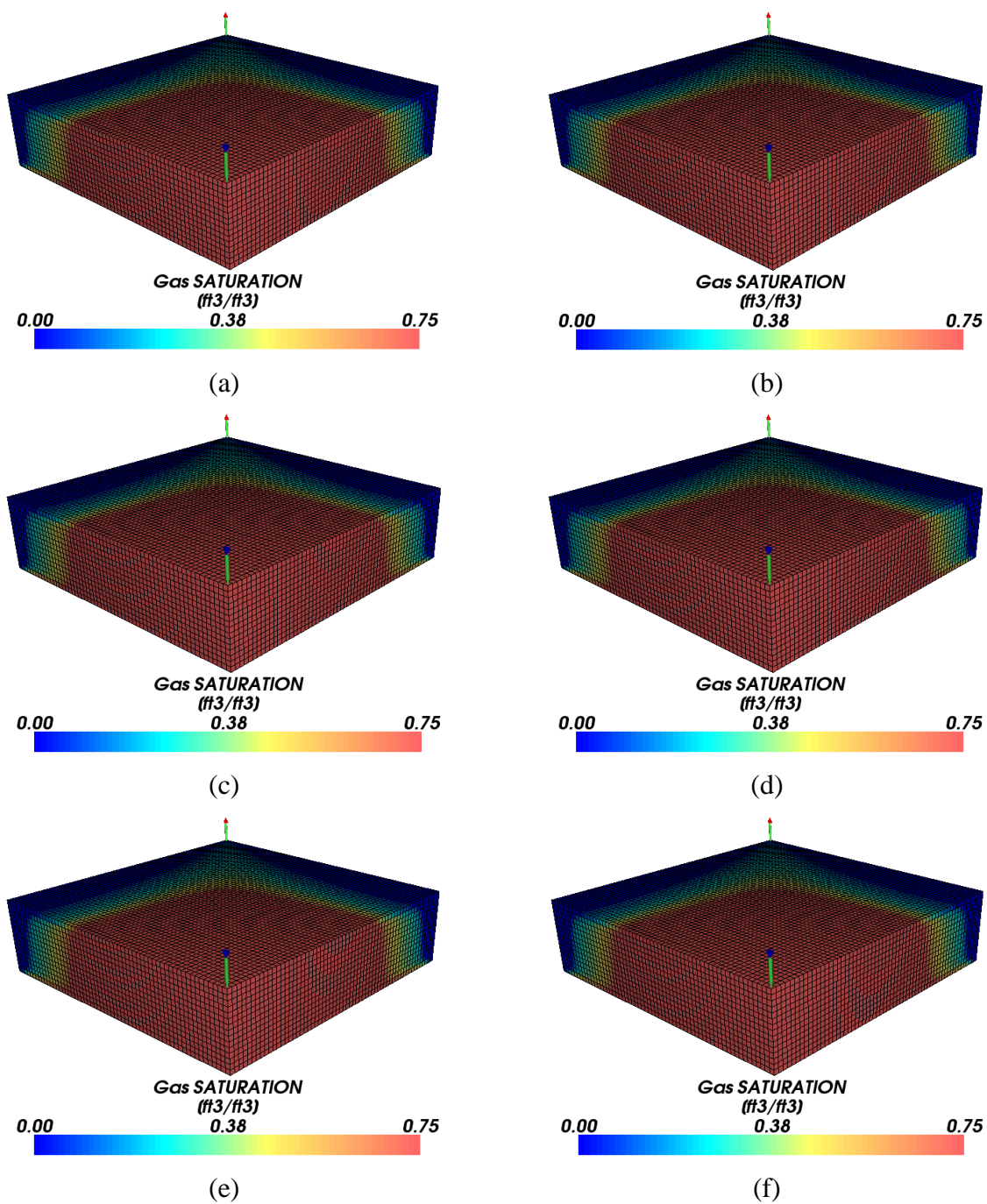
Figure 5.18 presents the gas saturation fields for the 60x60x15 grid at 700 days, for all formulations. Once again, it is possible to infer a good agreement between all the formulations. One can observe that the gas flows faster at the bottom of the 3D reservoir. Such behaviour cannot be obtained with the 2D discretization.

The CPU times for 3D Cartesian grids are presented in Table 5.7. From this table, once again, it is possible to observe that the performance of the FI approaches increase with the grid refinement.

Table 5.7 – CPU time (s) of all simulations - Case 1 using 3D Cartesian grids.

<b>Formulation</b>	<b>20x20x5</b>	<b>40x40x10</b>	<b>60x60x15</b>
IMPEC	22.2	772.8	5663.3
IMPSAT-0	22.7	512.7	4727.2
IMPSAT-1	21.8	552.7	6704.9
IMPSAT-2	31.6	824.1	8599.0
FI-0	34	520.1	3667.8
FI-1	32.3	520	3693.8

Figure 5.18 – Gas saturation fields at 700 days for all formulations - Case 1 using a 60x60x15 Cartesian grid. a) IMPEC; b) IMPSAT-0; c) IMPSAT-1; d) IMPSAT-2; e) FI-0; and f) FI-1



### 5.1.3 Case study 1: 2D EbFVM

Using unstructured grids, it is important to see if the grid uniformity has any impact in the performance of the formulations. Since unstructured grids are used to map complex geometries, it is not possible to use uniform grids for these cases. Therefore, a convenient feature of the formulations is that the results must be independently of the grid distortion. In order to test this characteristic, the formulations are first run for three regular grids of quadrilateral elements (Figure 5.19), and then run for non-uniform grids of quadrilateral (Figure 5.20) and triangular (Figure 5.21) elements.

Figure 5.19 – 2D regular quadrilateral element grids - Case 1. a) 20x20; b) 40x40; and c) 60x60.

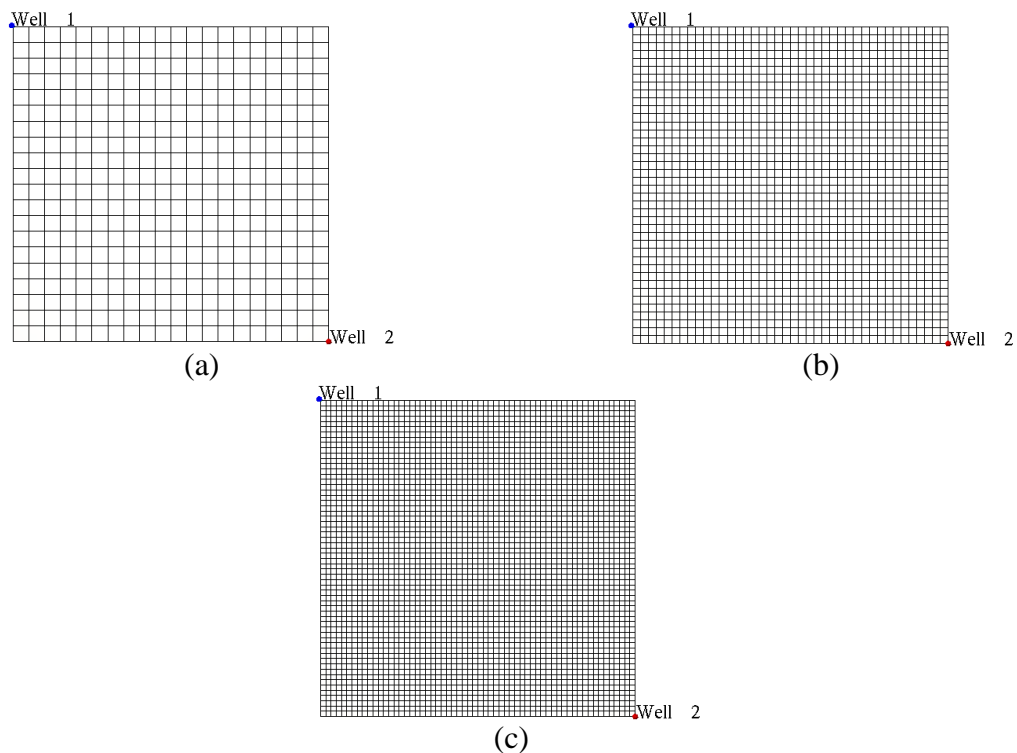




Figure 5.20 – 2D unstructured quadrilateral grids - Case 1. a) 1199 vertices (1134 elements); b) 2661 vertices (2568 elements); and c) 3387 vertices (3282 elements).

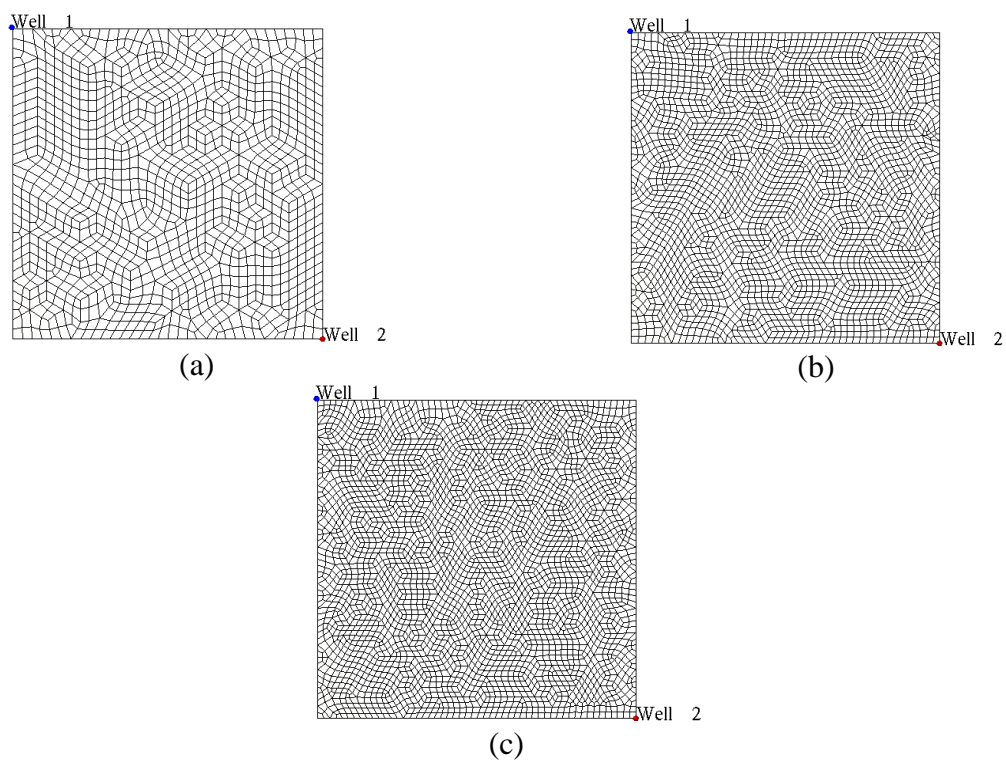
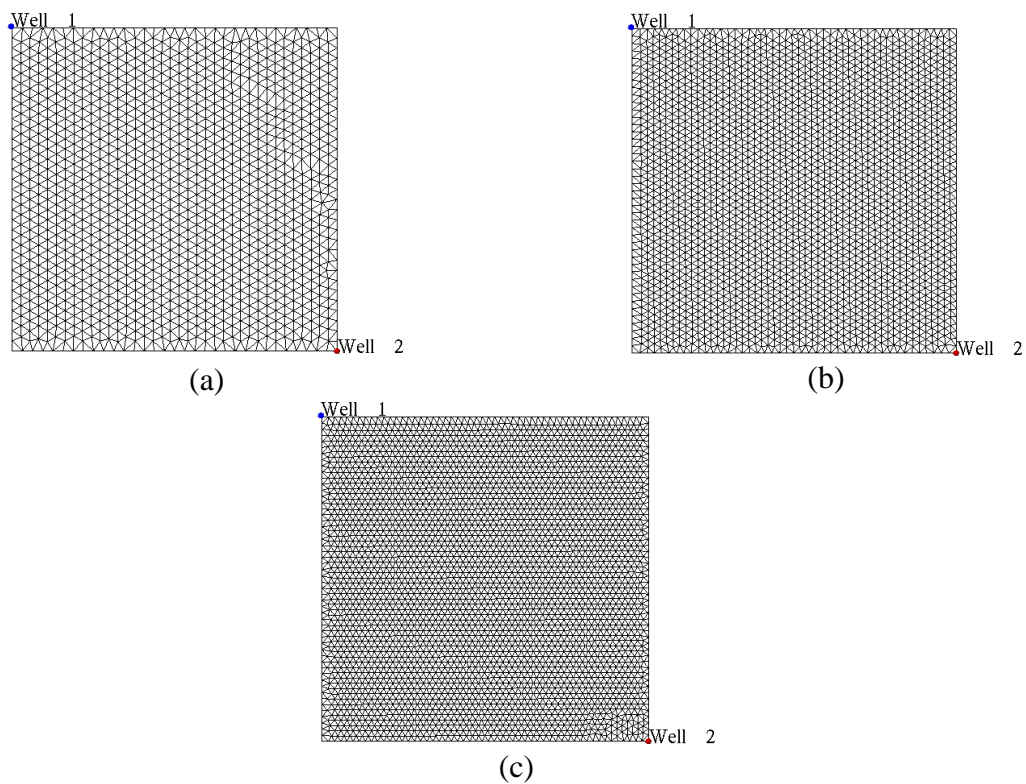


Figure 5.21 – 2D unstructured triangular grids - Case 1. a) 1220 vertices (2310 elements); b) 2330 vertices (4482 elements); and c) 3329 vertices (6444 elements).



For the same reasons described above, Figures 5.22 and 5.23 present the comparison of the oil and gas rates using the 60x60 regular quadrilateral grid only for the IMPSAT-0 and FI-0 approaches with the IMPEC approach, respectively.

Figure 5.22 – Production rates comparison between IMPEC and IMPSAT-0 - Case 1, using 2D regular quadrilateral grids. a) oil; and b) gas.

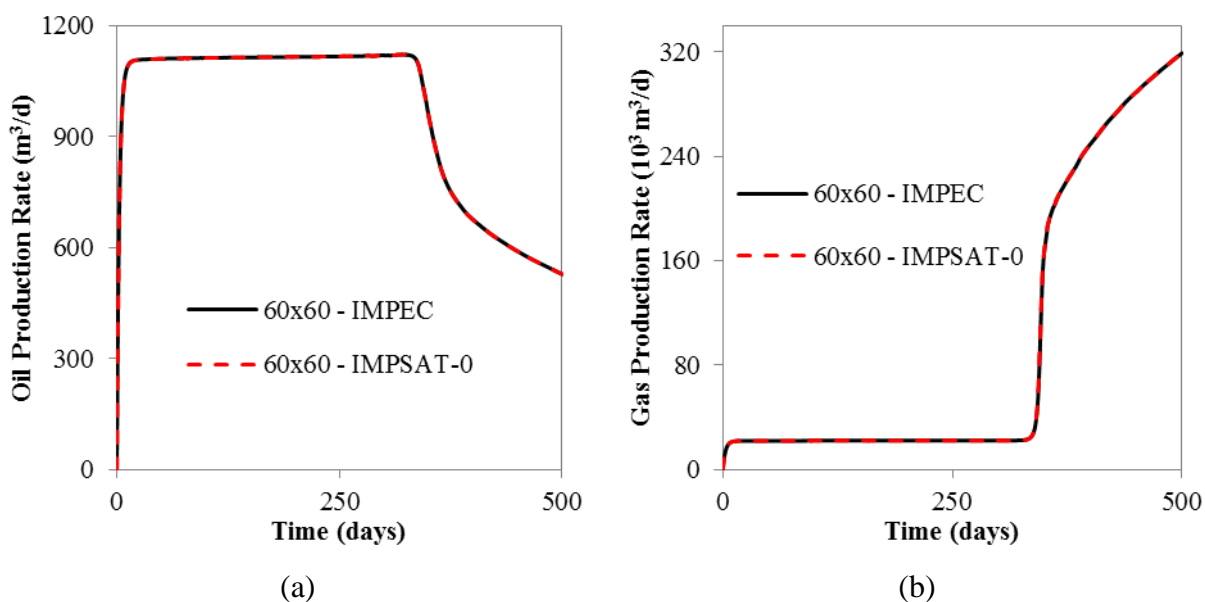
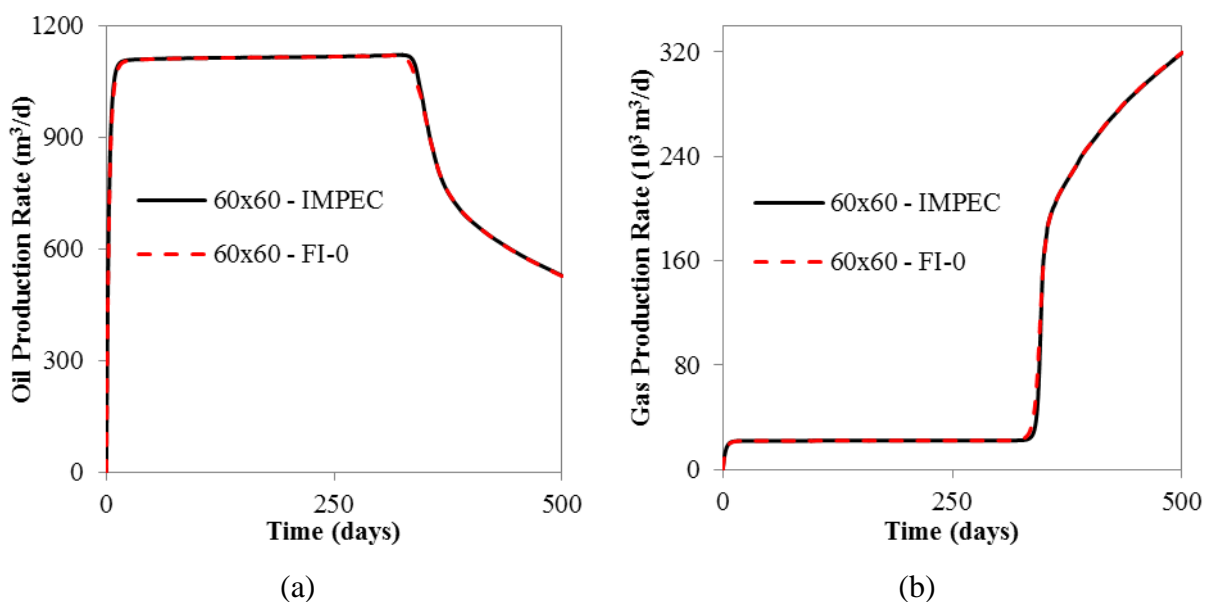


Figure 5.23 – Production rates comparison between IMPEC and FI-0 - Case 1, using 2D regular quadrilateral grids. a) oil; and b) gas.



Figures 5.24 and 5.25 present the comparison between the IMPEC and the IMPSAT-0 and FI-0, respectively, for unstructured quadrilateral grid with 3387 vertices.

Figure 5.24 – Production rates comparison between IMPEC and IMPSAT-0 - Case 1 for 2D unstructured quadrilateral grid. a) oil; and b) gas.

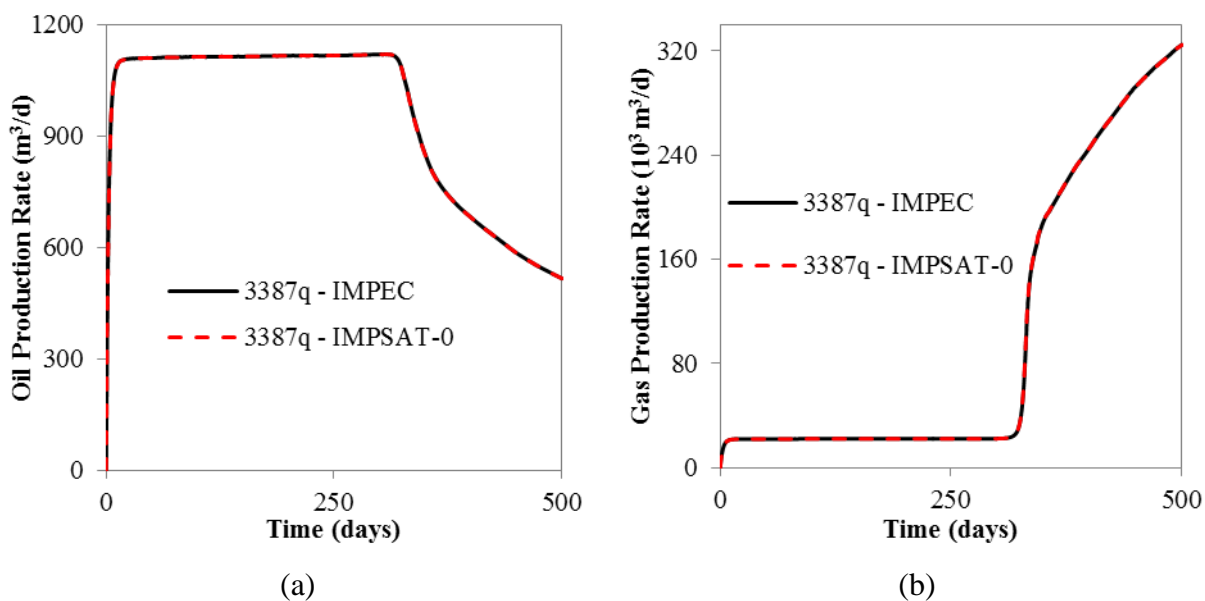
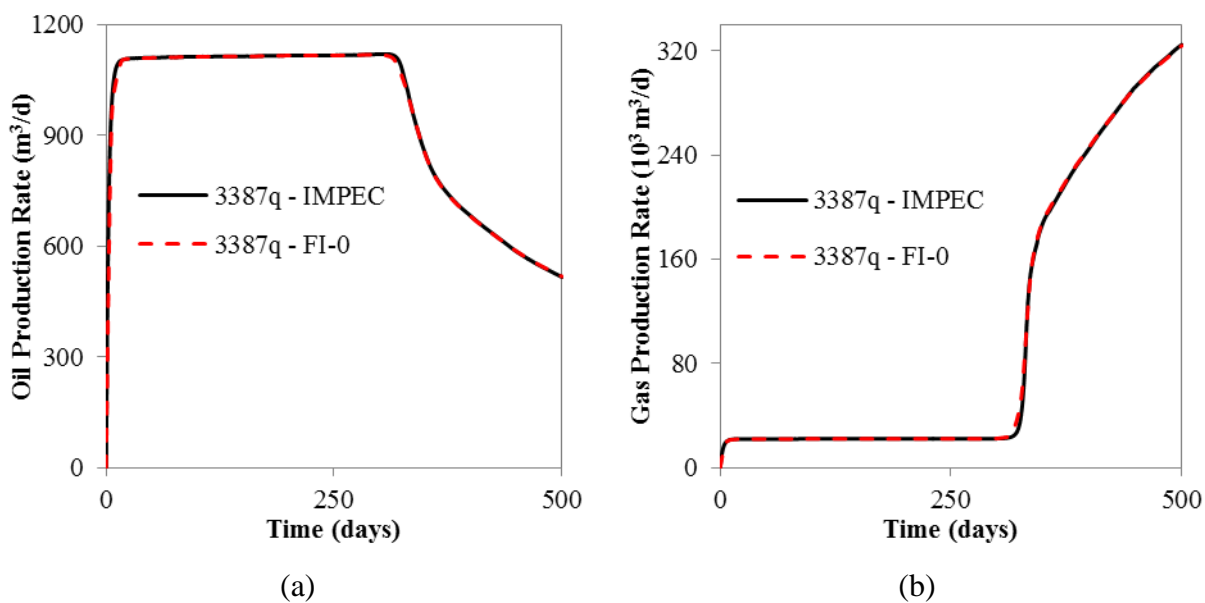


Figure 5.25 – Production rates comparison between IMPEC and FI-0 - Case 1 for 2D unstructured quadrilateral grid. a) oil; and b) gas.



Finally, the comparison between the IMPEC and the IMPSAT-0 and FI-0 using a 2D unstructured triangular grid with 3329 vertices are presented in Figures 5.26 and 5.27, respectively.



Figure 5.26 – Production rates comparison between IMPEC and IMPSAT-0 - Case 1 for 2D unstructured triangular grid. a) oil; and b) gas.

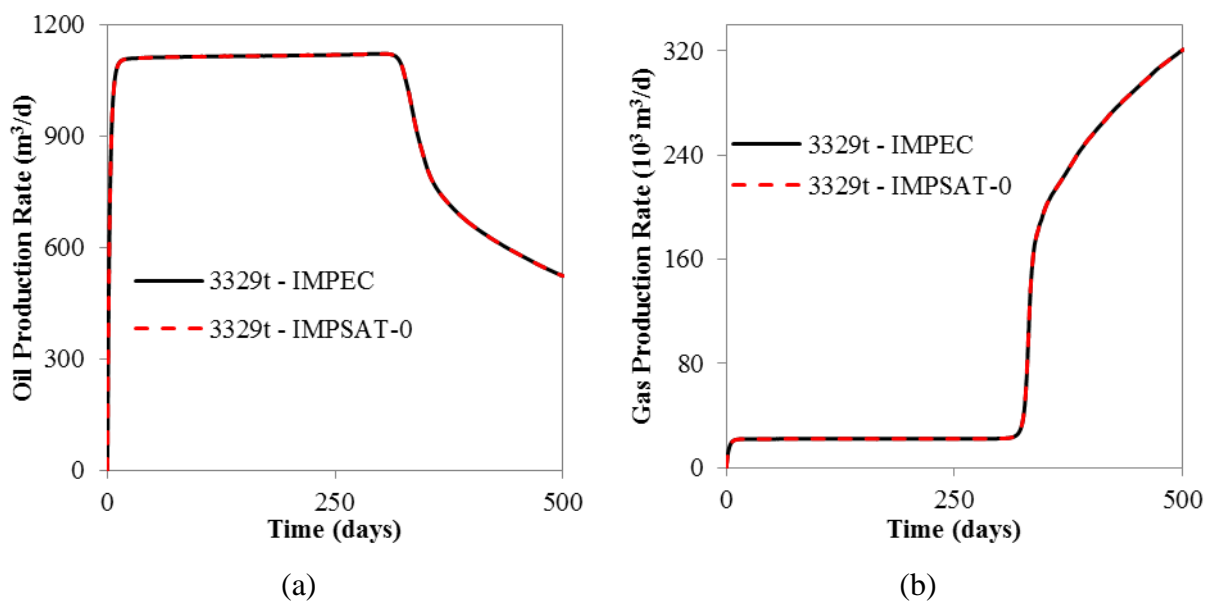
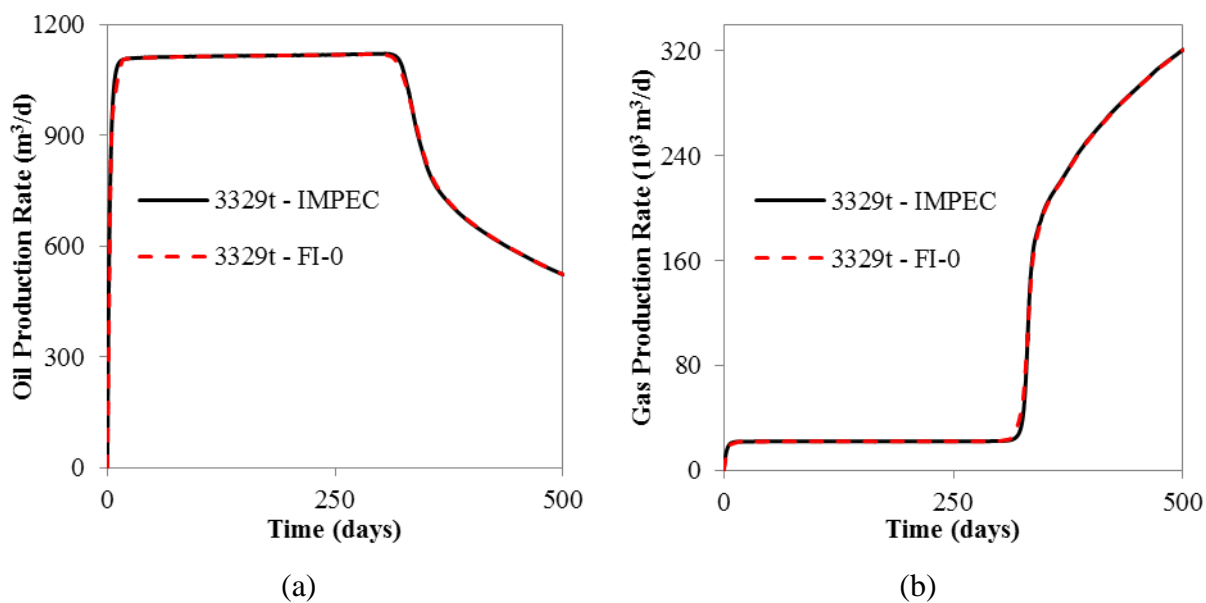
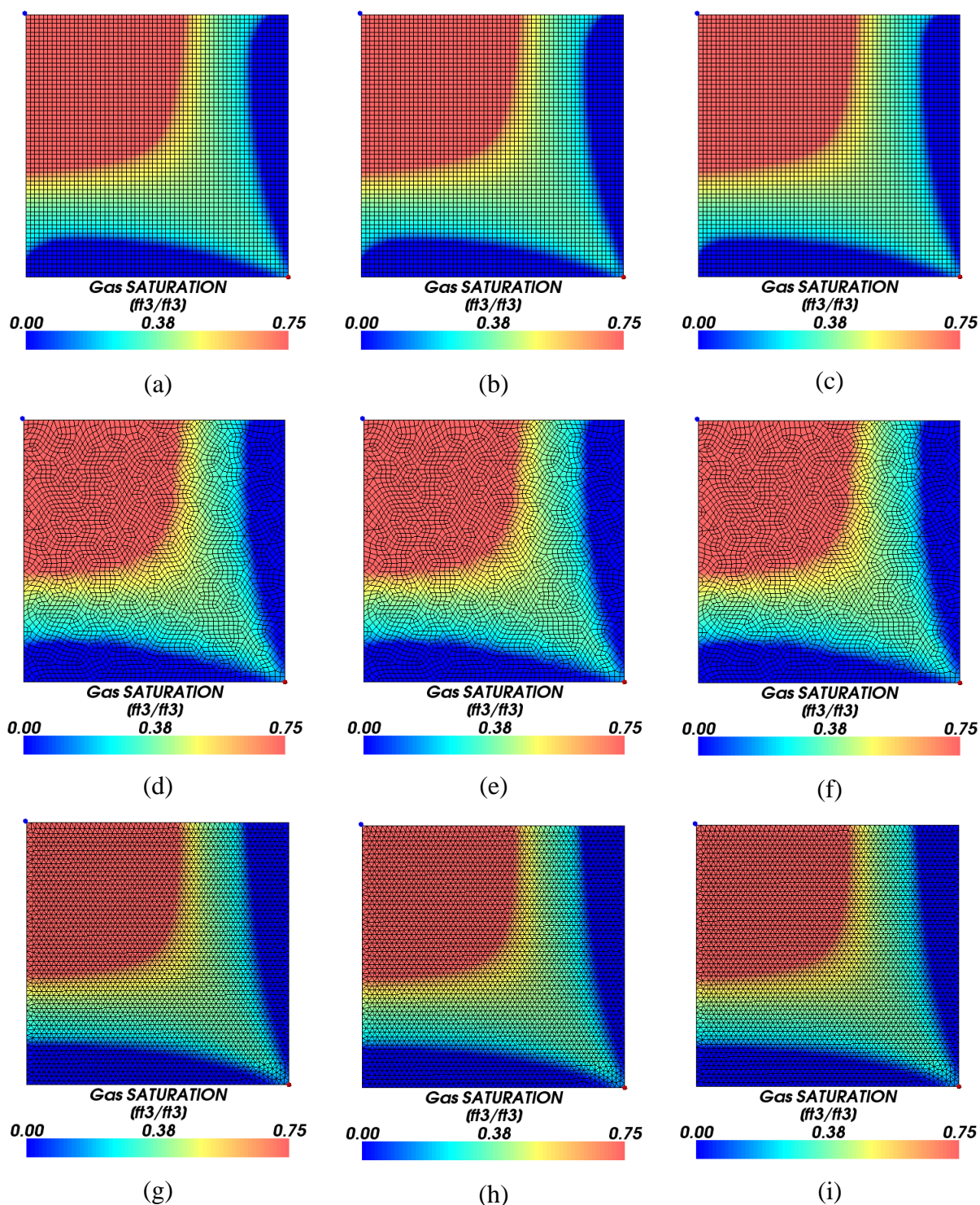


Figure 5.27 – Production rates comparison between IMPEC and FI-0 - Case 1 for 2D unstructured triangular grid. a) oil; and b) gas.



The gas saturation fields at 500 days are presented in Figure 5.28 for the finest grids investigated. A good agreement between the saturation field obtained with all formulations and grids is observed in this figure.

Figure 5.28 – Gas saturation field at 500 days for 2D EbFVM - Case 1. a) quadrilateral 60x60 IMPEC; b) quadrilateral 60x60 IMPSAT-0; c) quadrilateral 60x60 FI-0; d) quadrilateral 3387 vertices IMPEC; e) quadrilateral 3387 vertices IMPSAT-0; f) quadrilateral 3387 vertices FI-0; g) triangle 3329 vertices IMPEC; h) triangle 3329 vertices IMPSAT-0; and i) triangle 3329 vertices FI-0;



The CPU time for all formulations using the regular quadrilateral grids is presented in Table 5.8. The same information is presented for unstructured quadrilateral grids

in Table 5.9, and for unstructured triangular grids in Table 5.10. Once again, the same perform pattern verified for the Cartesian is verified for the EbFVM formulation. It is worthwhile to mention that the 60x60 regular grid has 3721 vertices, which is larger than the number of vertices of the finest unstructured grids used for quadrilateral and triangular elements. For this reason, the CPU time for the 60x60 grid will be larger than the CPU times for the finest grids shown in Tables 5.9 and 5.10.

Table 5.8 – CPU time (s) of all simulations - Case 1 using 2D regular quadrilateral grids.

<b>Formulation</b>	<b>20x20</b>	<b>40x40</b>	<b>60x60</b>
IMPEC	15.2	272.6	1540.7
IMPSAT-0	10.3	171.2	997.5
IMPSAT-1	10.8	176.5	966.0
IMPSAT-2	14.3	224	1192.6
FI-0	18.6	179.3	797.4
FI-1	18.7	184.6	732.5

Table 5.9 – CPU time (s) of all simulations - Case 1 using 2D unstructured quadrilateral grids.

<b>Formulation</b>	<b>1199 vertices</b>	<b>2661 vertices</b>	<b>3387 vertices</b>
IMPEC	113.8	699.2	954.6
IMPSAT-0	71.6	458.3	588
IMPSAT-1	75.3	478.3	629.2
IMPSAT-2	106	564.7	779.7
FI-0	110	470.3	463.3
FI-1	108.6	402.5	420.1

Table 5.10 – CPU time (s) of all simulations - Case 1 using 2D unstructured triangular grids.

<b>Formulation</b>	<b>1220 vertices</b>	<b>2330 vertices</b>	<b>3329 vertices</b>
IMPEC	109.6	649.2	1354.4
IMPSAT-0	97.3	445.4	1002.5
IMPSAT-1	101.3	500.4	1128.2
IMPSAT-2	128.7	653.5	1502.5
FI-0	89.1	301.2	582.8
FI-1	85.9	269.6	566

### 5.1.4 Case study 1: 3D EbFVM

Four sets of 3D unstructured grids were used for each element type in this analysis. These sets are presented in Figures 5.29, 5.30, 5.31 and 5.32 for hexahedrons, tetrahedrons, prisms and pyramids, respectively.

Figure 5.29 – 3D hexahedron element grids - Case 1. a) 1024 vertices; b) 6480 vertices; and c) 11767 vertices.

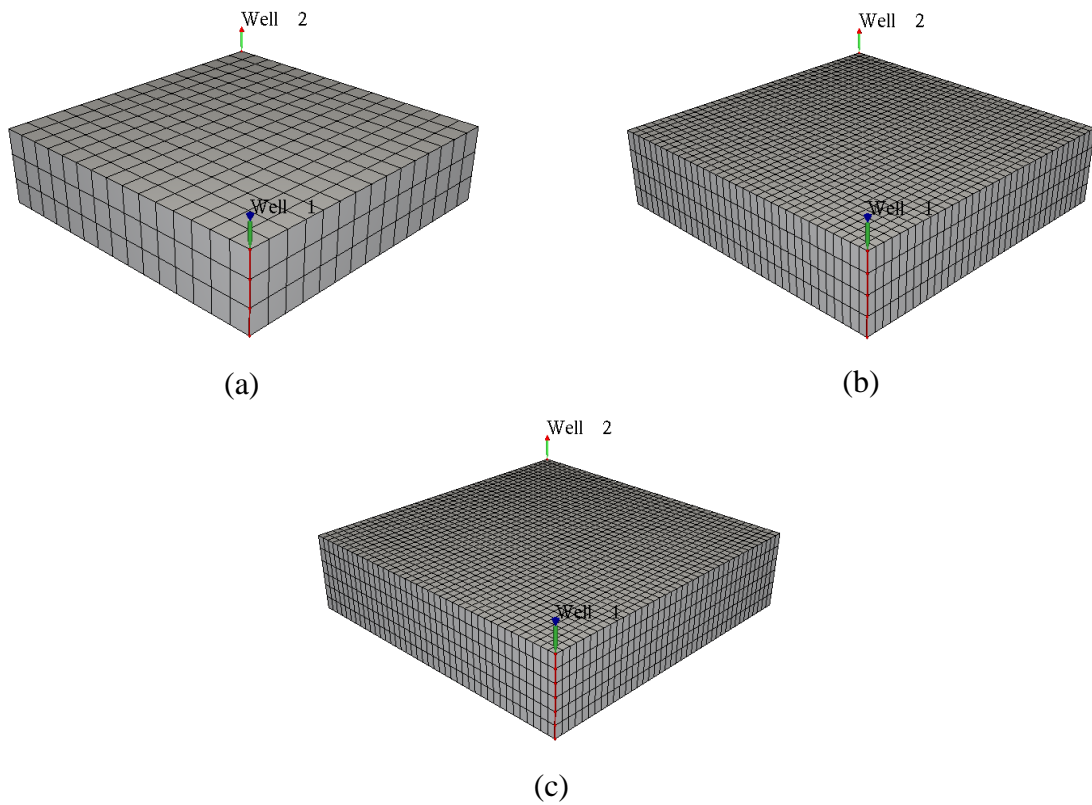


Figure 5.30 – 3D tetrahedron element grids - Case 1. a) 1024 vertices; b) 4056 vertices; and c) 16810 vertices.

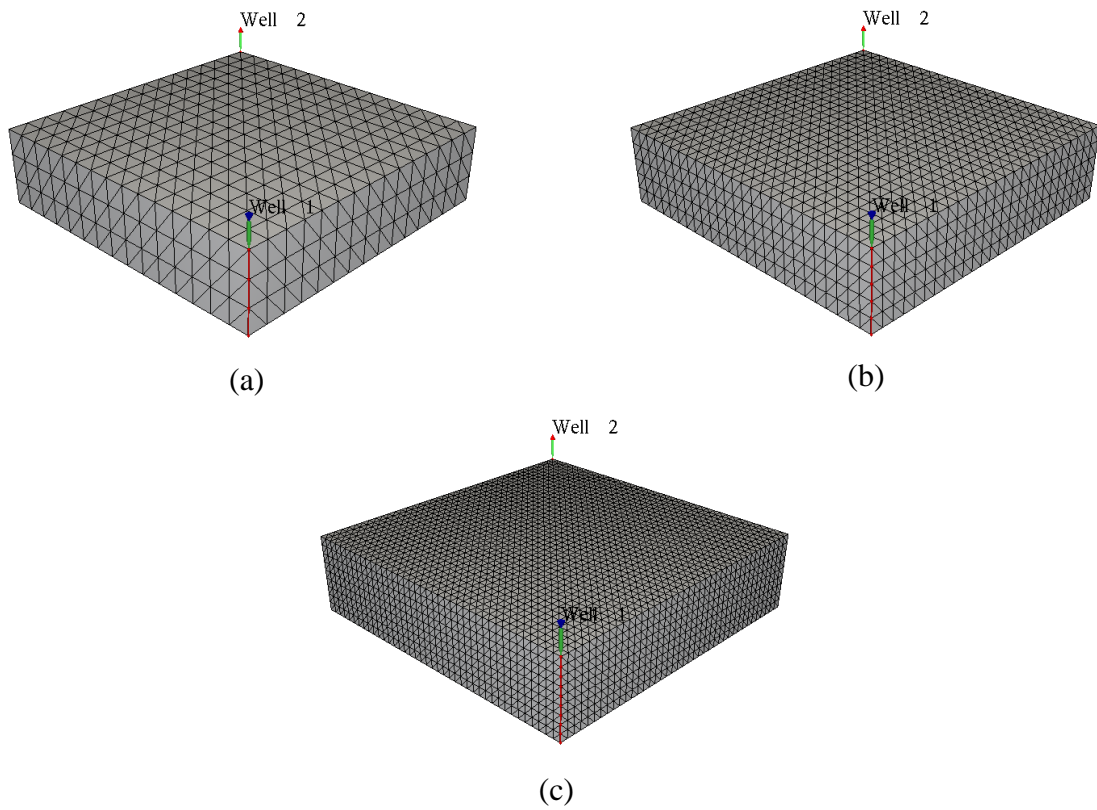


Figure 5.31 – 3D prism element grids - Case 1. a) 1024 vertices; b) 4056 vertices; and c) 13448 vertices.

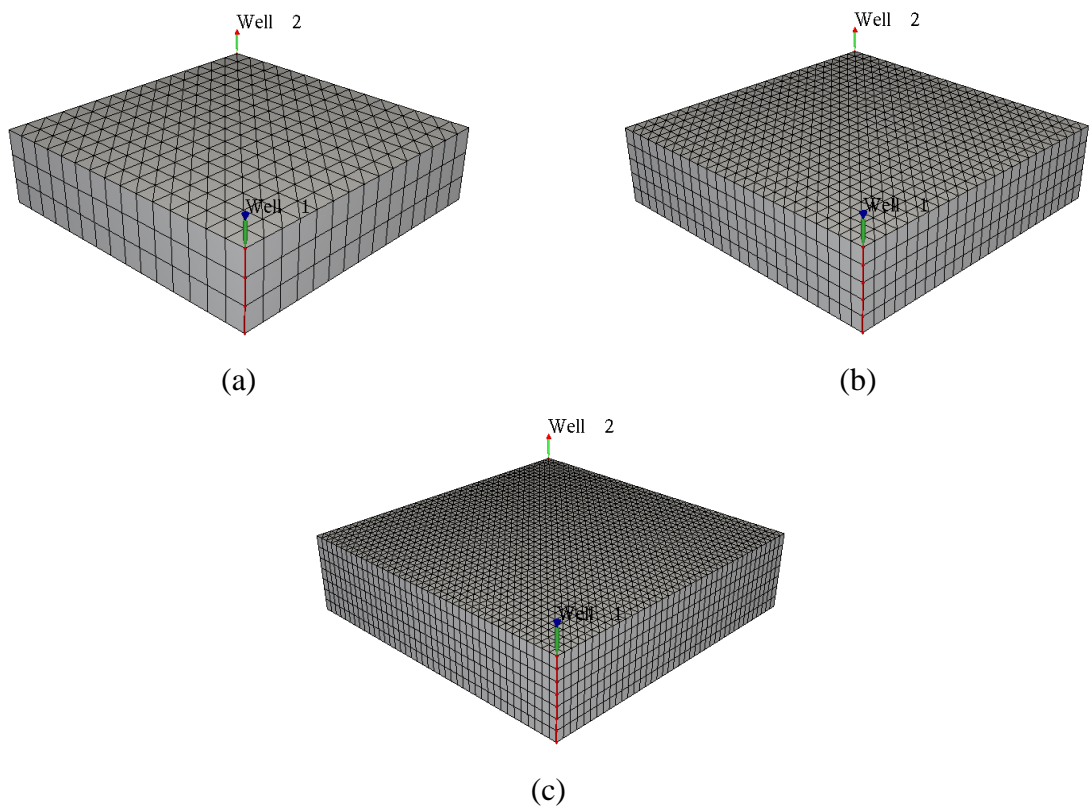
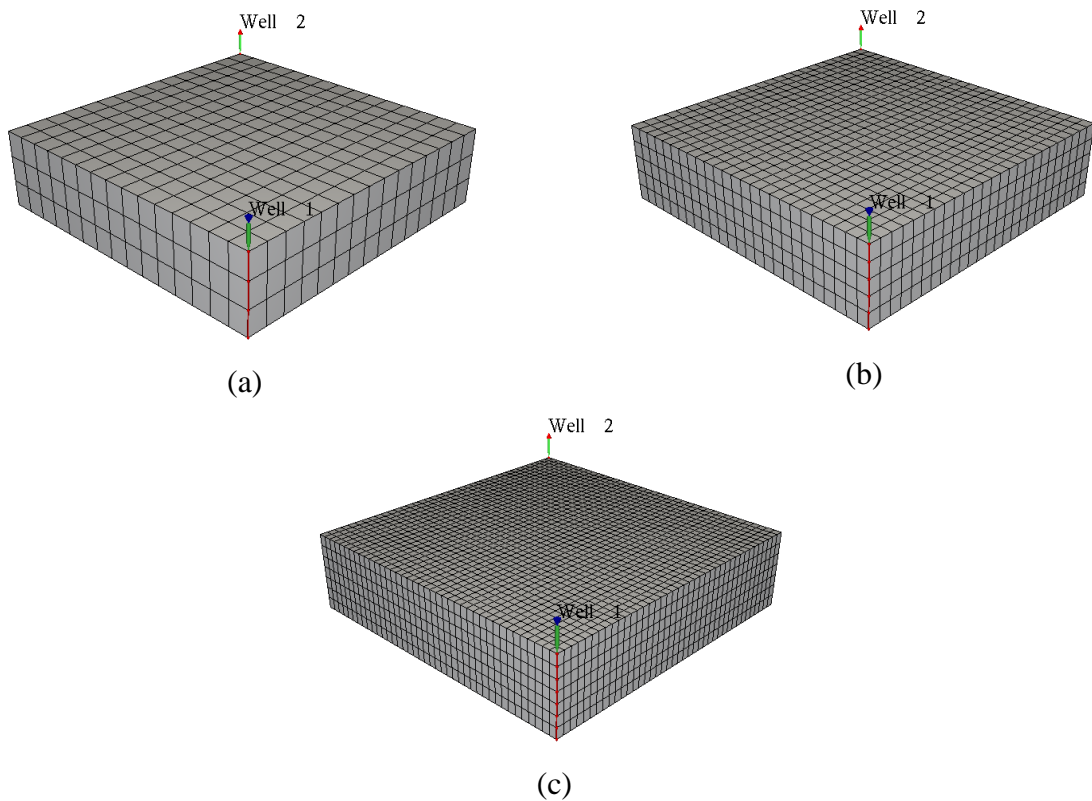




Figure 5.32 – 3D pyramid element grids - Case 1. a) 1699 vertices; b) 7181 vertices; and c) 24648 vertices.



Figures 5.33 and 5.34 present the comparison of the oil and gas rates using the hexahedron grid with 11767 vertices for the IMPSAT-0 and FI-0 approaches with the IMPEC approach, respectively. Figures 5.35 and 5.36 present the same study for tetrahedron grids as well as Figures 5.37 and 5.38 for prisms, and Figures 5.39 and 5.40 for pyramids. From these figures, it is possible to verify a good agreement between the formulations for all grid configurations investigated.

Figure 5.33 – Production rates comparison between IMPEC and IMPSAT-0 - Case 1 for 3D unstructured hexahedron grid. a) oil; and b) gas.

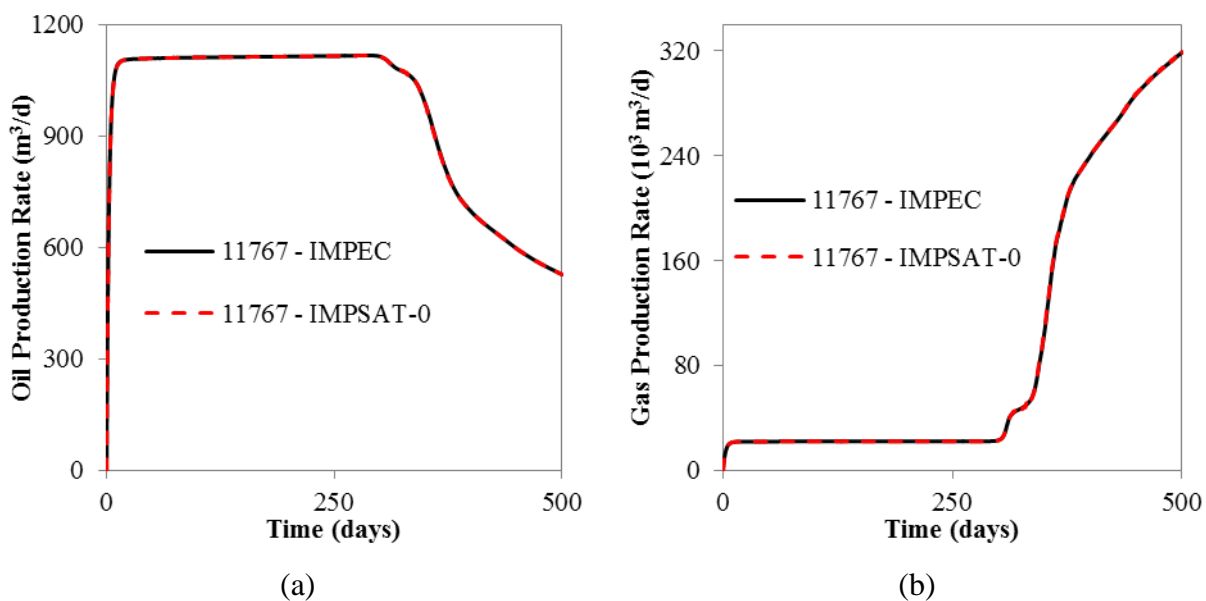


Figure 5.34 – Production rates comparison between IMPEC and FI-0 - Case 1 for 3D unstructured hexahedron grid. a) oil; and b) gas.

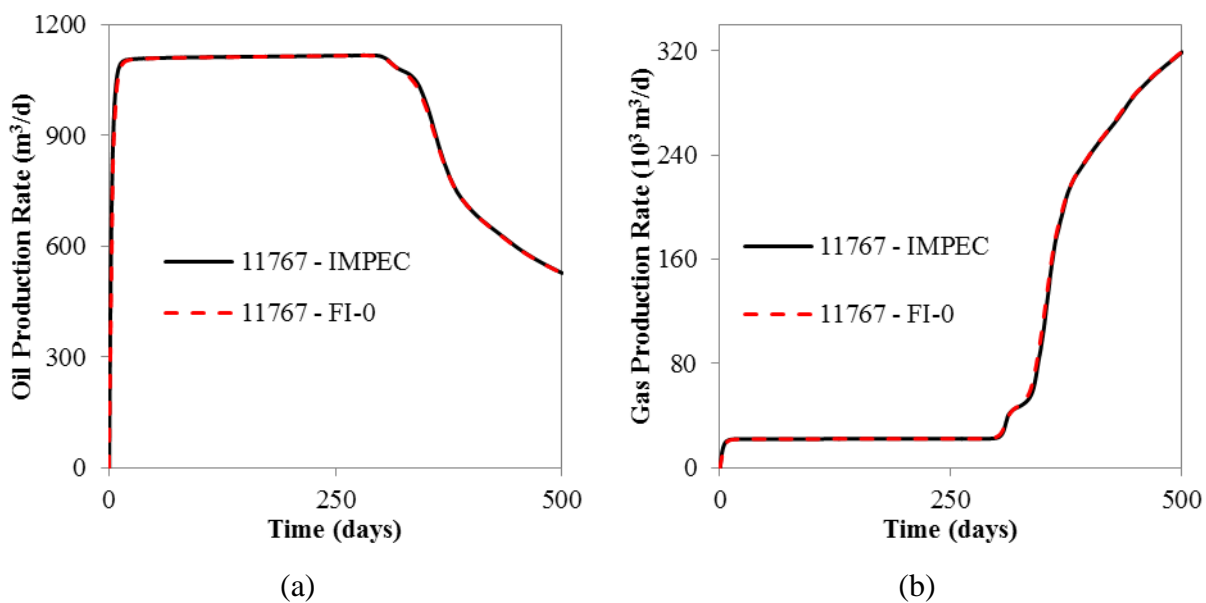


Figure 5.35 – Production rates comparison between IMPEC and IMPSAT-0 - Case 1 for 3D unstructured tetrahedron grid. a) oil; and b) gas.

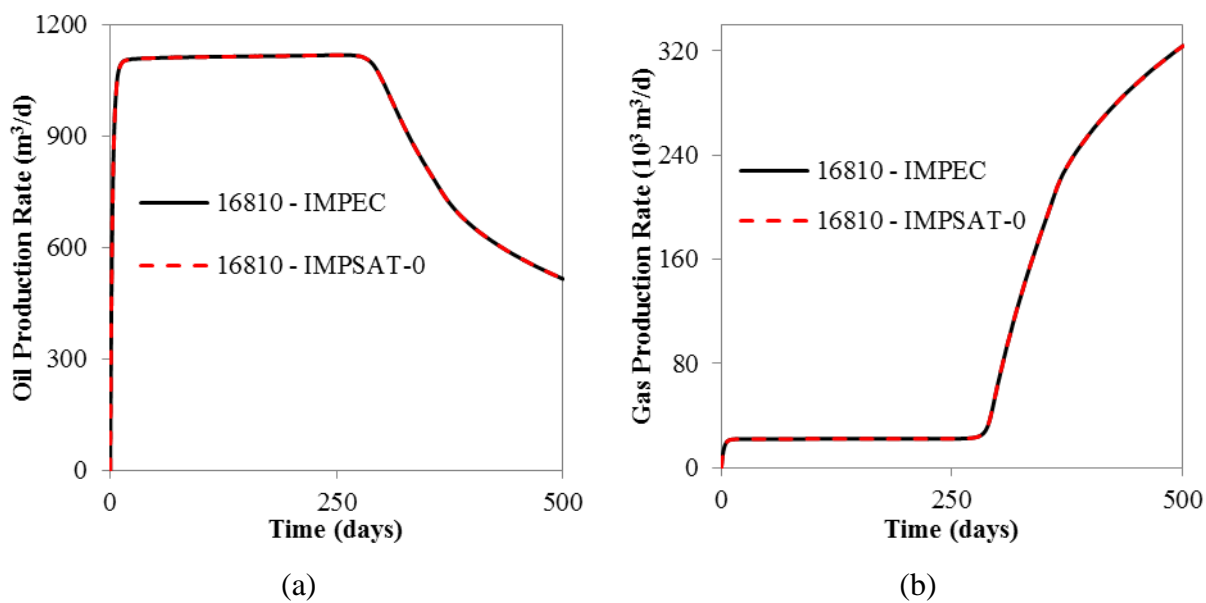


Figure 5.36 – Production rates comparison between IMPEC and FI-0 - Case 1 for 3D unstructured tetrahedron grid. a) oil; and b) gas.

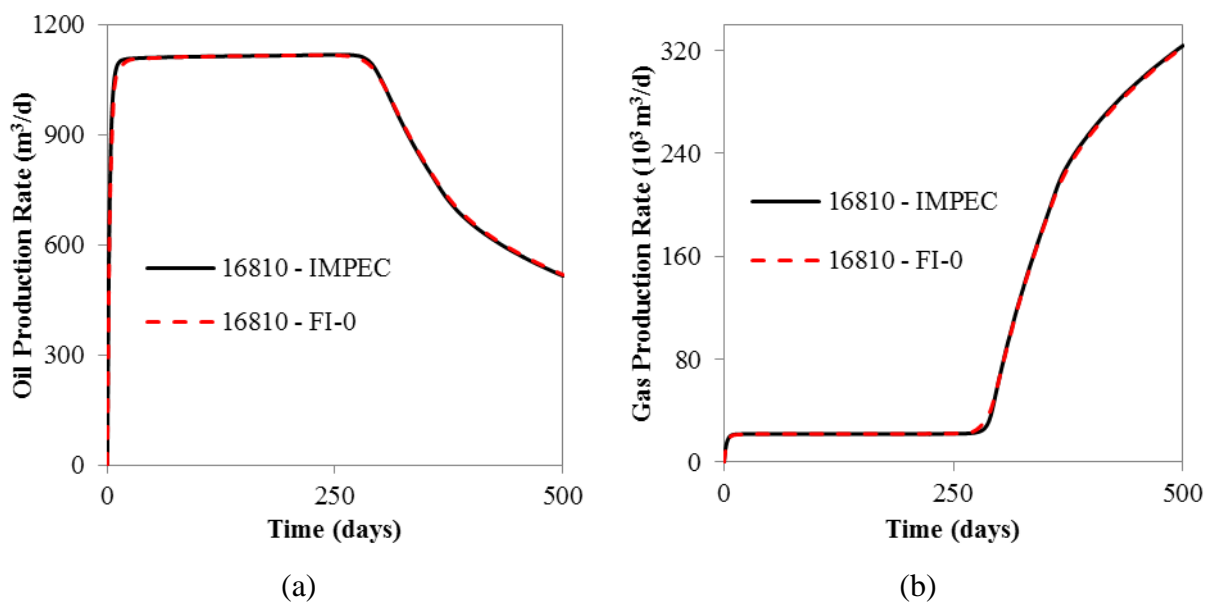




Figure 5.37 – Production rates comparison between IMPEC and IMPSAT-0 - Case 1 for 3D unstructured prism grid. a) oil; and b) gas.

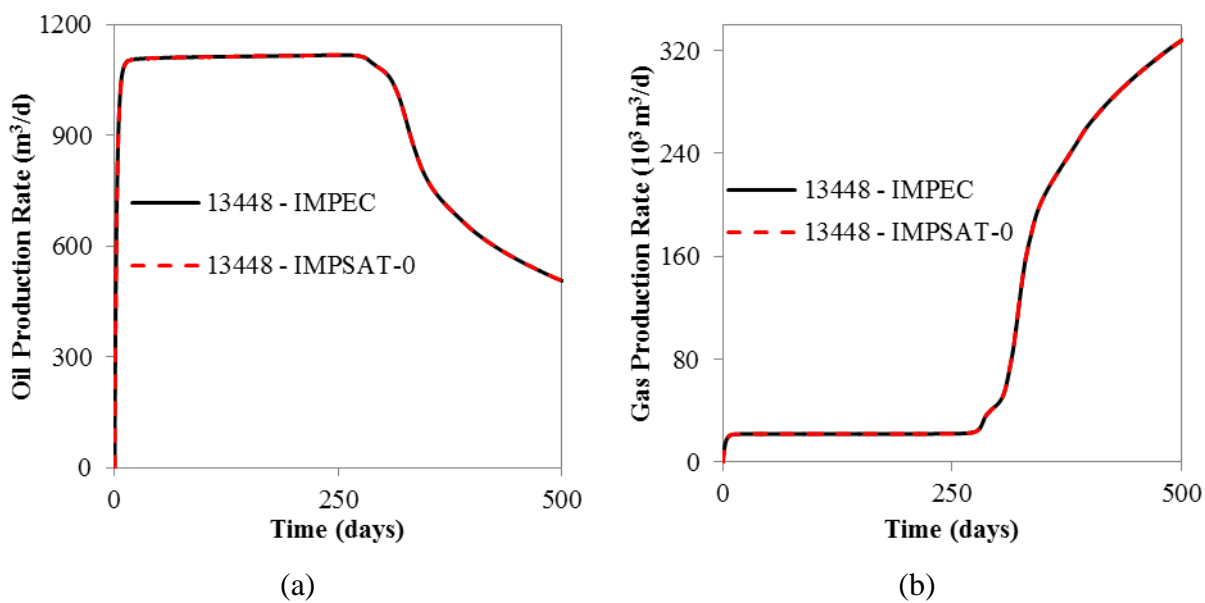


Figure 5.38 – Production rates comparison between IMPEC and FI-0 - Case 1 for 3D unstructured prism grid. a) oil; and b) gas.

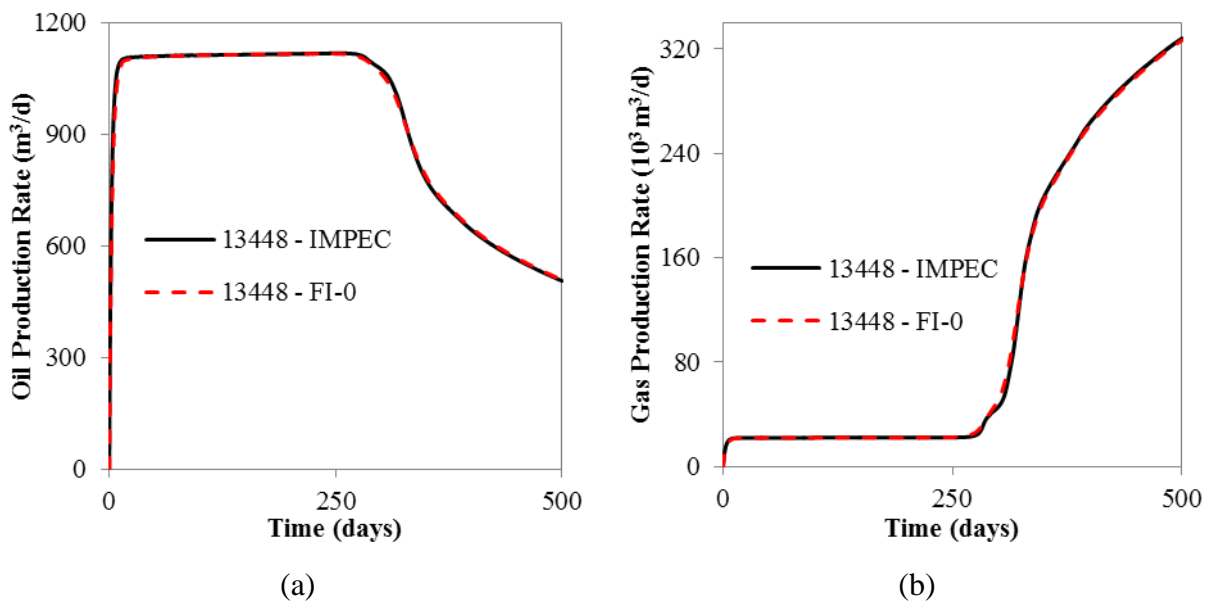


Figure 5.39 – Production rates comparison between IMPEC and IMPSAT-0 - Case 1 for 3D unstructured pyramid grid. a) oil; and b) gas.

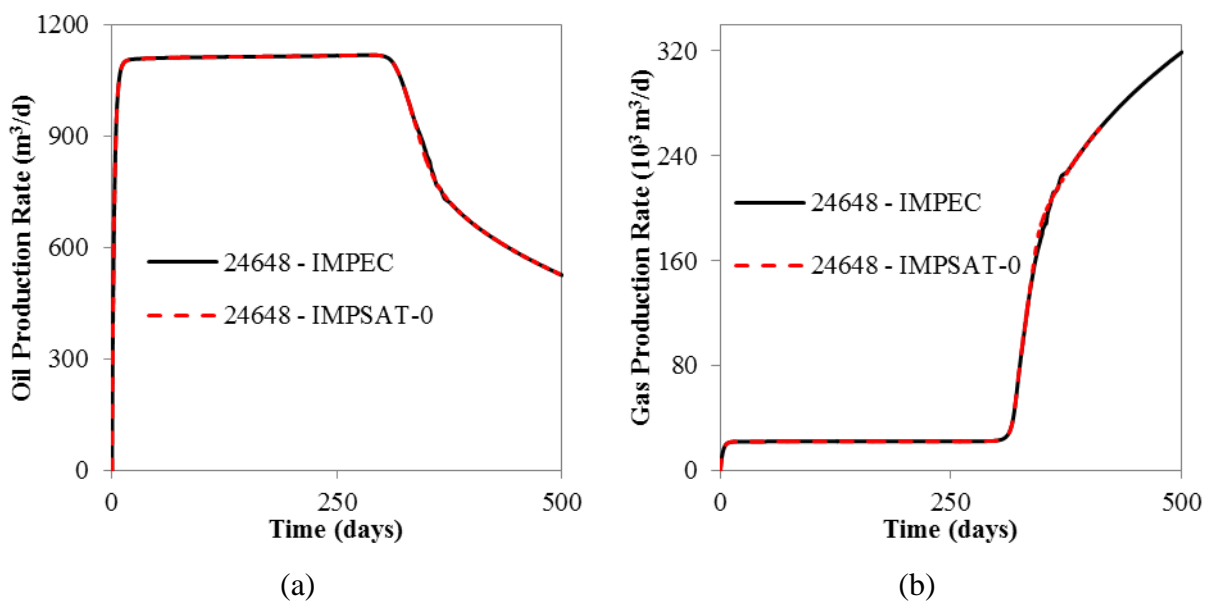
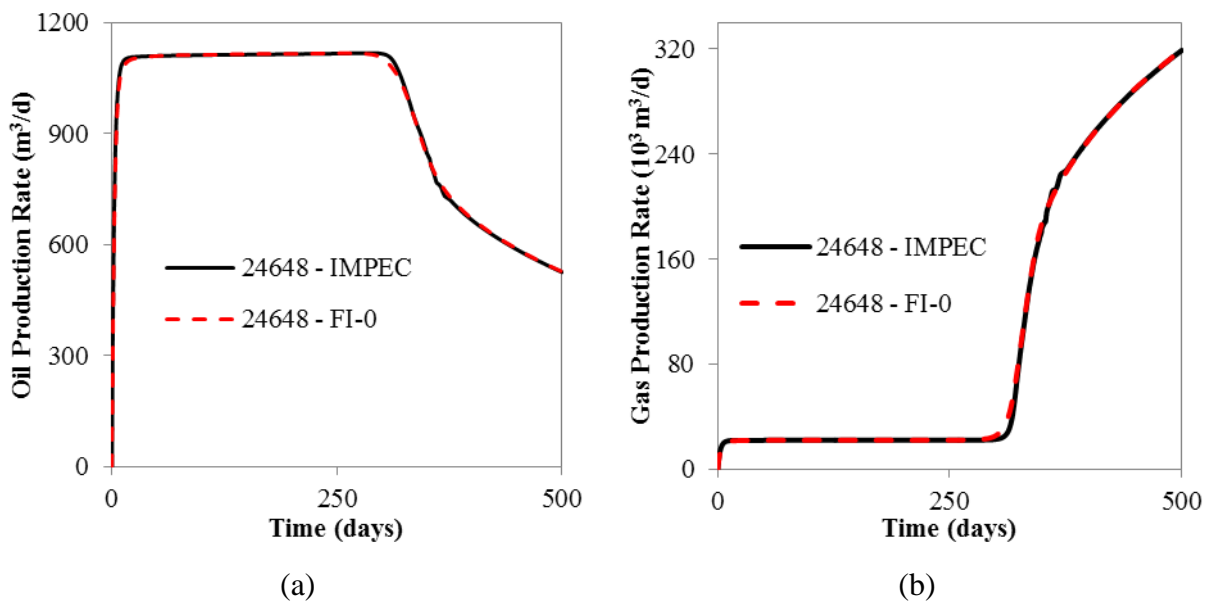


Figure 5.40 – Production rates comparison between IMPEC and FI-0 - Case 1 for 3D unstructured pyramid grid. a) oil; and b) gas.



The gas saturation fields at 700 days of production are shown in Figures 5.41, 5.42, 5.43 and 5.44 for hexahedron, tetrahedron, prism, and pyramid grids, respectively. From these figures, it is possible to infer that the results between the formulations are in good agreement.

Figure 5.41 – Gas saturation field at 700 days for 3D hexahedron EbFVM with 11767 vertices  
- Case 1. a) IMPEC; b) IMPSAT-0; and c) FI-0.

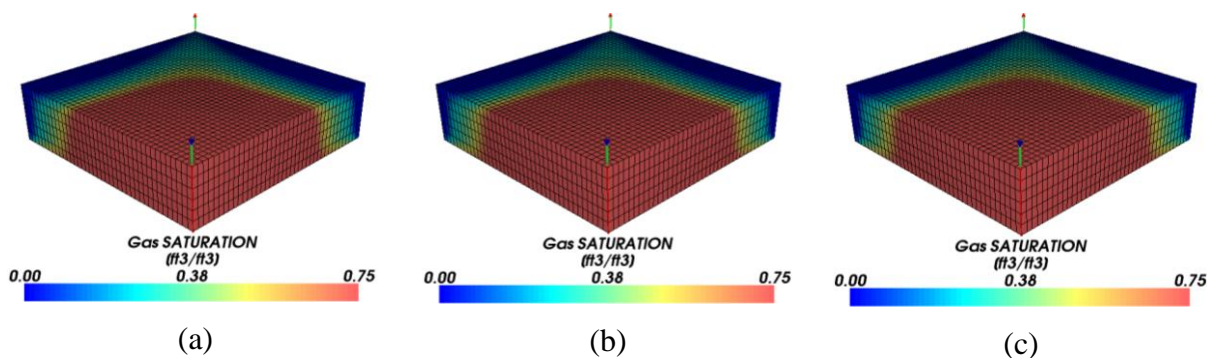


Figure 5.42 – Gas saturation field at 700 days for 3D tetrahedron EbFVM with 16810 vertices  
- Case 1. a) IMPEC; b) IMPSAT-0; and c) FI-0.

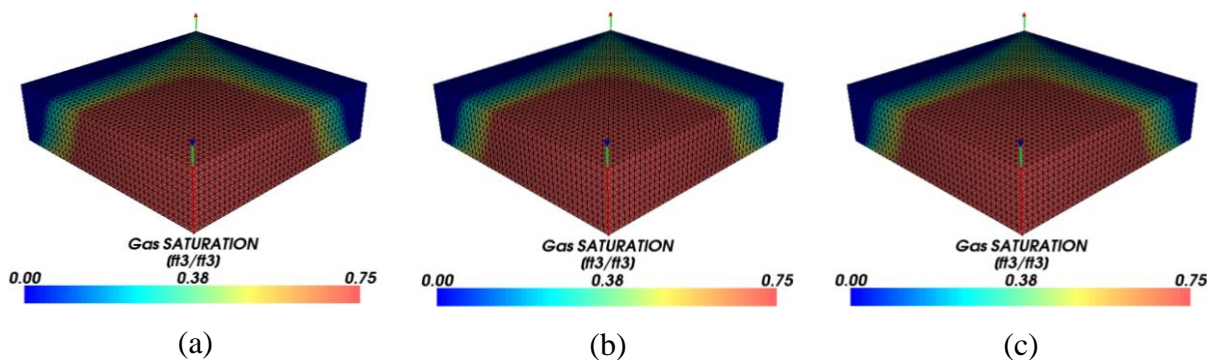


Figure 5.43 – Gas saturation field at 700 days for 3D prism EbFVM with 13448 vertices -  
Case 1. a) IMPEC; b) IMPSAT-0; and c) FI-0.

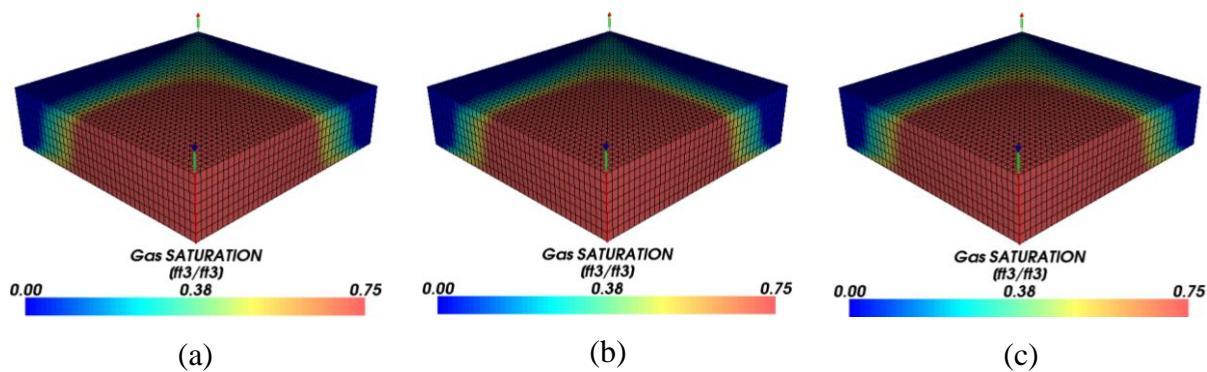
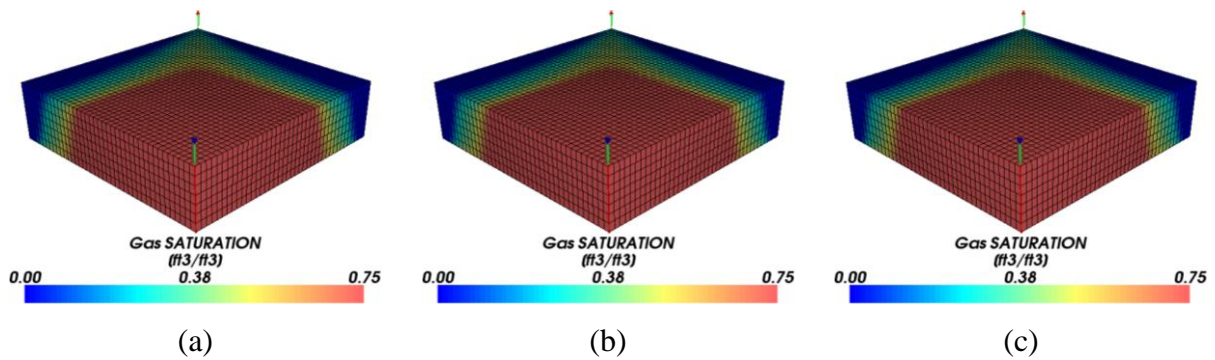


Figure 5.44 – Gas saturation field at 700 days for 3D pyramid EbFVM with 24648 vertices - Case 1. a) IMPEC; b) IMPSAT-0; and c) FI-0.



The CPU times for each formulation for the hexahedron, tetrahedron, prism, and pyramid grids are presented in Tables 5.11, 5.12, 5.13 and 5.14, respectively. Once again, from these tables, it is possible to observe that the FI approaches are better as the grid refines, as observed previously. However, all IMPSAT formulations were worse in performance than the IMPEC and FI approaches for all grids, unlike the previous simulations.

Table 5.11 – CPU time (s) of all simulations - Case 1 using 3D hexahedron grids.

<b>Formulation</b>	<b>1024 vertices</b>	<b>6480 vertices</b>	<b>11767 vertices</b>
IMPEC	36.1	1325.7	3590.8
IMPSAT-0	37.1	1504.9	3326.2
IMPSAT-1	39.7	1569.3	3343.3
IMPSAT-2	59.4	2233.3	4585.0
FI-0	170.4	1525.5	3191.2
FI-1	179.9	1335.7	3188.6

Table 5.12 – CPU time (s) of all simulations - Case 1 using 3D tetrahedron grids.

<b>Formulation</b>	<b>1024 vertices</b>	<b>4056 vertices</b>	<b>16810 vertices</b>
IMPEC	57.4	769.6	6395.2
IMPSAT-0	89.0	1072.5	9627.7
IMPSAT-1	94.9	1334.9	12242.2
IMPSAT-2	141.2	1738.5	14931.5
FI-0	115.7	532.5	2915.7
FI-1	114.7	504.3	3025.1

Table 5.13 – CPU time (s) of all simulations - Case 1 using 3D prism grids.

<b>Formulation</b>	<b>1024 vertices</b>	<b>4056 vertices</b>	<b>13448 vertices</b>
IMPEC	32.4	437.5	3762.6
IMPSAT-0	38.4	451.0	4483.9
IMPSAT-1	41.5	486.4	5314.3
IMPSAT-2	63.6	686.4	6770.1
FI-0	65.1	359.7	2071.3
FI-1	65.7	391.4	2395.0

Table 5.14 – CPU time (s) of all simulations – Case 1 using 3D pyramid grids.

<b>Formulation</b>	<b>1699 vertices</b>	<b>7181 vertices</b>	<b>24648 vertices</b>
IMPEC	98.5	1796.2	20546.0
IMPSAT-0	145.0	2333.6	14619.5
IMPSAT-1	156.7	2231.0	16129.9
IMPSAT-2	243.4	3165.1	26068.5
FI-0	149.0	1169.9	5839.4
FI-1	153.9	1224.4	6137.3

## 5.2 Case study 2: 2D EbFVM

Case study 2 is a gas flooding process in a 2D irregular reservoir using the EbFVM. The fluid in place is characterized by the following hydrocarbon components: C<sub>1</sub>, C<sub>3</sub>, C<sub>6</sub>, C<sub>10</sub>, C<sub>15</sub>, and C<sub>20</sub>. The reservoir initially contains oil, gas, and immobile water. The reservoir data used for this case is shown in Table 5.15.

Table 5.15 – Reservoir data for Case 2.

Property	Value
Superficial reservoir area and thickness	1134826.24 m <sup>2</sup> , 30.48 m
Porosity at reference pressure	0.35
Initial water saturation	0.17
Initial pressure	10.34 MPa
Permeability in X, Y, and Z directions	1.97×10 <sup>-14</sup> m <sup>2</sup> , 1.97×10 <sup>-14</sup> m <sup>2</sup> , and 1.97×10 <sup>-14</sup> m <sup>2</sup>
Formation temperature	344.26 K
Gas injection rate	2.83×10 <sup>5</sup> m <sup>3</sup> /d
Producer's bottom hole pressure	8.96 MPa

The original in place composition and the injected fluid composition for this case is shown in Table 5.16.

Table 5.16 – Fluid composition data for Case 2.

Component	Initial Reservoir Composition	Injection Fluid Composition
C <sub>1</sub>	0.050	0.770
C <sub>3</sub>	0.030	0.200
C <sub>6</sub>	0.070	0.010
C <sub>10</sub>	0.200	0.010
C <sub>15</sub>	0.150	0.005
C <sub>20</sub>	0.050	0.005

The components properties are displayed in Table 5.17.

Table 5.17 – Component data for Case 2.

Component	$P_c$ (MPa)	$T_c$ (K)	$v_c$ (m <sup>3</sup> /kmol)	$MW$ (kg/kmol)	<i>Acentric Factor (<math>\omega</math>)</i>
C <sub>1</sub>	4.60	190.56	$9.98 \times 10^{-2}$	16.0	0.013
C <sub>3</sub>	4.25	369.83	$2.00 \times 10^{-1}$	44.1	0.152
C <sub>6</sub>	3.01	507.44	$3.70 \times 10^{-1}$	86.2	0.301
C <sub>10</sub>	2.10	617.67	$6.30 \times 10^{-1}$	142.3	0.488
C <sub>15</sub>	1.38	705.56	1.04	206.0	0.650
C <sub>20</sub>	1.12	766.67	1.34	282.0	0.850

The binary interaction coefficients and the relative permeabilities parameters are given in Tables 5.18 and 5.19, respectively.

Table 5.18 – Binary interaction coefficients for Case 2.

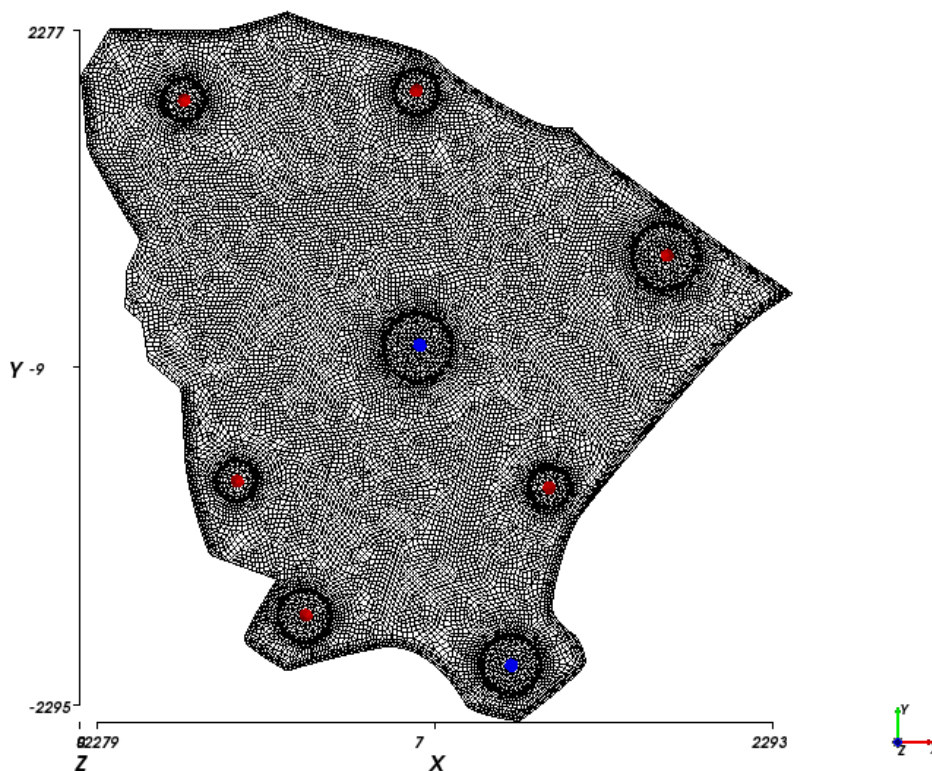
Component	C <sub>1</sub>	C <sub>3</sub>	C <sub>6</sub>	C <sub>10</sub>	C <sub>15</sub>	C <sub>20</sub>
C <sub>1</sub>	-	-	-	-	0.05	0.05
C <sub>3</sub>	-	-	-	-	0.005	0.005
C <sub>6</sub>	-	-	-	-	-	-
C <sub>10</sub>	-	-	-	-	-	-
C <sub>15</sub>	0.05	0.005	-	-	-	-
C <sub>20</sub>	0.05	0.005	-	-	-	-

Table 5.19 – Relative permeability data for Case 2.

Parameter	Value
Model	Modified Stone II
End point relative permeabilities ( $k_{rw}^0$ , $k_{row}^0$ , $k_{rog}^0$ and $k_{rg}^0$ )	0.4, 0.9, 0.9 and 0
Residual saturations ( $S_{wr}$ , $S_{orw}$ , $S_{org}$ and $S_{gr}$ )	0.3, 0.1, 0.1 and 0
Exponents ( $e_w$ , $e_{ow}$ , $e_{og}$ and $e_g$ )	3, 2, 2 and 2

The grid used for this case is shown in Figure 5.45. The reservoir in Figure 5.45 is an hypothetical reservoir and has the shape of Ceará State. Two injector and six producers wells are considered for this case. All injectors are operated under constant gas injection and the producers under constant bottom hole pressure. In order to reduce the grid orientation effect, a radial mesh is used around all the wells.

Figure 5.45 – Hybrid grid: 20298 vertices; 3254 triangle elements and 18195 quadrilateral elements - Case 2.



Figures 5.46 and 5.47 present the comparison of the production rates of the IMPEC formulation with the IMPSAT-0 and FI-0, respectively. From these figures, it is possible to observe a good agreement of the production rates for all the formulations.

Figure 5.46 – Production rates comparison between IMPEC and IMPSAT-0 - Case 2. a) oil; and b) gas.

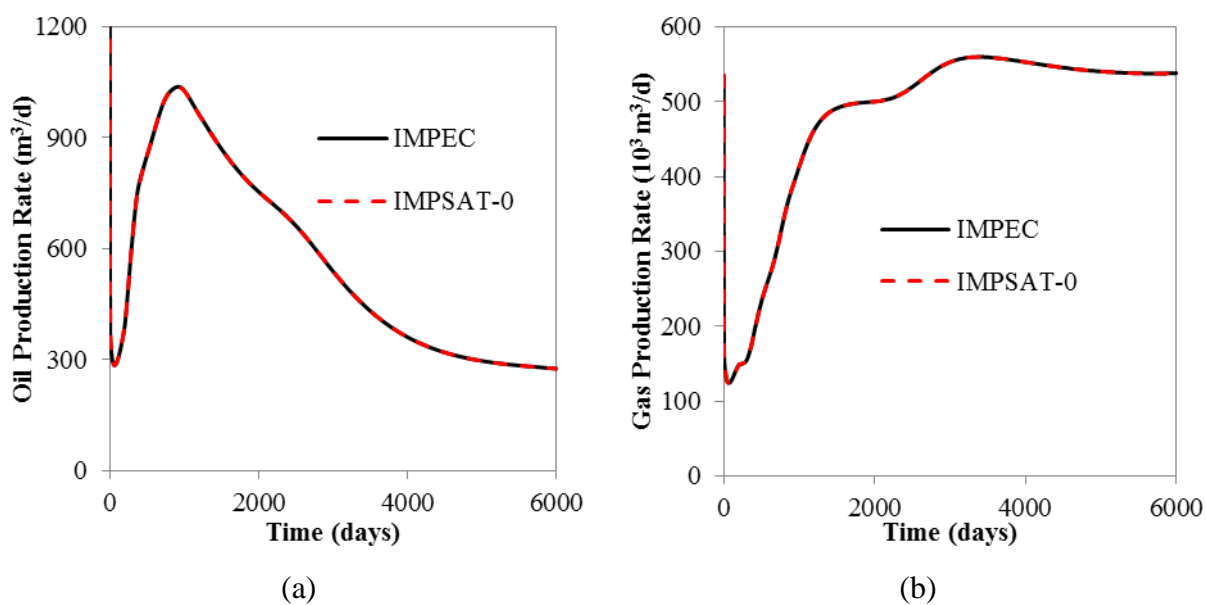
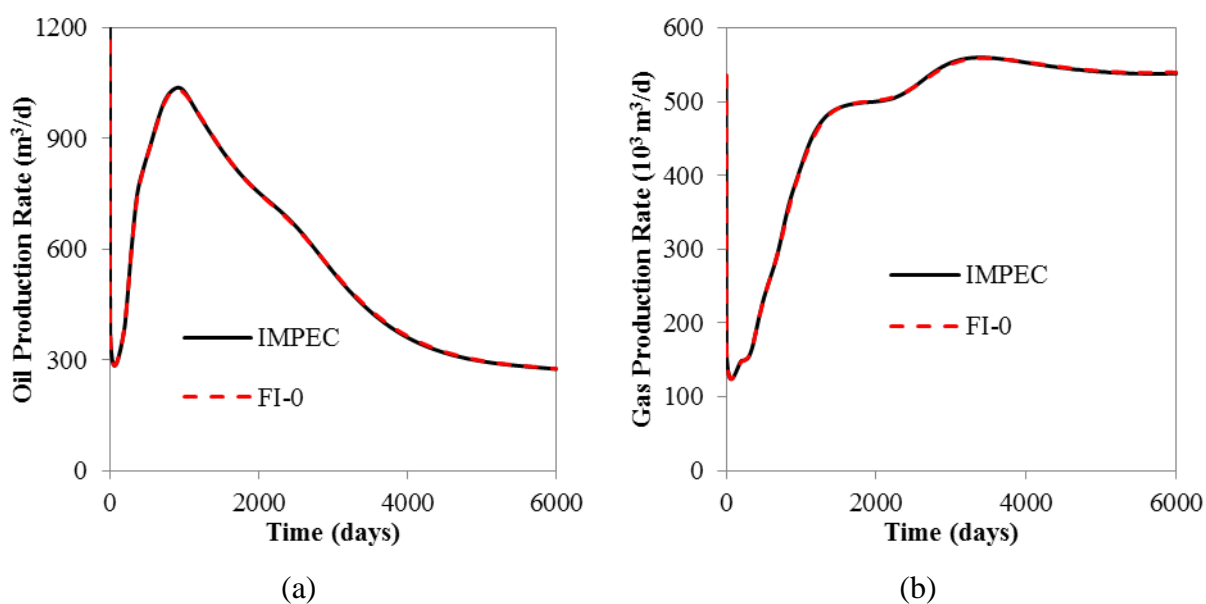


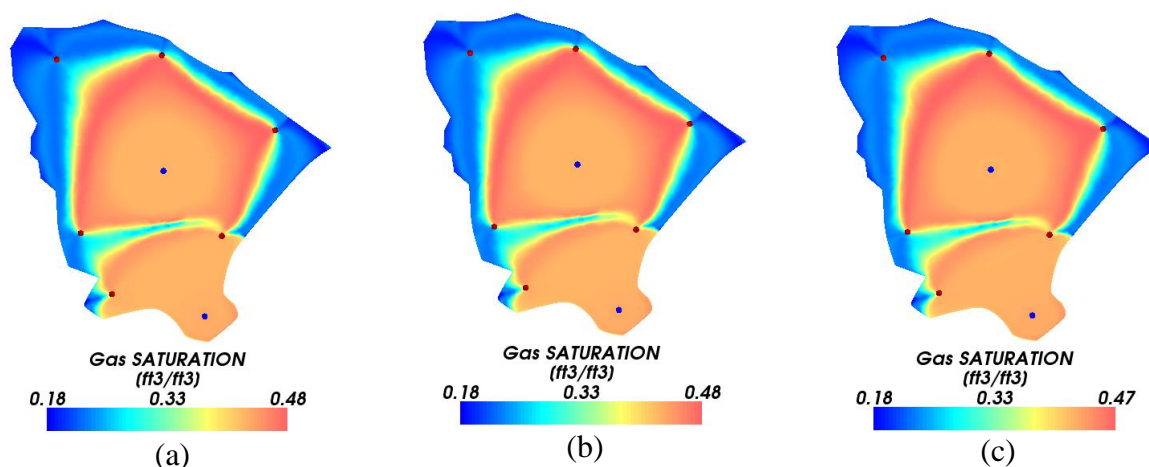


Figure 5.47 – Production rates comparison between IMPEC and FI-0 - Case 2. a) oil; and b) gas.



The gas saturation fields at 6000 days of simulation for the IMPEC, IMPSAT-0, and FI-0 formulations are presented in Figure 5.48. From this figure, one can observe a good agreement between the formulations results.

Figure 5.48 – Gas saturation fields at 6000 days of simulation - Case 2. a) IMPEC; b) IMPSAT-0; and c) FI-0.



The CPU time for all formulations are presented in Table 5.20. It can be observed that the IMPEC formulation was faster than the IMPSAT-1 and IMPSAT-2. The fastest formulation for this case was the FI-0, followed by the FI-1 and IMPSAT-0.

Table 5.20 – CPU time (s) of all simulations – Case 2.

<b>Formulation</b>	<b>CPU TIME</b>
IMPEC	6450.64
IMPSAT-0	5913.98
IMPSAT-1	6953.31
IMPSAT-2	7487.51
FI-0	4234.84
FI-1	4566.00

### 5.3 Case study 3

Case study 3 is a CO<sub>2</sub> injection process in a 2D reservoir. The fluid in place is characterized by the following components: CO<sub>2</sub>, C<sub>1</sub>, C<sub>2-3</sub>, C<sub>4-6</sub>, C<sub>7-15</sub>, C<sub>16-27</sub>, and C<sub>28</sub>. The reservoir initially contains only oil and immobile water. As CO<sub>2</sub> is injected, gas and a second liquid hydrocarbon phases are formed. One injector and one producer wells are considered, both operating at constant bottom hole pressure (BHP). Table 5.21 presents the reservoir data used for this case.

Table 5.21 – Reservoir data for Case 3.

<b>Property</b>	<b>Value</b>
Length, width, and thickness	152.4 m, 304.8 m, and 6.09 m
Porosity at reference pressure	0.25
Initial water saturation	0.25
Initial pressure	7.58 MPa
Formation temperature	313.71 K
Injector's bottom hole pressure	8.62 MPa
Producer's bottom hole pressure	7.58 MPa

The original in place composition and the injected fluid composition for this case is shown in Table 5.22.

Table 5.22 – Fluid composition data for Case 3.

<b>Component</b>	<b>Initial Reservoir Composition</b>	<b>Injection Fluid Composition</b>
CO <sub>2</sub>	0.0337	0.95
C <sub>1</sub>	0.0861	0.04999
C <sub>2-3</sub>	0.1503	0.000002
C <sub>4-6</sub>	0.1671	0.000002
C <sub>7-15</sub>	0.3304	0.000002
C <sub>16-27</sub>	0.1611	0.000002
C <sub>28</sub>	0.0713	0.000002

The components properties are displayed in Table 5.23.

Table 5.23 – Component data for Case 3.

Component	$P_c$ (MPa)	$T_c$ (K)	$v_c$ (m <sup>3</sup> /kmol)	$MW$ (kg/kmol)	<i>Acentric Factor (<math>\omega</math>)</i>
CO <sub>2</sub>	7.37	304.2	$9.40 \times 10^{-2}$	44.01	0.2250
C <sub>1</sub>	4.60	190.6	$9.90 \times 10^{-2}$	16.04	0.0080
C <sub>2-3</sub>	4.49	344.2	$1.81 \times 10^{-1}$	37.2	0.1305
C <sub>4-6</sub>	3.39	463.2	$3.07 \times 10^{-1}$	69.5	0.2404
C <sub>7-15</sub>	2.17	605.7	$5.99 \times 10^{-1}$	140.96	0.6177
C <sub>16-27</sub>	1.65	751.0	1.13	280.99	0.9566
C <sub>28</sub>	1.64	942.5	2.09	519.62	1.2683

The binary interaction coefficients and the relative permeabilities parameters are given in Tables 5.24 and 5.25, respectively.

Table 5.24 – Binary interaction coefficients for Case 3.

Component	CO <sub>2</sub>	C <sub>1</sub>	C <sub>2-3</sub>	C <sub>4-6</sub>	C <sub>7-15</sub>	C <sub>16-27</sub>	C <sub>28</sub>
CO <sub>2</sub>	-	0.055	0.055	0.055	0.105	0.105	0.105
C <sub>1</sub>	0.055	-	-	-	-	-	-
C <sub>2-3</sub>	0.055	-	-	-	-	-	-
C <sub>4-6</sub>	0.055	-	-	-	-	-	-
C <sub>7-15</sub>	0.105	-	-	-	-	-	-
C <sub>16-27</sub>	0.105	-	-	-	-	-	-
C <sub>28</sub>	0.105	-	-	-	-	-	-

Table 5.25 – Relative permeability data for Case 3.

Parameter	Value
Model	Corey
End point relative permeabilities ( $k_{rw}^0$ , $k_{ro}^0$ , $k_{rg}^0$ and $k_{rl}^0$ )	0.21, 0.7, 0.35, and 0.35
Residual saturations ( $S_{wr}$ , $S_{orw}$ , $S_{org}$ , $S_{gr}$ , $S_{lrw}$ , and $S_{lrg}$ )	0.25, 0.2, 0.2, 0.05, 0.2, and 0.2
Exponents ( $e_w$ , $e_{ow}$ , $e_{og}$ , $e_g$ , $e_{lw}$ , and $e_{lg}$ )	1.5, 2.5, 2.5, 2.5, 2.5, and 2.5

This case is run for both Cartesian and unstructured grids.

### 5.3.1 Case study 3: 2D Cartesian grid

Figure 5.49 shows the regular 40x80 grid used for this case. An isotropic but heterogeneous permeability field in x and y directions is used for this investigation. The absolute permeability field is presented in Figure 5.50. In order to better visualize the whole variation of the permeability field, Fig. 5.50b,c show two different zooms of the whole scale presented in Fig. 5.50a.

Figure 5.49 – 2D 40x80 Cartesian grid - Case 3.

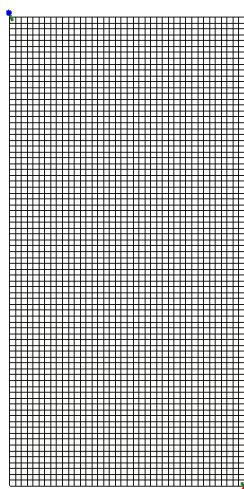
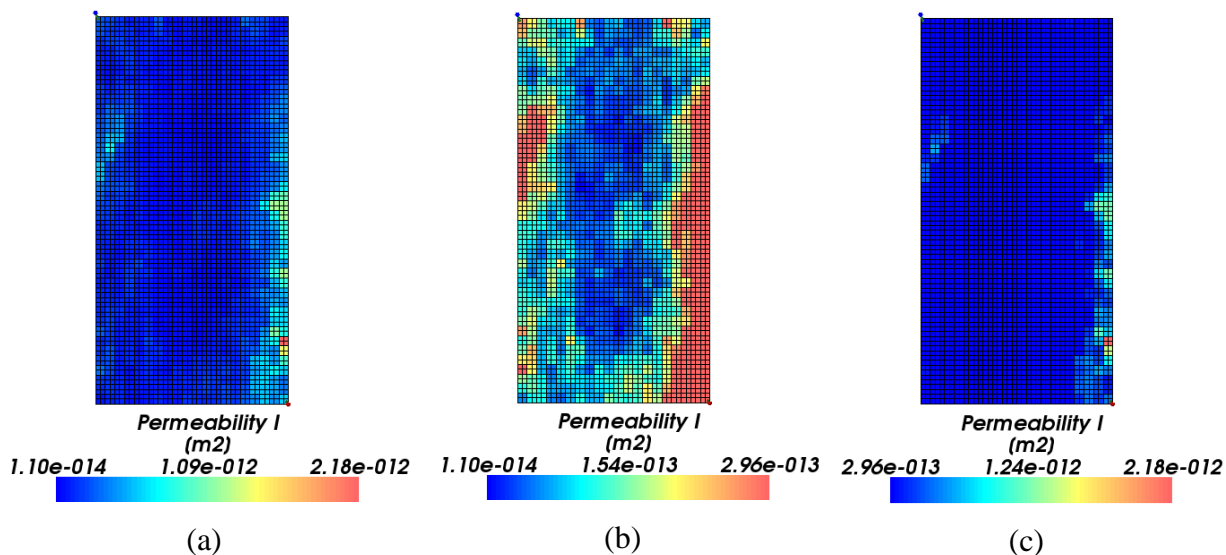


Figure 5.50 – Heterogeneous absolute permeability in X and Y directions field - Case 3.



The oil and gas production rates obtained with the IMPEC and IMPSAT-0, and IMPEC and FI-0 are presented in Figures 5.51 and 5.52, respectively. From these figures, it is possible to observe that the production curves are in a good agreement.

Figure 5.51 – Production rates comparison between IMPEC and IMPSAT-0 - Case 3 for the Cartesian grid. a) oil; and b) gas.

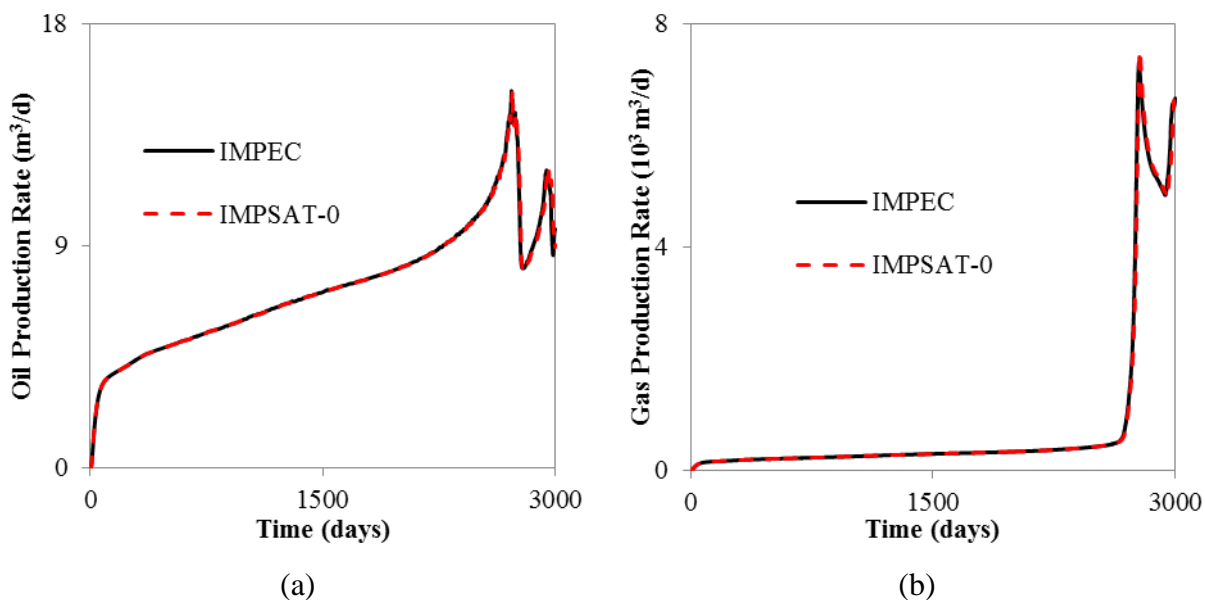
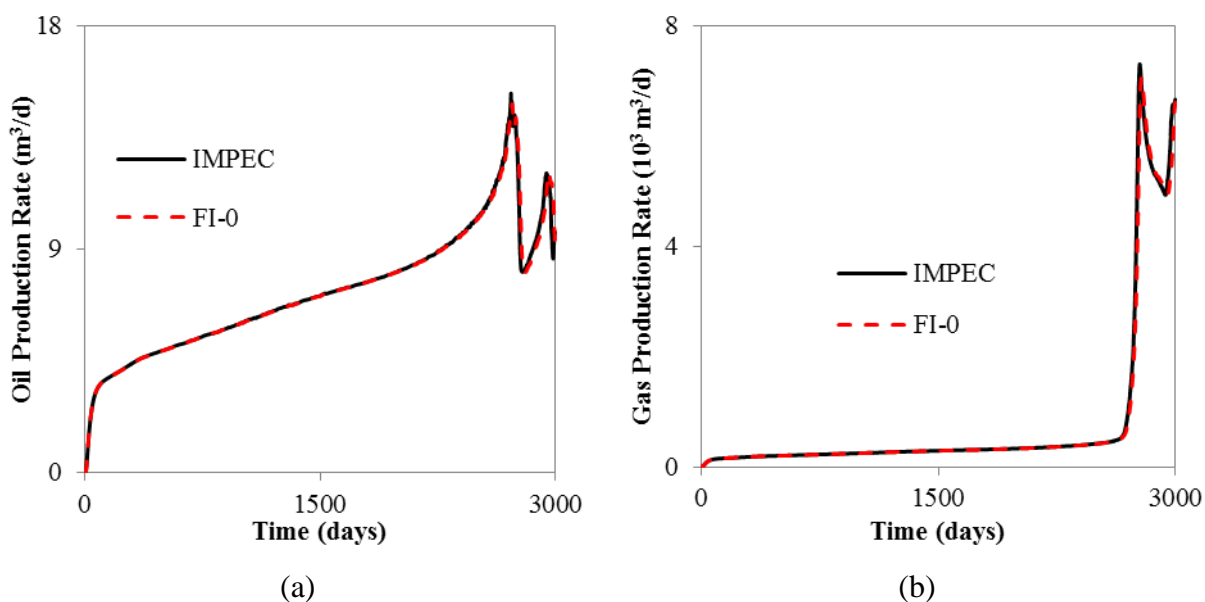


Figure 5.52 – Production rates comparison between IMPEC and FI-0 - Case 3 for the Cartesian grid. a) oil; and b) gas.



The gas saturation and the second hydrocarbon liquid fields at 3000 days for the IMPEC, IMPSAT-0, and FI-0 are presented in Figure 5.53 and 5.54, respectively. From these

figures, it can be seen a good agreement between each one of two saturation fields for all formulations investigated.

Figure 5.53 – Gas saturation field at 3000 days for 2D Cartesian grid - Case 3. a) IMPEC; b) IMPSAT-0; and c) FI-0.

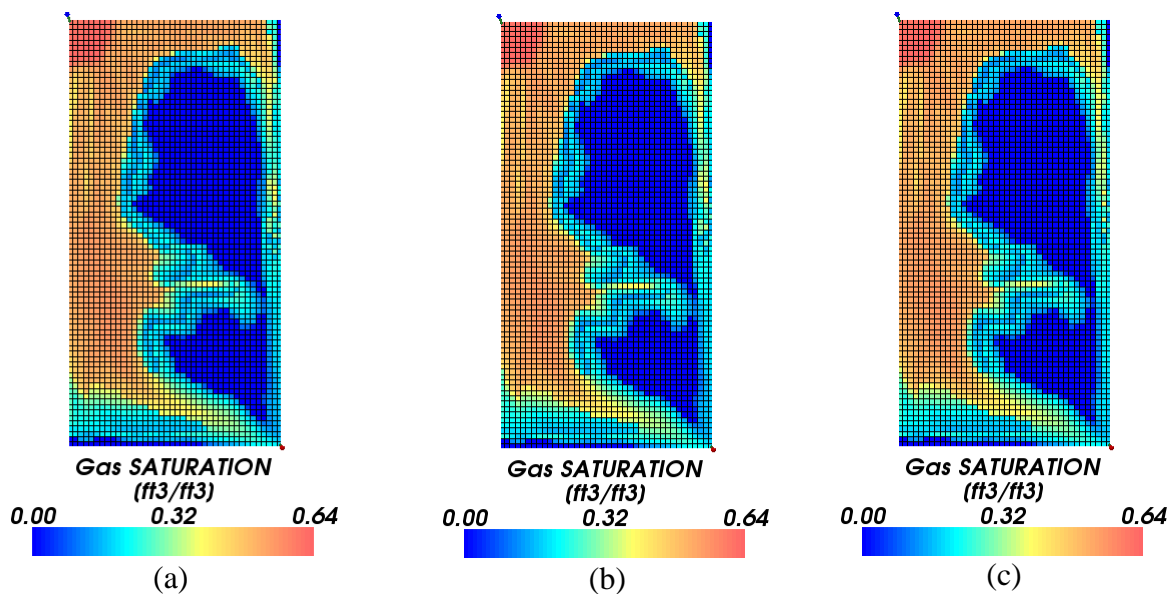
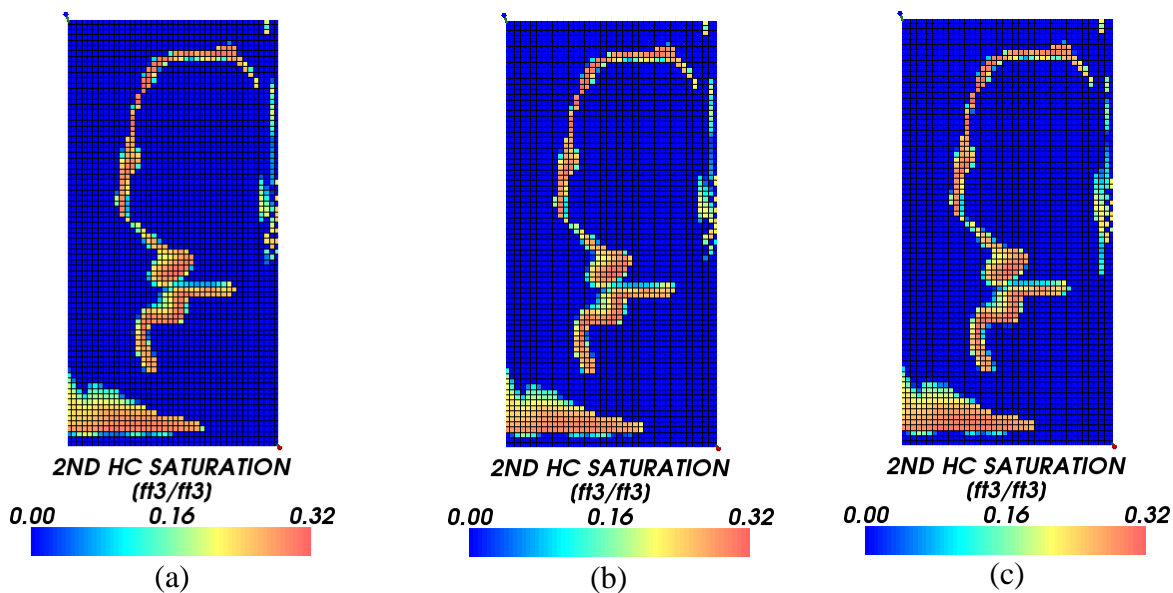


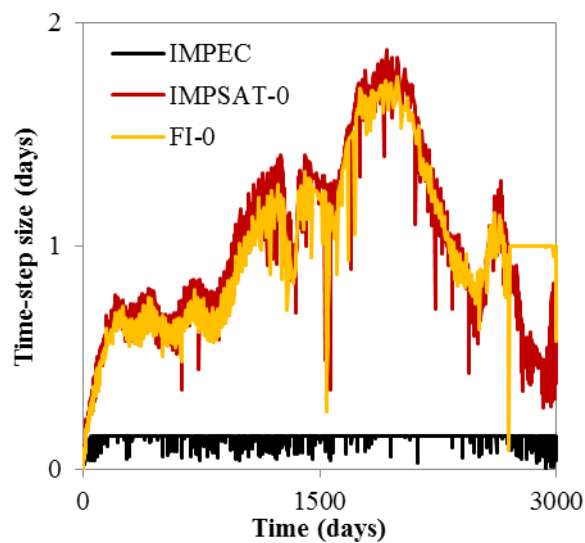
Figure 5.54 – Second hydrocarbon liquid saturation field at 3000 days for 2D Cartesian grid - Case 3. a) IMPEC; b) IMPSAT-0; and c) FI-0.



The best time-step profiles obtained for the IMPEC, IMPSAT-0, and FI-0 formulations are presented in Figure 5.55. The IMPEC formulation had many difficult to run this case without any spurious oscillation. Several runs were performed in order to find

feasible time-step control parameters. In fact, the parameters used for the IMPEC were the only ones that allowed the simulation to run the whole case without spurious oscillation or crash. The run was much easier to be carried out for the IMPSAT formulations, and little effort had to be performed to obtain a good time-step control parameters. The FI approaches allowed the use of large time-steps; however when production curves were compared, it was verified that time refinement were necessary. Therefore, for this case we used the same maximum time-steps for both FI and IMPSAT approaches.

Figure 5.55 – Time-stepping profiles for the IMPEC, IMPSAT-0 and FI-0 formulations – Case 3 using Cartesian grid.



The CPU time for all formulations are presented in Table 5.26. It can be observed that the IMPEC required the largest CPU time. In fact, it is unfeasible to use the IMPEC formulation alone to solve this problem, since several runs were necessary to achieve the time-step control parameters that allowed to obtain a solution without numerical oscillation. For this case, the IMPSAT formulations were the best choice, showing robustness and small CPU time.



Table 5.26 – CPU time (s) for all simulations - Case 3 using a 40x80 2D Cartesian grid.

<b>Formulation</b>	<b>CPU TIME</b>
IMPEC	3917.38
IMPSAT-0	1061.22
IMPSAT-1	1119.99
IMPSAT-2	1425.03
FI-0	3165.60
FI-1	2951.34

### 5.3.2 Case study 3: 2D EbFVM

The same reservoir and fluid shown in section 5.3.1 are used to test the formulations in conjunction with 2D EbFVM. In order to reduce the grid orientation effect a radial grid is used around the wells. The hybrid grid used for this investigation is shown in Figure 5.56. The heterogeneous absolute permeability in X and Y directions from Fig. 5.50 converted to the grid configuration of Fig. 5.56 is presented in Fig. 5.57.

Figure 5.56 – 2D 3016 vertices grid with 818 triangular and 2490 quadrilateral elements - Case 3.

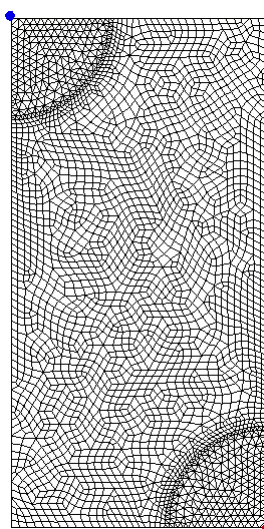
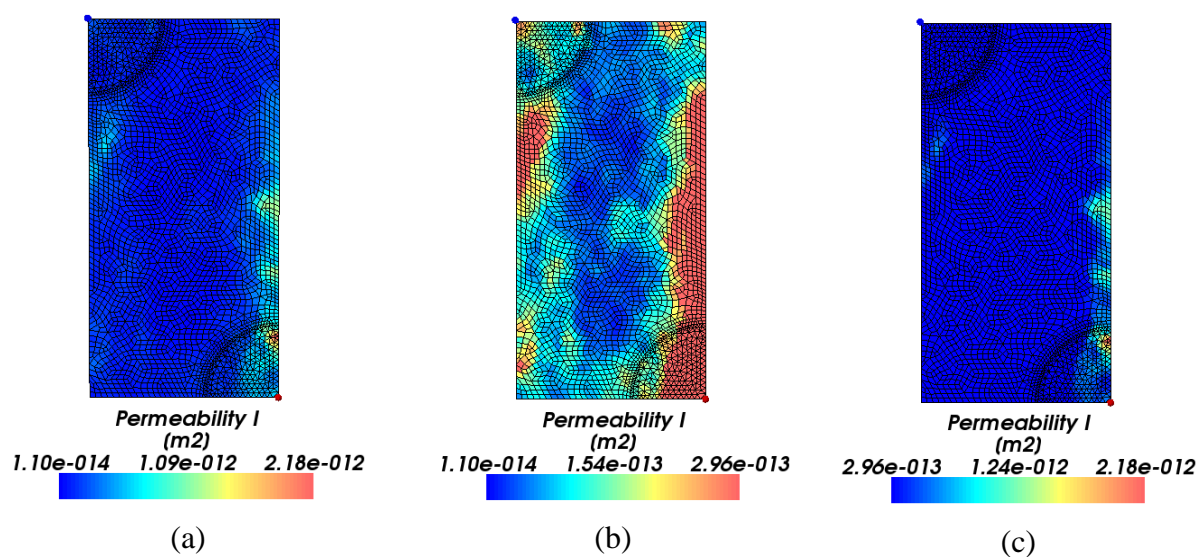
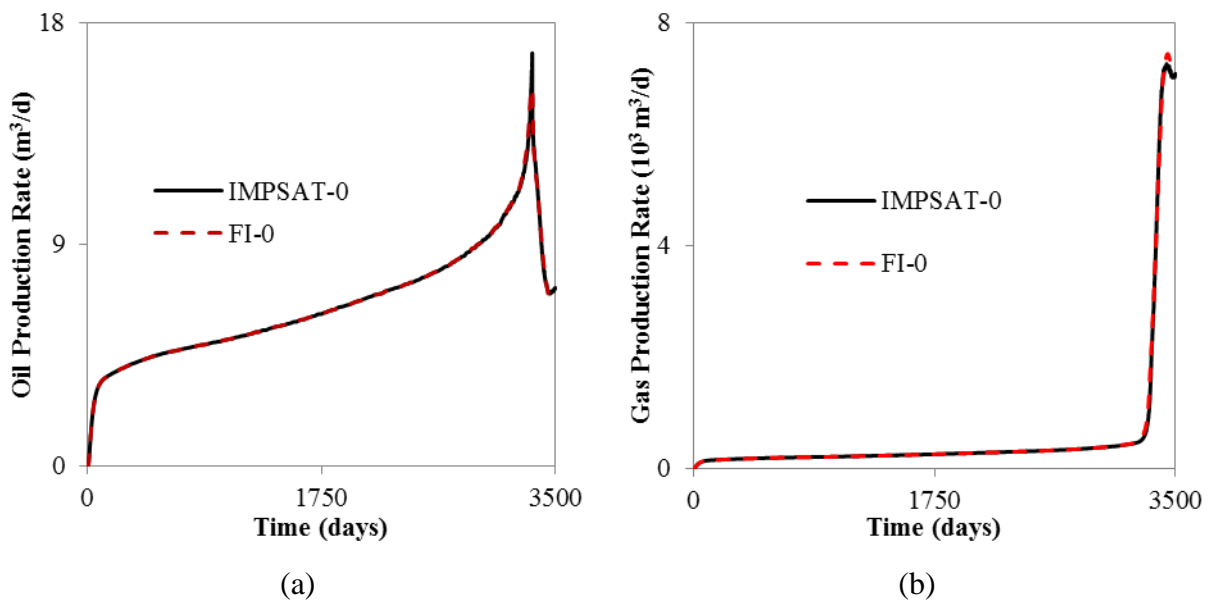


Figure 5.57 – Heterogeneous absolute permeability in X and Y directions field for 2D EbFVM - Case 3.



For this case, it was not found any time-step control parameters that allowed the IMPEC formulation to be carried out the whole run without either spurious oscillations or crash. Therefore, only the results of the IMPSAT-0 and FI-0 approaches will be compared. This comparison is shown in Figure 5.58. From this figure, it is possible to observe a good agreement between the oil and gas production curves obtained with the two approaches.

Figure 5.58 – Production rates comparison between IMPSAT-0 and FI-0 - Case 3 for 2D EbFVM. a) oil; and b) gas.



The gas saturation and the second liquid phase fields at 3500 days for the IMPSAT-0 and FI-0 are presented in Figures 5.59 and 5.60, respectively. Once again, from these figures, it is possible to see a good agreement in the two saturation fields obtained with the two approaches.

Figure 5.59 – Gas saturation field at 3500 days for 2D EbFVM - Case 3. a) IMPSAT-0; and b) FI-0.

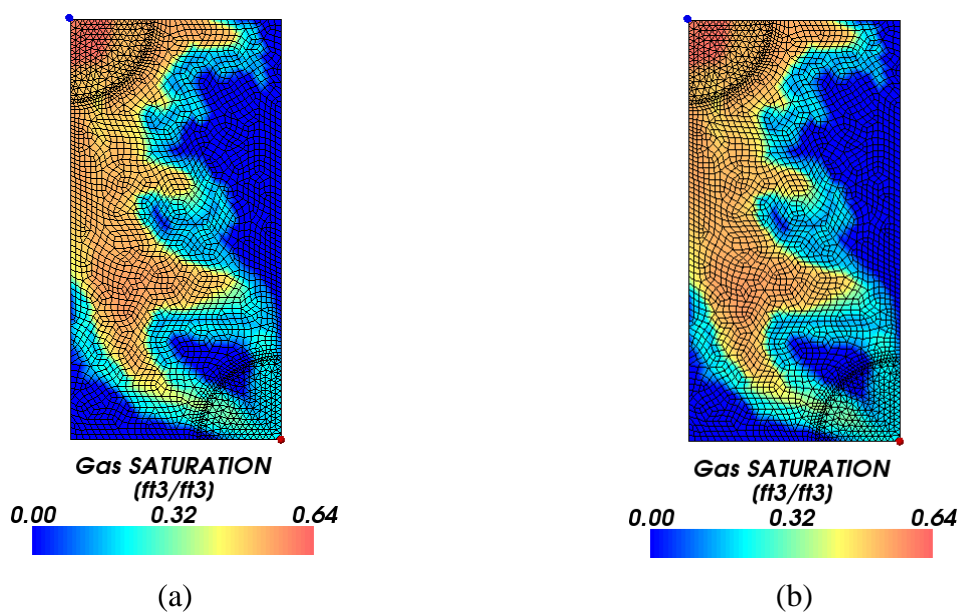
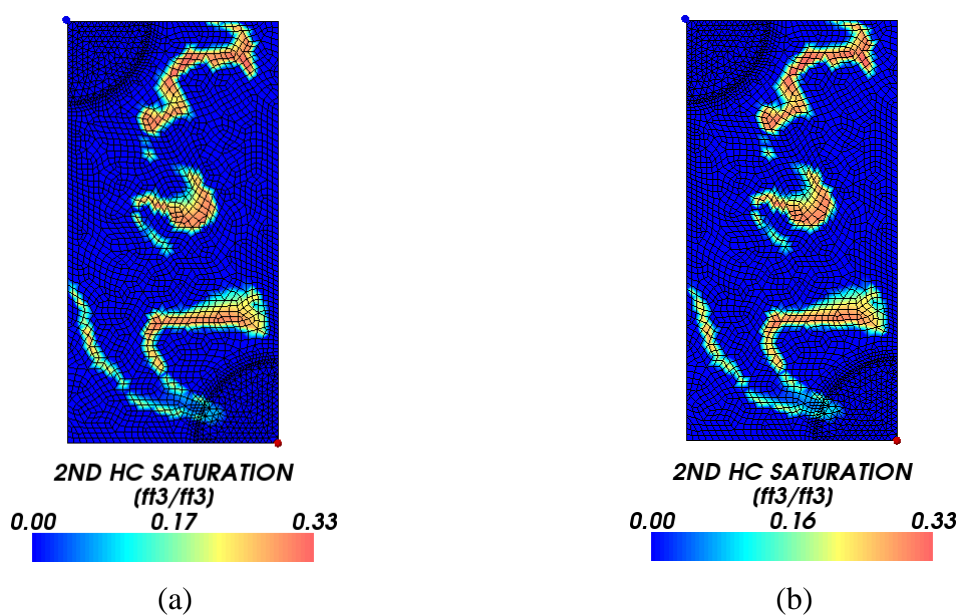
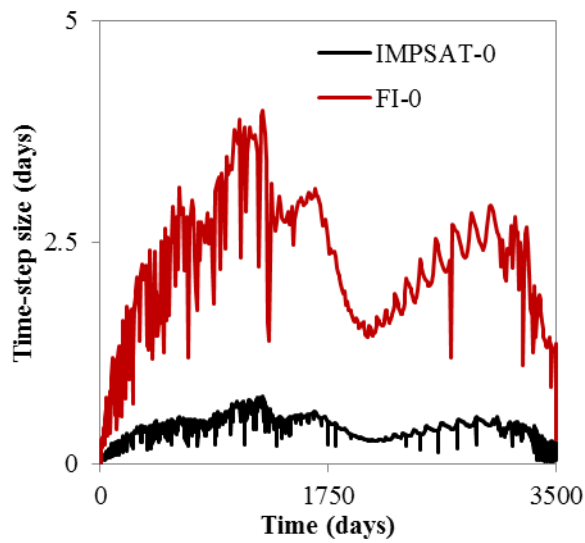


Figure 5.60 – Second liquid hydrocarbon phase saturation field at 3500 days for 2D EbFVM-Case 3. a) IMPSAT-0; and b) FI-0.



The time-step profiles for the IMPSAT-0 and FI-0 are presented in Figure 5.61. For this case, the FI approaches were able to reach larger time-step sizes without great penalty in the accuracy.

Figure 5.61 – Time-stepping profiles for the IMPSAT-0 and FI-0 formulations – Case 3 using the element grid.



The CPU Times for all formulations are presented in Table 5.27. From this table, we can infer that both classes of formulations have approximately the same performance.

Table 5.27 – CPU time (s) for all simulations - Case 3 using a hybrid grid with 3016 vertices.

<b>Formulation</b>	<b>CPU TIME</b>
IMPEC	FAILED
IMPSAT-0	2956.91
IMPSAT-1	3173.69
IMPSAT-2	3673.88
FI-0	3212.71
FI-1	2455.11

#### 5.4 Case study 4: 3D Cartesian

The last case study investigated in this work is a CO<sub>2</sub> injection process in a 3D isotropic heterogeneous reservoir in x and y directions. Differently from the previous cases investigated, water is mobile during the whole simulation, and the fluid is characterized with seven components. Only water, oil and gas phases are considered. Table 5.28 presents the reservoir data for this case. The in place original composition and the injected fluid composition for this case are shown in Table 5.29. The components and pseudo-components properties are presented in Table 5.30. The binary interaction coefficients and relative permeability parameters are presented in Tables 5.31 and 5.32, respectively.

Table 5.28 – Reservoir data for Case 4.

<b>Property</b>	<b>Value</b>
Length, width, and thickness	146.3 m, 146.3 m, and 19.05 m
Porosity at reference pressure	0.163
Initial water saturation	0.65
Initial pressure	9.65 MPa
Permeability in z direction	$1.576 \times 10^{-14} \text{ m}^2$
Formation temperature	333.15 K
Injector's bottom hole pressure	10.0 MPa
Producer's bottom hole pressure	6.89 MPa

Table 5.29 – Fluid composition data for Case 4.

<b>Component</b>	<b>Initial Reservoir Composition</b>	<b>Injection Fluid Composition</b>
CO <sub>2</sub>	0.0077	1.0
C <sub>1</sub>	0.2025	-
C <sub>2-3</sub>	0.1180	-
C <sub>4-6</sub>	0.1484	-
C <sub>7-14</sub>	0.2863	-
C <sub>15-24</sub>	0.1490	-
C <sub>25+</sub>	0.0881	-

Table 5.30 – Component data for Case 4.

Component	$P_c$ (MPa)	$T_c$ (K)	$v_c$ (m <sup>3</sup> /kmol)	$MW$ (kg/kmol)	<i>Acentric Factor</i> ( $\omega$ )
CO <sub>2</sub>	7.39	304.21	2.60×10 <sup>-2</sup>	44.01	0.225
C <sub>1</sub>	4.60	190.60	1.00×10 <sup>-1</sup>	16.043	0.008
C <sub>2-3</sub>	4.50	343.64	1.81×10 <sup>-1</sup>	38.3985	0.1301
C <sub>4-6</sub>	3.35	466.41	3.13×10 <sup>-1</sup>	72.824	0.2436
C <sub>7-14</sub>	2.42	603.07	5.55×10 <sup>-1</sup>	135.8191	0.6
C <sub>15-24</sub>	1.80	733.79	1.01	257.7499	0.903
C <sub>25+</sub>	1.73	923.20	1.25	479.9548	1.229

Table 5.31 – Binary interaction coefficients for Case 4.

Component	CO <sub>2</sub>	C <sub>1</sub>	C <sub>2-3</sub>	C <sub>4-6</sub>	C <sub>7-15</sub>	C <sub>16-27</sub>	C <sub>28</sub>
CO <sub>2</sub>	-	0.12	0.12	0.12	0.09	0.09	0.09
C <sub>1</sub>	0.12	-	-	-	-	-	-
C <sub>2-3</sub>	0.12	-	-	-	-	-	-
C <sub>4-6</sub>	0.12	-	-	-	-	-	-
C <sub>7-15</sub>	0.09	-	-	-	-	-	-
C <sub>16-27</sub>	0.09	-	-	-	-	-	-
C <sub>28</sub>	0.09	-	-	-	-	-	-

Table 5.32 – Relative permeability data for Case 4.

Parameter	Value
Model	Stone II
End point relative permeabilities ( $k_{rw}^0$ , $k_{ro}^0$ , and, $k_{rg}^0$ )	0.21, 0.71, and 1.0
Residual saturations ( $S_{wr}$ , $S_{orw}$ , $S_{org}$ , and, $S_{gr}$ )	0.49, 0.25, 0.25, and 0.05
Exponents ( $e_w$ , $e_{ow}$ , $e_{og}$ , and $e_g$ )	2.0, 2.7, 2.7, and 2.5

The reservoir and grid used for this case is presented in Figure 5.62, while the absolute permeability in x and y directions is presented in Figure 5.63.

Figure 5.62 – 40x40x5 Cartesian grid - Case 4.

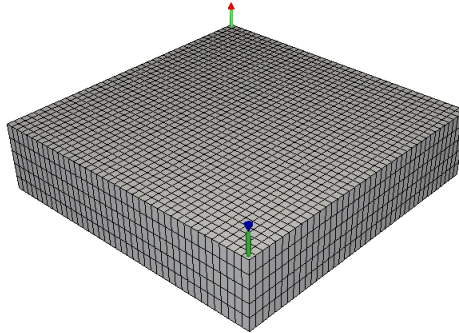


Figure 5.63 – Heterogeneous absolute permeability in x and y directions field - Case 4.

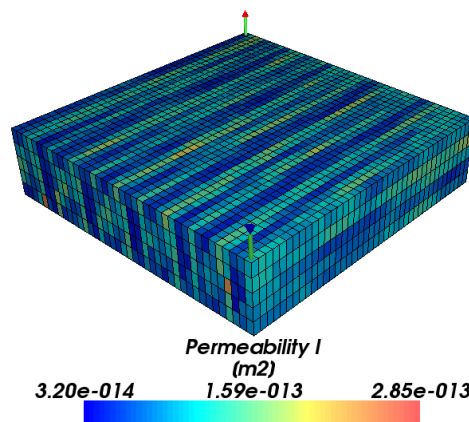


Figure 5.64 presents the comparison in terms of oil and gas production rates between the IMPEC and IMPSAT-0 formulations. As it can be observed from this figure, the gas breakthrough was delayed for the IMPSAT-0 formulation. This inaccuracy was observed to be reduced when the time-step sizes were decreased. The production rates comparison for the IMPSAT-1 and IMPSAT-2 with IMPEC are shown in Figures 5.65 and 5.66, which show a good agreement of the production curves. It is important to mention that both the IMPSAT-1 and IMPSAT-2 did not require time-step reduction in order to obtain the production curves shown in Figs. 5.65 and 5.66. This result suggests that the IMPSAT-0 formulation is less accurate in terms of time than the other two approaches, and it can be not well suitable for cases where the solution strongly changes during the simulation. The production rate curves for the FI-0, FI-1 formulations are compared with the IMPEC formulation in Figures 5.67 and 5.68, respectively. Once again, a good agreement of the production curves can be observed from these figures.

The gas saturation fields for all formulations at 250 days are presented in Figure 5.69. From this figure, we can observe a good agreement of the field obtained for all



formulations, except for the IMPSAT-0 formulation where a little difference can be observed near the producer well.

Figure 5.64 – Production rates comparison between IMPEC and IMPSAT-0 - Case 4. a) oil; and b) gas.

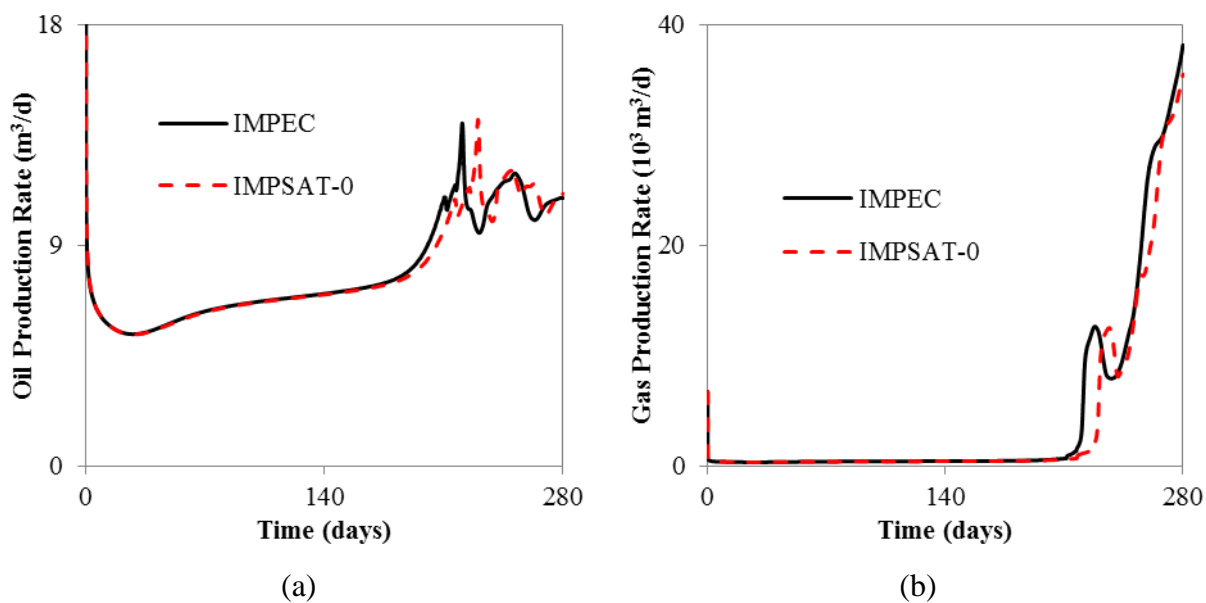


Figure 5.65 – Production rates comparison between IMPEC and IMPSAT-1 - Case 4. a) oil; and b) gas.

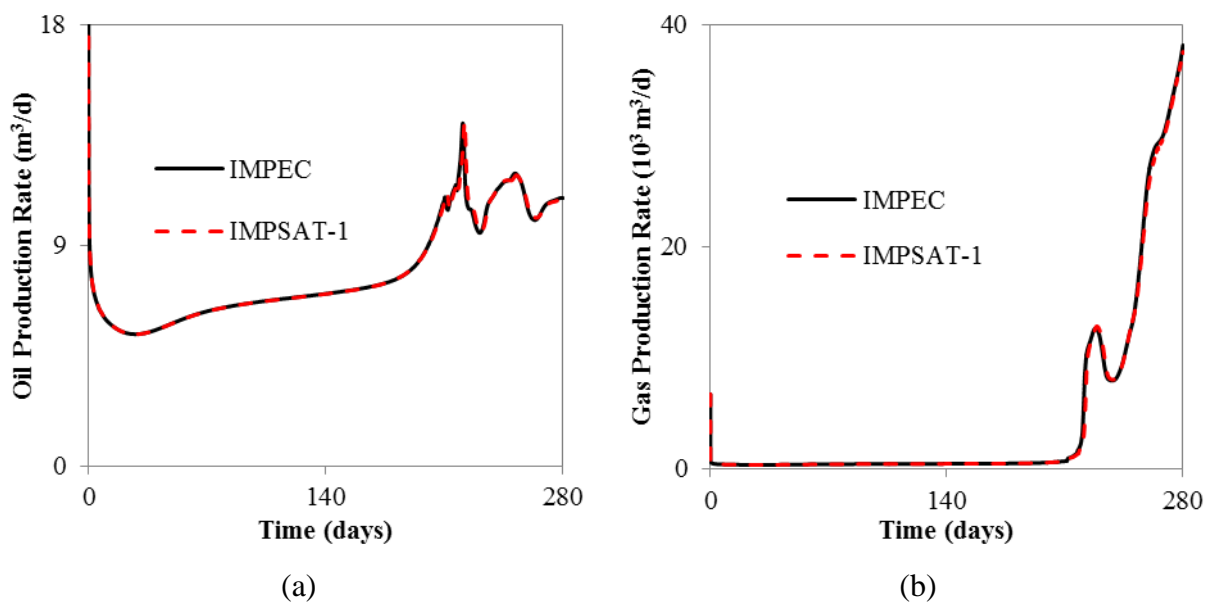


Figure 5.66 – Production rates comparison between IMPEC and IMPSAT-2 - Case 4. a) oil; and b) gas.

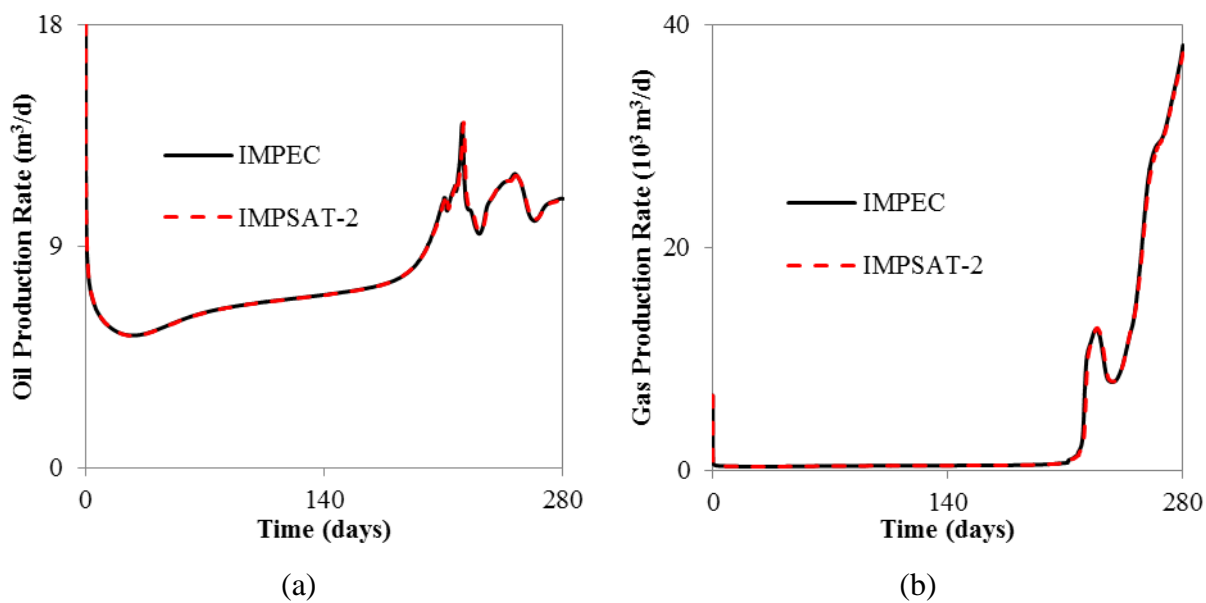


Figure 5.67 – Production rates comparison between IMPEC and FI-0 - Case 4. a) oil; and b) gas.

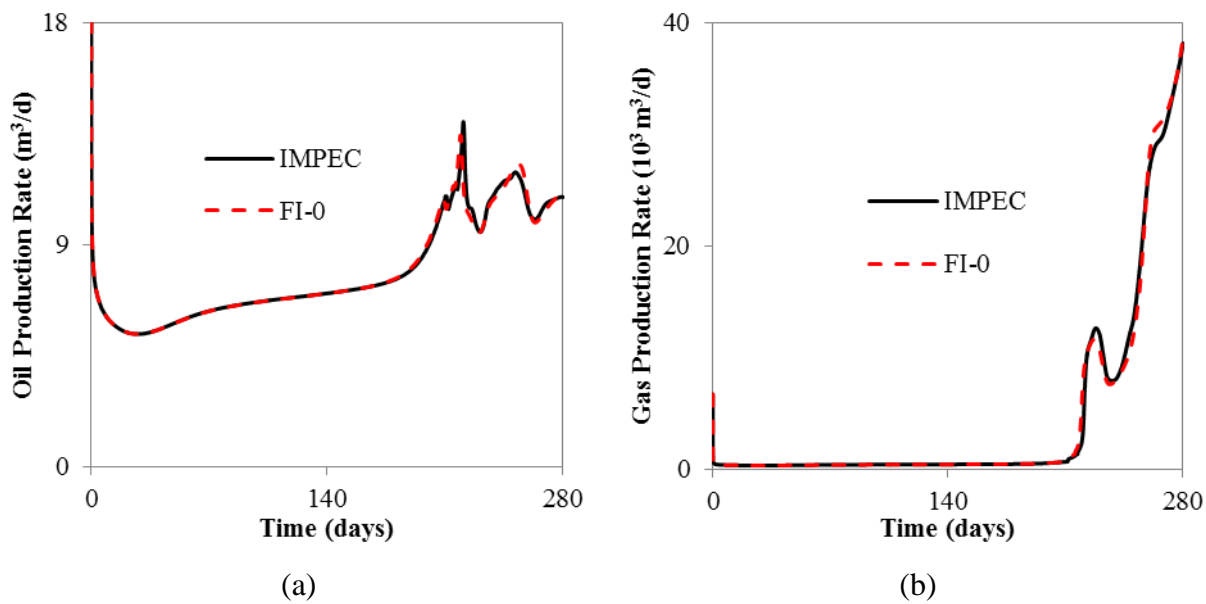


Figure 5.68 – Production rates comparison between IMPEC and FI-1 - Case 4. a) oil; and b)

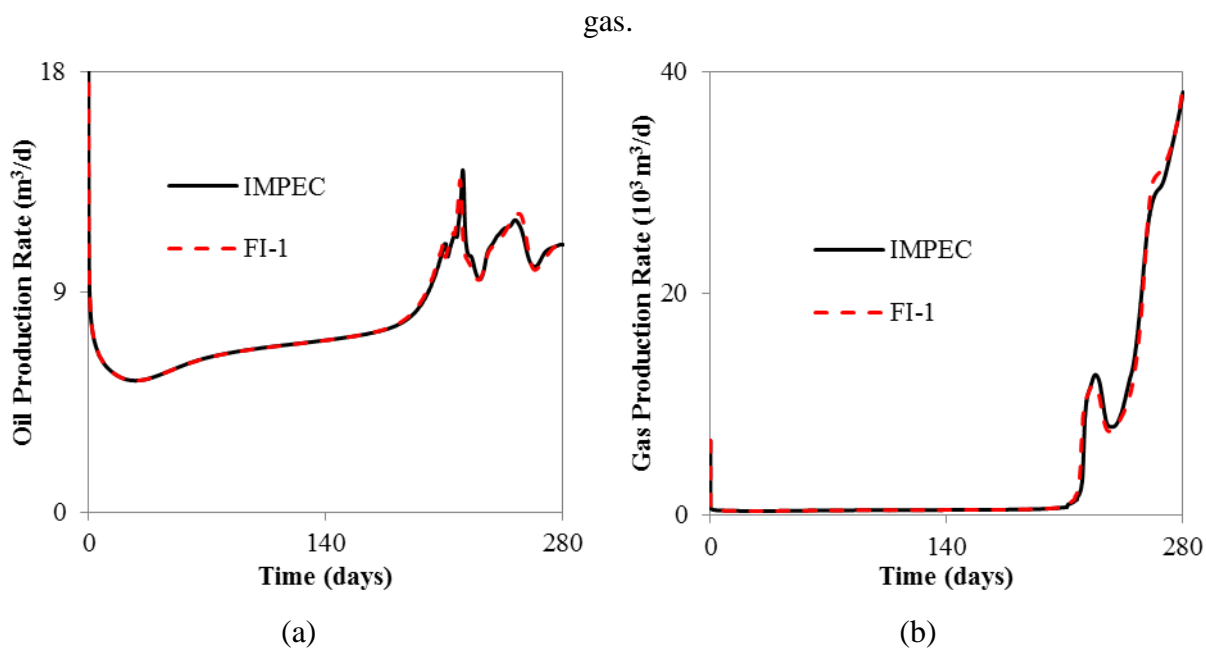
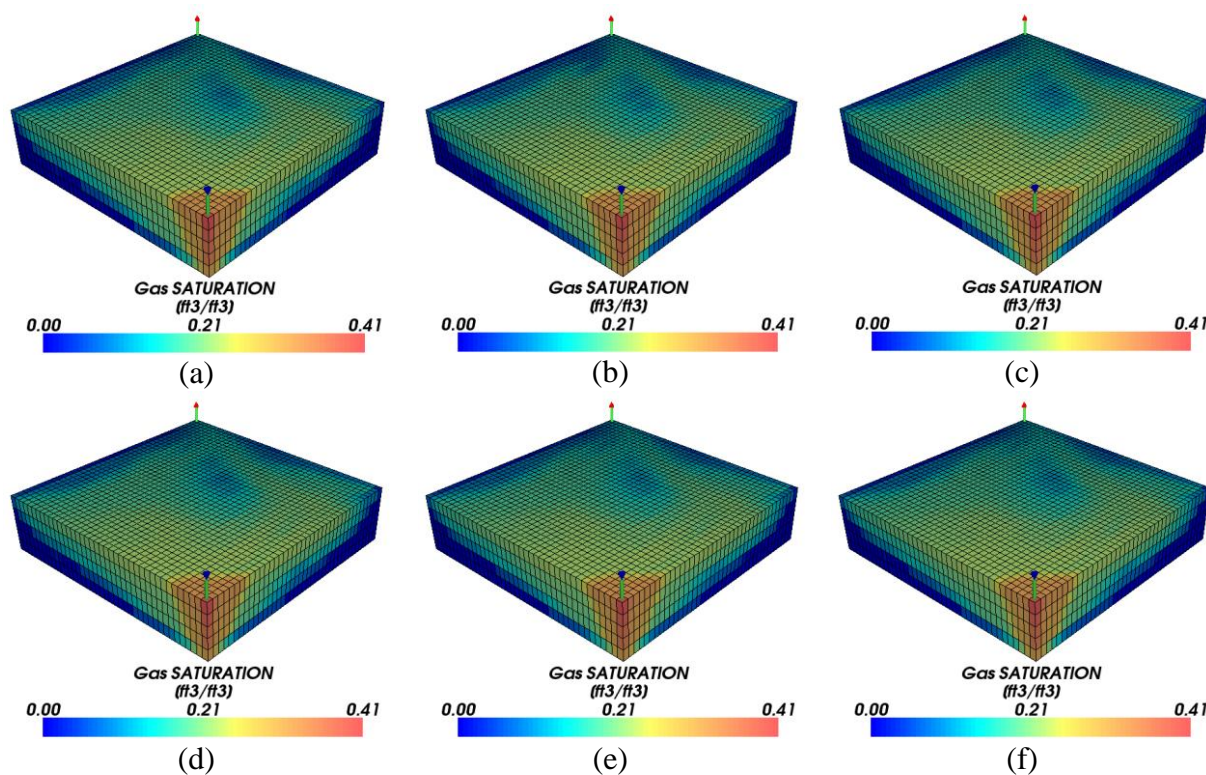


Figure 5.69 – Gas saturation field at 250 days - Case 4. a) IMPEC; b) IMPSAT-0; c) IMPSAT-1; d) IMPSAT-2; e) FI-0; and f) FI-1.



The time-step profile for all formulations is presented in Figure 5.70 and the CPU times are presented in Table 5.33. The IMPSAT-0 was the fastest formulation for this case. However, as the accuracy of this formulation was not good as the other formulations it cannot be considered. Further test using smaller time-step for the IMPSAT-0 that produced the correct answer, gives rise to a CPU time of 2769 seconds, which is much large than the CPU time of the other formulations. Therefore, the best formulation for this case was the IMPSAT-1. The FI approaches could not use greater time-steps for keeping the solution accuracy and were not that fast one.

Figure 5.70 – Time-stepping profiles – Case 4. a) IMPEC and IMPSAT formulations; and b) IMPEC and FI formulations.

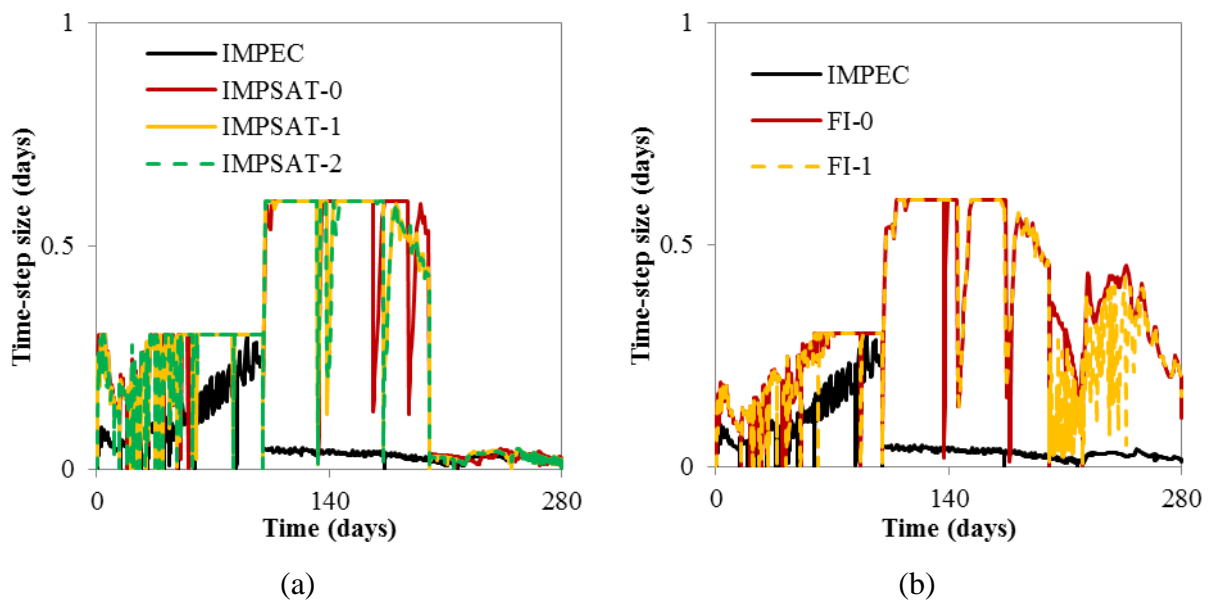


Table 5.33 – CPU time (s) of all simulations – Case 4.

Formulation	CPU TIME
IMPEC	1821.71
IMPSAT-0	1233.36
IMPSAT-1	1249.47
IMPSAT-2	1430.35
FI-0	2131.27
FI-1	2199.48

## 6 CONCLUSIONS AND FUTURE WORK

This thesis presented the implementation of several numerical formulations in an in-house compositional reservoir simulator called UTCOMP. UTCOMP was developed at the Center for Petroleum and Geosystems Engineering at The University of Texas at Austin for the simulation of enhanced recovery processes. UTCOMP is a multiphase/multi-component compositional equation of state simulator which can handle the simulation of several enhanced oil recovery processes. The original formulation of this simulator was based in an IMPEC approach proposed by Ács et al. (1985). As a contribution of this work, the original IMPSAT formulation of Watts (1986) and a fully implicit (FI) of Collins et al. (1992) were successfully implemented in this study. These two approaches were called IMPSAT-0 and FI-0, respectively. Additionally, two modifications of the IMPSAT of Watts (1986) were implemented: IMPSAT-1 and IMPSAT-2. The IMPSAT-1 tries to correct the explicit terms of the saturation when evaluating the total number of moles of each component, and the IMPSAT-2 evaluates pressure and saturations in an iterative procedure. In addition to these formulations, another FI formulation was implemented (FI-1). This new FI formulation is an extension of the IMPEC of Ács et al. (1985) approach. All the implementations were performed for 2D and 3D reservoirs using Cartesian and unstructured grids in conjunction with the EbFVM (Element based Finite-Volume Method). Four case studies were designed to test and to analyze the performance of the formulations. All cases were related to gas injection processes.

From the several tests performed in this work, it was observed that the FI approaches were slower than the other formulations for coarse grids, and faster for fine grids. On the other hand, the IMPSAT formulations were faster for intermediate grids, we mean, neither coarse nor refined grids. The iterative IMPSAT (IMPSAT-2) was unable to achieve large time-step than the original Watts' formulation (IMPSAT-0), showing that in general, original level of implicitness of the Watts' formulation is enough for this formulation to overcome the CPU time of the IMPEC approach.

It was observed that the FI approaches cannot have a good performance for cases that are very sensible to time variation, such as cases 3 and 4. Since the investigated FI approaches could not provide good solutions for large time-steps, the IMPSAT formulations showed much better performance for these case studies.

On the other hand, the original Watts' formulation, IMPSAT-0, was inaccurate for the last case study four, where water, oil and gas flow into an 3D heterogeneous reservoir. It was found that the modification done in this formulation, IMPSAT-1, was very effective to keep the numerical accuracy obtained by the IMPSAT-2. Also, the iterative IMPSAT, IMPSAT-2, was able to handle this case properly, but with an increase in the total CPU time due to the large computational time per time-step when compared to the IMPSAT-1.

### ***6.1 Future work***

Several new features can complement the implementations of the present work. First, for completing the formulations implemented in this work, it is needed to implement the dispersion terms for each one of the formulations.

Second, an approximated CFL criteria could be used for control of the time-step selection, which could help the simulator to achieve better CPU times, since the time-step size is controlled in the UTCOMP simulator only by variation of physical properties.

Third, the use of parallel processing can reduce the CPU time of all formulations and is an important feature already in use by many commercial simulators. To verify the behavior of each formulation when using parallel processing is an important issue for this study.

Fourth, the use of high-order schemes is known to reduce the stability of explicit formulations. Verify the performance of each formulation when using high-order schemes is important since these schemes can sharply reduce grid refinement and therefore reduce the efforts used to carry out the simulation of real fields.

Finally, the implementation of an adaptive implicit method could be used to select the regions where the material balance equations could be solved by the IMPEC approach, and the regions where due to numerical instabilities the conservative equations should be solved by FI approach. This Adaptive Implicit Method is already in use in the literature and it is known to get the best of the IMPEC and FI formulations. It is important to mention that a stability criterion is an important key parameter when these two formulations are combined.

## 7 REFERENCES

- ÁCS, G.; DOLESCHALL, S. and FARKAS, E., General Purpose Compositional Model, SPE Journal, vol. 25, pp. 543-553, 1985.
- ARAÚJO, J.J.P., Tridimensional Simulation of Petroleum Reservoirs Using the Black-Oil Model with Formulation in Mass Fractions (In Portuguese). 2005. 115p. Thesis (Master in Chemical Engineering) – Department of Chemical Engineering, Federal University of Ceará, 2005.
- BALAY, S.; GROPP, W.D.; MCINNES, L.C. and SMITH, B.F., Efficient Management of Parallelism in Object-Oriented Numerical Software Libraries, In: Arge E. and Langtangen H.P. (eds.), Modern Software Tools in Scientific Computing, pp. 163-202, 1997.
- BALAY, S.; ADAMS, M.F.; BROWN, J.; BRUNE, P.; BUSCHELMAN, K.; EIJKHOUT, V.; GROPP, W.D.; KAUSHIK, D.; KNEPLEY, M.G.; MCINNES, L.C.; RUPP, K.; SMITH, B.F. and ZHANG, H., PETSc User's Manual, In: <http://www.mcs.anl.gov/petsc>, Argone National Laboratory, 2013.
- BALAY, S.; ADAMS, M.F.; BROWN, J.; BRUNE, P.; BUSCHELMAN, K.; EIJKHOUT, V.; GROPP, W.D.; KAUSHIK, D.; KNEPLEY, M.G.; MCINNES, L.C.; RUPP, K.; SMITH, B.F. and ZHANG, H., PETSc User's Manual, In: <http://www.mcs.anl.gov/petsc>, Argone National Laboratory, 2014.
- BALIGA, B.R. and PATANKAR, S.V., A New Finite-Element Formulation for Convection-Diffusion Problems, Numerical Heat Transfer, vol. 3, pp. 393-409, 1980.
- BRANCO, C.M. and RODRÍGUEZ, F., A Semi-Implicit Formulation for Compositional Reservoir Simulation, vol. 4, no. 1, pp. 171-177, 1996.
- BUCKLEY, S.E. and LEVERETT, M.C., Mechanism of Fluid Displacement in Sands, Transactions of the AIME, vol. 146, no. 1, pp. 107-116, 1942.
- CHANG, Y.-B., Development and Application of an Equation of State Compositional Simulator. 1990. 502p. Dissertation (Ph.D. in Petroleum Engineering) – Department of Petroleum and Geosystems Engineering, The University of Texas at Austin, 1990.
- CHIEN, M.C.H.; LEE, S.T. and CHEN, W.H., A New Fully Implicit Compositional Simulator, Paper SPE 13385, proceedings of the 8<sup>th</sup> SPE Symposium on Reservoir Simulation, Dallas, TX, February 10-13, 1985.
- CHOPRA, A.K. and CARTER, R.D., Proof of the Two-Phase Steady-State Theory for Flow through Porous Media, SPE Formation Evaluation, vol. 1, no. 6, 1986.

- CHU, W.H., Development of a General Finite Difference Approximation for a General Domain – Part I: Machine Transformation, *Journal of Computational Physics*, vol. 8, pp. 392-408, 1971.
- COATS, K.H., An Equation of State Compositional Model, *SPE Journal*, vol. 20, pp. 363-376, 1980.
- COATS, K.H., Reservoir Simulation: State of Art, *Journal of Petroleum Technology*, vol. 34, pp. 1633-1642, 1982a.
- COATS, K.H., “Reservoir Simulation”, *Petroleum Engineering Handbook*, H. B. Bradley (ed.), SPE, 1982b.
- COLLINS, D.A.; NGHIEM, L.X.; LI, Y.-K. and GRABENSTETTER, J.E., An Efficient Approach to Adaptive-Implicit Compositional Simulation with an Equation of State, *SPE Reservoir Engineering*, vol. 7, no. 2, pp. 259-264, 1992.
- CORDAZZO, J., Petroleum Reservoir Simulation Using the EbFVM Method and Algebraic Multigrid (In portuguese). 2006. 250p. Thesis (Doctorate in Mechanical Engineering) – Programa de Pós-Graduação em Engenharia Mecânica. UFSC, Florianópolis. 2006.
- COREY, A.T., *Mathematics of Immiscible Fluids in Porous Media*, Water Resources Publication, Littleton, CO, 1986.
- COUTINHO, B.G., Numerical Solution of Petroleum Reservoir Problems using Generalized Coordinates (In Portuguese). 2002. 115p. Thesis (Master in Mechanical Engineering) – Department of Mechanical Engineering, Federal University of Campina Grande, 2002.
- CUNHA, A.R.; MALISKA, C.R.; SILVA, A.F.C. and LIVRAMENTO, M.A., Two-Dimensional Two-Phase Petroleum Reservoir Simulation Using Boundary-Fitted Grids, *Proceedings of the V ENCIT*, pp. 359-362, São Paulo, Brazil, 1994.
- DARWISH, M.S. and MOUKALLED, F., TVD Schemes for Unstructured Grids, *International Journal of Heat and Mass Transfer*, vol. 46, no. 4, pp. 599-611, 2003.
- EDWARDS, M.G., Cross Flow Tensors and Finite Volume Approximation with Deferred Correction, *Computer Methods in Applied Mechanics and Engineering*, vol. 51, pp. 143-161, 1998.
- EPRI, Enhanced Oil Recovery Scoping Study, Report TR-113836, 1999.
- FERNANDES, B.R.B., Compositional Simulation of Petroleum Reservoir Simulation Using the Element based Finite Volume Method (In Portuguese). 2011. 52p. Monograph (B.Sc. in Chemical Engineering) – Department of Chemical Engineering, Federal University of Ceará, 2011.



- FERNANDES, B.R.B.; LIMA, I.C.M.; ARAÚJO, A.L.S., MARCONDES, F. and SEPEHRNOORI, K., 2D Compositional Reservoir Simulation Using Unstructured Grids in Heterogeneous Reservoirs, 10<sup>th</sup> Congress on Computational Mechanics, São Paulo, Brazil, 2012
- FERNANDES, B.R.B.; MARCONDES, F. and SEPEHRNOORI, K., Investigation of Several Interpolation Functions for Unstructured Meshes in Conjunction with Compositional Simulation, Numerical Heat Transfer Part A: Applications, vol. 64, no. 12, pp. 974-993, 2013.
- FERNANDES, B.R.B.; MARCONDES, F.; VARAVEI, A. and SEPEHRNOORI, K., Comparison of an IMPEC and a Semi-Implicit Formulation for Compositional Reservoir Simulation, Brazilian Journal of Chemical Engineering, accepted to publication, 2014a.
- FERNANDES, B.R.B.; GONÇALVES, A.D.R.; DRUMOND FILHO, E.P.; LIMA, I.C.M.; MARCONDES, F.; VARAVEI, A. and SEPEHRNOORI, K., A 3D Total Variation Diminishing Scheme for Compositional Reservoir Simulation Using the Element-based Finite Volume Method, Numerical Heat Transfer Part A: Applications, accepted to publication, 2014b.
- FUNG, L.S.-K.; HIEBERT, A.D. and NGHIEM, L.X., Reservoir Simulation with a Control-Volume Finite-Element Method, SPE Reservoir Engineering, vol. 7, pp.349-357, 1992.
- FUSSELL, L.T. and FUSSELL, D.D., An Iterative Technique for Compositional Reservoir Models, SPE Journal, vol. 19, pp. 211-220, 1979.
- HAUKAS, J.; AAVATSMARK, I. and ESPEDAL, M., A Black-Oil and Compositional IMPSAT Simulator with Improved Compositional Convergence, Proceedings of the 9<sup>th</sup> European Conference on the Mathematics of Oil Recovery, Cannes, France, 30 Aug. – 2 Sep., 2004.
- HAUKAS, J.; AAVATSMARK, I.; ESPEDAL, M. and REISO, E., A Volume Balance Consistent Compositional IMPSAT Formulation with Relaxed Stability Constraints. Computational Geosciences, 2005.
- HAUKAS, J., Compositional Reservoir Simulation with Emphasis on the IMPSAT Formulation. 2006. 71p. Dissertation (Ph.D. in Applied Mathematics) - Department of Mathematics, The University of Bergen, Norway, 2006.
- HEINEMANN, Z.E. and BRAND, C.W., Gridding Techniques in Reservoir Simulation, Proceedings of the First International Forum on Reservoir Simulation, Alpbach, Austria, 1988.

- HEINEMANN, Z.E.; BRAND, C.W.; MUNKA, M. and CHEN, Y.M., Modelling Reservoir Geometry with Irregular Grids, SPE Reservoir Engineering, vol. 6, no. 2, 1991.
- HERNING, F. and ZIPPERER, L., Calculation of the Viscosity of Technical Gas Mixtures from the Viscosity of Individual Gases, Gas and Wasserfach, vol. 79, pp. 49-54; 69-73, 1936.
- HIRASAKI, G.J. and O'DELL, P.M., Representation of Reservoir Geometry for Numerical Simulation, SPE Journal, vol. 10, no. 4, pp. 393-404, 1970.
- HURTADO, F.S.V.; MALISKA, C.R.; da SILVA, A.F.C and CORDAZZO, J., A Quadrilateral Element-based Finite Volume Method Formulation for the Simulation of Complex Reservoirs, SPE Latin American and Caribbean Petroleum Engineering Conference, Buenos Aires, Argentina, 2007.
- GLASBY, G.P., Abiogenic Origin of Hydrocarbons: An Historical Overview, Resource Geology, vol. 56, no. 1, pp. 85-98, 2006.
- JHAVERI, B.S. and YOUNGREN, G.K., Three-Parameter Modification of the Peng-Robinson Equation of State to Improve Volumetric Prediction, SPE Reservoir Engineering, vol. 3, no. 3, pp. 1033-1040, 1988.
- JOSSI, J.A.; STIEL, L.I. and THODOS, G., The Viscosity of Pure Substances in the Dense Gaseous and Liquid Phases, AIChE Journal, vol. 8, no. 1, pp. 59-63, 1962.
- KAZEMI, H.; VESTAL, C.R. and SHANK, G.D., An Efficient Multicomponent Numerical Simulator, SPE Journal, vol. 18, no. 5, pp. 355-368, 1978.
- KENDALL, R.P.; MORRELL, G.O.; PEACEMAN, D.W.; SILLIMAN, W.J. and WATTS, J.W., Development of a Multiple Application Reservoir Simulator for Use on a Vector Computer. Paper SPE 11483 presented at the 1983 SPE Middle East Oil Technical Conference, Manama, Bahrain, Março 14-17, 1983.
- KOREN, B., A Robust Upwind Discretization Method for Advection, Diffusion and Source Terms, in C.B. Vreugdenhil and B. Koren (eds.), Numerical Methods for Advection-Diffusion Problems, pp. 117-138, 1993.
- LEVENTHAL, S.H.; KLEIN, M.H. and CULHAM, W.E., Curvilinear Coordinate Systems for Reservoir Simulation, SPE Journal, vol. 25, no. 6, pp. 893-904, 1985.
- LI, X., A Collection of Case Studies for Verification of Reservoir Simulators. 2012. 227p. Thesis (M.Sc. in Petroleum Engineering) – Department of Petroleum and Geosystems Engineering, The University of Texas at Austin, 2012.

- LOHRENZ, J.; BRAY, B.G. and CLARK, C.R., Calculating Viscosities of Reservoir Fluids from their Compositions, *Journal of Petroleum Technology*, vol. 16, no. 10, pp. 1171-1176, 1964.
- MACLEOD, D.B., On a Relation Between Surface Tension and Density, *Transactions of the Faraday Society*, vol. 19, pp. 38-41, 1923.
- MALISKA, C.R.; CUNHA, A.R.; LIVRAMENTO, M.A. and SILVA, A.F.C., Tridimensional Petroleum Reservoir Simulation Using Generalized Curvilinear Grids, *Proceeding of the V ENCIT*, pp. 363-366, São Paulo, Brazil, 1994.
- MALISKA, C.R.; da SILVA, A.F.C.; CZESNAT, A.O.; LUCIANETTI, R.M. and MALISKA JR., C.R. Three-Dimensional Multiphase Flow Simulation in Petroleum Reservoirs Using the Mass Fractions as Dependent Variables, *Latin American and Caribbean Petroleum Engineering Conference*, Rio de Janeiro, Brazil, 1997.
- MALISKA, C.R., *Computational Heat Transfer and Fluid Mechanics (In portuguese)*, 2<sup>nd</sup> ed., Livros Técnicos e Científicos, Rio de Janeiro, 2004.
- MANSOORI, J., Discussion of Compositional Modelling With an Equation of State, *SPE Journal*, vol. 22, no. 2, pp. 202-203, 1982.
- MARCONDES, F.; HAN, C. and SEPEHRNOORI, K., Implementation of Corner Point Mesh into a Parallel, Fully Implicit, Equation of State Compositional Reservoir Simulator, 18<sup>th</sup> International Congress of Mechanical Engineering (COBEM), Ouro Preto, Brazil, 2005.
- MARCONDES, F.; HAN, C. and SEPEHRNOORI, K., Effect of Cross Derivatives in Discretization Schemes in Structured Non-Orthogonal Meshes for Compositional Reservoir Simulation, *Journal of Petroleum Science and Engineering*, vol. 63, no. 1-4, pp. 53-60, 2008.
- MARCONDES, F. and SEPERHNOORI, K., An Element-Based Finite Volume-Method Approach for Heterogeneous and Anisotropic Compositional Reservoir Simulation, *Journal of Petroleum Science & Engineering*, vol. 73, pp. 99-106, 2010.
- MARCONDES, F.; SANTOS, L.O.S.; VARAVEI, A. and SEPERHNOORI, K., A 3D Hybrid Element-based Finite Volume Method for Heterogeneous and Anisotropic Compositional Reservoir Simulation, *Journal of Petroleum Science and Engineering*, vol. 108, pp. 342-351, 2013.
- MASSON, C.; SAABAS, H.J. and BALIGA, B.R., Co-Located Equal-Order Control-Volume Finite-Element Method for Two-Dimensional Axisymmetric Incompressible Fluid Flow, *International Journal for Numerical Methods in Fluids*, vol. 18, no. 1, pp. 1-26, 1994.

- MEHRA, A.R.; HEIDEMANN, R.A. and AZIZ, K., An Accelerated Successive Substitution Algorithm, Canadian Journal of Chemical Engineering, vol. 61, pp. 590-596, 1983.
- MICHELSSEN, J.L., The Isothermal Flash Problem. Part I. Stability, Fluid Phase Equilibria, vol. 9, pp. 1-19, 1982.
- NGHIEM, L.X.; FONG, D.K. and AZIZ, K., Compositional Modelling with an Equation of State, SPE Journal, vol. 21, pp. 687-698, 1981.
- NGHIEM, L.X., Author's Reply to Discussion of Compositional Modelling With an Equation of State, SPE Journal, vol. 22, no. 2, p. 204, 1982.
- NOGUEIRA, R.L., Petroleum Reservoir Simulation Using the Black-Oil Model based on Mass Fractions in Conjunction with Unstructured Grids. 2011. 95p. Thesis (Master in Chemical Engineering) – Department of Chemical Engineering, Federal University of Ceará, 2011.
- PEACEMAN, D.W., Interpretation of Well-Block Pressures in Numerical Reservoir Simulation, SPE Journal, vol. 18, no. 3, pp. 183-194, 1978.
- PEACEMAN, D.W., Interpretation of Well-Block Pressure in Numerical Reservoir Simulation with Nonsquare Grid Blocks and Anisotropic Permeability, SPE Journal, vol. 23, no. 3, pp. 531-543, 1983.
- PENG, D-Y. and ROBINSON, D.B., A New Two-Constant Equation of State, Industrial & Engineering Chemistry Fundamentals, vol. 15, no. 1, pp. 59-64, 1976.
- PERSCHKE, D.R., Equation of State Phase Behavior Modelling for Compositional Simulator. 1988. 456p. Dissertation (Ph.D. in Petroleum Engineering) – Department of Petroleum and Geosystems Engineering, The University of Texas at Austin, USA, 1988.
- QUANDALLE, P. and SAVARY, D., An Implicit in Pressure and Saturations Approach to Fully Compositional Simulation, Proceedings of the 10<sup>th</sup> SPE Symposium on Reservoir Simulation, Houston, TX, 1989.
- RACHFORD, R.H. and RICE, J.D., Procedure for Use of Electronic Digital Computers in Calculating Flash Vaporization Hydrocarbon Equilibrium, Journal of Petroleum Technology, vol. 4, 1952.
- REDLICH, O. and KWONG, J.N.S., On the Thermodynamics of Solutions. V. An Equation of State. Fugacities of Gaseous Solutions, Chemical Reviews, vol. 44, pp. 233-244, 1949.
- POLING, B.E.; PRAUSNITZ, J.M. and O'CONNELL, J.P., The Properties of Gases and Liquids, 5<sup>th</sup> Ed., McGraw-Hill, 2001.
- ROE, P.L., Some Characteristic-based Schemes for the Euler Equations, Annual Review of Fluid Mechanics, vol. 18, pp. 337-365, 1986.

- ROZON, B.J., A Generalized Finite Volume Method for Reservoir Simulation, Reservoir Simulation 1989, Reservoir Simulation Symposium, Houston, USA, 1989.
- SAABAS, H.J. and BALIGA, B.R., Co-Located Equal-Order Control-Volume Finite-Element Method for Multidimensional, Incompressible, Fluid Flow – Part I: Formulation, Numerical Heat Transfer Part B: Fundamentals, vol. 26, no. 4, pp. 381-407, 1994a.
- SAABAS, H.J. and BALIGA, B.R., Co-Located Equal-Order Control-Volume Finite-Element Method for Multidimensional, Incompressible, Fluid Flow – Part II: Verification, Numerical Heat Transfer Part B: Fundamentals, vol. 26, no. 4, pp. 409-424, 1994b.
- SARMENTO, D.C., Three-Phase Simulation of Petroleum Reservoirs Using the Black-Oil Model with Formulation in Mass Fractions (In Portuguese). 2009. 99p. Thesis (Master in Chemical Engineering) – Department of Chemical Engineering, Federal University of Ceará, 2009.
- SHELDON, J.W. and DOUGHERTY, E.D., The Approximation of Secondary Recovery Projects Using Moving Interfaces, 36<sup>th</sup> Annual fall Meeting of SPE, Dallas, USA, 1961.
- SILLETTE, A.G.; HILLESTAD, J.G. and STONE, H.L., A High-Stability Sequential Solution Approach to Reservoir Simulation, Fall Meeting of the Society of Petroleum Engineers of AIME.SPE, Las Vegas, Nevada, USA, 1973.
- STIEL, L.I. and THODOS, G., The Viscosity of Nonpolar Gases at Normal Pressure, AUChe Journal, vol. 7, no. 4, pp. 611-615, 1961.
- STONE, H.L., Estimation of Three-Phase Relative Permeability and Residual Oil Data, Journal of Canadian Petroleum Technology, vol. 12, no. 4, pp. 53-61, 1973.
- SUBRAMANIAN, G.; TRANGENSTEIN, J.A.; MOCHIZUKI, S. and SHEN, E.I-C., Efficient Fluid Behavior Computations in a Sequential Compositional Reservoir Simulator, 9<sup>th</sup> SPE Symposium on Reservoir Simulation, San Antonio, Feb. 1-4, 1987.
- SUGDEN, S., A Relation Between Surface Tension, Density, and Chemical Composition, Journal of the Chemical Society, vol. 125, pp. 1177-1189, 1924.
- SWAMINATHAN, C.R. and VOLLER, V.R., Streamline Upwind Scheme for Control-Volume Finite Elements, Part I: Formulations, Numerical Heat Transfer Part B: Fundamentals, vol. 22, no. 1, pp. 95-107, 1992a.
- SWAMINATHAN, C.R. and VOLLER, V.R., Streamline Upwind Scheme for Control-Volume Finite Elements, Part II: Implementation and Comparison with SUPG Finite-Element Scheme, Numerical Heat Transfer Part B: Fundamentals, vol. 22, no. 1, pp. 109-124, 1992a.

- THELE, K.J., A Comparison of Three Equation of State Compositional Simulators. Dissertation (Ph.D. in Petroleum Engineering) – Department of Petroleum and Geosystems Engineering, The University of Texas at Austin, USA, 1984.
- THOMPSON, J.F., THAMES, F.C. and MASTIN, C.W., Automatic Numerical Generation of Body Fitted Curvilinear Coordinates Systems for Fields Containing any Number of Arbitrary Two-Dimensional Bodies, *Journal of Computational Physics*, vol. 15, pp. 299-319, 1974.
- TRANGENSTEIN, J.A., Customized Minimization Techniques for Phase Equilibrium Computations in Reservoir Simulation, *Chemical Engineering Science*, vol. 42, pp. 2847-2863, 1988.
- U.S. Department of Energy, Enhanced Oil Recovery, In: <http://energy.gov/fe/science-innovation/oil-gas/enhanced-oil-recovery>, accessed in April 13, 2014, 2011.
- WADSLEY, W.A., Modelling Reservoir Geometry with Non-Rectangular Coordinates Grids, 55<sup>th</sup> Annual Fall Technical Conference and Exhibition of Society of Petroleum Engineers of AIME, Dallas, USA, 1980.
- WANG, P.; WHEELER, M.; PARASHAR, M. and SEPEHRNOORI, K., A New Generation EOS Compositional Reservoir Simulator: Part I – Formulation and Discretization, SPE Reservoir Simulation Symposium, June 8-11, Dallas, US.
- WATTS, J.W., A Compositional Formulation Based on Pressure and Saturation Equations, *SPE Reservoir Engineering Journal*, vol. 1, pp. 243-252, 1986.
- WONG, T.W. and AZIZ, K., Considerations in the Development of Multipurpose Reservoir Simulation Models, First and Second International Forum on Reservoir Simulation, July, 1989.
- WONG, T.W.; FIROOZABADI, A.; NUTAKKI, A. and AZIZ, K., A Comparison of Two Approaches to Compositional and Black Oil Simulation, 9<sup>th</sup> SPE Symposium on Reservoir Simulation, San Antonio, TX, Feb. 1-4, 1987.
- YOUNG, L.C. and STEPHENSON, R.E., A Generalized Compositional Approach for Reservoir Simulation, *SPE Journal*, vol. 23, No. 5, pp. 727-742, 1983.
- ZUDKEVITCH, D. and JOFFE, J., Correlation and Prediction of Vapor-Liquid Equilibria with the Redlich-Kwong Equation of State, *AIChE Journal*, vol. 16, no. 1, pp. 112-119, 1970.

**APPENDIX A**  
**TIME-STEPPING CONTROL PARAMETERS**

Table A.1. Time-stepping control parameters for Case 1 using 2D Cartesian grids.

<b>Formulation</b>	$\Delta t_{max}$ (d)	$\Delta t_{min}$ (d)	$\Delta P_{lim}$	$\Delta S_{lim}$	$\Delta V_{lim}$	$\Delta N_{lim}$
IMPEC – 20x20	0.9	$10^{-4}$	0.1	0.1	0.1	0.25
IMPSAT-0 – 20x20	2.4	$10^{-4}$	0.1	0.1	0.1	0.25
IMPSAT-1 – 20x20	2.4	$10^{-4}$	0.1	0.1	0.1	0.25
IMPSAT-2 – 20x20	2.4	$10^{-4}$	0.1	0.1	0.1	0.25
FI-0* – 20x20	25	$10^{-4}$	1	1	1	10
FI-1* – 20x20	25	$10^{-4}$	1	1	1	10
FI-0 – 20x20	3	$10^{-4}$	0.1	0.1	0.1	0.25
FI-1 – 20x20	3	$10^{-4}$	0.1	0.1	0.1	0.25
IMPEC – 40x40	0.2	$10^{-4}$	0.1	0.1	0.1	0.25
IMPSAT-0 – 40x40	0.7	$10^{-4}$	0.1	0.1	0.1	0.25
IMPSAT-1 – 40x40	0.7	$10^{-4}$	0.1	0.1	0.1	0.25
IMPSAT-2 – 40x40	0.7	$10^{-4}$	0.1	0.1	0.1	0.25
FI-0* – 40x40	25	$10^{-4}$	1	1	1	10
FI-1* – 40x40	25	$10^{-4}$	1	1	1	10
FI-0 – 40x40	1	$10^{-4}$	1	1	1	0.25
FI-1 – 40x40	1	$10^{-4}$	1	1	1	0.25
IMPEC – 80x80	0.06	$10^{-4}$	0.1	0.1	0.1	0.25
IMPSAT-0 – 80x80	0.17	$10^{-4}$	0.1	0.1	0.1	0.25
IMPSAT-1 – 80x80	0.17	$10^{-4}$	0.1	0.1	0.1	0.25
IMPSAT-2 – 80x80	0.17	$10^{-4}$	0.1	0.1	0.1	0.25
FI-0* – 80x80	25	$10^{-4}$	1	1	1	10
FI-1* – 80x80	25	$10^{-4}$	1	1	1	10
FI-0 – 80x80	1	$10^{-4}$	1	1	1	0.25
FI-1 – 80x80	1	$10^{-4}$	1	1	1	0.25

Table A.2. Time-stepping control parameters for Case 1 using 3D Cartesian grids.

<b>Formulation</b>	$\Delta t_{max}$ (d)	$\Delta t_{min}$ (d)	$\Delta P_{lim}$	$\Delta S_{lim}$	$\Delta V_{lim}$	$\Delta N_{lim}$
IMPEC – 20x20x5	0.8	$10^{-4}$	0.1	0.1	0.1	0.25
IMPSAT-0 – 20x20x5	2.4	$10^{-4}$	0.1	0.1	0.1	0.25
IMPSAT-1 – 20x20x5	2.4	$10^{-4}$	0.1	0.1	0.1	0.25
IMPSAT-2 – 20x20x5	2.4	$10^{-4}$	0.1	0.1	0.1	0.25
FI-0 – 20x20x5	3	$10^{-4}$	1	1	1	10
FI-1 – 20x20x4	3	$10^{-4}$	1	1	1	10
IMPEC – 40x40x10	0.2	$10^{-4}$	0.1	0.1	0.1	0.25
IMPSAT-0 – 40x40x10	0.7	$10^{-4}$	0.1	0.1	0.1	0.25
IMPSAT-1 – 40x40x10	0.7	$10^{-4}$	0.1	0.1	0.1	0.25
IMPSAT-2 – 40x40x10	0.7	$10^{-4}$	0.1	0.1	0.1	0.25
FI-0 – 40x40x10	2	$10^{-4}$	1	1	1	10
FI-1 – 40x40x10	2	$10^{-4}$	1	1	1	10
IMPEC – 60x60x15	0.15	$10^{-4}$	0.1	0.05	0.1	0.05
IMPSAT-0 – 60x60x15	0.3	$10^{-4}$	0.1	0.05	0.1	0.4
IMPSAT-1 – 60x60x15	0.3	$10^{-4}$	0.1	0.05	0.1	0.4
IMPSAT-2 – 60x60x15	0.3	$10^{-4}$	0.1	0.05	0.1	0.4
FI-0 – 60x60x15	1	$10^{-4}$	1	1	1	10
FI-1 – 60x60x15	1	$10^{-4}$	1	1	1	10



Table A.3. Time-step control parameters - Case 1 using 2D uniform quadrilateral grids.

<b>Formulation</b>	$\Delta t_{max}$ (d)	$\Delta t_{min}$ (d)	$\Delta P_{lim}$	$\Delta S_{lim}$	$\Delta V_{lim}$	$\Delta N_{lim}$
IMPEC – 20x20	0.25	$10^{-4}$	0.05	0.01	0.05	0.4
IMPSAT-0 – 20x20	0.7	$10^{-4}$	0.05	0.01	0.05	0.4
IMPSAT-1 – 20x20	0.7	$10^{-4}$	0.05	0.01	0.05	0.4
IMPSAT-2 – 20x20	0.7	$10^{-4}$	0.05	0.01	0.05	0.4
FI-0 – 20x20	1	$10^{-4}$	1	1	1	10
FI-1 – 20x20	1	$10^{-4}$	1	1	1	10
IMPEC – 40x40	0.065	$10^{-4}$	0.05	0.01	0.05	0.4
IMPSAT-0 – 40x40	0.18	$10^{-4}$	0.05	0.01	0.05	0.4
IMPSAT-1 – 40x40	0.18	$10^{-4}$	0.05	0.01	0.05	0.4
IMPSAT-2 – 40x40	0.18	$10^{-4}$	0.1	0.1	0.1	0.25
FI-0 – 40x40	1	$10^{-4}$	1	1	1	10
FI-1 – 40x40	1	$10^{-4}$	1	1	1	10
IMPEC – 60x60	0.025	$10^{-4}$	0.05	0.01	0.05	0.1
IMPSAT-0 – 60x60	0.075	$10^{-4}$	0.05	0.01	0.05	0.1
IMPSAT-1 – 60x60	0.075	$10^{-4}$	0.05	0.01	0.05	0.1
IMPSAT-2 – 60x60	0.075	$10^{-4}$	0.05	0.01	0.05	0.1
FI-0 – 60x60	1	$10^{-4}$	1	1	1	10
FI-1 – 60x60	1	$10^{-4}$	1	1	1	10

Table A.4. Time-step control parameters for Case 1 using 2D unstructured quadrilateral grids.

<b>Formulation</b>	$\Delta t_{max}$ (d)	$\Delta t_{min}$ (d)	$\Delta P_{lim}$	$\Delta S_{lim}$	$\Delta V_{lim}$	$\Delta N_{lim}$
IMPEC – 1199 vertices	0.1	$10^{-4}$	0.05	0.01	0.05	0.4
IMPSAT-0 – 1199 vertices	0.3	$10^{-4}$	0.05	0.01	0.05	0.4
IMPSAT-1 – 1199 vertices	0.3	$10^{-4}$	0.05	0.01	0.05	0.4
IMPSAT-2 – 1199 vertices	0.3	$10^{-4}$	0.05	0.01	0.05	0.4
FI-0 – 1199 vertices	1	$10^{-4}$	1	1	1	10
FI-1 – 1199 vertices	1	$10^{-4}$	1	1	1	10
IMPEC – 2661 vertices	0.04	$10^{-4}$	0.05	0.01	0.05	0.4
IMPSAT-0 – 2661 vertices	0.12	$10^{-4}$	0.05	0.01	0.05	0.4
IMPSAT-1 – 2661 vertices	0.12	$10^{-4}$	0.05	0.01	0.05	0.4
IMPSAT-2 – 2661 vertices	0.12	$10^{-4}$	0.1	0.1	0.1	0.25
FI-0 – 2661 vertices	1	$10^{-4}$	1	1	1	10
FI-1 – 2661 vertices	1	$10^{-4}$	1	1	1	10
IMPEC – 3387 vertices	0.035	$10^{-4}$	0.05	0.01	0.05	0.1
IMPSAT-0 – 3387 vertices	0.1	$10^{-4}$	0.05	0.01	0.05	0.1
IMPSAT-1 – 3387 vertices	0.1	$10^{-4}$	0.05	0.01	0.05	0.1
IMPSAT-2 – 3387 vertices	0.1	$10^{-4}$	0.05	0.01	0.05	0.1
FI-0 – 3387 vertices	1	$10^{-4}$	1	1	1	10
FI-1 – 3387 vertices	1	$10^{-4}$	1	1	1	10

Table A.5. Time-step control parameters for Case 1 using 2D unstructured triangular grids.

<b>Formulation</b>	$\Delta t_{max}$ (d)	$\Delta t_{min}$ (d)	$\Delta P_{lim}$	$\Delta S_{lim}$	$\Delta V_{lim}$	$\Delta N_{lim}$
IMPEC – 1220 vertices	0.1	$10^{-4}$	0.05	0.01	0.05	0.4
IMPSAT-0 – 1220 vertices	0.21	$10^{-4}$	0.05	0.01	0.05	0.4
IMPSAT-1 – 1220 vertices	0.21	$10^{-4}$	0.05	0.01	0.05	0.4
IMPSAT-2 – 1220 vertices	0.21	$10^{-4}$	0.05	0.01	0.05	0.4
FI-0 – 1220 vertices	1	$10^{-4}$	1	1	1	10
FI-1 – 1220 vertices	1	$10^{-4}$	1	1	1	10
IMPEC – 2330 vertices	0.035	$10^{-4}$	0.05	0.01	0.05	0.4
IMPSAT-0 – 2330 vertices	0.09	$10^{-4}$	0.05	0.01	0.05	0.4
IMPSAT-1 – 2330 vertices	0.09	$10^{-4}$	0.05	0.01	0.05	0.4
IMPSAT-2 – 2330 vertices	0.09	$10^{-4}$	0.1	0.1	0.1	0.25
FI-0 – 2330 vertices	1	$10^{-4}$	1	1	1	10
FI-1 – 2330 vertices	1	$10^{-4}$	1	1	1	10
IMPEC – 3329 vertices	0.025	$10^{-4}$	0.05	0.01	0.05	0.1
IMPSAT-0 – 3329 vertices	0.06	$10^{-4}$	0.05	0.01	0.05	0.1
IMPSAT-1 – 3329 vertices	0.06	$10^{-4}$	0.05	0.01	0.05	0.1
IMPSAT-2 – 3329 vertices	0.06	$10^{-4}$	0.05	0.01	0.05	0.1
FI-0 – 3329 vertices	1	$10^{-4}$	1	1	1	10
FI-1 – 3329 vertices	1	$10^{-4}$	1	1	1	10

Table A.6. Time-step control parameters for Case 1 using 3D unstructured hexahedron grids.

<b>Formulation</b>	$\Delta t_{max}$ (d)	$\Delta t_{min}$ (d)	$\Delta P_{lim}$	$\Delta S_{lim}$	$\Delta V_{lim}$	$\Delta N_{lim}$
IMPEC – 1024 vertices	0.35	$10^{-4}$	0.05	0.01	0.05	0.4
IMPSAT-0 – 1024 vertices	1.0	$10^{-4}$	0.1	0.1	0.1	0.4
IMPSAT-1 – 1024 vertices	1.0	$10^{-4}$	0.1	0.1	0.1	0.4
IMPSAT-2 – 1024 vertices	1.0	$10^{-4}$	0.1	0.1	0.1	0.4
FI-0 – 1024 vertices	1	$10^{-4}$	1	1	1	10
FI-1 – 1024 vertices	1	$10^{-4}$	1	1	1	10
IMPEC – 6480 vertices	0.07	$10^{-4}$	0.05	0.01	0.05	0.4
IMPSAT-0 – 6480 vertices	0.2	$10^{-4}$	0.1	0.1	0.1	0.4
IMPSAT-1 – 6480 vertices	0.2	$10^{-4}$	0.1	0.1	0.1	0.4
IMPSAT-2 – 6480 vertices	0.2	$10^{-4}$	0.1	0.1	0.1	0.4
FI-0 – 6480 vertices	1	$10^{-4}$	1	1	1	10
FI-1 – 6480 vertices	1	$10^{-4}$	1	1	1	10
IMPEC – 11767 vertices	0.05	$10^{-4}$	0.05	0.01	0.05	0.4
IMPSAT-0 – 11767 vertices	0.2	$10^{-4}$	0.1	0.1	0.1	0.4
IMPSAT-1 – 11767 vertices	0.2	$10^{-4}$	0.1	0.1	0.1	0.4
IMPSAT-2 – 11767 vertices	0.2	$10^{-4}$	0.1	0.1	0.1	0.4
FI-0 – 11767 vertices	1	$10^{-4}$	1	1	1	10
FI-1 – 11767 vertices	1	$10^{-4}$	1	1	1	10

Table A.7. Time-step control parameters for Case 1 using 3D unstructured tetrahedron grids.

<b>Formulation</b>	$\Delta t_{max}$ (d)	$\Delta t_{min}$ (d)	$\Delta P_{lim}$	$\Delta S_{lim}$	$\Delta V_{lim}$	$\Delta N_{lim}$
IMPEC – 1024 vertices	0.4	$10^{-4}$	0.05	0.01	0.05	0.4
IMPSAT-0 – 1024 vertices	1.1	$10^{-4}$	0.05	0.1	0.05	0.4
IMPSAT-1 – 1024 vertices	1.1	$10^{-4}$	0.05	0.1	0.05	0.4
IMPSAT-2 – 1024 vertices	1.1	$10^{-4}$	0.05	0.1	0.05	0.4
FI-0 – 1024 vertices	2	$10^{-4}$	1	1	1	10
FI-1 – 1024 vertices	2	$10^{-4}$	1	1	1	10
IMPEC – 4056 vertices	0.15	$10^{-4}$	0.05	0.01	0.05	0.4
IMPSAT-0 – 4056 vertices	0.35	$10^{-4}$	0.05	0.01	0.05	0.4
IMPSAT-1 – 4056 vertices	0.35	$10^{-4}$	0.05	0.01	0.05	0.4
IMPSAT-2 – 4056 vertices	0.35	$10^{-4}$	0.05	0.01	0.05	0.4
FI-0 – 4056 vertices	3	$10^{-4}$	1	1	1	10
FI-1 – 4056 vertices	3	$10^{-4}$	1	1	1	10
IMPEC – 16810 vertices	0.07	$10^{-4}$	0.05	0.01	0.05	0.4
IMPSAT-0 – 16810 vertices	0.2	$10^{-4}$	0.05	0.01	0.05	0.4
IMPSAT-1 – 16810 vertices	0.2	$10^{-4}$	0.05	0.01	0.05	0.4
IMPSAT-2 – 16810 vertices	0.2	$10^{-4}$	0.05	0.01	0.05	0.4
FI-0 – 16810 vertices	3	$10^{-4}$	1	1	1	10
FI-1 – 16810 vertices	3	$10^{-4}$	1	1	1	10

Table A.8. Time-step control parameters for Case 1 using 3D unstructured prism grids.

<b>Formulation</b>	$\Delta t_{max}$ (d)	$\Delta t_{min}$ (d)	$\Delta P_{lim}$	$\Delta S_{lim}$	$\Delta V_{lim}$	$\Delta N_{lim}$
IMPEC – 1024 vertices	0.5	$10^{-4}$	0.05	0.01	0.05	0.4
IMPSAT-0 – 1024 vertices	1.4	$10^{-4}$	0.05	0.1	0.05	0.4
IMPSAT-1 – 1024 vertices	1.4	$10^{-4}$	0.05	0.1	0.05	0.4
IMPSAT-2 – 1024 vertices	1.4	$10^{-4}$	0.05	0.1	0.05	0.4
FI-0 – 1024 vertices	3	$10^{-4}$	1	1	1	10
FI-1 – 1024 vertices	3	$10^{-4}$	1	1	1	10
IMPEC – 4056 vertices	0.15	$10^{-4}$	0.05	0.01	0.05	0.4
IMPSAT-0 – 4056 vertices	0.45	$10^{-4}$	0.05	0.01	0.05	0.4
IMPSAT-1 – 4056 vertices	0.45	$10^{-4}$	0.05	0.01	0.05	0.4
IMPSAT-2 – 4056 vertices	0.45	$10^{-4}$	0.05	0.01	0.05	0.4
FI-0 – 4056 vertices	3	$10^{-4}$	1	1	1	10
FI-1 – 4056 vertices	3	$10^{-4}$	1	1	1	10
IMPEC – 13448 vertices	0.07	$10^{-4}$	0.05	0.01	0.05	0.4
IMPSAT-0 – 13448 vertices	0.17	$10^{-4}$	0.05	0.01	0.05	0.4
IMPSAT-1 – 13448 vertices	0.17	$10^{-4}$	0.05	0.01	0.05	0.4
IMPSAT-2 – 13448 vertices	0.17	$10^{-4}$	0.05	0.01	0.05	0.4
FI-0 – 13448 vertices	3	$10^{-4}$	1	1	1	10
FI-1 – 13448 vertices	3	$10^{-4}$	1	1	1	10

Table A.9. Time-step control parameters for Case 1 using 3D unstructured pyramid grids.

<b>Formulation</b>	$\Delta t_{max}$ (d)	$\Delta t_{min}$ (d)	$\Delta P_{lim}$	$\Delta S_{lim}$	$\Delta V_{lim}$	$\Delta N_{lim}$
IMPEC – 1699 vertices	0.35	$10^{-4}$	0.05	0.01	0.05	0.4
IMPSAT-0 – 1699 vertices	0.9	$10^{-4}$	0.05	0.1	0.05	0.4
IMPSAT-1 – 1699 vertices	0.9	$10^{-4}$	0.05	0.1	0.05	0.4
IMPSAT-2 – 1699 vertices	0.9	$10^{-4}$	0.05	0.1	0.05	0.4
FI-0 – 1699 vertices	3	$10^{-4}$	1	1	1	10
FI-1 – 1699 vertices	3	$10^{-4}$	1	1	1	10
IMPEC – 7181 vertices	0.1	$10^{-4}$	0.05	0.01	0.05	0.4
IMPSAT-0 – 7181 vertices	0.28	$10^{-4}$	0.05	0.01	0.05	0.4
IMPSAT-1 – 7181 vertices	0.28	$10^{-4}$	0.05	0.01	0.05	0.4
IMPSAT-2 – 7181 vertices	0.28	$10^{-4}$	0.05	0.01	0.05	0.4
FI-0 – 7181 vertices	3	$10^{-4}$	1	1	1	10
FI-1 – 7181 vertices	3	$10^{-4}$	1	1	1	10
IMPEC – 24648 vertices	0.04	$10^{-4}$	0.05	0.01	0.05	0.4
IMPSAT-0 – 24648 vertices	0.14	$10^{-4}$	0.05	0.01	0.05	0.4
IMPSAT-1 – 24648 vertices	0.14	$10^{-4}$	0.05	0.01	0.05	0.4
IMPSAT-2 – 24648 vertices	0.14	$10^{-4}$	0.05	0.01	0.05	0.4
FI-0 – 24648 vertices	3	$10^{-4}$	1	1	1	10
FI-1 – 24648 vertices	3	$10^{-4}$	1	1	1	10

Table A.10. Time-step control parameters for Case 2.

<b>Formulation</b>	$\Delta t_{max}$ (d)	$\Delta t_{min}$ (d)	$\Delta P_{lim}$	$\Delta S_{lim}$	$\Delta V_{lim}$	$\Delta N_{lim}$
IMPEC	0.5	$10^{-4}$	0.1	0.1	0.1	0.1
IMPSAT-0	1.05	$10^{-4}$	0.1	0.1	0.1	0.1
IMPSAT-1	1.05	$10^{-4}$	0.1	0.1	0.1	0.1
IMPSAT-2	1.05	$10^{-4}$	0.1	0.1	0.1	0.1
FI-0	10	$10^{-4}$	0.1	0.1	0.1	0.1
FI-1	10	$10^{-4}$	0.1	0.1	0.1	0.1

Table A.11. Time-step control parameters for Case 3 using Cartesian grid.

<b>Formulation</b>	$\Delta t_{max}$ (d)	$\Delta t_{min}$ (d)	$\Delta P_{lim}$	$\Delta S_{lim}$	$\Delta V_{lim}$	$\Delta N_{lim}$
IMPEC	0.15	$10^{-3}$	0.05	0.005	0.05	0.02
IMPSAT-0	4.5	$10^{-4}$	0.1	0.1	0.05	0.045
IMPSAT-1	4.5	$10^{-4}$	0.1	0.1	0.05	0.045
IMPSAT-2	4.5	$10^{-4}$	0.1	0.1	0.05	0.045
FI-0 from 0 to 2700 days	4.8	$10^{-4}$	1	1	1	0.04
FI-0 from 2700 to 3000 days	1.0	$10^{-1}$	1	1	1	0.1
FI-1 from 0 to 2700 days	4.8	$10^{-4}$	1	1	1	0.04
FI-1 from 2700 to 3000 days	1.0	$10^{-1}$	1	1	1	0.1

Table A.12. Time-step control parameters for Case 3 using the element grid.

<b>Formulation</b>	$\Delta t_{max}$ (d)	$\Delta t_{min}$ (d)	$\Delta P_{lim}$	$\Delta S_{lim}$	$\Delta V_{lim}$	$\Delta N_{lim}$
IMPEC	2	$10^{-3}$	0.05	0.1	0.05	0.005
IMPSAT-0	2	$10^{-3}$	0.05	0.01	0.05	0.015
IMPSAT-1	2	$10^{-3}$	0.05	0.01	0.05	0.015
IMPSAT-2	2	$10^{-3}$	0.05	0.01	0.05	0.015
FI-0	5	$10^{-3}$	0.05	0.01	0.05	0.080
FI-1	5	$10^{-3}$	0.05	0.01	0.05	0.080



Table A.13. Time-step control parameters for Case 4.

<b>Formulation</b>	$\Delta t_{max}$ (d)	$\Delta t_{min}$ (d)	$\Delta P_{lim}$	$\Delta S_{lim}$	$\Delta V_{lim}$	$\Delta N_{lim}$
IMPEC from 0 to 100	2.2	$10^{-5}$	0.05	0.05	0.03	0.1
IMPEC from 100 to 200	2.2	$10^{-5}$	0.001	0.01	0.01	0.1
IMPEC from 200 to 280	2.2	$10^{-5}$	0.001	0.01	0.001	0.012
IMPSAT-0 from 0 to 100	0.3	$10^{-4}$	0.1	0.1	0.1	0.38
IMPSAT-0 from 100 to 200	0.6	$10^{-3}$	0.05	0.07	0.07	0.20
IMPSAT-0 from 200 to 280	1	$10^{-3}$	0.05	0.01	0.001	0.015
IMPSAT-1 from 0 to 100	0.3	$10^{-4}$	0.1	0.1	0.1	0.38
IMPSAT-1 from 100 to 200	0.6	$10^{-3}$	0.05	0.07	0.07	0.20
IMPSAT-1 from 200 to 280	1	$10^{-3}$	0.05	0.01	0.001	0.015
IMPSAT-2 from 0 to 100	0.3	$10^{-4}$	0.1	0.1	0.1	0.38
IMPSAT-2 from 100 to 200	0.6	$10^{-3}$	0.05	0.07	0.07	0.20
IMPSAT-2 from 200 to 280	1	$10^{-3}$	0.05	0.01	0.001	0.015
FI-0 from 0 to 100	0.3	$10^{-4}$	0.1	0.1	0.1	0.2
FI-0 from 100 to 200	0.6	$10^{-2}$	0.05	0.07	0.07	0.18
FI-0 from 200 to 280	1	$10^{-3}$	0.05	0.01	0.001	0.15
FI-1 from 0 to 100	0.3	$10^{-4}$	0.1	0.1	0.1	0.2
FI-1 from 100 to 200	0.6	$10^{-2}$	0.05	0.07	0.07	0.18
FI-1 from 200 to 280	1	$10^{-3}$	0.05	0.01	0.001	0.15